POWER SYSTEM NETWORK SPLITTING AND LOAD FREQUENCY CONTROL OPTIMIZATION USING ABC BASED ALGORITHMS

KANENDRA NAIDU A/L VIJYAKUMAR

THESIS SUBMITTED IN FULFILMENT OF THE REQUIREMENTS FOR THE DEGREE OF DOCTOR OF PHILOSOPHY

FACULTY OF ENGINEERING
UNIVERSITY OF MALAYA
KUALA LUMPUR

2015

UNIVERSITY OF MALAYA

ORIGINAL LITERARY WORK DECLARATION

Name of Candidate: **Kanendra Naidu A/L Vijyakumar** (I.C No: **841129-14-5857**)

Registration/Matric No: **KHA 110103**

Name of Degree: **Doctor Of Philosophy**

Title of Thesis ("this Work"): **POWER SYSTEM NETWORK SPLITTING AND LOAD FREQUENCY CONTROL OPTIMIZATION USING ABC BASED ALGORITHMS**

Field of Study: **Power System**

I do solemnly and sincerely declare that:

(1) I am the sole author/writer of this Work;
(2) This Work is original;
(3) Any use of any work in which copyright exists was done by way of fair dealing and for permitted purposes and any excerpt or extract from, or reference to or reproduction of any copyright work has been disclosed expressly and sufficiently and the title of the Work and its authorship have been acknowledged in this Work;
(4) I do not have any actual knowledge nor do I ought reasonably to know that the making of this work constitutes an infringement of any copyright work;
(5) I hereby assign all and every rights in the copyright to this Work to the University of Malaya ("UM"), who henceforth shall be owner of the copyright in this Work and that any reproduction or use in any form or by any means whatsoever is prohibited without the written consent of UM having been first had and obtained;
(6) I am fully aware that if in the course of making this Work I have infringed any copyright whether intentionally or otherwise, I may be subject to legal action or any other action as may be determined by UM.

Candidate's Signature Date:

Subscribed and solemnly declared before,

Witness's Signature Date:

Name:

Designation:

ABSTRACT

Blackout is the worst case scenario that could occur in the power system network. The cascading failure from one part of the system can propagate throughout the network and cause total system blackout. In order to mitigate the effect of blackout which causes the system to split into infeasible islands, the intentional islanding method is considered. It is applied to split the system into operational smaller island of network until system restoration is carried out. With regards to this, an optimization technique is required to identify the optimum system splitting solution and at the same time ensure the post-islanding frequency stability in the system. This research presents a modified optimization program for the system splitting problem in large scale power system based on Artificial Bee Colony algorithm and graph theory. The post-islanding frequency stability is maintained by optimizing the Load Frequency Control's parameters. The graph theory is used to represent the power system based on interconnection between the buses through the adjacency matrix. The edge reduction algorithm is initially applied to reduce the search space to obtain the initial solution. Subsequently, the modified optimization is implemented in order to find the optimum system splitting solution which ensures minimal power flow disruption. The power balance is checked and transmission line power flow analysis is carried out in each island to ensure stability is maintained. In the event the power balance criteria are violated, load shedding scheme is further applied to meet generation-load equilibrium. In the post-islanding phase, the load frequency control for each islanded area is optimally tuned using multi objective ABC optimization technique to maintain nominal system frequency at all times. The online wavelet filter is further implemented to filter out the noise in the LFC model. The IEEE 30-bus, 39-bus and 118-bus test system are chosen to validate the proposed method in MATLAB.

ABSTRAK

Salah satu senario buruk yang boleh berlaku dalam sistem kuasa adalah putus bekalan. Kegagalan melata dari satu bahagian sistem boleh tersebar ke seluruh rangkaian dan menyebabkan putus bekalan secara menyeluruh. Untuk mengurangkan kesan putus bekalan yang menyebabkan rangkaian berpisah kepada sistem terpulau tak tersaur, kaedah sistem pemulauan terancang dipertimbangkan. Kaedah ini digunakan untuk memisahkan rangkaian kuasa kepada sistem terpulau tersaur yang masih berfungsi. Oleh yang demikian, satu kaeadah pengoptimuman diperlukan untuk mengenalpasti sistem terpulau yang optimum dan dalam masa yang sama, memastikan agar kestabilan dan operasi pasca sistem pemualaun dijamin. Kajian ini membentangkan atur cara pengoptimuman diskret untuk masalah sistem terpulau dalam sistem kuasa skala besar berpandukan algoritma 'Artificial Bee Colony' dan 'graph theory'. Kestabilan pasca sistem terpulau dijamin dengan mengoptimasi parameter pengawal frekuensi beban. 'Graph theory' digunakan untuk mewakili saling hubungan antara bas melalui matriks bersebelahan. Algoritma 'edge reduction' digunakan untuk mengurangkan ruang gelintaran untuk memperolehi penyelesaian awal. Atur cara pengoptimuman diskret dilaksanakan untuk mencari penyelesaian optimum berpandukan gangguan aliran kuasa minima. Keseimbangan kuasa dipantau dan analisis talian penghantaran aliran kuasa dijalankan di setiap pulau bagi memastikan kestabilan dikekalkan. Sekiranya kriteria keseimbangan kuasa dilanggar, skim penanggalan beban akan diaplikasikan. Dalam fasa operasi pasca pemulauan, parameter optimum pengawal frekuensi beban untuk setiap sistem terpulau ditala menggunakan atur cara 'ABC' multiobjektif untuk mengekalkan frekuensi sistem nominal. Penapis 'wavelet' dugunakan untuk menapis hingar dalam model LFC. Sistem ujian IEEE 30, 39 dan 118 bas dipilih untuk mengesahkan kaedah yang dicadangkan dalam MATLAB.

ACKNOWLEDGEMENTS

First and foremost, I would like to kindly express my sincere thanks and deepest gratitude to my supervisors, Associate Professor Dr. Hazlie Bin Mokhlis and Dr. Ab Halim Bin Abu Bakar for all the help and guidance provided. Their advice, enthusiasm and motivation in assisting me to successfully complete this project is wholeheartedly appreciated.

I would like to sincerely thank my co-supervisor, Professor Vladimir Terzija for his advice and feedback in completing my PhD work. I would like to also thank Universiti Malaya for providing academic support and encouragement and also the necessary facility in ensuring a conducive atmosphere in order to accomplish my project.

I would like to take this opportunity to thank all my friends in the power group laboratory for all their assistance. I would also like to extend my gratitude and sincere thanks to my parents, my brother and sister who played an instrumental role in helping me by providing their full support and encouragement.

Last but not least, my heartfelt gratitude and appreciation to all of you and others who has contributed towards the successful completion of this project.

TABLE OF CONTENTS

LIST OF FIGURES

LIST OF TABLES

LIST OF SYMBOLS AND ABBREVIATIONS

AGC	:	Automatic Generation Control
ABC	:	Artificial Bee Colony
ACE	:	Area Control Error
H	:	Generator inertia constant
K_p	:	Proportional gain
K_r	:	Reheat gain
LFC	:	Load Frequency Control
PID	:	Proportional Integral Derivative
PSO	:	Particle Swarm Optimization
P_{Gmax}	:	Highest maximum power rating
P_G	:	Power generated
P_{Load}	:	Load demand
P_{loss}	:	Power losses in transmission line
$P_{imbalance}$	:	Power imbalance
P_{flow}	:	Power flow in transmission lines
P_{max}	:	Maximum power rating of the lines
P_{util}	:	Power utilized by transmission line
P_{min}	:	Minimal power flow disruption
T_i	:	Integral time constant
T_d	:	Derivative time constant
T_H	:	Hydraulic time constant
T_r	:	Reheat element time constant
T_T	:	Steam turbine time constant
p.u.	:	Per Unit

LIST OF APPENDICES

CHAPTER 1: INTRODUCTION

1.1 Introduction

Power system is an important and significant element that plays a major part in humans' daily lives. The power system is an intricate web of connection that acts as a single unit and mainly comprises of three important power system elements which are power system generation, transmission and distribution. This intricate and complex interconnection is often referred to as a power grid. Due to rapid growth in technology, humans' dependence on reliable source of electricity has increased tremendously. As such, the reliability of the electricity is heavily dependent on the successful operation of each part of the system which is composed of multiple interconnected elements (Rosas-Casals & Solé, 2011).

The electrical power system has five main operating states which are normal, alert, emergency, *in extremis* state and restorative state (X. Wang et al., 2005). In the normal and alert state the system is still able to operate in stable condition. The emergency state denotes the state in which the safety threshold of the system is compromised and is the final state where major preventive measures need to be taken. Failure to do so will lead to the extremis state in which the system will experience cascaded failure which will lead to total system blackout. After blackout, the re-energization of the power system is referred to as the restoration state (Sakaguchi & Matsumoto, 1983).

More often than not, the power system blackout is caused by the malfunction of the transmission system. The blackout problem is also quite often associated by the transient or dynamic stability of the system rather than the steady state condition (Tiranuchit & Thomas, 1988). From this point of view, the generation part of the system

is at fault as the inability of the generator to maintain synchronism with the rest of the system after a huge disturbance leads to network collapse. Through this, it can be said that the power system generation and transmission plays a major role in ensuring system stability and power system reliability and security.

Many cases of blackouts in the world have been documented and published as reported in (Andersson et al., 2005; Hain & Schweitzer, 1997; Union for the Coordination of Transmission of Electricity, 2003; Vournas et al., 2006; Wong et al., 2007). One of the most common phenomena observed during system blackouts is that the frequency instability of the system causes the generator in the system to trip. This will in turn cause a cascaded effect that affects the supply and demand in the system as the protection elements of the system operates based on threshold of system parameters such as frequency, voltage or current (Wong et al., 2007). These unguided tripping will result in unintentional islanding. The formation of uncontrolled islands during cascading failure is one of the main causes of blackout in power system. Figure 1.1 shows the System Average Interruption Duration Index (SAIDI) based on the data from 1992 until 2001 (Committee on Enhancing the Robustness and Resilience of Future Electrical Transmission and Distribution in the United States to Terrorist Attack, 2012).

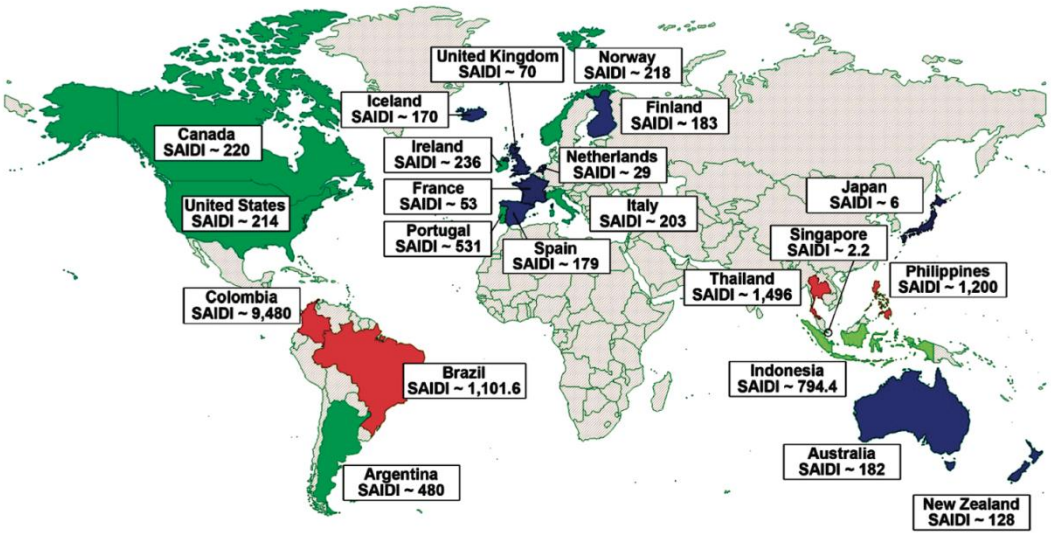

Figure 1.1: SAIDI based on a sample of countries

The figure which is taken based on a sample number of countries across the world indicates the measure of total power outage (number of minutes per year) experienced by an average customer. The trend highlights the fact that power outages are still being experienced by the customers despite major technological advancement in power systems.

Figure 1.2 shows the power outages due to extreme events during the first quarter of 2013(Klinger & Owen Landeg, 2014). Extreme events are events attributed to storms, winds, snow and other events due to estimate variation in weather pattern. Fifty two power outages were recorded across nineteen different countries. This evidently points to the presence of blackout in recent times.

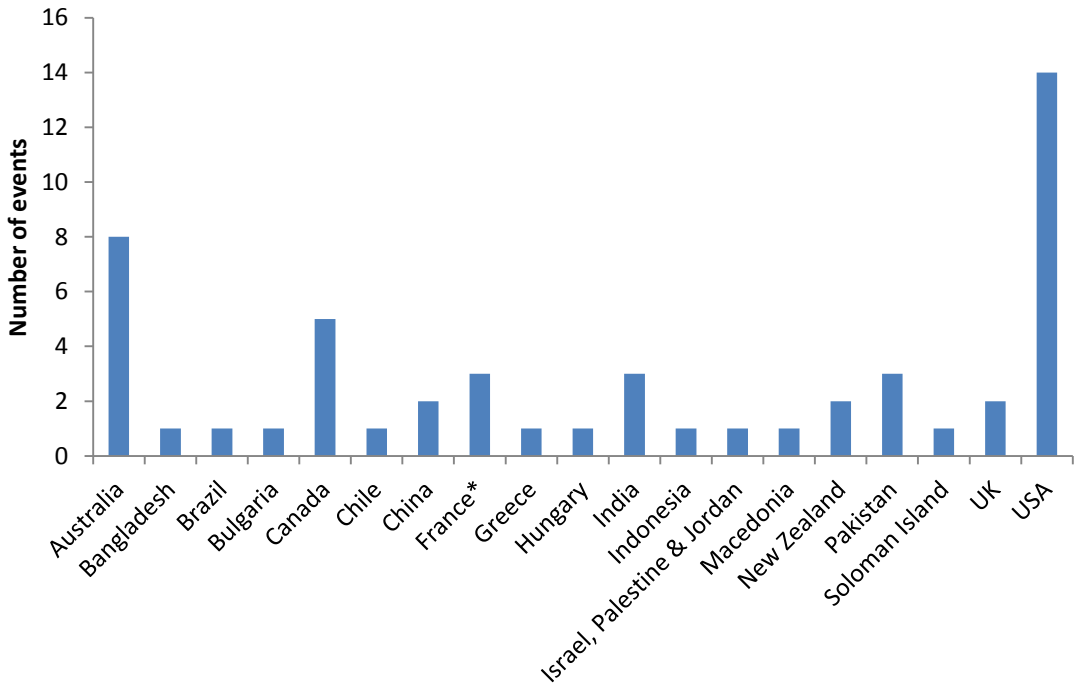

Figure 1.2: Reported cases of power outages during the first quarter of 2013

The best way to handle the blackout problem would be through intentional or planned islanding. The main premise of intentional islanding is to split the network into 'proper' islands. This is done to ensure that the islands continue providing power supply to meet the load demand. This means that by obtaining information on when the blackout is going to occur or observing the condition of the system in the extremis state, proper techniques have to be employed to split the power system network into different islands thus preserving the load generation capability which will ensure system stability. The weak area of the system will be partitioned off and reliable electrical supply to the customers can be guaranteed until the power system is fully restored. During the islanded operation, important system parameters such as voltage and frequency stability have to be carefully monitored in order to ensure proper operation of the islanded areas. In order to ensure successful post-islanding operation, the transient criteria of the system such as generator coherency and steady state criteria of the system such as

power balance and transmission line capability has to be considered (Najafi et al., 2010).

Intentional islanding or controlled islanding as it is commonly referred to has gained researchers attention throughout the years. Intentional islanding for transmission network is a potential approach in defense strategy of power system to prevent total power blackout. Early research work in identifying the best network splitting solution has been reported in (Zhao et al., 2003) up to the most recent research in this area as reported in (Ding et al., 2013). In the intentional islanding approach, network splitting is carried out to separate the network into two or several islands. Each island will operate as a standalone network with generation capability to meet the island's load demand. However, less research work has been undertaken to identify the optimum network splitting solution and at the same time addressing the post-islanding frequency stability.

1.2 Problem Statement

There are certain issues that have to be considered before intentional islanding can be carried out, such as:

a. Optimization program for network splitting algorithm
b. Load shedding and transmission line power flow analysis
c. Post-islanding frequency stability

The main issue involved in determining the optimum network splitting solution is the combinatorial explosion of search space. A large scale power system usually contains extensive number of lines and the process to scour each possible configuration is a huge task which requires enormous effort. Furthermore, since the problem is discrete in nature, the conventional optimization program will not be able to efficiently find a

feasible network splitting solution. Combined with further constraints such as generator coherency and desired number of islands to be formed, the task of obtaining feasible network splitting solutions which are optimal is extremely difficult. The transmission lines to be disconnected have to be carefully selected in order to ensure minimal power flow disruption to maintain preserve transient stability in the system. Improper disconnection of transmission lines in forming the islands could further cause the islanded areas to collapse due transient instability. The power imbalance in each island should also be taken into account as deficit in generation could also trigger system instability.

The post-islanding frequency stability is also a crucial aspect in the intentional islanding problem. This is due to the fact that once the system has been islanded into different areas, each island has to sufficiently cater the load demand as a standalone network. The stability of the island in terms of the power flow in the transmission line has to be maintained within the maximum allowable capacity of the existing lines. The load frequency control of the generators should also be optimally tuned to address the changes in the system in the event there is increase or decrease in load demand. Hence, an optimization algorithm to optimally spit the network has to be developed based on practical constraints in order to obtain the feasible network splitting solutions. The post-islanding frequency stability should also be ensured in order to ascertain a successful islanding operation.

1.3 Research Objectives

The aim of this research is to propose an optimal network splitting solution using a modified optimization program based on discrete values and to analyze the post-islanding frequency stability by implementing an adaptive load frequency control to

maintain the frequency of each islanded area to its nominal value. The following are the objectives that are needed to be achieved:

a. To propose an optimum network splitting solution based on minimal power flow disruption using modified Artificial Bee Colony (ABC) optimization technique and compared with modified Particle Swarm Optimization (PSO) technique.
b. To incorporate load shedding and transmission line power flow analysis in order to maintain post-islanding frequency stability
c. To determine the optimum Proportional-Integral-Derivative (PID) parameters for the Load Frequency Control (LFC) for split network using multi objective ABC optimization technique and compared with multi objective PSO technique based on weighted sum in order to ensure the frequency stability in the post-islanding phase is maintained.
d. To implement online wavelet filter to effectively filter out the high frequency noise in the LFC signal input

1.4 Methodology and Scope of Research

The main scope of this research is to find the optimal network spiting solution for the intentional islanding scenario and to analyze and evaluate the post-islanding frequency stability. It would like to be stressed here that intentional islanding is achieved via system splitting or network splitting. Often, these terms are used interchangeably. However, in line with the title of the investigation, the term network splitting is used hereon. In order to successfully carry out the proposed research, the following methodologies are carried out:

- Modeling of large scale power system based on graph theory
- Developing an intelligent algorithm to reduce the search space

- Modified optimization technique based on discrete values for network splitting will be implemented
- Load shedding scheme in order to maintain power balance criteria in each island will be carried out
- Optimal tuning of the load frequency control using multi objective ABC optimization based on weighted sum to ensure the successful operation of islanded areas will be realized
- Implementation of online wavelet filter to effectively filter out the high frequency noise while maintaining signal integrity at the same time
- Verification and validation of the proposed optimization process will be carried out using Matlab software

This research proposes a modified optimization technique for network splitting problem based on discrete values and subsequently ensure the post-islanding frequency stability. The graph theory is utilized as the core of the algorithm to identify and split the large scale power system accordingly. Modified Artificial Bee Colony (ABC) optimization based on discrete values and modified Particle Swarm Optimization (PSO) technique based on discrete values are implemented to find the optimal network splitting solution. The proposed optimization method takes into account all practical constraints in the system to obtain the feasible splitting solution. Load shedding scheme is also introduced to maintain power balance equilibrium. The multi objective ABC optimization technique and multi objective PSO technique is implemented to optimally tune the load frequency control (LFC) to ensure post-islanding frequency stability of the system. The online wavelet filter is then integrated to the LFC model to effectively filter out the noise in the input signal to the controller.

The large scale power system based on the standard IEEE 30-bus, 39-bus and 118-bus test systems are modeled in Matlab software. The modified optimization technique is also developed and tested in Matlab software. The load frequency control model is designed and tested using Matlab's Simulink software.

The scope and limitation of this research are as follows:

- The main focus of this research is to present an optimum solution for the network splitting problem. This is particularly useful for network planning engineers and future researchers to benchmark their result. As such, the time constraint in finding the solution is neglected in this investigation. This also enables Newton Raphson load flow method to be used instead of DC load flow.
- The test cases currently considered are standard IEEE test cases and the desired islands are set to a maximum number of four based on current research carried out.
- The coherent group of generators and the resultant number of desired islands are obtained from published results and investigations.
- The automatic generation control (AGC) model of the multiple generator single area interconnected reheat thermal system is based on the model developed by (Rerkpreedapong et al., 2003). The designed model is a Laplace equivalent model of the power system.
- Since the reactive power in the system can be compensated locally, only the active power is considered in the system. In regards to that, only the active power is considered in this investigation.

1.5 Thesis Outline

This thesis consists of six chapters and one appendix, which are organized in the following order:

Chapter 1: Introduction

This chapter presents an overview of the complete thesis by presenting a general introduction on the effect of blackout on the power system network. The importance of optimum network splitting algorithm is briefly discussed and the need for maintaining post-islanding frequency stability is also explained. The research objectives and the methodology employed are presented followed by the outline of the thesis.

Chapter 2: An overview of Network Splitting, Graph Theory and Load Frequency Control (LFC)

This chapter starts of by presenting a general overview of power system and the main causes of cascading failure in power system. The general outlook of power system security is then shown and the failures in the system that can lead to blackout in the power system are then highlighted. Several case studies on the blackout are presented and various blackout mitigation techniques are shown. The network splitting technique and the various algorithms used to successfully split the network is further discussed. Graph theory and the application of graph theory in power system network splitting are also presented here. The final part of these chapter discuses in great detail on the load frequency control (LFC) implementation. This chapter ends off by presenting a summary of the literatures and the techniques chosen to be implemented to develop the proposed methodology in line with the objectives of the research.

Chapter 3: Proposed Optimum Network Splitting Algorithm and Load Frequency Control Optimization

This chapter deals with two major aspects of the investigation which are the proposed optimum network splitting algorithm and load frequency control optimization. The proposed optimum network splitting algorithm is divided and explained in three subsequent tasks. The first task details on how the graph theory is utilized to model the large scale power system based on the IEEE test system. The second task presents the proposed edge reduction algorithm which is developed to produce the initial number of transmission lines to be disconnected. The third task presents the modified ABC optimization technique based on discrete values which shows how the optimum network splitting solution is found. The power balance criteria and transmission line power flow analysis is also described in this section. The second aspect of the investigation which is the load frequency control (LFC) optimization to ensure post-islanding frequency stability is described in detail. The ABC optimization used for the controller optimization technique is discussed and the self-tuning algorithm used by the PID controller is also shown.

Chapter 4: Validation of Proposed Optimum Network Splitting Algorithm

Three different IEEE test systems – IEEE 30-bus, IEEE 39-bus and IEEE 118-bus tests system are modeled using graph theory. Initially the edge reduction algorithm is applied and the selected edges to be disconnected are shown. Subsequently, the optimum network splitting algorithm is applied to obtain the optimum line configuration of the system based on the given system constraints. The solution obtained is compared with published results and alternative discrete optimization algorithm to validate the proposed technique.

Chapter 5: Validation of Proposed Load Frequency Control Optimization

This chapter will present LFC optimization technique. The LFC model of each test case – IEEE 30-bus, IEEE 39-bus and IEEE 118-bus tests system is designed in Simulink. The LFC is optimally tuned using multi objective ABC optimization technique based on weighted sum. The ABC optimization technique is compared with PSO technique to highlight the performance of the proposed technique. The load variation tests are carried out to observe and analyze the performance of each islanded areas as a standalone network. The system performance in terms of settling time and maximum overshoot is observed to determine the performance of the optimization technique. The online wavelet filter is implemented to effectively filter out the high frequency noise while maintaining the signal integrity.

Chapter 6: Conclusion and Future Work

The final chapter in the thesis summarizes the research conclusion and the contribution made in this research project. This chapter closes with recommendation for future work that can be carried out based on this research project.

CHAPTER 2: AN OVERVIEW OF NETWORK SPLITTING, GRAPH THEORY AND LOAD FREQUENCY CONTROL

2.1 Power System Overview

Power system security and reliability is a paramount necessity in ensuring continuous power supply to the customer. In order to ensure that continuous power is delivered to the customers, many measures have been undertaken by the electrical utility board at each and every level of the power network. The three main levels of power system are power system generation, transmission and distribution. Detail planning of the system such as forecasting load demand right up to the protection of main elements in the system has been carried out by the power system operators to ensure minimum interruption. Despite such preventive measures being taken, failures in power system network still do occur.

Failures in power system can occur in any level and there are measures to overcome different type of faults. Faults such as single line to ground fault, double line to ground fault, fault due to lighting and or false relay tripping could occur at any time. Equipment such as circuit breakers, relays and other protection equipment are used to mitigate these faults. Due to the size of the power system which comprises of thousands of different equipment, the malfunction of single equipment is not uncommon. The failure of one of the equipment can further aggravate the instability of the whole network and is known as cascading failure.

Cascading failure can be defined as failure in a part of the network which can trigger failures in successive part of the network. This will lead to a catastrophic event known as blackout. Blackouts which are power outages in the network are detrimental towards

the stability of power system network as blackouts can result in partial or total collapse of the power grid. Among the main causes of faults that could lead to cascading failure are frequency collapse, thermal overload, transient instability, voltage instability and hidden failures (Kirschen, 2002).

2.2 Power System Security

Power system security is an important term which is synonymous to providing reliable power supply in power system. Security in a broader term reflects the ability of the system, to a certain degree to provide reliable and continuous power supply to the customer during imminent disturbances (contingencies). The term power system security and power system stability are often used to denote the reliability of the power supply. However, upon further scrutiny, it can be observed that the power system security, which is the wider term, encompasses power system stability as one of its sub-terms. When a power system is subjected to inadequate level of security, very often than not, the power grid will suffer a catastrophic failure. This catastrophic failure, known as blackout could cause economic loss and even in extreme cases, injuries and loss of life (Morison et al., 2004).

The power system should be able to meet the specified security criteria in both the transient and steady state. Failure to do so in any one of the state would deem the system incapable of providing a reliable supply of power to the consumers. The system should be able to provide power supply within the boundaries specified in the operating constraints during pre and post fault operations. Among the main aspects of security assessments are:

a) Frequency – Underfrequency
b) Voltage – Overvoltage and Undervoltage

c) Thermal Loading – Thermal Overload

In order to further characterize and classify the overall operating condition of system, the power system operating states have been developed by (Dy Liacco, 1967). The operating states that has been defined embodies the whole structure and the operating state of the of the power system. The operating state of the system has to be identified in order for the control action to take the necessary measures to ensure the reliable operation of the power system.

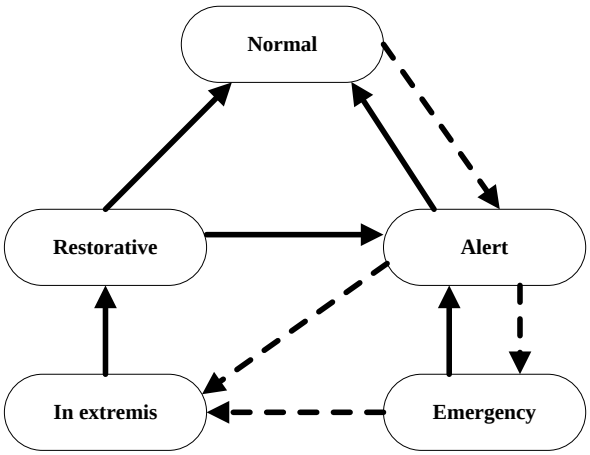

Figure 2.1: Operating States of Power System (Morison et al., 2004)

Figure 2.1 shows the five important operating states of the power system. The dashed arrows represent the contingencies resulting from unavoidable circumstances or events that are unplanned. The solid arrows in the diagram represent the control action that needs to be taken to return to normal operating state of the system. One of the main control objectives is to ensure that the power system is operating in the normal stage and in any event there is any disturbance, the power supply outage duration should be kept to the bare minimum. The operating states are:

1. *Normal state:* All system parameters are within operating conditions specified by power system operator to provide continuous power supply to customers. Any

plausible contingencies within the technical constraints can be handled properly to ensure normal operation.

2. *Alert state:* Due to contingency measures, parameters or technical constraints of the system is violated. However, power is still being continued to be served to the customers. Preventive and restorative action has to be undertaken to return the system back to normal state. Failure to do so might cause system to be subjected to further instability which could lead to the emergency state or in worst case scenario, *in extremis* state.
3. *Emergency state:* In the event of severe contingencies in the alert state, the emergency state will be the resultant outcome. Thus, failure to carry out proper preventive or restorative action in the alert state might result the system deteriorating even further. System is still intact and power is still being continued to be served. Active corrective and control actions have to be undertaken to return the system to alert state and subsequently to normal state. Emergency control action such as generator tripping and fault clearing need to be done to prevent the system from going to *in extremis* state.
4. *In extremis state:* The worst case scenario in power system as the system is no longer intact. Major portion of the network will experience the absence of power supply and the system will either be in partial or complete blackout. In this state, any possible control action should be taken to minimize the damage as cascading failure can further cause widespread damage.
5. *Restorative state:* In order to ensure that system is restored back to normal operating conditions, the restorative action is taken by applying appropriate control actions such as restoring parts of areas in which the power plants have black start capability. If the damage done by blackout is extensive, the system will be returned to the alert state before restoring it back to normal state.

2.3 Failures in Power System

Reduction in predictability of the power system operation has given rise to many possible factors that could influence the normal operation of the power system. These factors could also be a possible cause to many disturbances in the system. These disturbances could be minor interruptions lasting for short period of time to huge disturbances that could eventually lead to blackout in the system. Predictability of power system is a very important aspect. This will ensure that the designed system will be able to mitigate any abnormal conditions that may arise from the system based on existing knowledge. As an example, power system operators often forecast the load demand of the system a day earlier to be able to dispatch generation units accordingly.

However, there are some factors that could influence the operation predictability of the power system (Morison et al., 2004). A failure in any one of these components could propagate and further result in cascading failure that could potentially lead to total system blackout. Among the factors that are related to the transmission and generation stability are:

1. *Lack of new transmission facilities:* The transmission lines are overloaded based on their initial capacity or rating in which the lines were designed. Thus, due to protection equipment operation, the lines might be overloaded whenever fault clearing is carried out. This could be attributed to the unplanned increase of load demand over period of time.
2. *Increased dependence on controls and special protection systems:* Incorrect control operations might lead to further issues as protection equipment's malfunction could sever connection of unfaulted lines. Thus, the control and special protection system has to operate without any errors.

3. *Increased dependence on communications and computer systems:* Software failures might result in erroneous control action. This has to be eliminated as the control actions that are initiated by software based on intelligent algorithms has to be robust in identifying faults and adapt to the dynamics of the network.
4. *Trend towards interconnection:* Since the development of power system has integrated many different geographical areas, the interconnection between different areas of the system has grown significantly. As such, dynamic properties of the system such as generator coherency and small signal stability, plays a major role in determining the characteristics of the system.

The blackout event is often caused by a single generation or transmission element. Different factor as described above can cause the system to experience multiple failures and lead to total disarray. This can however be prevented if corrective actions are taken when these faults are detected earlier in the system. However disturbances, especially during the peak load condition can be quite detrimental as any amount of corrective action might not be able to save the system from entering the emergency state. The flowchart in Figure 2.2 provides a clearer description on the process leading to blackout (Pourbeik et al., 2006).

The power system initially operates under normal operating conditions. In this state, there is no major disturbance in the system as the power system provides reliable and secure supply to meet the load demand. When a disturbance or any event that could cause fault in the system is initiated, the system operator is made aware of this condition. This is made possible by monitoring the changes in important system parameters such as voltage, frequency, current and power values.

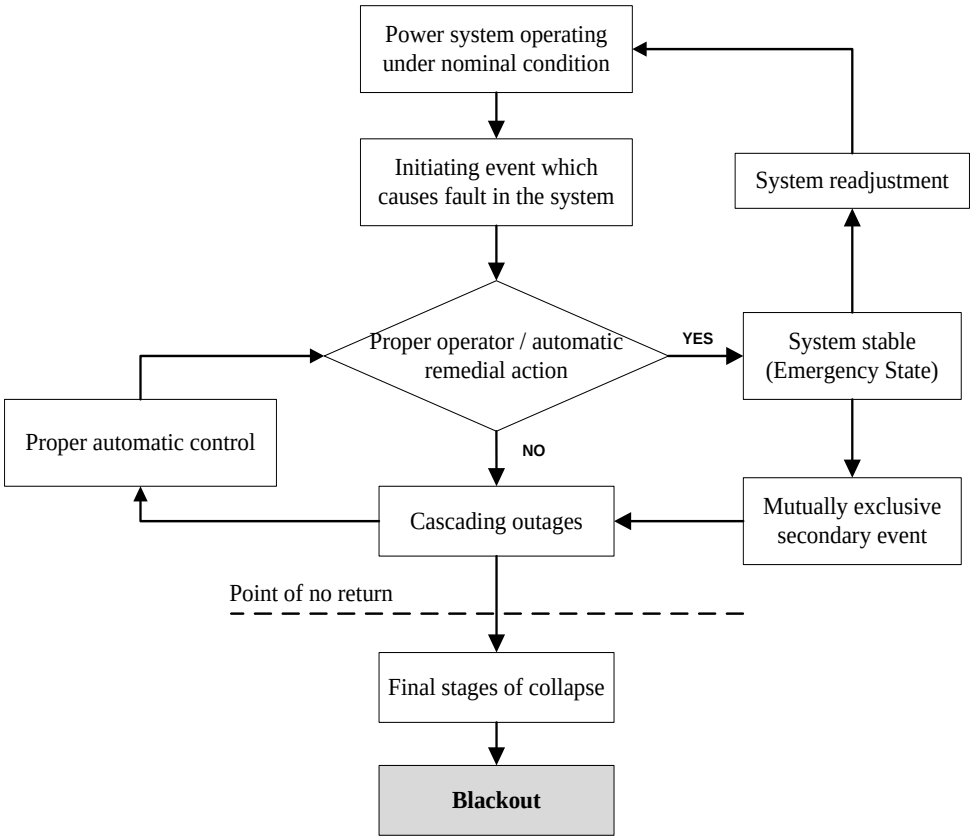

Figure 2.2: General process of events leading to total system blackout

Manual or automatic action is then initiated to recover the system from the faulted condition. If the corrective or remedial action is successful, the system is back to its stable state. However, the system is still considered to be in an emergency state as a certain amount of time is required to recover the system to its pre-fault condition. If the system is proven to be stable, readjustment is carried out and the system returns back to its normal operating condition.

If the remedial action is unsuccessful, then the system will start to experience cascading failure. Multitude of equipment starts to fail or maloperate. This will further cause other parts of the system which was initially operating in normal condition to be affected. This could also occur during the stable state when the system is observed for a period of time before readjustment is carried out. At this state, if a major secondary event occurs, then the system would also experience cascading failure. At this stage,

extreme remedial action is required such as under frequency load shedding or under voltage load shedding. This is of critical importance to return the control of the system back to the operator.

If the corrective action in the cascading outage stage is unsuccessful, then the system enters to point of no return in which the system will experience the final stages of total system collapse. The system might split into uncontrollable islands. When this happens, the islands might experience a large mismatch between generation and load demand. At this point, no amount of measures could be undertaken to save the system as the system will eventually end in total system blackout.

2.4 Blackout

Blackout is the worst case scenario in power system. A blackout can cause either partial or total collapse of the system. Blackouts can last for short period or a long period of time. As discussed by (Rosas-Casals & Solé, 2011), the failure of the transmission system due to cascading failure could also be considered as a blackout. There are many reported cases of blackout and the subsequent impact to the affected customers. From these cases, we will be able to observe and analyze the cause and effect of the events that lead to the blackout.

1. *Israel (Hain & Schweitzer, 1997):* The Israeli Electric Corporation has an electrical network which consists of 400 kV, 161 kV, and 110 kV circuits. The generation capacity of the system is 6388 MW (Union for the Coordination of Transmission of Electricity, 2003) and the recorded peak load is 5538 MW. During the event that leads to blackout, double circuit tripping occurred on the 161 kV line. The 161 kV line connects the northern and southern part of the system. The remaining interconnecting line was also tripped due to power oscillations. This has caused the

system to be split into two islands – "northern" and "southern" island. The load-generation equilibrium in "southern" island was not met as the demand exceeded the available supply in the island by 900 MW. This caused the frequency in the island to decreases rapidly and ultimately the generating units in the area were tripped off leading to blackout in the southern part of the system.

2. *United States and Canada (Andersson et al., 2005):* The U.S / Canadian blackout was a severe case of blackout as 50 million people were affected. The total load demand of the system was approximately 630 GW. Due to generator fault, the active power generation was severely limited. Cascading failure due to transmission line overload and inadequate load shedding further aggravated the instability of the system. The generators in the system were not able to meet the load-generation equilibrium, thus tripping off the remaining generating units. Finally, due to loss of major tie lines, the power flow in the system was affected as reverse power flow was recorded. The remaining transmission lines were heavily loaded and the cascading failures lead to the devastating blackout in the system.

3. *Athens (Vournas et al., 2006):* The blackout that occurred in southern Greece affected approximately 5 million people. The network in Greece consists of 400 kV and 150 kV transmission lines. The recorded peak load was 9500 MW. The reason for voltage instability in the system is due to the distance between generating units and load which are far apart. Due to heavy demand during summer, in which the usage of air conditioning units increases, one of the generating units was tripped off and failure in load shedding occurred when another generating unit was tripped off at the same time. Due to reduction in power supply and no proper load shedding initiated, the load-generation equilibrium was not met and the voltage collapse in the

system was experienced. This caused the system to split unintentionally into two islands – north and south. The northern part of the system had surplus of generation and the over frequency relays were able to operate and bring back the system to stable operation. The southern part of the island experienced further issues as the voltage stability was compromised leading to undervoltage relays tripping off the generating units. This eventually led to blackout.

4. *Italy (Union for the Coordination of Transmission of Electricity, 2003):* The power system in Italy involves four other different countries (Austria, France, Slovenia and Switzerland) which are interconnected. The northern part of comprises tie lines connected to neighboring country (Switzerland) rated at 220 kV and 380 kV. A flashover occurred on the 380 kV line causing the line to be disconnected. The other lines in the system were then tasked to take over the load to resume normal operation. However, due to the overloading conditions of other lines, the line overload was only acceptable for a short period of time. Due to overheating, the resultant voltage sag caused the tripping of the remaining interconnecting line (380 kV). Losing both important tie lines (380 kV), the overload condition on the remaining lines which were rated lower made the scenario become even worse. The high overload conditions attributed to voltage instability in the area causing several generating units to trip. Load shedding was further initiated to save part of the network, however due to absence of adequate power supply, the Italian power network faced total blackout.

5. *Taiwan (Wong et al., 2007):* The Taiwan Power Company is the power system operator in Taiwan which is responsible for power system operation throughout the island. The Taiwan power system comprises of 69 kV, 161 kV and 345 kV

transmission lines. The generation capacity of the system is 28,480 MW and the recorded peak load is 24,206 MW. A ground fault occurred due to tower collapse which was carrying the 345 kV line. This further caused successive relay tripping in the system and the network was split into two areas comprising “north” and “south” of Taiwan. The generation-load balance in the northern area experienced a deficit in power supply as the surplus power generated in the southern area could not be transferred. The southern part on the network had surplus generation which led to overfrequency in the area. Due to this, the frequency in the northern area start to collapse and generating units in the area were tripped off. Several generating units in the northern area had to be tripped off to maintain the generation-load equilibrium and to ensure the proper operation of the island.

6. *Malaysia (P Kundur et al., 2007; Smith, 2003):* Malaysia has its fair share of major power blackouts thorough its history. On 29 September 1992, a total power blackout occurred due to lighting strike on the transmission facility. This caused a cascaded effect in the transmission and distribution system. On the 3rd of August 1996, peninsular Malaysia experienced a 16-hour blackout due to transmission problem. This massive power failure was due to the tripping of a transmission line near one of the power stations which caused a cascaded effect which shut down all the other power stations in a sequential manner. Another total system blackout was experienced on 18th November 1998, where the distance protection relay was not able to clear the fault on transmission line which occurred due to flashover. This caused the 275 kV lines connecting the North/East to the Central/South system to trip and further separating the system into two islands. In January 2005, another blackout case was reported which caused the power outage on the northern states of the country (Perak, Penang, Kedah, and Perlis). The opening of a breaker to clear

fault in the system inadvertently cause the adjacent breaker to open and split the main substation into northern and southern section. Different blackout cases has also been reported in 2013 (New Straits Times, 2015).

The six major blackout cases highlight the severity of the event. The customers are hugely affected by this catastrophic event. The bar chart in Figure 2.3 shows the power disturbance in North America. It can be seen that the number of power outages in the American grid has increased. This paints a very gloomy outlook as power outages are becoming a norm to be associated with the power system operation.

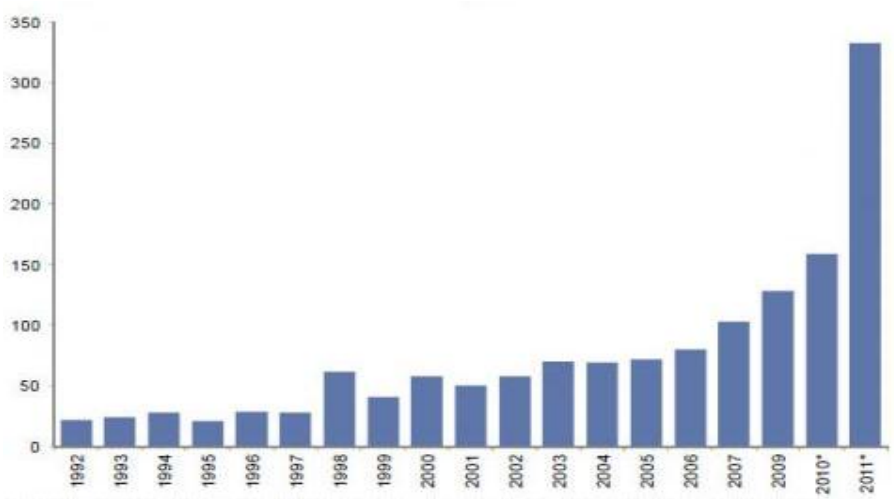

Figure 2.3: Major power disturbances in North America (NERC, Eaton Blackout Tracker, Goldman Sachs Research estimates)

2.4.1 Blackout Summary

Observing the sample cases of the different blackout events that occurred, the following points can be concluded:

1. When the power system is subjected to cascading failure, the system is unintentionally split into different islands. The islands are split without any criteria

to ensure stability of the island as the point of tripping is based upon the location of the interconnecting transmission line between areas.

2. The system plunges into instability as the load-generation balance or equilibrium is not met. This is one of the main reasons why unintentionally split island lead to blackout.
3. Load frequency control are often overlooked in preserving the frequency stability of the system as the controller should be able to bring the system's frequency back to steady state or nominal value as fast as possible without much oscillation in the system.
4. The voltage stability of the system is often compromised when transmission line connection are severed. This could be seen in cases where the voltage collapse in the system becomes the contributing factor towards the blackout. Priority of line tripping should be a major consideration to ensure transient stability in the islanded areas.
5. Adaptive load shedding should be applied at the very instant when cascading failure is detected as time is of crucial importance. Any delay in load shedding application will be an inadequate measure to save the system.

2.4.2 Blackout Mitigation

In order to reduce the risk or the possibility of cascading failures, certain approaches or techniques have been implemented. These methods or techniques are based upon system response and system characteristics during blackout event. Reviewing cases of existing system blackouts, contingencies or preventive measures were analyzed to reduce the cascading outage and thus minimizing the risk of total system blackout.

1. *Adaptive load shedding method:* As seen in the blackout cases presented in Section 2.4, the need for adaptive load shedding is apparent as this measure is considered and emergency control action designed to maintain the generation-load balance. The generation-load balance is crucial for the normal operation of power system. Load shedding schemes are categorized as either centralized or decentralized schemes. Centralized load shedding schemes rely on overall information of the system whereas the decentralized load shedding scheme are based upon local area's information. The decentralized load shedding information is more robust as the decision making process is independent and takes into account only the local area's parameter to ensure local or decentralized stability. As stated by (Zin et al., 2004), most of the decentralized load shedding schemes which are based upon under frequency load shedding, sheds a particular amount of load when a frequency drop is detected. Other load shedding techniques are based upon under voltage load shedding schemes. These types of load shedding techniques are oblivious to other aspects of power system operation.

   As proposed by (Ford et al., 2009), the decentralized load shedding scheme should not only be able to provide protection when the frequency drops but the load shedding should also protect the system from line overloading. The local information obtained from the areas will further enable the scheme to adapt to size and behavior of the disturbance. Without protection on line overloading, the load shedding alone will not be enough to prevent cascading failures as seen from the blackout cases. (Dola & Chowdhury, 2006) has also highlighted the importance of an automated load shedding process to prevent cascading outages which lead to total system blackout. The load shedding technique together with a defensive mechanism could further provide a secure power system operation.

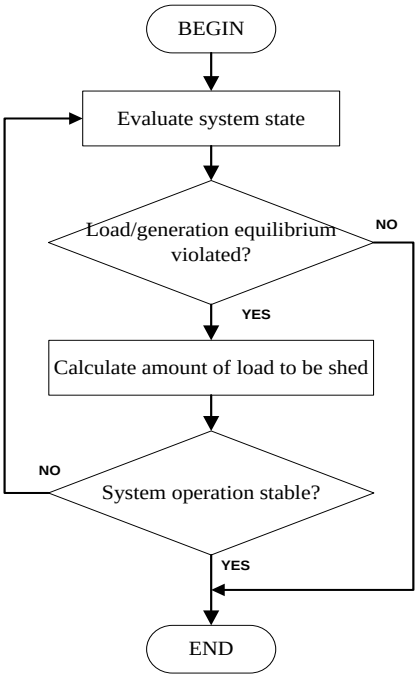

Figure 2.4: Flowchart of load shedding process

The flowchart in Figure 2.4 shows the general overview of the adaptive load shedding procedure employed to mitigate cascading failure. The system is monitored and the system state is evaluated to determine the load generation equilibrium. In the event the equilibrium is violated, the df/dt (changes in frequency over changes in time) is calculated and the amount of load to be shed is determined. The system is further probed to check if it is stable. If it is not stable, the load shedding process is carried out again. If the system is able to maintain the load generation equilibrium after load shedding, then the system is deemed stable.

2. *Line overloading - Voltage stability:* The overloading of transmission line or tripping of generating units could lead to voltage instability in the system. An index such as voltage stability margin (VSM) should be developed to ensure system stability. (Fu & Wang, 2011) has approached the problem by subdividing the task into two sub problems. This is done to ensure that the decomposed system has power flow solvability. During system instability, the power flow solution is

unsolvable. Due to this, the correct operating points of the system will not be obtained thus leading to system collapse. The proposed method can be seen in the flowchart shown in Figure 2.5.

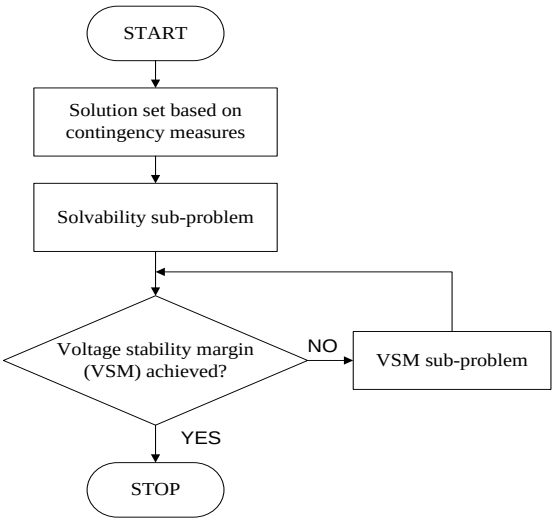

Figure 2.5: Proposed algorithm flowchart

It can be seen from the flowchart that the solution is checked for voltage stability margin every time the network is decomposed into sub problems for solvability. The obtained solution is checked for voltage stability margin and if the criterion is fulfilled, the algorithm is stopped. In this way, the power flow solution of the system can be obtained and the voltage stability margin can be ensured.

3. *Preventive control:* Preventive control as the term suggests is a method which prevents the system from going into catastrophic failure by preparing the system in the normal state. This will ensure the system to respond to any uncertain events that may occur in a predefined manner to avoid unexpected operation of the system which lead to system failure. In this proposed approach by (Maharana & Swarup, 2010), the graph theory approach is used to reschedule generators. The Direct Acyclic Graph (DAG) is used to detect the power flow in the system so that the generating units in the area can be rescheduled to accommodate load demand. This

will ensure load-generation equilibrium in the system as the alternative generators selected have to ensure adequate power supply is met to serve the load. This technique will assist the power system operator prevent tripping of generating units in the early stages of the cascading event. The graph theory property of detecting paths in a network is utilized to determine the reach of a generator (ROG) to identify the buses which can be reached by the generating units to provide power. However in this approach, the optimality of the generating units due to rescheduling is ignored as the utmost importance is to prevent cascading failure in the system.

(Makarov et al., 2005) has further highlighted the importance of preventive control as part of the defense mechanism of the power system to avoid total system blackout. Figure 2.6 shows the typical scenario in cascading failure which ultimately leads to blackout as analyzed by (Hardiman et al., 2004).

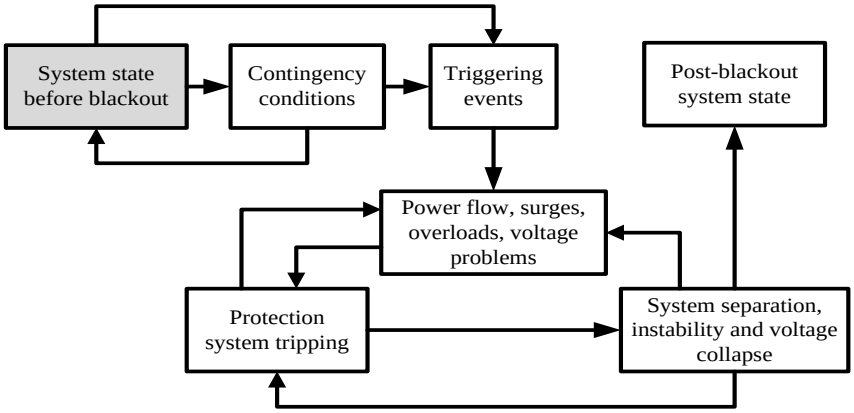

Figure 2.6: Typical scenario of cascading failure

In the cases analyzes, it was found that the 'triggering events' represent a cumulative state of multiple factors that indirectly lead to power outage in the system. In view of this, three line of defense was implemented by Russia's United Power System (UPS) to prevent the system from entering the point of no return. The multiple lines of defense cover different features of the power system i.e. from the

Wide Area monitoring of the network down to the technical aspects such as overfrequency and overvoltage protection. The extensive framework of the defense mechanism dispatches different aspects of power system operation as dedicated tasks. The approach taken clearly signifies the need for a thorough and extensive preventive control to avoid the blackout in power system. This importance of detecting and preventing the failure before it cascades or accumulates is also highlighted by (Phadke & Thorp, 1996). Hidden failures which are defined as permanent defect in the system which causes maloperation of protection devices has to be monitored and eliminated to minimize the risk of cascading failures.

4. *Intentional Islanding:* Intentional islanding which is also known as network splitting is used to split the network to two or more islands depending on the power system operating criteria. In the earlier cases of blackout, unplanned splitting often occurs and one of the islanded areas will face a deficit in power supply while the other area will have a surplus of generation. Through controlled islanding and proper load shedding, this could be prevented. The resultant islands will remain theoretically in balance and continuous power supply can be delivered to customers with minimal disruption. (Sun et al., 2003; Zhao et al., 2003) has applied binary decision technique to split the system into desired number of islands as shown in Figure 2.7.

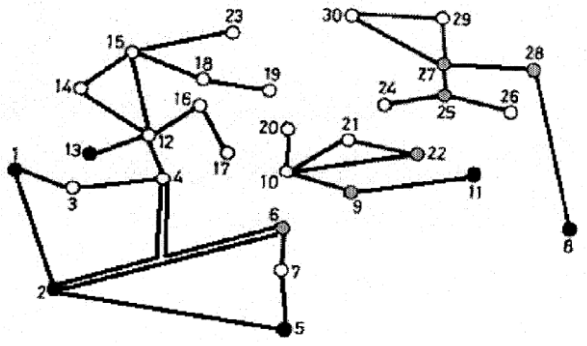

Figure 2.7: Splitting strategy for IEEE 30- bus system (Zhao et al., 2003)

Figure 2.7 shows the splitting strategy implemented for the IEEE 30-bus system. Using the binary decision technique, the system is split into three different islands. The splitting strategy is considered successful when the resultant islands are feasible island solutions. The feasible network splitting solution has to adhere to the following system constraints:

a) Separation and Synchronization Constraint (SSC): The islanded areas in the system should contain group of generators which are coherent to each other. Asynchronous group of generators have to be separated based on their coherency.
b) Power balance constraint (PBC): The power balance constraint which is basically the load-generation balance should be met to ensure that islanded areas are stable and no further frequency drop occurs after islanding.
c) Rated value and limit constraints (RLC): The transmission line thermal limit and transmission capacity should not be exceeded in order to ensure steady state stability of the system.

Similar work has also been reported in different literatures (L. Liu et al., 2009; Senroy et al., 2006; Yang et al., 2006; You et al., 2004). Majority of the work uses similar variation of the system constraints shown above to island the power system. The islanding solution will then determine the transmission lines to be disconnected based on a predefined fitness or objective function. Figure 2.8 shows a typical islanding solution based on investigation published by (L. Liu et al., 2009).

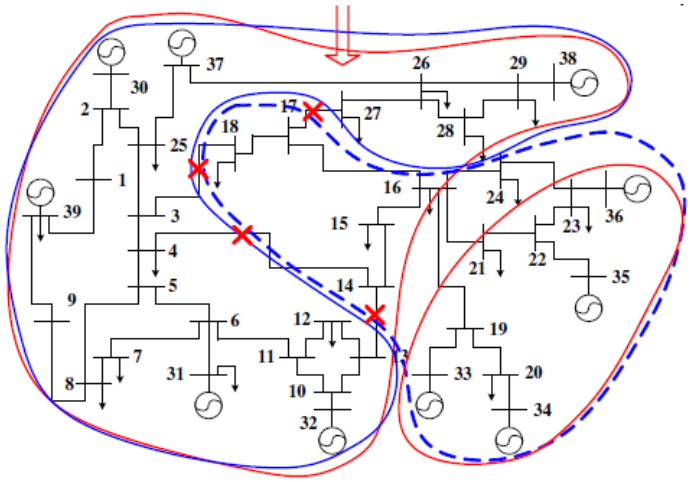

Figure 2.8: Intentional islanding of the IEEE test system

In order to implement intentional islanding, (Aghamohammadi & Shahmohammadi, 2012) has outlined the three main tasks involved in successful execution of intentional islanding. These tasks have to be carried out in a sequential order.

1. *Task 1 - Identification of cascading outage:* The initial task in the process is to identify the operating instant when the cascading outage is unavoidable. This task is synonymous to identifying when the system is going to face unplanned splitting that could lead to uncontrollable islands.
2. *Task 2 - System splitting strategy:* Once task of identifying the instant of uncontrolled islanding is carried out, the system splitting strategy can be employed to split the network into predetermined number of islands. The system constraints such as load-generation balance and system stability has to be preserved.
3. *Task 3 - Post-islanding stability and operation:* Once the system has been split and the islands have been formed, the post island stability and operation has to be monitored so that the islands are able to operate as normal system without any further problems. The frequency and voltage stability of the islands are of paramount importance.

2.4.3 Blackout mitigation summary

Analyzing all the available methods to mitigate the blackout phenomenon, the intentional islanding method is a robust method comprising all the important aspects in ensuring system stability during and after islanding. In this technique, the network is split into controllable islands. Furthermore, load shedding can be applied and stability criteria of the islands can be determined by incorporating the intentional islanding method with the above mentioned system constraints. This will further enhance intentional islanding technique as an important defense mechanism in the power system. Practically, intentional islanding has been carried out by Western System Coordinating Councils (WSCC) in the western region of USA. Similarly an intentional islanding system has also been installed in Brazil, South America. The controlled opening of the interconnections has proven to minimize the impact of disturbance (P Kundur et al., 2007).

2.5 Network Splitting Techniques

In order to implement network splitting in large scale power system network, there are many techniques or methods that can be used. These methods are based upon the premise of network splitting by considering stability criteria of the power system network. Different objective functions are considered by each technique. The framework of the technique also differs based on the system methodology. Among the algorithms used for network splitting are listed as per the following.

2.5.1 Binary Decision Diagram (BDD)

The binary decision diagram (BDD) enables standard Boolean operations to be performed on functions (Brace et al., 1991). It is considered as mathematical

expressions used to represent the Boolean functions. This has been particularly useful in solving large class of complex problems. However in combinational problem such as in the large scale power system, further manipulation of the BDD is required by imposing restrictions on it to produce a compact representation of the problem in hand (Bryant, 1992). As such the ordered binary decision diagram (OBDD) is formulated as a canonical form to solve the problem.

OBDD has been used to determine network splitting strategies in power system. (Zhao et al., 2003) has used a two phase method to implement the splitting strategy. The first phase is used to check for the load-generation balance while the second phase is used to check for transmission line constraints. This is done using conventional power flow analysis. The solution of the splitting problem is obtained after the execution of phase 2. The advantage of OBDD is the search space reduction as the network splitting problem poses combinatorial explosion of the search space. In the investigation carried out by (Jin et al., 2007), the OBDD was used to determine the splitting strategy. Subsequently the unified stability control framework was implemented to find the best splitting point with respect to different emergency control measures. (Sun et al., 2003) on the other hand used a three phase method with OBDD to solve the splitting problem. The difference is that, to further reduce the search space, graph theory is used in phase 1 to decompose the network to reduce the search space as shown in Figure 2.9.

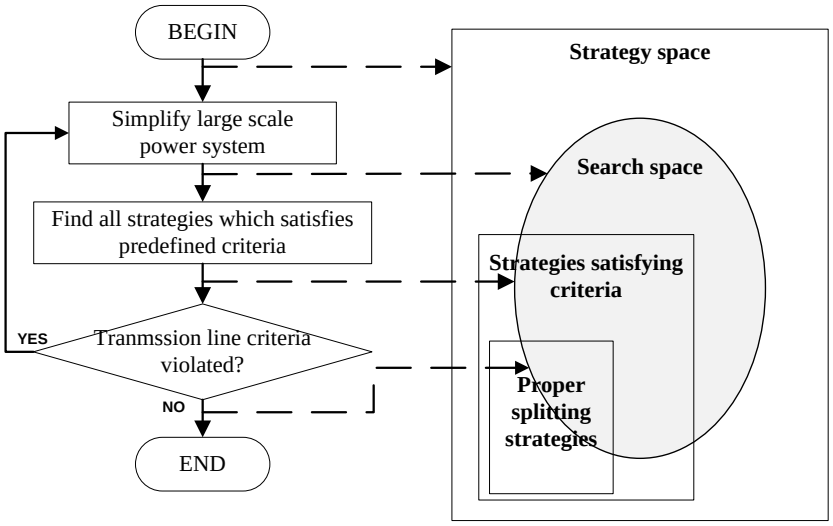

Figure 2.9: Flowchart of search space reduction process

This phase will initially reduce the complex large scale power system into a smaller network. The overall possible combination is identified as the strategy space. This space is reduced to a more manageable search space by using rules and heuristic knowledge. The search space is reduced again by obtaining solutions which satisfies the PBC and SSC criteria. This space is further reduced in the final step when the RLC criterion is checked. Phase 2 and phase 3 are similar to the two phase implementation carried out by (Zhao et al., 2003). The effectiveness of graph theory in decomposing the large scale power system is obvious as the number of edges to be disconnected is reduced to a feasible search space.

2.5.2 Clustering technique

Subsequent recent research in this area and the BDD algorithm has been further improved by using clustering technique. The l clustering method is based upon the graph theory approach in which the graph of the power system comprising vertices and edges are initially built. The eigenvalues are then computed to partition the graph as shown in Figure 2.10 (Peiravi & Ildarabadi, 2009).

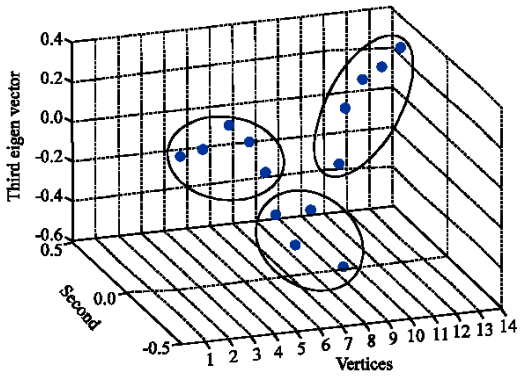

Figure 2.10: Graph partitioning based on eigenvectors with respect to vertices.

The figure shows how the 14 bus power system which is modeled by graph theory is portioned into three groups using the Multilevel Kernel k-Means approach. The approach is then further improved by implementing a weighted Multilevel Kernel k-Means to improve the performance of the clustering technique (Peiravi & Ildarabadi, 2009). (Ding et al., 2013) has proposed the possibility of implementing the controlled spectral clustering technique for the network splitting problem. A two-step controlled clustering is implemented in which the first step consists of grouping the coherent group of generators and in the second step, the islanding solution meeting all the prescribed constraints are verified. The graph theory is applied to the problem in the preliminary stages to convert the optimization problem into a graph-cut problem. The graph-cut problem is then solved using the spectral clustering method to split the system into desired number of islands.

2.5.3 Two time-scale theory

The two time-scale theory which decomposes the time based on their speed is used by researchers in the power system area. The slow coherency approach which exploits the two time-scale theory evaluates the generators response by subjecting the system to disturbances (Chow et al., 1995). In the slow coherency approach, the generator coherency is developed based on the fact that they are not dependent on the disturbance

size (L. Liu et al., 2009). The mathematical model developed for the generator coherency is a linearized model and details of generators are often ignored in formulating the generator model. The details which are excluded do not influence the network or power system characteristic in a radical manner. (Tortós & Terzija, 2012) have further manipulated the slow coherency theorem to propose a methodology to split the system based on the strength of the area. The "weak" areas are defined as areas from which comprise of transmission lines which are most likely to split in the event of large disturbance. By identifying the weak links, the splitting strategy disconnects the links which has minimum power exchange. (You et al., 2004) has proposed the use of slow coherency in determining the splitting problem of the power system. The coherency indices are initially computed to determine the grouping of the generators using the formula shown in Equation 2.1.

$$d_{ij} = \frac{W_i {W_j}^T}{\|W_i\| \|W_j\|} \tag{2.1}$$

where W_i and W_j are obtained from the eigenvector transfer matrix which corresponds to the rotor angle of the i^{th} and j^{th} generators.

Subsequently, the power system operating constraints are imposed and the feasible islands are found. The assumption that the disturbance occurrence in the system does not influence the islanding solution is verified by applying the proposed algorithm on a 179 bus network. The proposed slow coherency algorithm for controlled islanding is then tested by (Yang et al., 2006) by applying the algorithm in US / Canada blackout case. In the practical case, the slow coherency method which identifies the weakest electrical link is combined with adaptive load shedding and graph theory to find the minimum cut sets in the island to ensure feasible network splitting solution. The feasible set of islands should be able to operate as a standalone system when it is disconnected

by the grid. The combination of all three methods makes the slow coherency theorem robust in dealing with practical cases.

2.5.4 Heuristic Technique

Due to the combinatorial explosion of the search space, different techniques are used in the splitting problem to obtain a solution which satisfies all constraint. However due to time constraints for on-line application, power system network simplification is carried out. This however will cause the search algorithm to miss some of the better solutions for the splitting problem. Since search for an optimum solution is a time consuming task, (W. Liu et al., 2007) have proposed method using binary particle swarm optimization to directly search from the large scale power system which is not simplified. This will allow the network to retain its characteristics and behavior and random search algorithm is used to find the solution. Using this proposed technique, the priority of the loads is considered together with isolation of possible impacted region. The proposed technique is applied on the IEEE 30 bus network and solutions which meet all the specified criteria are obtained. The binary based optimization is used due to the fact that the transmission lines that are "cut off": are real values, thus continuous based optimization will not be able to solve the splitting problem. This is because, the continuous based optimization approach takes into account the floating point numbers or numbers in decimal format based on the continuous plane. The network splitting problem is a discrete problem based on whole numbers.

(Aghamohammadi & Shahmohammadi, 2012) has proposed a search technique using ant search mechanism which is based upon probabilistic search method. The numbers of islands in the system are predefined based on the generator coherency in the IEEE 39 bus network. Using existing knowledge on the coherency of the system, the initial

search point to find islands in the system are carried out in parallel. The generators on each of the islands are assigned with an identification corresponding to the number of island and this will be used throughout the algorithm to group potential buses and generator to form an island bounded by power system constraints such as load-generation balance and transmission line criteria. The boundary lines for tripping are obtained through this search mechanism and post-islanding stability is determined based on the steady state constraint to determine percentage of load shedding and generation increase through spinning reserve.

2.5.5 Piecewise Linear AC Power Flow and Mixed Integer Linear Programming

The piecewise linear function is a function entirely made of straight lines. A function is said to piecewise linear if the graph is constructed by polygonal lines connecting the points in a sequential manner in the Cartesian plane (Imai & Iri, 1987). The mixed integer linear programming is a variant of the integer programing. The mixed integer linear programming (MILP) is used to find the solution to an equation bounded by integer constraints. The piecewise linear approach and MILP (Trodden et al., 2014) has used the piecewise linear approximation to AC problems approach to develop the splitting solution to isolate the impacted area. (P. A. Trodden et al.) and (Trodden et al., 2014) also highlighted the importance of AC power flow in finding the optimum islanding solution compared to the DC-based approach which is commonly used. In this technique, the mathematical formulation of the power system network is formulated before the splitting point is evaluated.

2.5.6 Network Splitting Techniques summary

Section 2.5 shows there are different techniques used in the network splitting problem. Each approach has its own advantages and disadvantages. However, it can be seen that the research effort undertaken to address the network splitting problem is still less. This is due to complexity of the network splitting problem. The BDD method is a powerful tool to decompose the network. However further improvement are required to be integrated with this method to find the optimum solution. The clustering technique is another powerful tool that can be used to identify the proper splitting solution however due to the complexity of the large scale power system, it is only able to assess the active power flow. This can limit the expansion of the work since reactive power or other stability criterion should be further considered to obtain an optimal splitting solution. The slow coherency theorem on the other hand is an effective technique to determine the resultant number of islands based on the coherency of the generators. However, further strategies or techniques are required to find the optimal splitting point of the network. The MILP and piecewise linear approach is extremely useful to decompose and aggregate the complex interconnection of the large scale power system. However, further research is still being carried out to find the optimal splitting solution.

Reflecting back on the objective of this research, it is appropriate for the heuristic technique to be chosen. This is due to the fact that the heuristic technique will be able to find the optimal network splitting solution which is in line with the objective of this research. The heuristic technique also enables us to incorporate the post-islanding stability verification into the algorithm. As described by different techniques in this section, the graph theory is a recurring term which is often observed. This is because the graph theory is capable of providing an accurate representation of the large scale power system network for further processing. In other words, the graph theory approach allows

the basic framework of the network to be designed while retaining the power system's characteristics. Furthermore, the adaptability of the graph theory allows other techniques to be applied in conjunction with the graph theory such as load shedding and power flow analysis to verify violation of transmission line constraints such as overloading of lines.

2.6 Graph Theory

Graph theory is a mathematical structure which is used to model the relation between edges and vertices in a system. The relation between the edges and vertices can be represented using $G(V, E)$ (Koren, 2005).

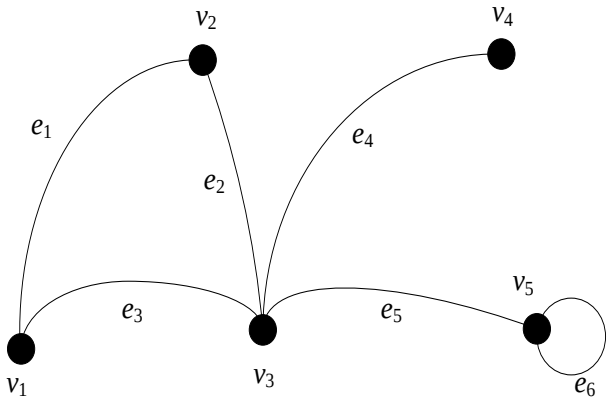

Figure 2.11: Typical graph model

In power system, the edges *(E)* which are the path connecting between vertices *(V)* are used to represent the transmission lines. The vertices are used to represent the buses in the system such as the load or the generator buses. The term node and vertex are used interchangeably as the vertices are often defined as nodes as well. The graph model in Figure 2.11 shows how the vertices and edges are interconnected for a typical graph model. There are five vertices in the system $\{v_1, v_2, v_3, v_4, v_5\}$ and six edges $\{e_1, e_2, e_3, e_4, e_5, e_6\}$.

In order to identify the connected vertices and edges in the graph, the graph has to be traversed. Two common search methods used to traverse the graph are Depth First Search (DFS) and Breadth First Search (BFS). The main difference between these search algorithms is the order in which the vertices are discovered (Ruohonen, 2008).

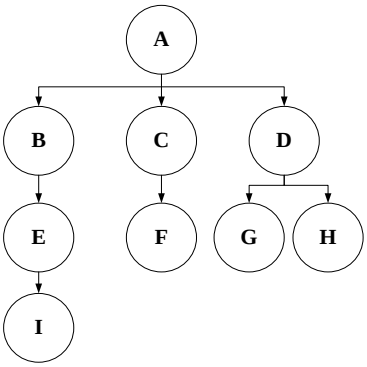

Figure 2.12: Search process in an arbitrary graph model

The depth first search method as the term implies searches on the basis of depth first order as shown for arbitrary graph in Figure 2.12. The starting node of the graph is A. The depth first order of the graph is given as: **A → B → E → I → C → F → D → G → H**

The breadth first search algorithm operates by searching through the system based on the width of the graph. The search algorithm begins at the starting node of the graph and moves forward to find the adjacent nodes that are near from the starting node in a series of layer. The breadth first search order of the graph is: **A → B → C → D → E → F → G → H → I**.

Various approaches in graph theory have been used in power system network splitting. The different properties of the graph theory have further facilitated researchers to implement their algorithm based on the desired application. The common implementation of the graph theory used in network splitting is as discussed below.

2.6.1 Graph model approach

In this approach, weightage is assigned to the nodes to represent the power network as a whole. The weightage for each node is calculated based on the differences in the generated apparent power and load. The graph theory relation will then be formulated as specified as $G(V, E, W)$. Application of weightage to the graph will result in node-weighted graph (Sun et al., 2003; Zhao et al., 2003). The graph model of the network is then further analyzed and processed in order to obtain the network splitting solution.

2.6.2 Minimal cutset

When the edges in the graph are removed, it is termed as a cut. The cut or cutset (more than one cut) can be used as splitting criteria. (X. Wang & Vittal, 2004) implemented the minimal cutset in the splitting problem to obtain feasible islands. The minimal cutset is the minimum number of cut required to split the graph. Since the number of edges is more than the vertices in the power system, the edges to be cut need to be selected based on certain criteria such as edge weightage to justify the basis of minimal cutset. Many different algorithms are developed to find the minimal cutset. Among the methods available are max-flow/min-cut theorem, Karger's minimum cut algorithm and Dijkstra's algorithm (Skiena, 1990). Each of the method will have different computation time as the method choice is based upon application.

2.6.3 Graph-cut approach

The graph-cut approach is a preliminary processing step before further analysis is carried out. The graph model of the power system is built where the graph is split into two different sub graphs based on their respective weightages. The minimum cut for the graph model is then found using recursive bisection. The sub-graphs formed due to this action represent the islands that have to be formed for intentional islanding.

2.6.4 Graph theory summary

The different approaches of graph theory in network splitting shows that graph theory can be utilized further rather than just to represent the power system network. In regards to this, in this investigation, the graph theory can be used to represent the different large scale power system network. The graph cut approach can also be utilized to reduce the search space in order to determine the minimal cutset. The graph model of the power system should also be traversed to determine the interconnected nodes in the network.

2.7 Post-islanding Frequency Stability - Load Frequency Control

The post-islanding frequency stability is carried out after the network has been successfully split to ensure the continuous operation of the islanded areas is carried out as per normal. The stability of the islanded areas is of great importance to the power system before system restoration is carried out. In order for successful restoration of the power system, the sequential tasks involved are:

a) Power system sectionalizing – network splitting in which the large scale power system is islanded based on operating parameters
b) Subsystem restoration – Each islanded area (subsystem) should be restored to their normal operating conditions
c) Subsystem synchronization - The operating parameters of the islanded areas have to be synchronized in order to restore the system back to its initial state (pre-splitting)

The post-islanding frequency stability of the islanded area which is the second task is defined as the subsystem restoration process. The main system parameters that need to

be monitored to ensure subsystem stability and system's security are the frequency and voltage parameters. The frequency of the islanded area should be maintained within its permissible limits to avoid underfrequency. The voltage criteria of the subsystem should also be monitored to ensure adequate voltage supply is maintained. The islanded areas have to maintain the stability and operate as standalone units as the restoration time is uncertain. Adaptive load shedding should be adapted to match load-generation balance (C. Wang et al., 2011). The load frequency control (LFC) which is a subset of automatic generation control (AGC) is used to regulate and maintain the power system's frequency based on its nominal value.

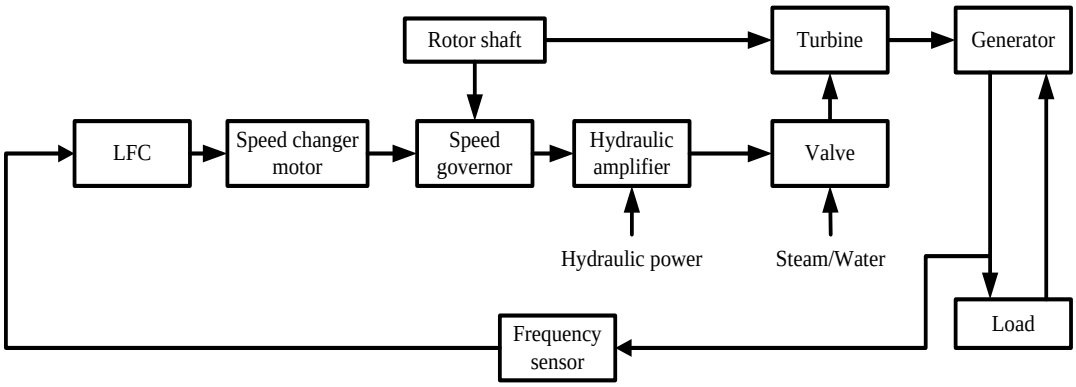

Figure 2.13: Block diagram of a standard synchronous generator with LFC

Figure 2.13 shows a block diagram representation of a standard synchronous generator with LFC. This generator which is based upon the thermal power plant model requires steam or water to spin the turbine to generate the power. The variation in load demand is sensed by the frequency sensor. If there is any deviation in this value with respect to the nominal value, the LFC is tasked to regulate the frequency of the system back to its nominal value. This is done by controlling the opening of the valve. If the load demand increases, the LFC will send a signal to initiate the governor to increase the speed by opening the valve. This will in turn cause the turbine to spin faster to produce more power to meet the load demand. The process is reversed when the load

demand decreases. The LFC implementation in stabilizing the frequency of the system can be seen in the linearized model shown in Figure 2.14.

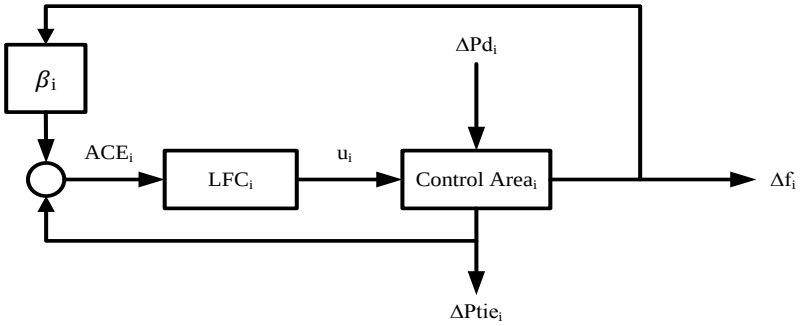

Figure 2.14: Single area LFC

The *Control Area*$_i$ represents the *i*th control area generator system. $\Delta Ptie_i$ represents the tie line power deviation and the ΔPd_i represent the load demand in the area. The ACE_i which represents the area control error in the *i*th area is a culmination of frequency bias (β_i) multiplied by frequency deviation (Δf_i). The u_i is the control signal given to the system by the LFC for compensation action. The generation load equilibrium or balance is important to ensure that the system frequency remains at a nominal value. The main objectives of LFC as stated by (H. Shayeghi et al., 2009) are:

a) Zero steady-state error for frequency deviation
b) Minimum unscheduled tie line power flow
c) Acceptable value for overshoot and steady state settling time for both frequency deviation and tie line power deviation

This underlines the importance of the LFC in ensuring frequency stability in the system. In the islanded system, the LFC operates in a similar manner to restore the nominal frequency in the respective areas when the network is split. The analysis carried out on the LFC has been extensive and researchers have implemented different technique and control strategies to optimize the LFC performance. The design methods

used to optimize the LFC can be broadly categorized as shown in Figure 2.15 below (Pandey et al., 2013; H. Shayeghi et al., 2009).

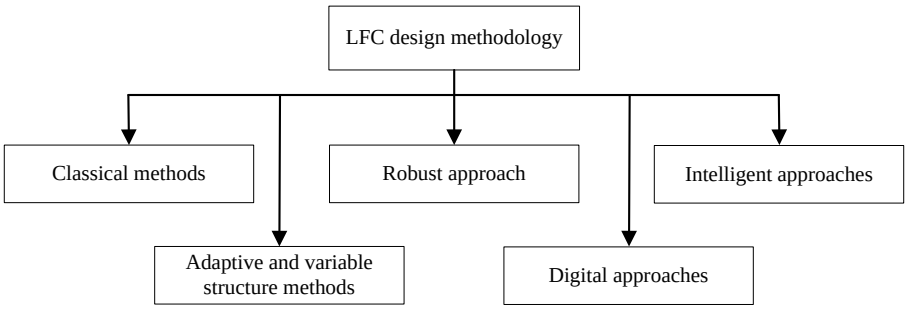

Figure 2.15: LFC design methodology

2.7.1 Classical methods

The classical methods as the term implies refers to the conventional used in the AGC. In this design, the flywheel type of governor is used to minimize the frequency deviation. Conventional methods in detecting magnitude and phase margin using bode and nyquist diagrams are commonly used. The integral of the control signal error is used as the input to the controller which will compensate the error.

Early work based on this particular control technique was reported by (Elgerd & Fosha, 1970). The cost function based on the integral squared error (ISE) was used to damp the oscillation and obtain good transient response. Based on the similar error criterion, (Nanda et al., 1983) used the linear discrete-time state-space model to design the integral controller to ensure frequency stability in the system. This however was not adequate enough to obtain an acceptable LFC performance due to poor dynamic performance. Large overshoots and comparatively long settling time is observed when the classical control approach is implemented.

In order to address the disadvantages and weakness in the conventional approach, optimal controller was developed. Significant improvement were achieved and this has been reported in (Bohn & Miniesy, 1972; Tacker et al., 1972). An optimal controller design was proposed by (Kwatny et al., 1975) in which the energy sources and power regulation are integrated as shown in Figure 2.16.

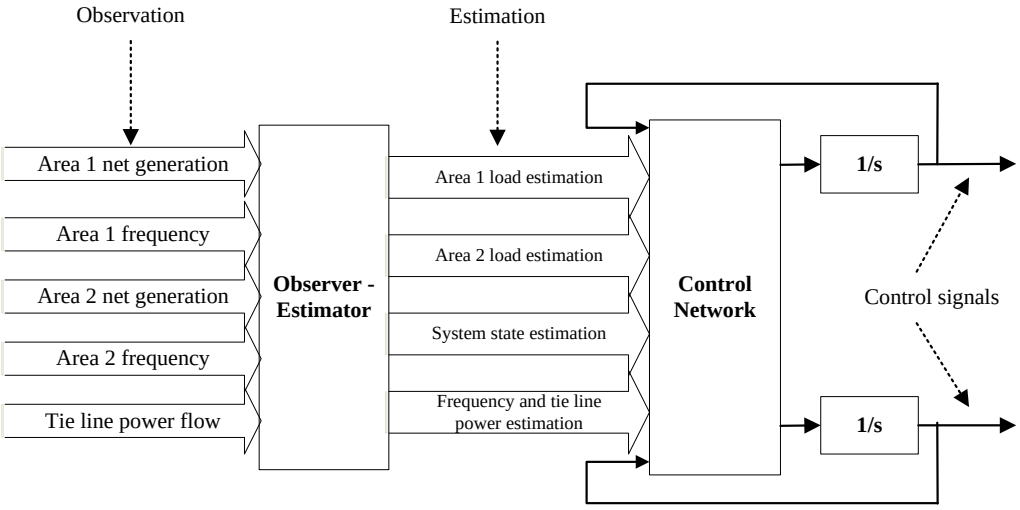

Figure 2.16: Configuration of optimal control for LFC

The observer–estimator model is an input output configuration which decides the state of the system. The estimated values are fed to the control system of the LFC to compensate and reset the frequency deviation back to zero. The optimal controllers, even tough are able to overcome the weakness posed by the classical controllers, are complicated to design. As such, in large scale power system, the optimal controller might not be a feasible option especially in an interconnected system comprising of more than two areas. Researcher have also further improved and introduced LFC based upon modern optimal control-theory as reported in (Aldeen & Trinh, 1992; Rubaai & Udo, 1992; Velusami & Romar, 1997).

2.7.2 Adaptive and variable structure methods

One of the major challenges in the frequency control and stability of a power system is the ever changing nature of the load demand. The dynamic nature of the load requires the LFC to be able to track the changes and compensate the error in the system accordingly. In order to keep the system performance at a satisfactory level, the controller design has to adapt to the different loading patterns and conditions in the power system.

Initial work in adaptive control was carried out by (C. Ross, 1966). The premise of the investigation centered on the adaptive nature of the controller which is able to discriminate against different types of disturbance in the system. The analog controller makes the decision to energize the various relay connected based on a set of logic rules. A different approach of the adaptive controller was proposed by (C. Pan & Liaw, 1989; Y. Wang et al., 1994). In these investigations, the controller was implemented to adapt to the plant parameter changes. Despite variation in system parameters, the controller is still able to perform and achieve good performance. The adaptive controller has also been tested for larger system such as the three area power system (Zribi et al., 2005). The controller still performed satisfactorily and displayed its robustness in view of variation in system parameters and load disturbances. Further enhancement to the adaptive controller has been carried out by integrating advance techniques such as fuzzy logic (Masiala et al., 2004; Talaq & Al-Basri, 1999).

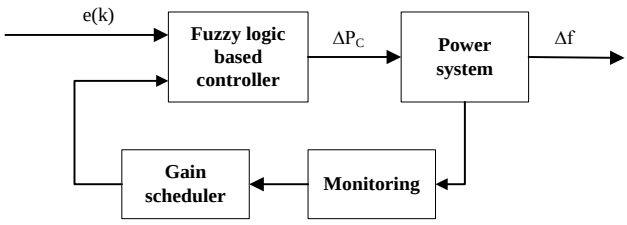

Figure 2.17: Block diagram of standard fuzzy logic based controller (FLC)

Figure 2.17 shows a standard block diagram of FLC. The input signal (e(k)) which is the error in the system is sent to the FLC. The output (ΔP_C) of the controller is then fed to the system and the frequency deviation (Δf) is continuously monitored. Any deviation in the load demand will be fed to gain scheduler and the fuzzy logic will tune the adaptive controller based on a set of predefined rules. The rules are designed based on user's knowledge on the system. Pattern recognition has also been incorporated in the design of adaptive controllers. The development of dynamic wavelet network (DWN) for the LFC problem has hasten the training process and at the same time reduce the size of process data (Hemeida, 2005; Oysal et al., 2005).

Self-tuning regulator which includes the adaptive control scheme is also seen as a viable approach for the LFC problem. The ability to self-regulate further enhances the flexibility of the controller as the controller is able to adjust based on the condition of the system in real time (Jovanovic, 1999). (Yeşil et al., 2004) designed a self-regulating controller based on the peak observer. The scaling factor of the fuzzy based PID controller is adjusted based on absolute peak value. The variable structure method which is well known for its robustness has been integrated with fuzzy logic control in (Ha & Trinh, 2000). The proposed controller implementation has been tested in large power system while including load disturbances in the system at the same time. However, one of the major drawbacks of the variable structure method is the chattering problem associated with it. (Kazemi & Andami, 2004) used the fuzzy logic to further reduce the chatter to ensure component dynamic performance. The chatter was reduced however, it was not completely eliminated.

2.7.3. Robust approach

Robustness can be termed as the ability of the system to tolerate disturbances and perturbations without jeopardizing its main function. In LFC, the robust controller should be able to perform to meet the objectives when the system is subjected to different types of uncertainties and disturbances. (Y. Wang et al., 1993) demonstrated the implementation of robust linear-feedback controller based on the Riccati-equation. Through this approach, the detail information on the time-varying parameters of the plant is not required. The robust controller only requires the bounds or the limits of the time-varying parameters to effectively ensure the stability of the system. This approach was further tested for a multi area power system as shown in (Lim et al., 1996). The *N* interlinked Riccati-equation was used to demonstrate the controller performance under system parametric uncertainties. Good performance was recorded even when non-linearity such as Generation Rate Constraint (GRC) was considered.

Different techniques have been used to further increase the efficiency of the robust controller. (Azzam, 1999) have used the Duan approach to enhance the dynamic performance of the LFC controller. The Duan approach enables the algorithm to locate the eigenvalues of the closed loop system. This makes the algorithm simple and less computational processing is required as it does not contain a going back procedure. Two different stability techniques have been included in the robust controller design proposed by (Ray et al., 1999). The 'matching conditions' and Lyapunov stability theory has been integrated with the robust controller and its performance further outperforms the robust LFC based on the Riccati equation proposed by (Y. Wang et al., 1993). A sequential design process was introduced by (Bevrani et al., 2004b) based on μ-synthesis. This approach is a systematic method which takes into account the previous

step in each design step. The synthesis procedure guarantees robust stability and performance for a variety of operating conditions.

The H-infinity (H_∞) methods have also been extensively used to address the LFC problem. The H_∞ method is a very effective method to be integrated with the robust controller. It has the advantage of solving complex problems involving multiple variables more efficiently than conventional techniques. In (J.-L. Chang, 2003) the H_∞ method is used to design a sliding-mode controller to ensure robust stability and disturbance attenuation. In a larger three area system, the H_∞ method is further integrated with iterative linear matrix inequalities algorithm to design the robust controller as presented in (Bevrani et al., 2004a). The controller is able to precisely track the nominal frequency and attenuate unwanted disruption in the system. A new robust controller design based on mixed H_2/H_∞ technique has been proposed by (Hossein Shayeghi, 2008).This mixed mode controller shows better performance compared to the H_∞ based robust controller. The robustness performance of the controller is better and effects of perturbation in the system are further reduced. The proposed model of the robust controller based H_2/H_∞ technique is shown in Figure 2.18.

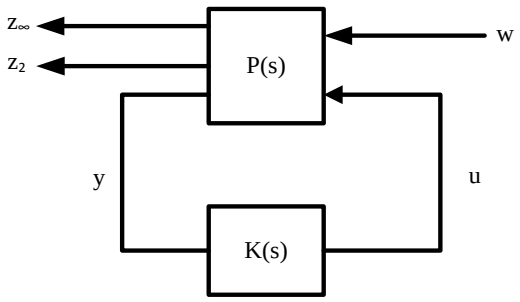

Figure 2.18: H_2/H_∞ design synthesis

The P(s) represents a linear time invariant system described by state-space equations and K(s) represents the controller. The y is the measured output value, the w is the disturbance vector the u is the output from the controller to compensate the deviation

from nominal value. The outputs of the system z_2 and z_∞ represent the performance of the system based on H_2 and H_∞ control technique respectively.

Other approaches have also been incorporated with the robust controller such as fuzzy logic approach (Lee et al., 2006) and Kharitonov's theorem (Toulabi et al., 2014). Other techniques such as Lyapunov stability theory and Q-parameterization have also been reported. The major design problem with the robust technique lies in the fact that due to numerous uncertainties in a large system, a multitude of approaches is required as there is no one single technique which can address all the issues (Stankovic et al., 1998). This can be seen by the various approaches recent researchers have undertaken by integrating two or more different approaches in the robust control design.

2.7.4 Digital approaches

Majority of the approach has focused on the time dependent continuous system. Digital and discrete approach for the LFC problem has also been considered as an alternative. Initially introduced by (C. W. Ross & Green, 1972), a comprehensive approach to the LFC problem was realized using the digital control. The approach included consideration of the dynamic state of the system and the system economics as well. The tie line flow and the frequency deviation value are discretized based on a sampling rate before being sent to the digital controller for remedial action in reducing the Area Control error (ACE). (DeMello et al., 1973; Mills & B'Rells, 1973) in their research pointed out the importance of filtering in digital control. The absence of proper filtering could defeat the objective of LFC as the aliasing effect could introduce an incorrect error signal to the controller. (Taylor & Cresap, 1976) in their research has carried out a simulation to model the digital controller of the LFC for the Pacific

Northwest power system. Through the simulation they were able to determine the accurate sampling rate to be used in the real-time digital controller

One of the major issues in automatic generation control (AGC) which is often overlooked is the accumulation of time error and inadvertent interchange. Due to practical difficulties in eliminating this problem, (Kothari et al., 1989) has proposed a modified expression of ACE to be implemented by the digital controller. The time error and inadvertent interchange is updated based on the sampling rate. The digital controller implemented based on a proportional integral (PI) control design was able to achieve zero steady state error and good dynamic performance. (Hari et al., 1991) has further extended the implementation of digital controller in the power system model by taking into account the Generation Rate constraint (GRC). This is a very important consideration to be taken into account as it further investigates and analyze the effect of GRC in presence of digital controllers. The investigation also addresses the drawback of prior research in which, for the sensitivity analysis, the controller and system were operating in continuous mode. In this research, the power system model is operated in continuous mode and the controller in digital mode. Despite imposing these constraints and making changes to the system parameters, the digital controller displayed robustness in its performance. Generally, the robust controller design based on integral control (K_i) action is based upon the following area control error (ACE) signal shown in Equation 2.2 (Hari et al., 1991).

$$u_i(t) = u_i(kT) - K_i ACE_i(k)[t - kT] \quad \text{for } kT \le t \le (k+1)T \tag{2.2}$$

where $u_i(t)$ represents the control signal of ith area, kT represents the signal sampling instants and T represents the sampling interval. The digital controller approach relies

heavily on the implementation rather than the tuning technique. Any form of technique can be implemented on the digital controller. However the designer has to bear in mind that the controller operates in a discrete form. In regards to this, the sampling time has to be taken into account when the tuning technique for the controller is designed. The risk of the controller responding inaccurately is highly possible if the discrete nature of the controller is not emphasized.

2.7.5 Intelligent approaches

The foray of artificial intelligence in LFC has been extensively reported and extensive amount of literature are available detailing this. The artificial intelligence techniques have an inherent capability in handling various scenarios posed by the operating conditions or system parameters. The artificial intelligence strength lies on the core of the algorithm which generally gives it the capability to learn and adapt to the system accordingly. This approach seems to be very favorable to researchers as detail understanding on the inner working and mechanism of the system is not of critical importance when the artificial intelligence based techniques are applied. A general understanding of the system regarding the input output process is sufficient enough to design the intelligence based controllers. However, a good understanding on the artificial intelligence technique is required before the controller can be designed. Various soft computing techniques such as neural network, fuzzy logic, genetic algorithms and swarm based optimization have been extensively used to tune the controller for the LFC problem.

2.7.5.1 Neural network

Neural network or artificial neural network (ANN) is a computer algorithm that is used to mimic the function of human neural system. The ANN requires an adequate set

of training data values to learn the pattern of the network. This information is then used to model the non-linear system and map the input and output variables. (Birch et al., 1994) carried out an investigation using feedforwad neural network to determine the effective combination of input data required in order to obtain the optimal system performance. The investigation reveals that the complete set of input training data comprising of frequency deviations, control signal, load values and forecasted load are required to ensure optimal system performance. Neglecting any one of these input data significantly increase the training and testing error of the system. The backpropagation network, which is another network architecture used in training the neural network, has been successfully implemented by (Beaufays et al., 1994). The LFC integrated with the intelligent controller was applied in a two area power system and results shows that the neural network is able achieve fast transient recovery while at the same time limiting overshoot when it is compared to an integral controller. Figure 2.19 below shows the standard model of the neural network.

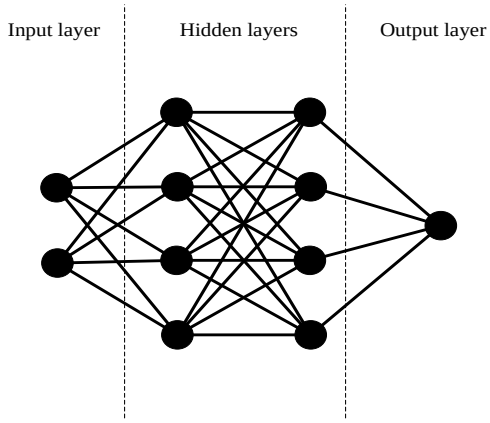

Figure 2.19: Typical neural network structure

One of the major issues in designing the ANN is the parameters of the network itself. This is highlighted by (Chaturvedi et al., 1999). The neural network typically consists of different number of neurons in its hidden layers. In a complex system, the number of hidden layers can be more than three. Coupled with the large set of training data, the computation time required to train the ANN could be very long. Thus a generalized

neural network was developed to hasten the training process by reducing the total number of hidden layers and number of neurons. Results show that the generalized version of ANN is able to perform well, however, a good working knowledge of the system is required so that the system performance is not jeopardized. The backpropagation network has been used in (Demiroren, 2001) by modeling the power system based on its state space equation. Different non-linear elements such as governor deadband effects, reheater effects and generating rate constraints were considered. In (Sharma et al., 2012) the ANN based LFC was implemented for a five area interconnected power system. The ANN based controller was still able to perform well despite the non-linearities involved or the size of network.

2.7.5.2 Fuzzy logic

Fuzzy logic has been widely used in many sectors of power system. The main advantage of fuzzy logic apart from the robustness and reliability is the ease of designing the fuzzy logic system. The design process is relatively easy and expert knowledge regarding the application is required. In the LFC tuning problem, fuzzy logic has been extensively used. The fuzzy logic has been used as a gain scheduling algorithm to tune the PI controller (C. Chang & Fu, 1997) and the PID controller (Yeşil et al., 2004). Due to the adaptability of the fuzzy logic system, hybrid approach has often been implemented to further heighten the tuning process of the LFC. In (Dhanalakshmi & Palaniswami, 2012) researchers have used the adaptive neuro-fuzzy inference system (ANFIS) to carry out a simulation study for AGC in a multi area system. The neuro-fuzzy hybrid system has also been successfully implemented in a four-area load frequency control based on the work carried out by (Prakash & Sinha, 2014), two area reheat interconnected power system with energy storage system (Redox Flow Batteries) (Chidambaram & Francis, 2011) and in two area power system with generation rate

constraint (Panda et al., 2009). The fuzzy logic has also been integrated with different techniques such as optimization based fuzzy logic (H Shayeghi et al., 2007) and swarm optimization based fuzzy logic (H Shayeghi et al., 2008).

2.7.5.3 Genetic algorithm

Genetic algorithm (GA) is one of the earliest optimization techniques commonly used to find the optimal solution for many different problems. GA searches the search space for the global minima based on the law of natural selection and survival of the fittest (Hassani & Treijs, 1975). The GA can be considered as a general optimization algorithm which finds the optimum solution based on certain objective function. In the LFC problem, GA has been successfully used to tune the ID and PID controller for a two-area interconnected power system. The GA tuned PID has also been recorded to provide the best dynamic performance based on the investigation reported by (Aditya, 2003). Since GA is a general purpose optimization technique, little changes are required to the configuration of the LFC in the power system (C. Chang et al., 1998). This eases the implementation of GA as a controller tuning technique despite the complexity of the system. Figure 2.20 shows the typical flowchart of the GA (Hussein).

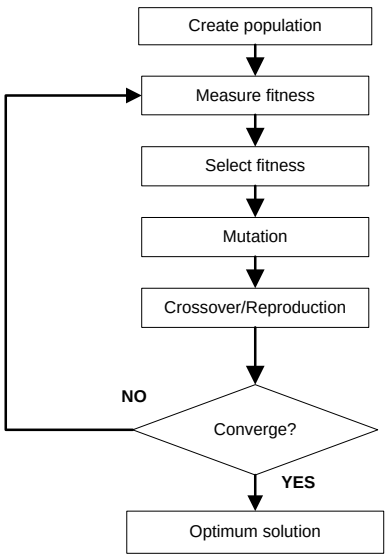

Figure 2.20: Flowchart of typical GA

The initial population which is the random PID parameters of the LFC are initially generated. The fitness function of the controller is then measured and the best fitness is selected. The corresponding PID parameter of the best fitness is the mutated and reproduced using probabilistic method. The convergence criteria is then checked. If convergence is met, the optimal solution is deemed to be found. Various studies pertaining to GA in LFC such as GA based LFC in multi-generator unit has been reported in (Daneshfar & Bevrani, 2010), real coded GA to tune interconnected power system with generation rate constraint and governor dead band as reported in (Ramesh & Krishnan, 2009) and GA based LFC for three area interconnected power system (Golpira & Bevrani, 2011). Based on the research conducted, satisfactory performance in obtaining the optimum LFC parameters has been reported.

2.7.5.4 Swarm based optimization

The swarm based optimization algorithm are usually derived from nature inspired interacting agents or biological entities interacting with the environment. Different swarm based optimization techniques have been used to tune the controller for LFC problem. Among them are particle swarm optimization (PSO) and artificial bee colony algorithm (ABC). PSO which is based is initially developed by (Kenndy & Eberhart, 1995) was able to overcome the premature convergence of GA in finding the optimal solution (Soundarrajan et al., 2010). The PSO has been successfully implemented to find the optimal gains of the controller for LFC. In (Soundarrajan et al., 2010), the PSO was used to find the optimum PID controller parameters for the LFC and automatic voltage regulator (AVR). (Hemmati et al., 2011) further showed the implementation of PSO based PID for a four area interconnected power system. In this work, the performance of PSO-PID in comparison with the GA-PID was carried out and it was further concluded that PSO outperforms the GA in finding the optimal PID parameters.

The multi objective PSO has also been developed and used to successfully tune the LFC in a two area power system (Sharifi et al., 2008).

The ABC algorithm which uses the bee as nature inspired interacting agent was developed by (Karaboga, 2005; Karaboga & Basturk, 2007b). The foray of ABC in LFC has also been extensively documented in many different literatures. In(Gozde, Taplamacioglu, et al., 2012) the authors have implemented the ABC based LFC for a two area interconnected thermal power system. In this investigation, the performance of ABC tuned LFC is highlighted in comparison to PSO tuned LFC. It is shown that the ABC tuned LFC performs better than PSO tuned LFC. The implementation of ABC algorithm for the LFC problem has also been carried out for a two and four area power system (Javidan & Ghasemi, 2013), two area restructured power system with system nonlinearities and parameter uncertainties (Ghasemi & A) and in power system with redox flow batteries (RFB) with unified power flow controller (UPFC) (Balasundaram & Akilandam, 2012).

2.7.6 LFC design methodology summary

This section shows the different approaches available to tune the controller for the LFC. Each of the approach has its own advantages and disadvantages. In order to choose the LFC design methodology, the objectives of this research are reviewed. Since one of the objectives of this research is to implement a load frequency control technique which is adaptive to the nature of the islanded solution, the intelligent based approach is chosen. The flexibility and adaptability of the artificial intelligent based approach far outperforms the other approaches which are more rigid in nature. The power system model of the area can be designed while considering practical constraints in the system without hindering the tuning process offered by the tuning technique. The load

frequency controller with adaptive tuning capabilities will prove to be instrumental in post-islanding phase as the network splitting might yield different islanding scenarios with different operating parameters. Hence, a controller with tuning adaptability is required to track the changes and carry out the LFC objectives as per system requirement.

The optimal parameters of the controller also can be found as the intelligent based controllers treat the LFC problem as a black box design problem. This basically means that the tuning technique is oblivious to the system parameters of the LFC. The technique will feed the inputs bounded by pre-defined system requirements to the process. The process is then run and the optimal output of the system is obtained. The optimal solution is dependent upon the objective function to be minimized. The set of parameters fed as the input to the process to be optimized are based upon the artificial intelligence used. Different artificial intelligence technique will have different performance. This is another important aspect of the intelligent approach. The user will be able to choose the technique to be implemented without carrying extensive modification to the system parameters. Various other techniques can be readily used as the intelligence based technique offers flexibility in implementation.

2.8 Discussion

In order to choose the best technique to be used in order to develop the optimization algorithm for the optimal network splitting problem and load frequency control, the ABC is chosen. The ABC algorithm is robust and simple to use. The flexibility in the algorithm enables the ABC algorithm to be integrated and implemented in various research disciplines (Karaboga & Basturk, 2008) (Karaboga et al., 2014). The main reasons why the ABC was chosen are due to the following factors:

1. The global optimization nature of the algorithm outperforms well known heuristic technique such as genetic algorithm, differential evolution and particle swarm optimization(Basturk & Karaboga, 2006) (Karaboga et al., 2007).
2. The ABC algorithm can be effectively used to solve discrete/combinatorial problem and also handle constrained optimization problems (Karaboga & Akay, 2009; Karaboga & Basturk, 2007a; Q.-K. Pan et al., 2011).
3. Efficient in solving multivariable and multimodal functions and at the same time it is capable of getting out of local minima (Karaboga & Basturk, 2007b).
4. The algorithm is also efficient in solving unimodal functions (Karaboga, 2005) and unconstrained optimization problems (Karaboga & Basturk, 2007a).
5. Only contains a single control parameter compared to other optimization techniques such as evolutionary algorithm and genetic algorithm which contains requires external parameters such as crossover rate, mutation rate, etc. These external parameters are difficult to determine a priori thus making the ABC algorithm easier to implement (Abu-Mouti & El-Hawary, 2009; Rao et al., 2008).
6. The structure of the algorithm maximizes the search process. The triple search capability presented by the three different groups of bee – employed, onlooker and scout bee prevents the stalling of solution by maximizing the search capability (Balasundaram & Akilandam, 2012; Gozde, Cengiz Taplamacioglu, et al., 2012). This is carried by the employed and onlooker bees phase which exploits the search space while the scout bee phase explores the search space for optimal solutions. The random generation of food source introduced by the scout bee phase and the greedy selection scheme used to update the fitness function heightens the local and global search capability of the algorithm (Huang & Liu, 2013).

The psuedocode for ABC program is as per following:

Initialization phase

REPEAT

Employed bee phase - Place employed bees on the food sources and calculate fitness function

Onlooker bee phase - Place onlooker bees on the food sources and calculate fitness function

Scout bee phase - Send scout bees to the search area for discovering new food sources

UNTIL (requirements are met)

The initial search process is carried out by the employed bee phase. The subsequent search phase carried out by the onlooker bee further forages the search space for better solutions. These search phases represent the exploitation process of the algorithm. The scout bee phase which represents the exploration phase of the algorithm further heightens the search process by testing random selection. This phase is very important to enhance the search process to discover new solutions.

2.9 Summary

In this chapter, a detailed literature review was conducted on the network splitting techniques and load frequency control (LFC). A review is first carried out to show the salient reasons on why cascading failures occur in power system. The reasons why power system security is important and the various types of failures in power system are subsequently highlighted. Case study based on blackout in five different countries is then analyzed and the need for a defensive mechanism is further shown to point out the reason why this investigation is important.

Various blackout mitigation techniques were described and each technique has its fair share of strength and weakness. In line with the objective of this research, the network splitting approach based on graph theory seems to be the most feasible and practical choice in mitigating the blackout effect. The optimum network splitting algorithm comprises of two parts. The first part is initial solution algorithm to reduce the search space. This can be carried out using graph theory as the graph theory consists of search mechanism to identify connected nodes in the system. This information can be further manipulated to identify the edges to be initially disconnected to reduce the search space.

The second part is modified optimization technique based on discrete values. In order to develop the modified optimization program to split the network successfully, the graph theory can be used as a useful tool to fit this purpose. This is because, the graph theory allow us to detect the interconnected vertices and edges in the system. Through this, we can easily split the network into desired number of islands. In order to obtain the optimum solution for network splitting problem, important constraints that have to be considered are the separation and synchronization constraints (generator coherency), power balance constraints, and transmission line constraints. The priority of transmission line based on minimal power flow disruption is considered before disconnecting the transmission lines to ensure transient stability in each island is maintained. The load shedding and transmission line power flow analysis can also be seamlessly integrated into the optimum network splitting algorithm.

The load frequency control implementation in order for post-islanding frequency stability is also analyzed in this section. This task is carried out to ensure that the island

is able to function in its normal state to continue supplying power to customers in islanded area. The Laplace model representation of the power system is designed and the controller is then tuned in order to obtain optimal system performance. This is made possible by tuning the LFC using intelligence based approach. The intelligence based approach ensures optimal system performance and flexibility in adaptation as a single controller in the post-islanding stage. The optimization technique in the intelligence based approach seems to be the best choice of tuning technique for the LFC in this investigation. This is because, the optimal parameters of the LFC can be easily found and the implementation of the technique is straightforward. The optimization technique is insensitive to the nature of parameters in the system as it treats the system as a black box. This is important as the islanded areas system parameters' could be different from one another based on the network splitting criteria.

CHAPTER 3: PROPOSED OPTIMUM NETWORK SPLITTING ALGORITHM AND LOAD FREQUENCY CONTROL OPTIMIZATION

3.1 Introduction

In this research, it is our best interest to find the optimal network splitting solution based on the transmission line tripping priority (minimal power-flow disruption). Subsequently, the post-islanding frequency stability is further analyzed to ensure that the frequency stability in the islanded areas is maintained. In this chapter, the investigation is divided into two main phases. In the first phase, network splitting is carried out to determine the optimal splitting point to isolate the network into desired number of islands. The second phase of the investigation deals with the implementation of load frequency control to ensure frequency stability and continuous operation in the islanded areas. In this chapter, the two main phases of the investigation is presented:

a) Proposed optimum network splitting algorithm.
b) Multi objective optimization for LFC

3.2 Optimum Network Splitting Algorithm

In order to find the optimum network splitting solution, the following tasks will be carried out sequentially.

a) Task 1: Modeling of Large Scale Power System
b) Task 2: Initial Solution Algorithm
c) Task 3: Discrete Optimization

3.2.1 Task 1: Modeling of Large Scale Power System

The large scale power system commonly used is based on the IEEE transmission network test cases. In order to model the large scale power system, the graph theory is

utilized. The reason why it is used is due to the inherent capability of the graph theory to effectively map out by providing a graphical representation of the entire power system. This is extremely useful for further analysis and research work pertaining to network splitting to be carried out as the buses and the transmission lines in the system can be easily identified.

Graph theory

A graph *G(V,E)* characterizes the relation between the set edges, *E* and set of vertices, *V*. If two vertices are connected to each other by an edge, the vertices are deemed to be adjacent. The adjacency matrix, *A* is a $|V| \times |V|$ matrix where the connection of vertex *i* to vertex *j*, $A_{ij} = 1$ if $(i, j) \in E$ and $A_{ij} = 0$ if otherwise (Koren, 2005). In the network splitting problem, the undirected graph is used since the flow of power is bidirectional, thus, $A_{ij} = A_{ji} = 1$ if $(i, j) \in E$. The sparse matrix which lists out all the connected vertices in pairs (excluding zero elements), is used to compress the data for faster processing and less storage space (Bondy & Murty, 1976; Chen & Li, 2012). (Zhao et al., 2003) demonstrates the implementation of graph theory to represent the IEEE 5-bus power system. The five bus power system shown in Figure 3.1 contains three generating units, (S_G^1, S_G^2 and S_G^3) and four loads (S_L^1, S_L^3, S_L^4 and S_L^5). The lines interconnecting the busses are given as (l_{12}, l_{23}, l_{14}, l_{24}, l_{35} and l_{45}).

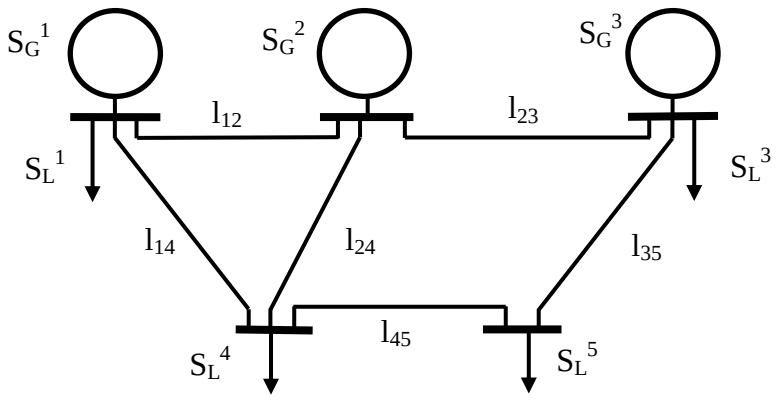

Figure 3.1: IEEE 5-bus power system

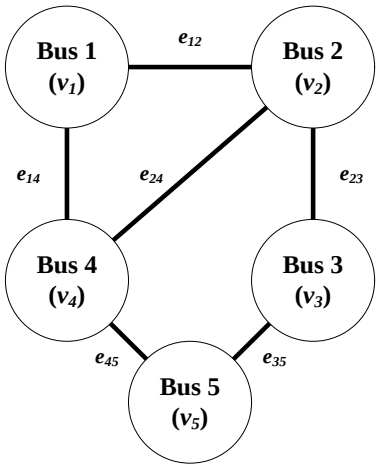

Figure 3.2: Graph model of IEEE 5-bus system

The graph model in Figure 3.2 shows how the IEEE 5-bus power system is visualized using graph theory. The vertices represent the buses (generator or load – v_1, v_2, v_3, v_4 and v_5) in the network and the edges (e_{12}, e_{23}, e_{14}, e_{24}, e_{35} and e_{45}) represent the transmission lines. The adjacency matrix, *A* of this system is given as:

$$A = \begin{vmatrix} 0 & 1 & 0 & 1 & 0 \\ 1 & 0 & 1 & 1 & 0 \\ 0 & 1 & 0 & 0 & 1 \\ 1 & 1 & 0 & 0 & 1 \\ 0 & 0 & 1 & 1 & 0 \end{vmatrix}$$

Matrix *A* shows the interconnected vertices of the system. The 1's and 0's indicate the connection between the buses. This is of crucial importance in the network splitting problem as the configuration of the buses and transmission lines which form the island varies based on system requirement. In this investigation, the vertex discovery order does not have a major influence on the outcome of the network splitting problem. Due to this, either search method can be chosen. In this study the breadth first search (BFS) is utilized. The information obtained is then further utilized for network splitting.

3.2.2 Task 2: Initial Solution Algorithm

The search space encompasses all the possible network splitting solution. It is imperative to reduce the search space to a smaller and more manageable region (Sun et al., 2003). A similar strategy is employed by (X. Wang & Vittal, 2004) and (You et al., 2003) in which the large scale power system is reduced to a smaller network in order to reduce the total number of nodes in the system. The reduced network will be faster and more feasible to process in terms of processing power and computation. The total number of possible combination based on the search space is:

$$\text{Search space} = 2^{\text{Total no.of lines}} - 1 \tag{3.1}$$

Equation 3.1 clearly shows that the search space grows exponentially based on the number of lines in the system. The IEEE 30-bus system which contains 41 lines has a search space of 2.199×10^{12}, the IEEE 39-bus system which contains 46 lines has a search space of 7.0369×10^{13} and the IEEE 118-bus system which contains 186 lines has a search space of 9.808×10^{55}.

In the modified ABC optimization technique based on discrete values, it is very important to obtain a good starting point or initial solution. The importance of initial solution in finding the optimal solution is highlighted in (Ng et al., 2007). The initial solution is able to guide the optimization algorithm to seek the global minima. In (Yongjian & Yumei, 2007) has further underlined the importance of initial solution in discrete based optimization. Results have shown that the global minimum is found when proper initial points are provided.

In this research, the edge reduction algorithm is developed to reduce the total number of possible combinations and provide a good initial solution. A good initial solution is

defined as a proper network splitting solution which meets the constraints and bounds defined by the system parameters. In order to verify the effectiveness of the proposed edge reduction algorithm, two other techniques are also investigated to find the initial solution. The techniques are random line configuration and generator coherency path elimination.

3.2.2.1 Edge reduction algorithm

The edge reduction algorithm, as the name implies reduces the number of edges to be disconnected to provide a good initial solution. The proposed algorithm reduces the number of edges that needs to be disconnected based on the shortest path distance of the vertices and the coherency grouping of the generators. The shortest path between the vertices is based on the Dijkstra algorithm (Skiena, 1990).This is the first phase of the optimal network splitting algorithm.

Initially the large scale power system is modeled using graph theory as shown in Task 1 (Section 3.2.1). Once the graph model of the system is completed, the load flow analysis is run to determine the power flow in each of the transmission lines. Figure 3.3 shows an arbitrary network based on the IEEE 14-bus test system. The coherent group of generators is also given as input to parameter in the algorithm. In Figure 3.3, two coherent groups of generators exist, which are:

a) Group 1: Generators 1, 2 and 6
b) Group 2: Generator 3 and 8

The first step in determining the edges not to be cut is by finding the shortest path between the vertices in the coherent group of generators. This will create the "backbone" of the network as shown by the red lines in Figure 3.3. The solid red line

represents the edges for the first group of coherent generators and the solid green line represents the edges for the second group of coherent generators. The shortest path between the coherent groups of generators ensures that the islanded solution is feasible. It is need to be noted here that identification of the shortest path is done sequentially i.e. from group 1 to group 2 and so on. Once the shortest path is determined, the edges not be disconnected is stored and an index is given to identify the group.

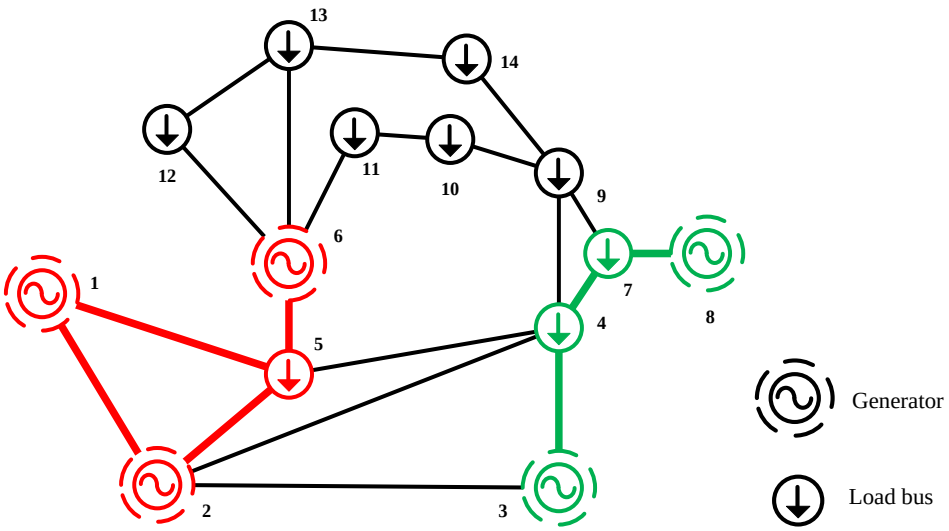

Figure 3.3: IEEE 14-bus test system

In this system, the edges 1-2, 1-5, 2-5 and 5-6 are identified as group 1 while edges 7-8, 4-7 and 3-4 are identified as group 2. This process is then repeated and if a direct connection is observed between two vertices, then the edge is identified as a cutset as shown in Figure 3.4.

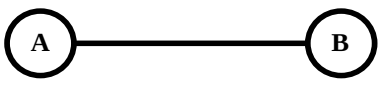

Figure 3.4: Direct connection

Figure 3.4 shows how the vertices are considered to be in direct connection to each other. In this case, vertex A is considered to be from group *n* and vertex B is from group *n+1*. As such, the edge A-B is considered as a line to be disconnected. Figure 3.5 shows

the resultant system after the 2nd iteration. Edges 2-3, 2-4 and 4-5 are considered as edges to be disconnected. The algorithm further proceeds to find any vertex connected to group 1 and group 2 and the paths are mapped out as shown in Figure 3.5. The dashed blue line represents the edges to be disconnected.

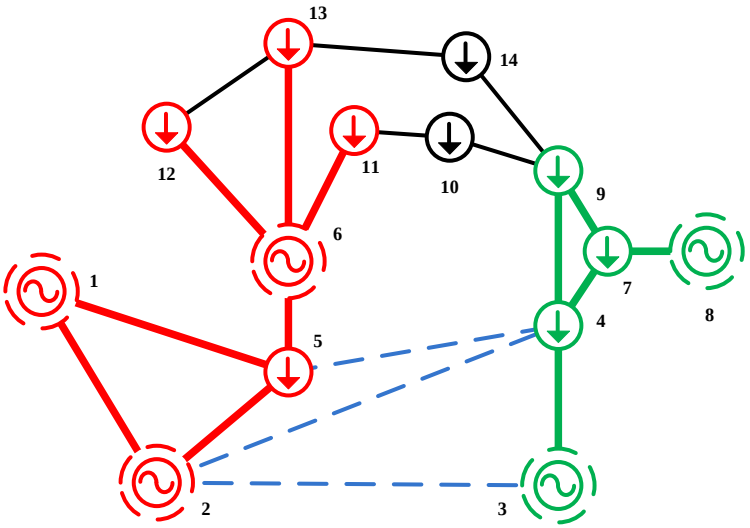

Figure 3.5: IEEE 14-bus test system after 2nd iteration

In the third iteration, the process is repeated and the shortest path for each group is mapped out sequentially starting from Group 1. Since the algorithm starts from group 1, the vertices connected to group one reaches out for other vertices based on the shortest path between them. Once this is completed, group 2 will further try to map any vertices connected to it and if direct connection are found, the respective edges will be considered to be possible edges to be disconnected.

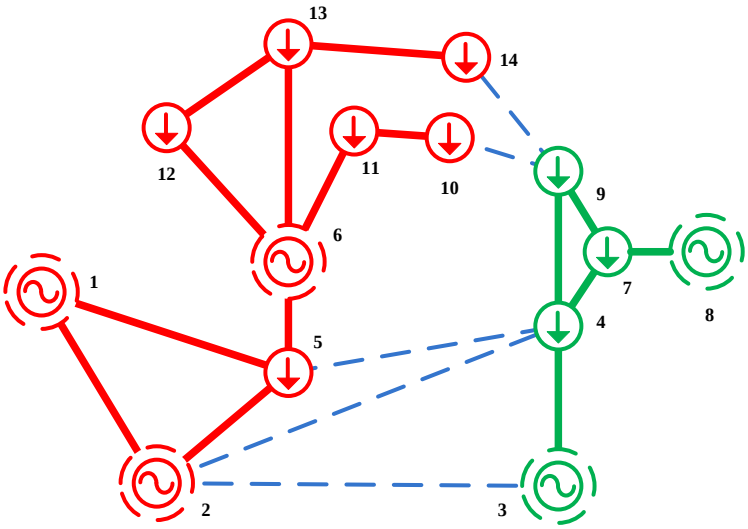

Figure 3.6: IEEE 14-bus test system after 3rd iteration

Figure 3.6 shows the final resultant network after the edge reduction algorithm is implemented. This basically provides us the information that is required for the initialization purposes, the edges 2 – 3, 2 – 4, 4 – 5, 9 – 10, and 9 – 14 are edges to be disconnected. The search space of the initial IEEE 14-bus test system has been reduced from a total number of 16383 ($2^{14} - 1$) to 31 ($2^5 - 1$) through this proposed algorithm and the initial line configuration solution is obtained. The flowchart of the edge reduction algorithm is shown below:

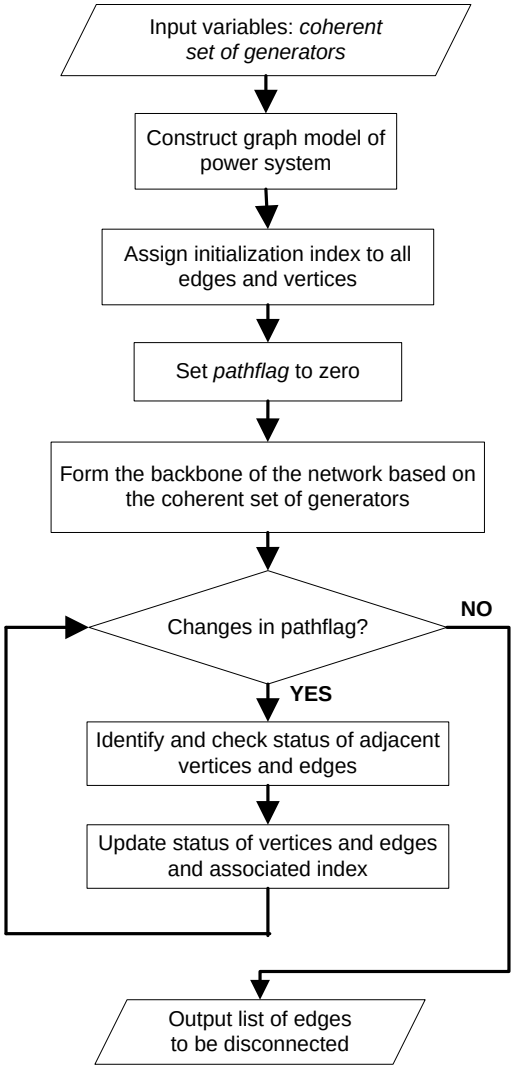

Figure 3.7: Edge reduction algorithm flowchart

Figure 3.7 shows the flowchart depicting the edge reduction algorithm. The input variables for the algorithm are the coherent group of generators (represented by variable *gen_coh*). The graph model of the test system is then constructed. Initialization index is assigned to every edge and vertex in the system. This index will assist the algorithm to keep track of the grouping of vertices and status of edges in the network. Initially all the edges are given a null index value to denote that these edges can be manipulated. Similarly the vertices also are given a null index value to denote they currently do not belong to any group. A variable called *pathflag* is initialized to zero. This is essentially

a flag that is used as an indicator to detect if there any more paths being mapped in the network.

The backbone of the coherent group of generators is formed and the vertices in the group are given an index value of 1 if they belong to the first group or 2 if the belong to the second group and so on. The edges are also given an index number based on the group that they are located in. Once this is done, the iteration process begins to sequentially map the adjacent vertices and edges. For example, the adjacent vertices and edges connected to group 1 are initially identified. The degree of adjacency is 1 meaning that only the first layer of adjacent network is identified. This process is then repeated for the second group and if there exists an edge which is in between different groups as shown in Figure 3.5, this edge is given an index value of '9' to signify that this is an edge to be cut. The *pathflag* variable is updated if there are any changes to the network pattern based on the edges being mapped in the previous iteration and current iteration. After certain number of iterations, when all the edges are mapped out, the *pathflag* detects that no edges to be manipulated exists and the algorithm stops. The final list of edges to be disconnected is then given as output of the algorithm for the next task.

3.2.2.2 Random line configuration

In this technique, the upper and lower bounds of the line configuration is specified and a random line configuration is generated as shown in Equation 3.2.

$$line\_config = round(rand(No\_sol,1))* Range + lb \quad (3.2)$$

where *line_config* is the possible line configuration

round is the command used to round up the floating point integer to a whole number

rand is the random number generator

No_sol is the number of line configuration required

Range is the difference between the upper bound (*ub*) value of $2^{\text{Total no. of lines}}$ and lower bound (*lb*) value 1.

The randomly generated line configuration is then evaluated based on the objective function to determine if a feasible network splitting solution is found. If not the process is continued until a feasible network splitting solution pertaining to the line configuration is found.

3.2.2.3 Generator coherency path elimination

In this technique, the path connecting the coherent group of generators is initially obtained based on the shortest distance connecting each set of coherent generators. This is similar to the first step of the edge reduction algorithm when the "backbone" of the network is identified as shown in Figure 3.8. Similar case study as shown in Section 3.2.2.1 is used here.

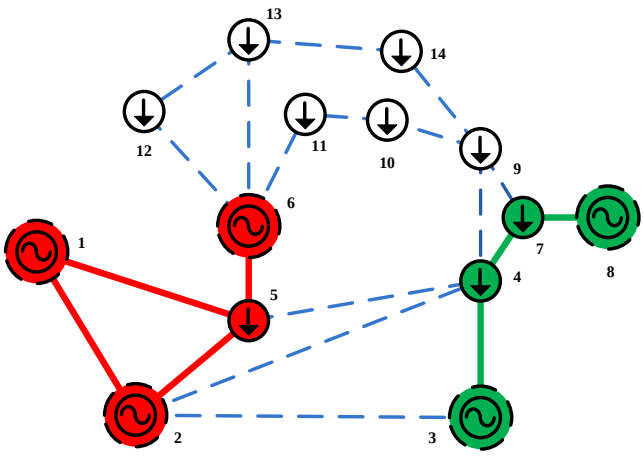

Figure 3.8: Generator coherency path

The edges of the network not to be disconnected are edges 1- 2, 1-5, 2- 5 and 5- 6 for coherency group 1 (solid red line) and edges 3-4, 4-7 and 7-8 for coherency group 2

(solid green line). Once these edges have been identified, the rest of the lines are deemed to be possible transmission lines to be disconnected (dashed blue line). The algorithm will then generate random line configuration based on the possible transmission lines to be disconnected in order to find a feasible network splitting solution as the initial solution.

3.2.3 Task 3: Modified ABC optimization based on discrete values

As explained earlier, the combinatorial explosion of search space involved in the network splitting problem is inevitable. The continuous optimization approach which takes into account integers and the value points that lie in between them (fractions) will be ineffective in the network splitting problem. The modified approach only deals with discrete numerical values. The transition between the integers will only consider whole numbers and not the fractions in between them.

3.2.3.1 Artificial Bee Colony (ABC) algorithm

In this investigation, the modified version of Artificial Bee Colony (ABC) optimization algorithm is used to obtain the optimum network splitting solution. The properties of the discrete optimization problem such as the system constraints, search space, proposed mutation algorithm and the objective function are further discussed.

3.2.3.2 Constraints

In order to obtain the optimum network splitting solution, it should satisfy all listed criteria – practical requirements and physical constraints. The system parameters which are the constraints for the modified optimization are:

1. Group of coherent generators [*gen_coh*].
2. The desired number of islands [*des_island* = 2, 3, 4, … *n*].

The parameter values are treated as system constraints for the modified optimization algorithm. Currently, the program is able to create up to 4 islands. The main input to the program is the group of coherent generators. The bus number of the coherent group of generators has to defined, e.g. *gen_coh1 = [1,2,6]* and *gen_coh2 = [3,8]*. The initial number of lines to be disconnected is obtained from the edge reduction algorithm as explained in Section 3.2.2. The desired number of islands which stems from the coherent group of generators is also taken into account as a system constraint. The information on the coherent group of generators is obtained from previous published works. The program ensures that none of these constraints are violated.

3.2.3.3 Input parameter

The transmission line configuration is regarded as the input variable to the network splitting problem. The line configuration (*line_config* variable) represents the transmission lines status in the power system network. In this approach, the integer number is used to represent the line status of the system. Since each line can be switched on or off (‘1’ – line connected, ‘0’ – line disconnected), the total number of possible combinations is equal to the search space based on the Equation 3.1. Due to combinatorial explosion of the search space, the edge reduction algorithm is used to obtain the initial solution *line_config* variable.

The following steps below shows how the *line_config* variable is constructed

Step 1: The edges to be disconnected are obtained from the edge reduction algorithm.

The edge reduction algorithm will present the initial set of edges to be disconnected to obtain the initial solution. For example, the edges to be disconnected (variable *edges_discon*) will be presented in the following form

edges_discon
2 – 3
2 – 4
4 – 5
9 – 10
9 – 14

The total number of edges disconnected is stored in a variable called *no_edges_discon*. In this case *no_edges_discon* = 5.

Step 2: Comparison with the linedata of the test system.

The edges will then be compared to the linedata of the particular test system to determine the lines to be disconnected. Binary values are assigned to each line segment in the linedata where the 1's indicate the lines which are connected and the 0's indicate the lines which are disconnected.

Step 3: Conversion to decimal number

Once the binary representation of the line configuration is obtained, the binary number is converted to decimal number (whole number). For example, a binary value of 1111111110011011111111111111111011011111 is represented by a decimal number of 2197345533663. This conversion is required for computational algorithmic purposes.

3.2.3.4 Mutation

The mutation process for the modified optimization need to be modified to suit the network splitting problem since it is a discrete problem. The conventional mutation process is not able to improve the solution since it is more suitable for continuous optimization operation. In this investigation three different phases of mutation process is carried out to generate mutated *line_config*.

Employed bee phase mutation

In the employed bee phase, the following mutation is proposed. The following steps show how the mutation process is carried out to generate the mutated *line_config*.

Step 1: The *line_config* variable is processed to obtain the *edges_discon* and *no_edges_discon*. A variable called *total_lines* is created to increase the *no_edges_discon* based on *line_factor* specified. The *line_factor* variable specifies the maximum number of *edges_discon* that can be increased. The pseudo code below shows the mutation process which is carried out.

---

for *total_lines = no_edges_discon* **until** *(no_edges_discon + line_factor)*
employed bee mutation process
end

Initially the variable *total_lines* is equal to the *no_edges_discon* and the mutation process shown in Table 3.1 is carried out.

Table 3.1: First run of the employed bee mutation process

edges_discon	$\mathbf{x_1}$	$\mathbf{x_2}$	$\mathbf{x_3}$	$\mathbf{x_4}$	**…**	$\mathbf{x}_{total\_lines}$	
First line is replaced	a_1	x_2	x_3	x_4	…	x_{total_lines}	Mutated *edges_discon*
Second line is replaced	x_1	a_2	x_3	x_4	…	x_{total_lines}	
Third line is replaced	x_1	x_2	a_3	x_4	…	x_{total_lines}	
Fourth line is replaced	x_1	x_2	x_3	a_4	…	x_{total_lines}	
.	.	.	.	.	.	.	
.	.	.	.	.	.	.	
.	.	.	.	.	.	.	
total_lines-th line is replaced	x_1	x_2	x_3	x_4	…	a_{total_lines}	

The variables $x_1, x_2 \ldots x_{total\_lines}$ represent the edges to be disconnected for a particular line configuration. In each step of the mutation process, one line segment of the disconnected transmission line is replaced by a randomly generated number (a_1, $a_2 \ldots a_{total\_lines}$). If the line configuration contains five edges which are disconnected (*no_edges_discon = 5)*, then each line segment is replaced one by one in a diagonal

manner from the first line until the fifth line. This is to ensure that a certain level of heuristic is maintained based on the original line configuration solution obtained earlier. In a single run, each line configuration will generate *total_lines* mutated solutions.

Step 2: In the second run, the *total_lines* counter is increased by one. If initially the *total_lines* was five, now the *total_lines* is increased to six. In this case a random line segment is updated for the newly created sixth line segment (x_6) as shown in Table 3.2.

Table 3.2: Second run of the employed bee mutation process

edges_discon	$\mathbf{x_1}$	$\mathbf{x_2}$	$\mathbf{x_3}$	**…**	$\mathbf{x_6}$	
First line is replaced	a_1	x_2	x_3	…	a_{16}	Mutated *edges_discon*
Second line is replaced	x_1	a_2	x_3	…	a_{26}	
Third line is replaced	x_1	x_2	a_3	…	a_{36}	
.	.	.	.	.		
.	.	.	.	.		
.	.	.	.	.		
Sixth line is replaced	x_1	x_2	x_3	…	a_{66}	

Random numbers are updated in the sixth line segment (a_{16},a_{26}…a_{66}) and the usual updating process explained in Step 1 is carried out to replace each line segment in diagonal manner. This means that each step of the mutation process in the second run, two random numbers are updated for the *edges_discon*.

Step 3: In the third run, the similar process as explained in Step 1 and Step 2 is carried out. However in this run, three random numbers are updated for the *edges_discon* in each step of the mutation process as shown in Table 3.3.

Table 3.3: Third run of the employed bee mutation process

edges_discon	$\mathbf{x_1}$	$\mathbf{x_2}$	$\mathbf{x_3}$	**…**	$\mathbf{x_6}$	$\mathbf{x_7}$	
First line is replaced	a_1	x_2	x_3	…	a_{16}	a_{17}	Mutated *edges_discon*
Second line is replaced	x_1	a_2	x_3	…	a_{26}	a_{27}	
Third line is replaced	x_1	x_2	a_3	…	a_{36}	a_{37}	
.	.	.	.	.			
.	.	.	.	.			
.	.	.	.	.			
Sixth line is replaced	x_1	x_2	x_3	…	a_{66}	a_{67}	
Seventh line is replaced	x_1	x_2	x_3	…	a_{66}	a_{77}	

These steps are repeated until the iteration described in Table 3.3 is met.

Step 4: The complete list of mutated *edges_discon* is then processed in order to obtain the mutated *line_config* based on the steps explained in Section 3.2.3.3. This means that the employed bee phase will generate a certain number of mutated *line_config* as shown in Equation 3.3.

$$\text{number of mutated } line\_config = \sum_{n=0}^{line\_factor} no\_edges\_discon + n \tag{3.3}$$

Onlooker bee phase mutation

In the onlooker bee phase, the following mutation has been proposed. The following steps show how the mutation process is carried out to generate the mutated *line_config*.

Step 1: The first step of the onlooker bee phase mutation is similar to the first step of the employed bee phase mutation is carried out to replace each line segment in diagonal manner (a_1, $a_2 \ldots a_{total\_lines}$).

Step 2: In this step, a null value is updated in each of the line segment in which a_1, $a_2 \ldots a_{total\_lines} = 0$. This process is shown in Table 3.4.

Table 3.4: Onlooker bee phase mutation process

edges_discon	$\mathbf{x_1}$	$\mathbf{x_2}$	•••	$\mathbf{x_{no\_edges\_discon}}$	
First line is replaced	$a_1 = 0$	x_2	…	$x_{no\_edges\_discon}$	Mutated *edges_discon*
Second line is replaced	x_1	$a_2 = 0$	…	$x_{no\_edges\_discon}$	
.	.	.	.	.	
.	.	.	.	.	
.	.	.	.	.	
no_edges_discon-th line is replaced	x_1	x_2	…	$a_{no\_edges\_discon} = 0$	

By carrying out this process, we are able to reduce the *edges_discon* to scour the search space to find a solution with lower *no_edges_discon*. For example if the initial *no_edges_discon* is five, the onlooker bee phase will try to find if a solution with *no_edges_discon* is four exists. In order to further improve and fasten the mutation process in finding the optimal solution, this mutation process in Step 1 and Step 2 are run twice

Step 3: The complete list of mutated *edges_discon* is further processed to obtain the mutated *line_config* based on the steps explained in Section 3.2.3.3. The onlooker bee phase will generate a certain number of mutated *line_config* as shown in Equation 3.4.

$$\text{number of mutated } line\_config = \sum_{n=0}^{1} (no\_edges\_discon - n) * 2 \tag{3.4}$$

Scout bee phase mutation

In the scout bee phase, the mutation process is activated when the maximum number of trials has been achieved. In this phase, the following mutation process shown in Table 3.5 is carried out.

Table 3.5: Scout bee phase mutation process

edges_discon	$\mathbf{x_1}$	$\mathbf{x_2}$	$\mathbf{x_3}$	**…**	$\mathbf{x}_{no\_edges\_discon-1}$	$\mathbf{x}_{no\_edges\_discon}$	
First line is replaced	a_1	a_2	x_3	…	$x_{no\_edges\_discon-1}$	$x_{no\_edges\_discon}$	Mutated *edges_discon*
Second line is replaced	x_1	a_2	a_3	…	$x_{no\_edges\_discon-1}$	$x_{no\_edges\_discon}$	
.	.	.	.	.	.	.	
.	.	.	.	.	.	.	
.	.	.	.	.	.	.	
no_edges_discon-th line is replaced	x_1	x_2	x_2	…	$a_{no\_edges\_discon-1}$	$a_{no\_edges\_discon}$	

In the scout bee phase, instead of replacing one line segment at a time, two adjacent line segments are replaced. This process is run twice in order to heighten search process.

This is to further explore the search space in order to find a better network splitting solution. Similar to the employed and onlooker bee phase, the complete list of mutated *edges_discon* is then processed in order to obtain the mutated *line_config* based on the steps explained in Section 3.2.3.3. The scout bee phase will generate a certain number of mutated *line_config* as shown in Equation 3.5.

$$\text{number of mutated } line\_config = (no\_edges\_discon)*2 \tag{3.5}$$

3.2.3.5 Objective Function

In this investigation, the minimal power-flow disruption as expressed in Equation 3.6 is considered. As explained earlier, the minimal power-flow disruption as the objective function will be able to improve the transient stability of the island due to the fact that extreme variation in the power-flow pattern is reduced.

$$f(x) = \left(\sum |P_{ij}|\right) \tag{3.6}$$

where P_{ij} represents the active power value on the transmission line between bus *i* and *j*. Since this is a minimization problem, we could also ensure that the optimum solution contains the lowest arithmetic sum of power flow in the line segments that are switched off. During the optimization process, the objective function is evaluated and the fitness function is stored. However, the values are ranked first before they are stored in order to determine the best fitness function. In this investigation, the objective function is the minimal power flow disruption (P_{min}). As such the ranking is based upon minimal power flow disruption. If similar values in minimal power disruption are found, the objective function is further ranked based on the minimum number of edges required to split the network.

3.2.3.6 Modified ABC optimization flowchart

The flowchart shown in Figure 3.9 depicts how the modified ABC optimization is realized for the network splitting problem.

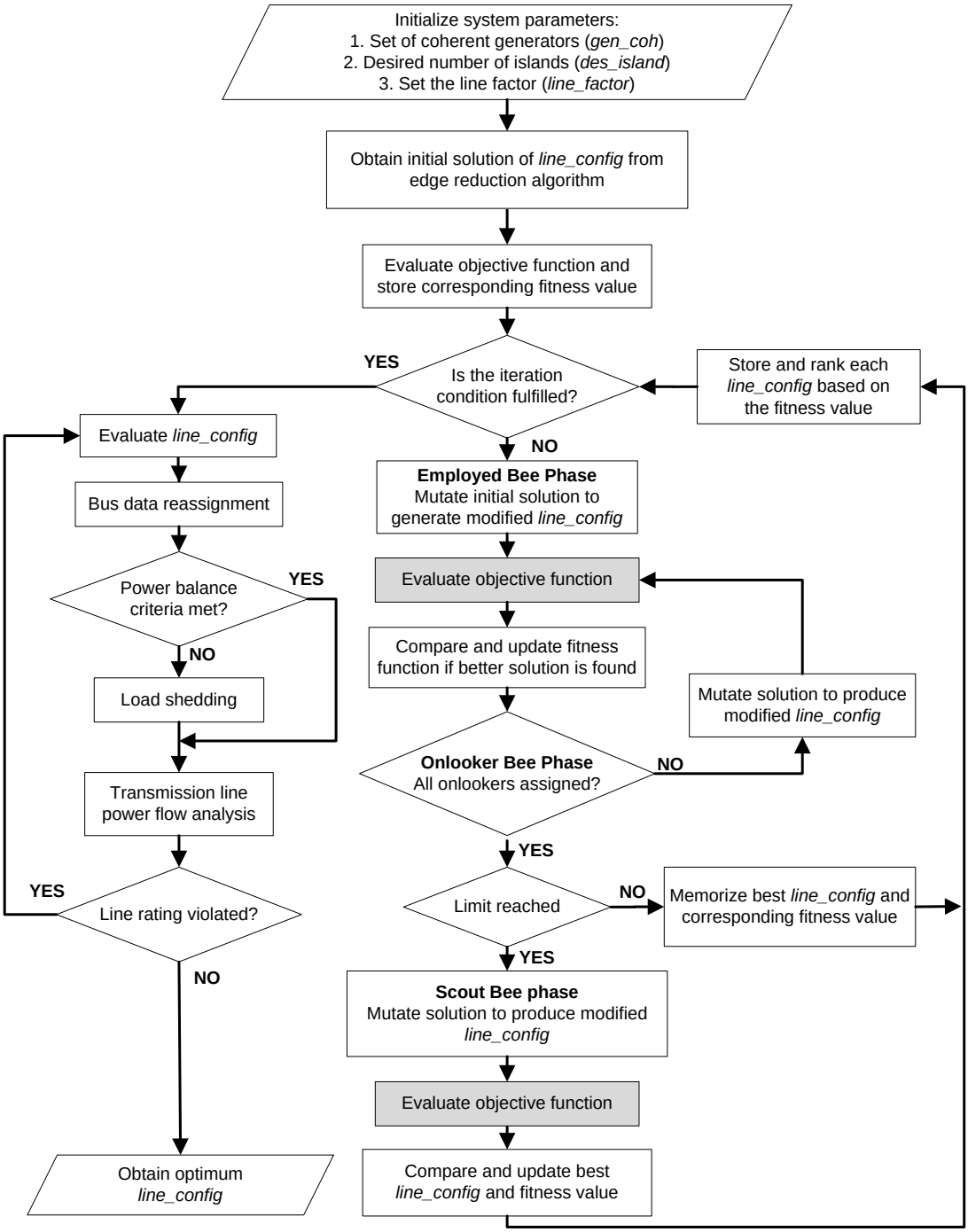

Figure 3.9: Modified ABC optimization flowchart

In the initialization phase, the set of edges to be disconnected is obtained from the edge reduction algorithm. Other information such as *des_island*, *gen_coh* and *line_factor* are

initialized. The line configuration (*line_config*) is based on the initial solution specified by the edge reduction algorithm. Due to the explosive nature of the search space, it is imperative to start the optimization process based on a set of feasible network splitting solutions. A feasible network splitting solution is defined as an islanding solution that is able to meet all specified criteria. The *line_config* generated by the edge reduction algorithm is used as the initial solution to be further processed by the optimization algorithm.

The objective function of the initial line configuration is evaluated and the fitness value is calculated and stored. The graph theory which is used to evaluate the objective function takes into account all constraints predefined by the user in order to identify feasible network splitting solutions based on the line configuration. The flowchart for the objective function via graph theory is shown in Figure 3.10.

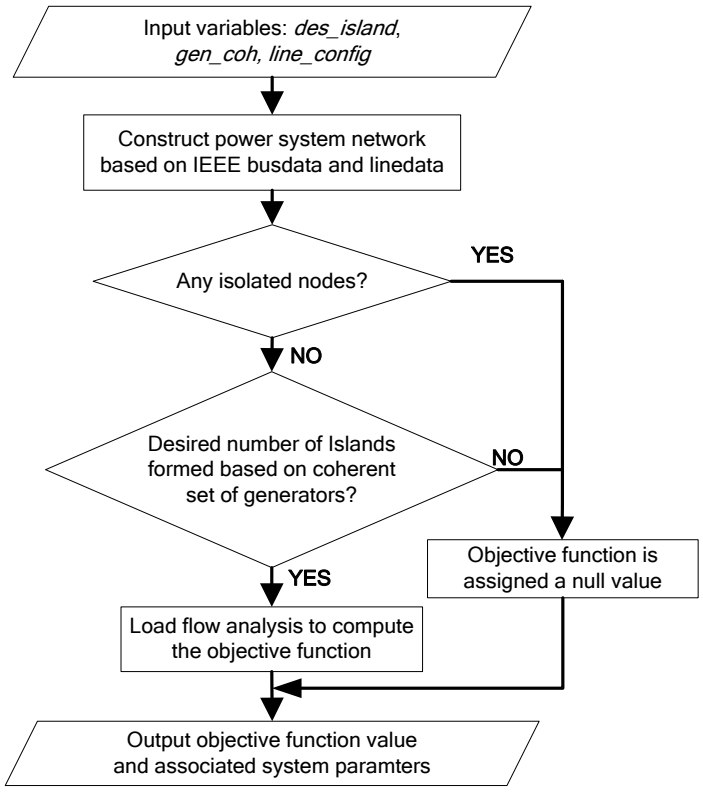

Figure 3.10: Objective function flowchart

The objective function for the network splitting algorithm is realized via graph theory as explained earlier. The input variables to the algorithm consist of *des_island*, *gen_coh* and *line_config*. This information is used to construct the graph model of the power system network as shown in Figure 3.2. The adjacency matrix which represents the interconnection between the nodes and edges is generated based on the *line_config*. The adjacency matrix is then checked for isolated nodes. In the event there are no isolated nodes and the *line_config* is able to split the network in accordance to *des_island*, each of the islands is checked to verify if they contain busses in accordance to *gen_coh*. If this is achieved, the load flow analysis is then carried out for each island and the summation of power flow in the lines that are tripped is evaluated as objective function. If none of this is achieved, then a null value is updated as the objective function to indicate that this line configuration does not result in a feasible network splitting solution.

In the employed bee phase, the line configuration contained in the *line_config* is mutated to generate modified line configurations. The employed bee mutation process is carried out and *n* number of mutated *line_config* is generated as shown in Equation 3.3. The objective function and the fitness value of each *line_config* are then evaluated and if better solution is found, the fitness function is updated. In the onlooker bee phase, the updated line configuration (if any) is further mutated based on the onlooker bee mutation process. The *n* number of modified *line_config* based on Equation 3.4 is generated and the objective function of the line configuration is evaluated and if better solution is found, the fitness function is updated.

An index called *no_trials* is updated every time a better fitness is not achieved in the employed and onlooker bee phase. If *limit* is reached, the scout bee phase is initiated

and it determines the abandoned food source and generates new line configuration based on the scout bee mutation process. The best line configuration and fitness function is updated and memorized until the iteration condition is fulfilled. The line configuration and corresponding objective function is then ranked based on their fitness values and stored in a matrix. The matrix containing all the information is then evaluated one by one as shown in Table 3.6.

Table 3.6: Complete line configuration array

Line Configuration	Objective Funciton
$line\_config_1$	$ObjFunc_1$
$line\_config_2$	$ObjFunc_2$
.	.
.	.
.	.
$line\_config_n$	$ObjFunc_n$

The complete line configuration array which contains a list of line configuration is used to determine the optimum network splitting solution. Since the values are ranked, the first line configuration usually denotes the best solution in the whole set. The size of the complete line configuration array is allocated to store a maximum number of ten *line_config* and *ObjFunc* values.

This line configuration is selected and the bus data reassignment is carried out. This has to be done as the system has been split and the power flow analysis has to be recalculated based on the current network configuration. When the network is split, one of the islands will contain the slack bus while the other islands will only contain the PV buses and the loads. Thus, a slack bus has to be selected in the other islands in order to carry out the power flow analysis. In this research, the slack bus is selected amongst the PV bus which has the highest maximum power rating (P_{Gmax}). If the island contains two

or more bus with the same P_{Gmax}, then the bus with the lower bus number is chosen. Once this is done, the load flow analysis is carried out to evaluate the power balance in each island. If the generated power in the island (P_G) is greater than the load demand (P_{Load}), then bus data reassignment is carried out and the generator will be scheduled accordingly (lower generation value) to meet the power balance equilibrium.

In order to benchmark the performance of the modified ABC optimization technique based on discrete values, the modified PSO technique based on discrete values is also developed to find the optimum network splitting solution.

3.2.3.7 Modified PSO flowchart

The modified PSO technique based on discrete values is developed to benchmark and validate the performance of the modified ABC optimization technique. The flowchart for the modified PSO technique is given below:

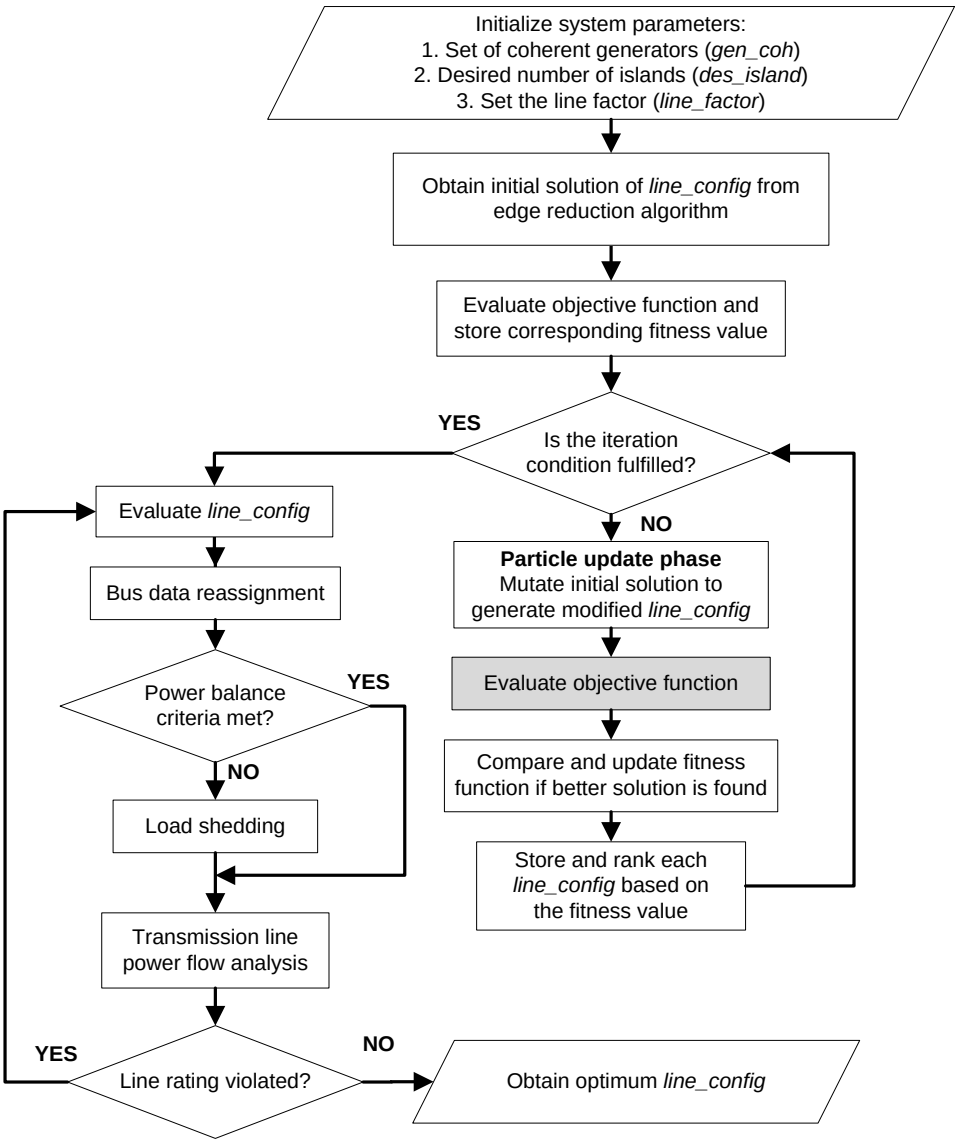

Figure 3.11: Modified PSO flowchart

Figure 3.11 shows the modified PSO flowchart. As it can be seen, the process to obtain the initial solution which is based upon the edge reduction algorithm is similar to the modified ABC optimization. The iteration condition is checked and particle update

phase is entered. In this phase, the initial solution is mutated based on the employed bee phase mutation process and onlooker bee phase mutation process shown in Section 3.2.3.4. The PSO technique does not contain different phases of optimization such as onlooker bee phase or scout bee phase. The fitness function is compared and updated if better fitness function is found. The iteration condition is checked again and if the maximum number of iteration has been reached, the optimization process stops. Similar to the modified ABC optimization, the *line_config* is further evaluated and bus data reassignment is carried out based on the islanding information. Power balance criteria is checked and transmission line power flow analysis is carried out further to determine the optimum network splitting solution.

3.2.3.8 Load Shedding Algorithm

In the event that the load demand (P_{Load}) is greater than the power generated (P_G), the load shedding algorithm is initiated. The following steps show the process of the load shedding algorithm which is initiated in order to meet the load demand:

Step 1: Calculate the power imbalance ($P_{imbalance}$) in the island.

Initially, the power imbalance in the island is calculated as shown in Equation 3.7.

$$P_{imbalance} = \sum P_G - (\sum P_{Load} + \sum P_{loss}) \quad (3.7)$$

In the pre-splitting phase, the total power generated by all the generators in the island is aggregated ($\sum P_G$). The load demand values ($\sum P_{Load}$) and the line losses ($\sum P_{loss}$) in the island are also aggregated and the difference between them shown in Equation 3.7 is calculated.

Step 2: Increase the generation capacity of slack bus to meet the power imbalance ($P_{imbalance}$) in the island.

In order to address the power imbalance in the island, the slack bus is tasked to compensate for the generation deficit. The slack bus can be increased further until its maximum power rating ($P_{Gmax(slack)}$). However if the slack bus maximum power rating has been met and there is still power imbalance as shown in Equation 3.8, then power imbalance is shared equally by the generators in the island.

$$P_{Gmax(slack)} - P_{imbalance} > 0 \tag{3.8}$$

Step 3: If the generation capacity has been increased to the maximum rating of the generators and the power balance criteria is still not met, the load shedding commences.

The load shedding is initiated if the power imbalance in the island is not met despite increasing all the generators in the island to their maximum generating capacity (P_{Gmax}). The load shedding technique is based on Equation 3.9.

$$\text{load shed}(\%) = \left(\frac{\text{Pimbalance}}{\sum P_G} \right) \times 100\% \tag{3.9}$$

Based on Equation 3.9, every active load in the system is reduced by the same load shed percentage. Once the load shedding is carried out, the power balance criteria is met.

The transmission line power flow analysis is then carried out to determine if the power flow (P_{flow}) violates the power rating of the lines (P_{max}). If the line ratings are not violated, the solution is deemed to be an optimum network splitting solution. However

if the transmission line ratings are violated, the algorithm will refer to the complete line configuration array to obtain the next best solution to be evaluated.

3.3 Post-Islanding Frequency Stability

The frequency stability is the main premise in the post-islanding stability phase for this investigation. In order to carry out this investigation, the automatic generation control (AGC) of the system is modeled. The system is modeled based on the areas and the number of interconnected generators within each area. The model will allow us to observe the frequency deviation and tie-line power of the system. In the post-islanding phase, the tie lines between the areas are disconnected and the generators operate in a deregulated environment. The control action is decentralized and the LFC in each area is tasked to regulate the frequency of the system. Figure 3.12 shows the block diagram of a typical control area *i (i = 1, 2 or 3)* which contains multiple (*n*) interconnected generators based on study carried out by (Rerkpreedapong et al., 2003).

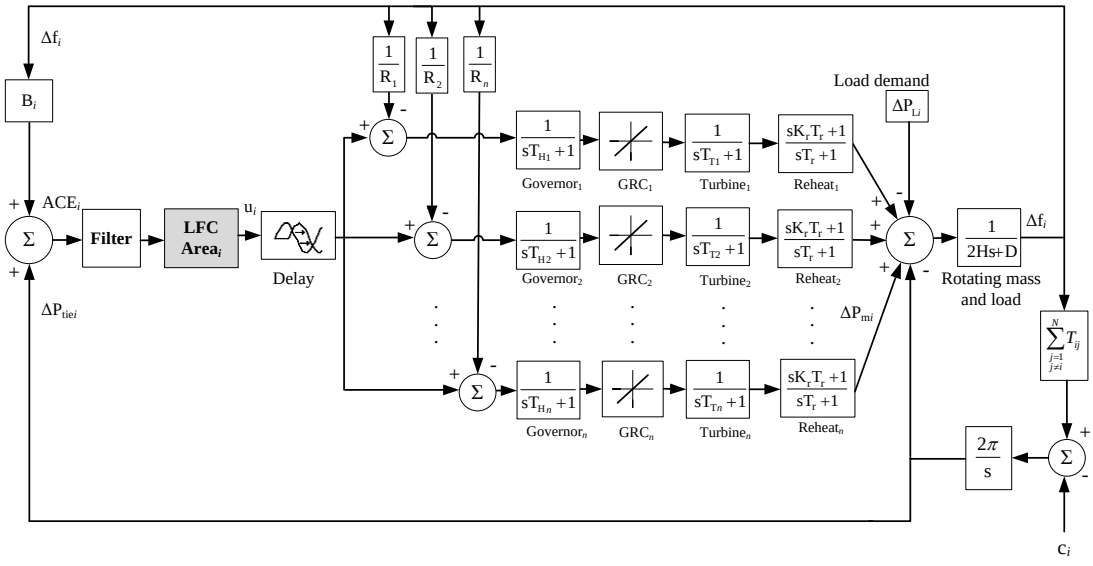

Figure 3.12: LFC model of control area *i* with *n* interconnected generators

The tie line equation can be defined as shown in Equation 3.10.

$$c_i = \sum_{\substack{j=1 \\ j \neq i}}^{N} T_{ij} \Delta f_j \tag{3.10}$$

where c_i is the area interface, T_{ij} represents the tie-line synchronizing coefficient between area i and j, $N = 1,2,\ldots\ldots$ represents the number of areas, $i = 1,2,\ldots\ldots$ and $j = 1,2,\ldots\ldots$ represents the corresponding area. The frequency deviation step response Δf_i and generator power response $\Delta P_{m,i}$ are the main outputs monitored and analyzed in LFC simulation study for post-islanding frequency stability. Various physical constraints should be considered in the AGC model of the power system to obtain a better response. This is important so that further analysis can be carried out while at the same time evaluating the practical behavior associated with the system. In this investigation, these physical constraints are incorporated into the power system model to further mimic the practical system and introduce non-linearities in the system:

1. Generation rate constraint (GRC): The GRC represents the physical limitation of the system so that the generation output is based on a specified rate. The standard GRC values used for the reheat thermal units are 3–10% pu MW/min (Lu et al., 1995).
2. Time delay:The time delay represents the time taken for the controller to react to changes in the system. The typical value for the time delay based on the LFC update rate is 2 seconds (Zhang et al., 2013).
3. Noise: The presence of high frequency noise in the system can impair the performance of the controller. Conventionally, the low pass filter is used to filter the ACE signal in order to reject fast control signal variation.

During post-islanding, the LFC plays a crucial role in maintaining frequency stability. The feedback mechanism of the LFC plays a major role in ensuring the load generation balance of the system is maintained. The Area Control Error (ACE) shown in Equation 3.11 characterizes the total deviation of the frequency (Δf) and tie-line power (ΔP_{tie}) of the system. The B represents the frequency bias factor.

$$ACE_i = \Delta P_{tie-i} + B_i \Delta f_i \tag{3.11}$$

The linear summation of these two properties (Δf and ΔP_{tie}) indicates the resultant error in the system and the ACE's value has to be driven to zero as fast as possible. This is to ensure that that the error is compensated in fastest time possible in order for the system to continue functioning in normal state of operation.

3.3.1 Multi objective optimization approach

Conventionally, only a single criterion such as the settling time or maximum overshoot is used to optimize the controller's parameters. In the multi objective optimization approach, both the settling time and maximum overshoot in the frequency deviation step response is considered. The main two performance criterion used to evaluate the transient closed loop response of the LFC in order to minimize the settling time and maximum overshoot are Integral of Time Multiplied Absolute Error (ITAE) and Integral of Time Weighted Squared Error (ITSE) (Killingsworth & Krstic, 2006). The ITAE formulation is shown in Equation 3.12 and the ITSE formulation is shown in Equation 3.13. The expressions of the objective functions are given as following:

$$ITAE = \int_0^t t.\left|ACE_i\right| dt \tag{3.12}$$

$$ITSE = \int_0^t t.\left(ACE_i\right)^2 dt \tag{3.13}$$

where t represents the simulation time. The ITSE imposes a time multiplier which will allow initial deviations but will penalize errors occurring later in time (Sepulveda et al., 2006). In other words, the ITSE provides a lower maximum overshoot value in the expense of a slightly higher settling time. The ITAE on the other hand allows larger overshoots with shorter settling time.

In order to realize the multi objective optimization, the weighted sum approach is considered. The weighted sum approach is one of the most easiest and practical

approach toward realizing the multi objective optimization. The weighted sum approach treats the multi objective optimization as a composite objective function (Hemamalini & Simon, 2010). The composite objective function is shown in Equation 3.14.

$$U = \sum_{i=1} w_i F_i(x) \tag{3.14}$$

where w_i are the positive weight values and $F_i(x)$ is the corresponding fitness function. Equation 3.14 is then minimized in order to find the optimal multi objective solution. In this investigation, it is our best interest to find the best compromise between two different objectives which are ITAE and ITSE. The expression of the multi objective composite function is as shown in Equation 3.15.

$$U = w_1 F_1(x) + w_2 F_2(x) \tag{3.15}$$

where w_1 and w_2 is the assigned weights and $F_1 = ITAE$ and $F_2 = ITSE$. The variable w_1 and w_2 are linked to each other based on the expression shown in Equation 3.16.

$$w_2 = 1 - w_1 \tag{3.16}$$

where w_1 is chosen is in the range of **[0 to 1]**. The weighted approach with a step size of 0.1 is chosen and the significance of the objective function is tuned based on the range of 0 to 1. In order to avoid the huge disparity in values between the two different objective functions, normalization is carried out. The normalization objective functions is a very important process as this allows the objective function to be scaled within the range of 0 to 1. The following normalization formula (Jain & Bhandare, 2011) expressed in Equation 3.17 is used:

$$fit_i' = \frac{fit_i - \min(fit_{overall}) x \delta}{\max(fit_{overall}) - \min(fit_{overall}) x \delta} \tag{3.17}$$

where fit_i represents the fitness to be normalized and $fit_{overall}$ represents the overall fitness. δ is chosen as 0.999 and is used to avoid zeroes during normalization process.

3.3.2 Objective function

In this investigation the PID controller is used. The reason why the PID controller is implemented is because the PID controller can further improve the performance of the LFC (Shabani et al., 2013). The PID controller's parameters are the proportional gain (K_p), integral time constant (T_i) and derivative time constant (T_d). The PID parameters are optimally tuned using the self-tuning algorithm (Astrom KJ & Hagglund T, 1995). The self-tuning algorithm which is a gain / parameter scheduling technique for the controller is shown in Figure 3.13.

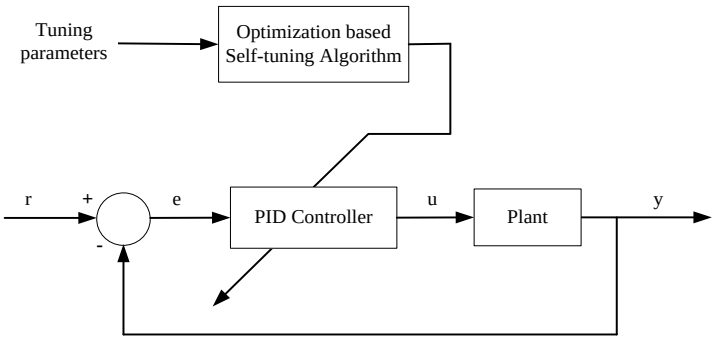

Figure 3.13: PID controller's self-tuning algorithm

The input to the controller is the ACE signal and based on this error value, the optimum set of controller's parameter – proportional gain (K_p), integral gain (K_i) and derivative gain (K_d) is tuned. The PID controller parameters are continuously tuned to accommodate the changes in the system and to obtain the optimum set of PID values to ensure stability in plant operation. The PID controller's expression is given as shown in Equation 3.18.

$$u_i = Kp_i(ACE_i + \frac{ACE_i}{sTi_i} + sTd_i ACE_i) \qquad i = 1,2,..... \tag{3.18}$$

where $K_i = K_p / T_i$ and $K_d = K_p * T_d$. The search space for the PID controller parameters are set in the range of [0.2,2] (Astrom KJ & Hagglund T, 1995; Gozde, Cengiz Taplamacioglu, et al., 2012).

3.3.3 Weightage value selection and performance index

In order to determine or select the proper weightage set, an index is proposed. This index would be able to provide the performance of each weightage set (w_{set}) towards the objective function. To evaluate the performance of each weightage set, a performance index based on the least average error (LAE) is proposed. The LAE is calculated using Equation 3.19.

$$LAE = \frac{\left(\frac{F_{1,w_{set,i}} - \min(F_{1,overall})}{\min(F_{1,overall})}\right) + \left(\frac{F_{2,w_{set,i}} - \min(F_{2,overall})}{\min(F_{2,overall})}\right)}{2} \tag{3.19}$$

where $F_{1,w_{set,i}}$ represents ITAE value and $F_{2,w_{set,i}}$ represents ITSE value at weightage set i (where $i = 1, 2 \ldots 11$). $F_{1,overall}$ and $F_{2,overall}$ represent the overall ITAE and ITSE values respectively. The performance index based on LAE (η_{LAE}) is expressed in Equation 3.20.

$$\eta_{LAE} = \frac{1}{LAE} \tag{3.20}$$

3.3.4 Multi objective optimization technique

In order to develop the multi objective optimization technique to optimize the controller's parameters, the continuous optimization methods are used. In this investigation the multi objective ABC optimization technique based on weight sum approach is implemented. However in order to validate the performance of the ABC optimization technique, a comparison is carried out against the multi objective PSO technique based on weighted sum.

3.3.4.1 Multi objective ABC optimization technique

The multi objective ABC based optimization technique is used in this investigation to tune the PID parameters of the LFC to ensure frequency stability in the islanded network. The advantages of the ABC optimization technique is shown in Chapter 2 (Section 2.8). The triple search capability which is one of the main advantages of ABC algorithm is able to find the optimal set of controller's parameters for each island. The application of ABC to tune the controller's parameters of the LFC has been recorded in many published works (Abedinia et al., 2011; Gozde, Taplamacioglu, et al., 2012; Javidan & Ghasemi, 2013; Jayanthi & Chidambaram, 2012; Paramasivam & Chidambaram, 2011; Rathor et al., 2011). One of the main strength of the ABC for the LFC problem is the adaptability to optimization technique to find the optimal set of controller parameters in various scenarios. The ABC based LFC has been able provide a robust performance even when it is used to tune two different objective functions (multi objective optimization). This further reinforces the choice of optimization technique to be used to tune the LFC in this research. The following steps show how the PID parameters are optimized using multi objective ABC optimization technique:

Initialization phase

Step 1: Define system parameters – number of colony size, number of food source, limit value, maximum iteration, and number of parameters, upper bound and lower bound.

Step 2: PID controller parameters for island *i* are randomly generated based on their upper bound, lower bound and number of colony size as shown in Equation 3.21.

$$PID\_param = rand(Food\_Number, Dimension) * Range + lb \quad (3.21)$$

where *PID_param* are the PID controller parameters (Kp_1,Ti_1,Td_1)

rand is the random number generator

Food_Number is the number of food source position

Dimension is the amount of variables to be optimized

Range is the difference between the upper bound (*ub*) value of 2 and lower bound (*lb*) value 0.2

Step 3: Objective value for each controller parameter set is calculated and pair of best PID parameters and best fitness function is stored. The objective functions are normalized based on Equation 3.17. The weightage set (w_1 and w_2) are then assigned to evaluate the composite objective function shown in Equation 3.22.

$$\text{Comp\_objfunc} = w_1 * \text{ObjFunc}_1 + w_2 * \text{ObjFunc}_2 \quad (3.22)$$

where *Comp_objfunc* represents the composite objective function

w_1 is the weight for first objective function

w_2 is the weight for second objective function

$ObjFunc_1$ is the ITAE objective function

$ObjFunc_2$ is the ITSE objective function

Employed Bee phase

Step 4: Modified PID controller parameters ($PID\_ param_{modified}$) are generated and if the PID parameter value is out of the predefined boundaries, the upper and lower bound value is taken. In order to produce the modified food solution, the following expression shown in Equation 3.23 is used.

$$v_{ij} = x_{ij} + \phi_{ij}\left(x_{ij} - x_{kj}\right) \quad (3.23)$$

where v_{ij} represents the modified food solution (modified PID parameters), x_{ij} represents the current food source, i represents the current iteration while j and k are random numbers with the condition that $k \neq i$. Φ_{ij} is a random number in the range of **[-1 to 1]**.

$$\text{if } (\text{PID\_ param}_{\text{modified}} > \text{ub})$$

$$\text{PID\_ param}_{\text{modified}} = \text{ub}$$

$$\text{if } (\text{PID\_ param}_{\text{modified}} < \text{lb})$$

$$\text{PID\_ param}_{\text{modified}} = \text{lb}$$

where $PID\_\ param_{modified}$ represents the modified PID parameters.

Step 5: Objective value for each modified solution is calculated and if better objective value is found, pair of best PID parameter and best fitness function is updated. If no better solution is found, trial counter is increased.

Step 6: The probability value of each solution is calculated based on the fitness value.

Onlooker Bee Phase

Step 7: Modified PID parameters based on the probability values are generated and if the parameter value is out of boundaries, the upper or lower bound value is taken. The food source's probability, ρ_i is calculated based on the expression shown in Equation 3.24.

$$\rho_i = \left(\frac{\alpha(fit_i)}{\max(fit_{overall})} \right) + \beta \qquad (3.24)$$

where fit_i represents the fitness value of the solution i as evaluated by the employed bees, and $max(fit_{overall})$ represents the maximum fitness value from the overall fitness derived from the employed bee phase ($fit_{overall} = fit_i, fit_{i+1}, \ldots . fit_{FN}$, where FN represents

the total number of food source). α and β represents the randomization variable which are typically in the range of [**0 to 1**]. The variable α and β are related based on Equation 3.25.

$$\beta = 1 - \alpha \tag{3.25}$$

where α is chosen as 0.9 and β as 0.1.

Step 8: Objective value for each modified solution is calculated and if better objective value is found, pair of best PID parameter and best fitness function is updated. If no better solution is found, trial counter is increased.

Scout Bee phase

Step 9: If the trial counter reaches limit value, random PID parameter confined to boundary values are generated. Any better solution found in this phase will be updated accordingly.

Repeat step 4 to step 9 until maximum iteration is reached. The optimum sets of PID parameters are obtained. A maximum iteration of 150 is defined as through trial and error it was found that the convergence towards global optima is obtained within this number of iteration.

3.3.4.2 Multi objective PSO technique

In order to verify and validate the performance of the multi objective ABC optimization technique, the multi objective PSO technique based on weighted sum is implemented. The PSO technique which is based upon the sociological behavior of birds flocking is used to find the global minima. The following steps show how the PID parameters are optimized using multi objective PSO technique:

Initialization phase

Step 1: Define system parameters – number of particles, maximum iteration, number of parameters, upper bound and lower bound.

Step 2: PID controller parameters for island *i* are randomly generated based on their upper bound, lower bound and number of colony size as shown in Equation 3.26.

$$\text{PID\_ param} = \text{rand(No\_particles, Dimension)} * \text{Range} + \text{lb} \quad (3.26)$$

where *PID_param* are the PID controller parameters (Kp_1,Ti_1,Td_1)

rand is the random number generator

No_particles is the number of particles

Dimension is the amount of variables to be optimized

Range is the difference between the upper bound (*ub*) value of 2 and lower bound (*lb*) value 0.2

Step 3: Objective value for each controller parameter set is calculated and pair of best PID parameters and best fitness function is stored. The objective functions are initially normalized based on Equation 3.17. The weightage set (w_1 and w_2) are then subsequently assigned to evaluate the composite objective function. Each particle's objective function is evaluated individually and stored as *pbest*. The groups best particle is evaluated and stored as *gbest*.

Particle update phase

Step 4: The movement of each particle (x_i) is based on a certain velocity (v_i). The speed of each particle changes according Equation 3.27.

$$v_i^{k+1} = w.v_i^k + c_1 r_1^k (p_{best_i}{}^k - x_i^k) + c_2 r_2^k (g_{best_i}{}^k - x_i^k) \quad (3.27)$$

where $i = 1,2,.....n_{swarm}$ (n_{swarm} = size of swarm derived from *No_particles*)

w is the inertia weight which is usually varied linearly from 0.9 to 0.4

r_1 and r_2 are random numbers in the range of [0,1]

c_1 and c_2 are acceleration factors and k represents the iteration number

Step 5: Modified PID controller parameters ($PID\_\ param_{modified}$) are generated based on the particle update function. The position of each particle is updated based on Equation 3.28.

$$x_i^{k+1} = x_i^{k} + v_i^{k+1} \tag{3.28}$$

where v_i represents the velocity

x_i represents the current PID parameter

x_i^{k+1} represents the updated PID parameter

If the PID parameter value is out of the predefined boundaries, the upper or lower bound value is taken.

$$\text{if } (\text{PID\_ param}_{\text{modified}} > \text{ub})$$

$$\text{PID\_ param}_{\text{modified}} = \text{ub}$$

$$\text{if } (\text{PID\_ param}_{\text{modified}} < \text{lb})$$

$$\text{PID\_ param}_{\text{modified}} = \text{lb}$$

Step 6: Objective value for each modified solution is calculated and if better objective value is found, pair of best PID parameter and best fitness function is updated. If no better solution is found, the current PID parameter remains.

Repeat step 4 to step 6 until maximum iteration is reached. The optimum sets of PID parameters are obtained. A maximum iteration of 150 is defined as through trial and error it was found that the convergence towards global optima is obtained within this number of iteration.

3.3.5 Wavelet filter

One of the focus of this research is to implement the online wavelet filter for the LFC of the islanded areas. The term online is used to denote that signals are filtered within a feedback control loop in real time. The wavelet transform is a signal processing technique which has been extensively used. The major advantage of wavelet transform is the ability of it to process the signal at different scale and resolutions (Graps, 1995). This process which is called the multiresolution analysis (MRA) is the main element of wavelet transform in extracting salient features from the signal. The discrete wavelet transform (DWT) which decomposes the signal in discreet manner is often used to obtain the high frequency and low frequency information from the signal. The details (high frequency) and approximation (low frequency) coefficients are obtained using DWT and the thresholding is applied to denoise the signal efficiently while maintaining signal integrity. Figure 3.14 shows how the wavelet transform is used to denoise the ACE signal.

Figure 3.14: Wavelet denoising overview

The input signal to the controller is the ACE. This ACE signal contains high frequency noise component. This signal is then processed using DWT to effectively denoise the signal and preserve the important information in the signal. In the wavelet transform phase, the signal is decomposed into its details and approximations. Then, the certain level of thresholding is applied to denoise the signal. The signal is then reconstructed using inverse wavelet transform and the denoised ACE signal is acquired. In this investigation, the daubechies wavelet of order 1 (db1) is selected as the default wavelet with five level of decomposition. The soft thresholding technique is applied to denoise the signal.

3.3.5.1 Wavelet filter implementation

The wavelet filter is designed using Matlab Simulink. The filter is then integrated to the LFC model. The input signal to the wavelet filter is the ACE signal. The filter design is shown in Figure 3.15.

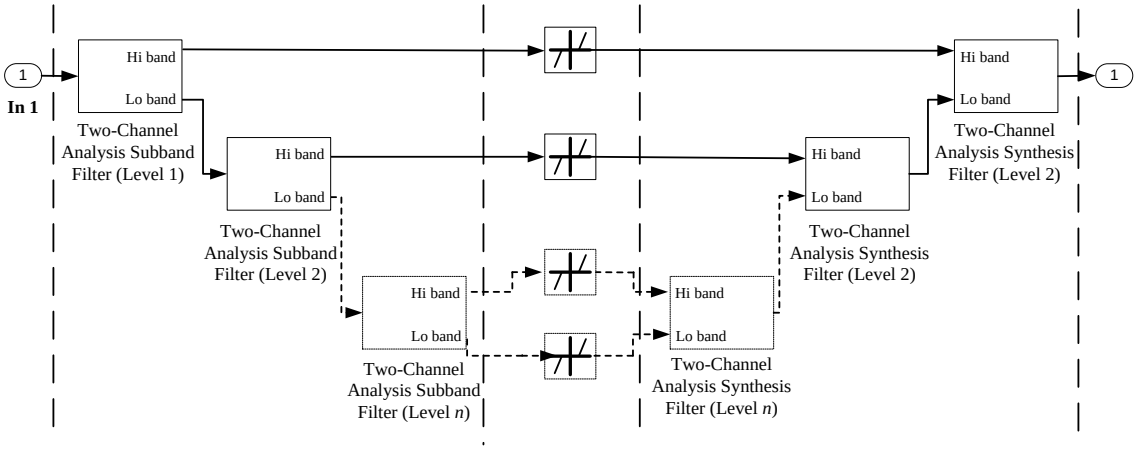

Figure 3.15: Wavelet filter design

Initially, the parameters of the wavelet are initialized based on the selected wavelet type. Once the input signal is obtained, the signal is decomposed into five levels of decomposition. The high frequency information (details) and low frequency information (approximations) are separated using a two channel subband filter. Soft thresholding is then applied on the wavelet coefficients to denoise the signal. Once the signal is denoised, it is reconstructed back using a two channel synthesis filter. The denoised signal is then propagated back to the LFC.

3.3.5.2 Signal integrity index

In order to evaluate the performance of the filter, the input signal to the filter which is the ACE has to be analyzed. The amount of noise present in the ACE signal will give a good indication on how well the filter has performed. In order to analyze the amount of noise present in the ACE signal, the Fast Fourier Transform (FFT) is carried out. Using the FFT, the signal is analyzed in the frequency domain. The important

characteristics of the signal are usually present in the form of low frequency while the noise is represented by the high frequency component. This can be seen in the clean ACE signal where the presence of high frequency noise is almost negligible. In this investigation, the Gaussian white noise function in Matlab Simulink is used to add the high frequency noise component in the LFC model.

In order to evaluate the amount of noise in the signal and further characterize the integrity of the signal, an index called signal integrity index is formulated. Initially based on the FFT, the statistical calculations shown in Equation 3.29 and Equation 3.30 are carried out:

$$sum_{\text{noise}} = \sum \left(\left| noise_i \right| \right) \tag{3.29}$$

$$mean_{\text{noise}} = \text{mean}\left(\left| noise_i \right| \right) \tag{3.30}$$

Once this information has been obtained, the signal integrity index as shown in Equation 3.31 is evaluated.

$$signal\ integrity\ index = \frac{(1/sum_{noise}) + (1/mean_{noise})}{2} \tag{3.31}$$

This index represents how clean and noise free the signal is. The complete structure of the system is shown Figure 3.16.

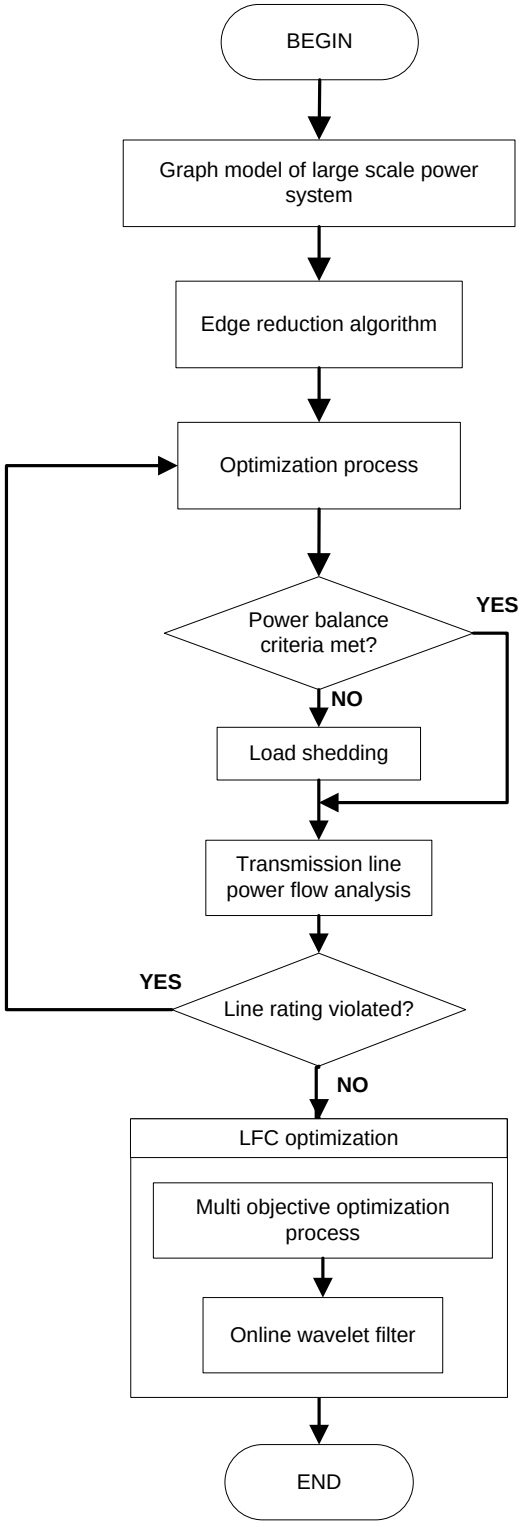

Figure 3.16: Complete network splitting flowchart

3.4 Summary

In this chapter, the proposed network splitting algorithm and load frequency control optimization is presented. The system methodology is divided into two phases. In the first phase, the optimum network splitting algorithm is shown. In order to obtain the

optimum network splitting solution, the large scale power system data containing the bus information and line configuration is initially processed by graph theory. The graph model of the large scale power system is built and the adjacency matrix of the system is obtained. This information is further used by the proposed edge reduction algorithm to reduce the search space of the power system. This initialization task is crucial in determining the optimal network splitting solution. As the combinatorial explosion of the search space is significantly reduced, the process to determine the optimal solution is hastened. This information is then fed into the proposed modified ABC optimization based on discrete values to obtain the optimal network splitting solution.

The load generation balance is further checked and load shedding is applied if it is required. The transmission line power flow analysis is then carried out to determine if the line ratings are violated. Once the optimum network splitting solution is obtained, the LFC optimization is carried out to determine the optimal LFC parameters for each islanded area. The multi objective ABC optimization based on weighted sum approach is used to determine the optimum set of PID control parameters. A performance index based on least average error (LAE) is formulated to evaluate the performance of the weightage set. The online wavelet filter is integrated in the LFC control area model to denoise the ACE signal. A signal integrity index is formulated to evaluate how clean and noise free the filtered signal is.

CHAPTER 4: VALIDATION OF PROPOSED OPTIMUM NETWORK SPLITTING ALGORITHM

4.1 Introduction

In this chapter, the proposed optimum network splitting algorithm developed in Chapter 3 is implemented. The algorithm is implemented for nine different test cases based on three different IEEE test systems. Initially the graph model of the test system is constructed. Subsequently the edge reduction algorithm is implemented to obtain the initial solution and finally the modified ABC optimization is carried out to determine the optimum network splitting solution. The optimum network splitting solution is also compared to results from reported investigation and modified PSO. The complete details of the islanding information and the one line diagram of the islanded solution are presented. The generator data of the IEEE test systems are included in the appendix section (Appendix A) and the graph model of the islanded solution is included in Appendix B.

4.2 Test System

In order to validate the effectiveness of the proposed optimum network splitting algorithm, three different test systems are used. These test systems are based on standard IEEE test systems obtained from the power systems test case archive (University of Washington, 1999). The maximum line rating for each test case is obtained from (Zimmerman et al., 2009) based on the double line configuration. The test systems used are:

a) IEEE 30-Bus Test System

In this test case, there are 6 generating units and 24 load buses. There are 41 lines in the system. The one line diagram of the test system is shown in Figure 4.1. The load flow analysis for this test system is shown in Table A-4.

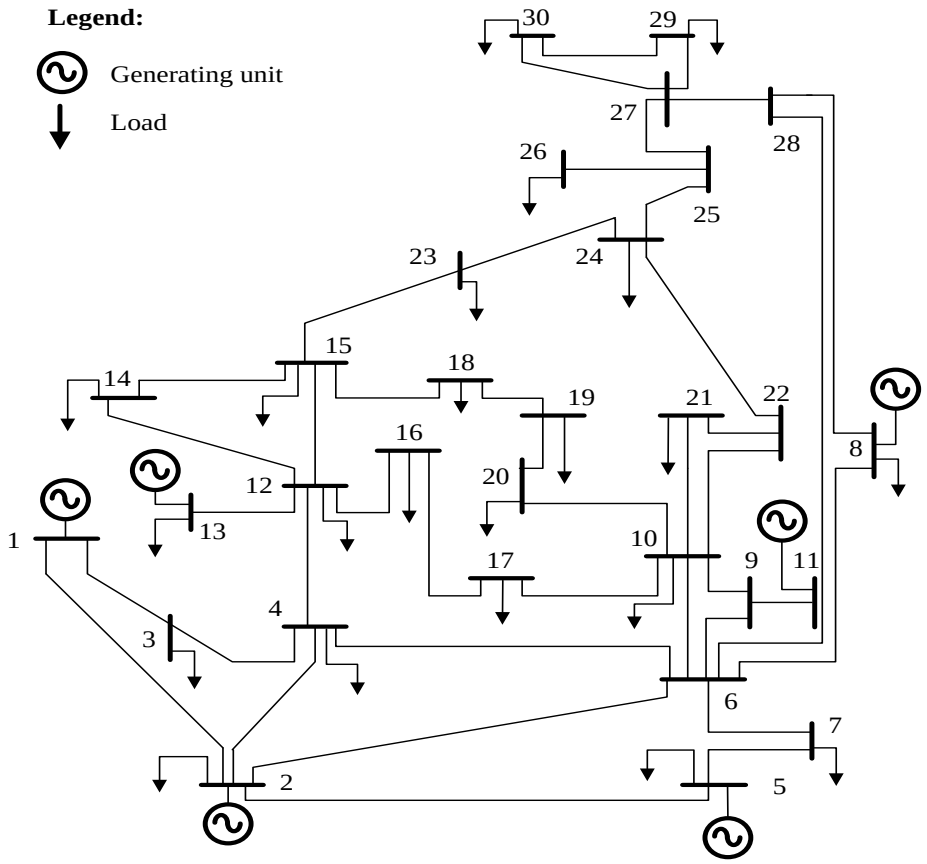

Figure 4.1: IEEE 30-bus test system one line diagram

b) IEEE 39-Bus Test System

This test case which is based upon the New England power system contains 10 generating units and 29 load buses. There are 46 lines in the system. A modified version of the IEEE 39-Bus test system with the same system parameters but with a different line configuration is also investigated. Figure 4.2 shows the one line diagram of the original IEEE 39-bus test system and Figure 4.3 shows the one line diagram of the modified IEEE 39-bus test system. The load flow

analysis for the original IEEE 39-bus and modified IEEE 39-bus test system is shown in Table A-5 and A-6 respectively.

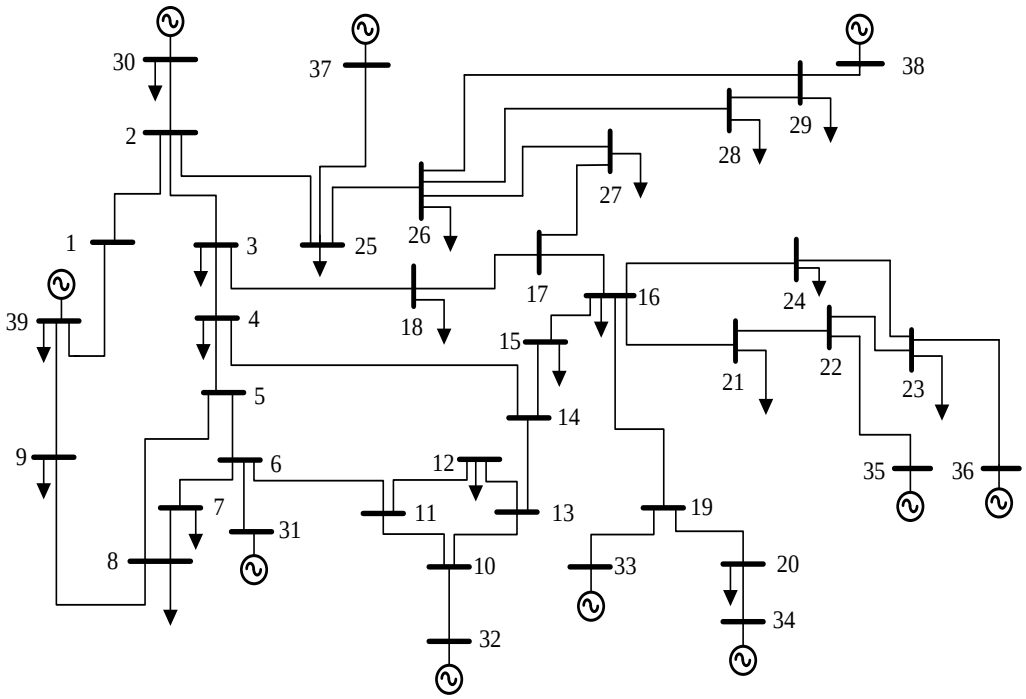

Figure 4.2: Original IEEE 39-bus test system one line diagram

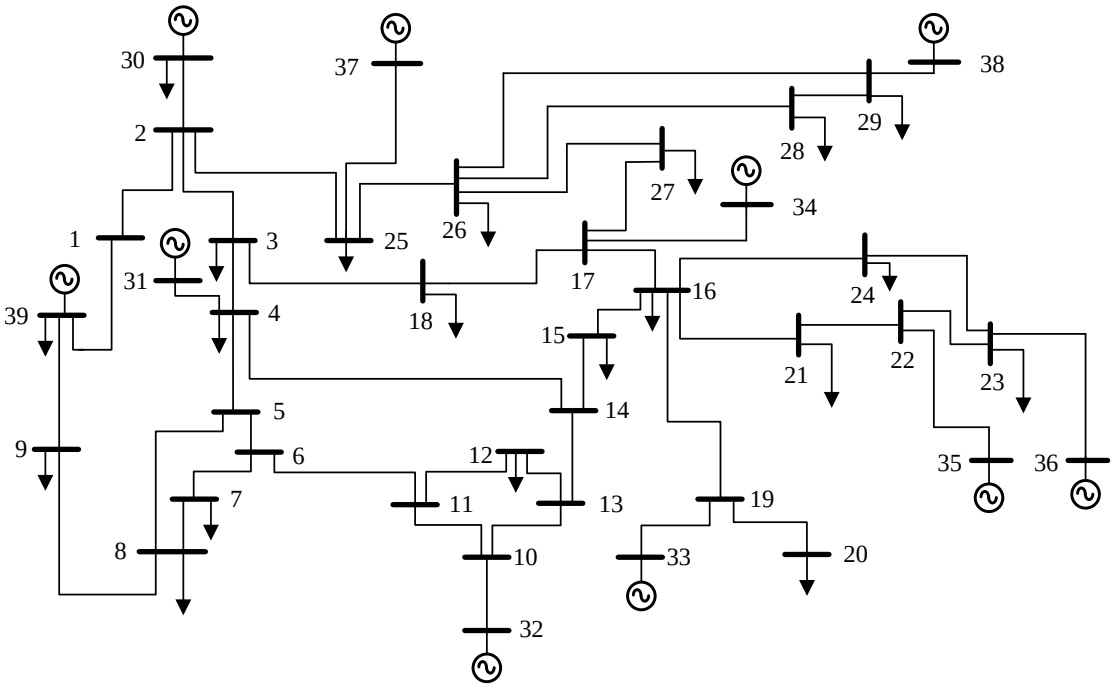

Figure 4.3: Modified IEEE 39-bus test system one line diagram

c) IEEE 118-Bus Test System

This test case contains 54 generating units and 64 load buses. However only 19 generating buses are considered as generating units while the other 35 buses are considered as loads due to insufficient amount of generation. There are 186 lines in the system. The one line diagram of the test system is shown in Figure 4.4. The load flow analysis for this test system is shown in Table A-7.

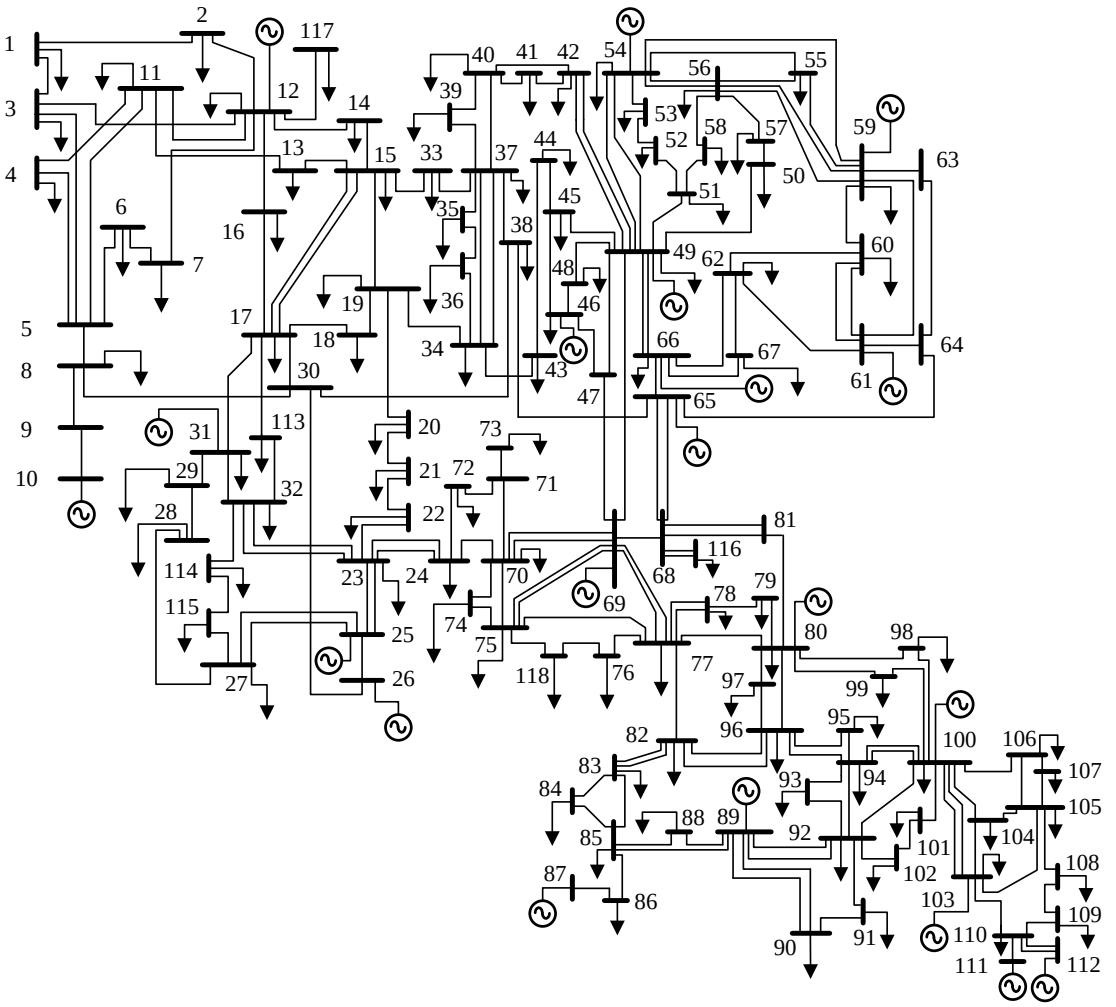

Figure 4.4: IEEE 118-bus test system one line diagram

In this chapter, the three test cases constituting of different coherency sets are evaluated for each test system. In total, there are nine test cases. In each case, the initial phase of investigation which is edge reduction is carried out to obtain the initial solution. The

modified ABC optimization is then carried out in the second phase of investigation to obtain the optimum network splitting solution.

4.3 Verification of Edge Reduction Algorithm

The edge reduction algorithm is important to determine the initial solution of the splitting problem. As explained in Chapter 3 (section 3.2.2), without an initial solution, it will take a large amount of time to determine the optimum network splitting solution. In order to verify this, an investigation is carried to compare the time taken to find the initial solution before the optimization process can be initiated. The investigation was carried out by comparing the time taken to find the initial solution based on three different initialization techniques explained in Chapter 3 (Section 3.2.2) for each test case. The techniques used are:

1. Random line configuration
2. Generator coherency path elimination
3. Edge reduction algorithm

Table 4.1 shows the information of time taken by each initialization technique.

Table 4.1: Simulation time information for different initialization technique

Initialization technique	**Time (s)**								
	IEEE 30-bus			**IEEE 39-bus**			**IEEE 118-bus**		
	t_{ave}	t_{min}	t_{max}	t_{ave}	t_{min}	t_{max}	t_{ave}	t_{min}	t_{max}
Random line configuration	4401.23	1251.15	11582.67	NA	NA	NA	NA	NA	NA
Generator coherency path elimination	1323.35	242.52	3263.78	NA	230.21	NA	NA	NA	NA
Edge reduction algorithm	0.76	0.69	0.87	0.82	0.71	0.99	7.39	7.18	7.74

NA – Not Available (initial solution not available after simulation of more than 24 hours)

The average time (t_{ave}) taken for each algorithm is evaluated based on ten separate runs. The maximum (t_{max}) and minimum (t_{min}) values of the time taken by each algorithm are also shown. The simulations are carried out on Case 1 of IEEE 30-bus, Case 6 of IEEE 39-bus and Case 9 of IEEE 118-bus to verify the performance of the edge reduction algorithm. It can be seen that for the IEEE 39-bus and IEEE-118 bus, the time taken to find the initial solution based on random line configuration was not available after simulation **(NA)** of more than 24 hours. The generator coherency path elimination on the other hand is able to find the solution for the IEEE 30-bus test system. However the average time taken is around 22 minutes. In the IEEE-39 bus test system, an initial solution was found 230.21s in one of the runs. However, this only happened once in the ten runs.

The edge reduction algorithm is not an iterative based procedure but rather a strategy to detect the possible lines that can be disconnected in order to obtain the initial islanding solution. Based on the information shown, it can be seen that the edge reduction algorithm requires minimal amount of time to find the initial solution compared to the other two initialization techniques. The simulation time for the IEEE 118-bus test system requires a bit more time compared to the other test systems due to the complexity of the network.

4.4 Case 1: IEEE 30-Bus Test System (Coherency set 1)

Figure 4.5 shows the graph model of the IEEE 30-bus test system. The numbered vertices represent the buses in the system and the bidirectional edges represent the transmission lines in the system.

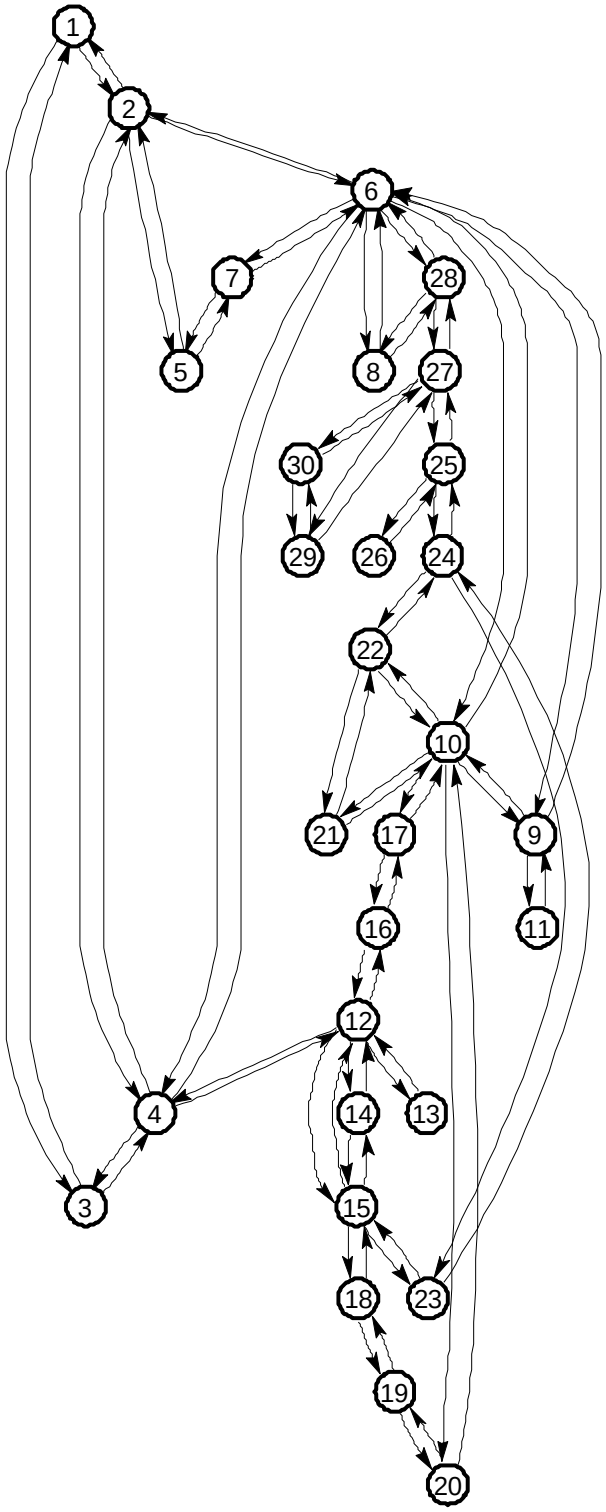

Figure 4.5: Graph model of IEEE 30-bus test system

4.4.1 First Phase: Edge reduction for Case 1

In this case, the IEEE 30-bus test system is analyzed based on investigation presented by (W. Liu et al., 2007). The system parameters as reported by (W. Liu et al., 2007) are listed in Table 4.2.

Table 4.2: System Parameters for Case 1

Desired number of islands:	2
Coherent group of generators:	Group 1 = {1, 2, 5, 13}
	Group 2 = {8, 11}

In the first phase of investigation, the edge reduction algorithm is carried out to determine the initial number of transmission lines which needs to be disconnected to result in the desired number of islands with the coherent group of generators. The red lines indicate transmission lines which remains intact while the blue lines indicate transmission lines that are disconnected. The edge reduction algorithm is applied for the IEEE 30-bus test system as shown in Figure 4.6. The initial search space of 41 possible transmission line combinations ($\approx 2.199 \times 10^{12}$) is reduced to 7 lines as an initial solution.

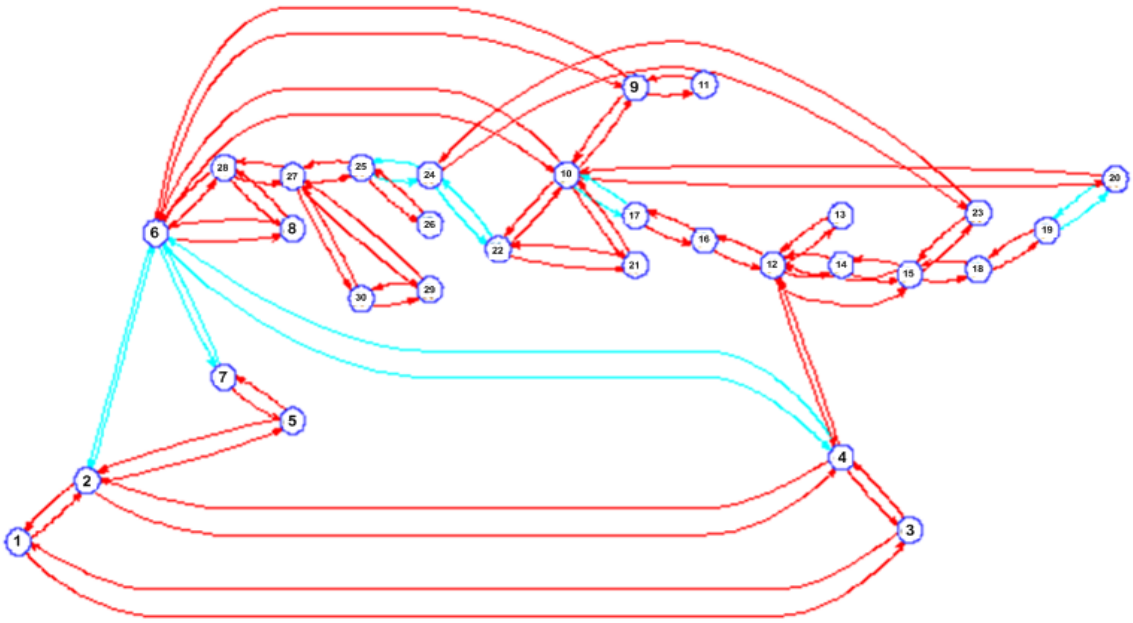

Figure 4.6: Edge reduction algorithm for Case 1

Table 4.3: Initial network splitting solution for Case 1

Initial splitting solution	Power flow (MW)
2 – 6	61.93
4 – 6	71.07
6 – 7	37.52
10 – 17	5.78
19 – 20	6.91
22 – 24	5.6
24 – 25	1.7
$\sum P_{min}$	190.53

Table 4.3 shows the initial network splitting solution obtained after the edge reduction algorithm has been implemented. The initial minimal power-flow disruption obtained ($\sum P_{min}$) is 190.53 MW. This initial solution is then passed on to the second phase to find the optimum network splitting solution.

4.4.2 Second Phase: Modified ABC optimization for Case 1

The proposed modified ABC optimization is applied to the test system and the optimum network splitting solution is obtained for the test case as shown in Table 4.4. The optimum number of lines to be disconnected is six and the minimal power-flow disruption obtained is 154.69 MW. This optimized minimal power-flow disruption value is lower than the reported value of 190.53 MW based on the reported investigation (W. Liu et al., 2007) and value of 182.93 MW based on the modified PSO. Furthermore, the number of lines disconnected is also lower than the reported value.

Table 4.4: Optimum network splitting solution for Case 1

Reported investigation (W. Liu et al., 2007)	Power flow (MW)	Modified PSO	Power flow (MW)	Modified ABC	Power flow (MW)
2 – 6	61.93	2 – 6	61.93	2 – 6	61.93
4 – 6	71.07	4 – 6	71.07	4 – 6	71.07
6 – 7	37.52	5 – 7	14.36	5 – 7	14.36
10 – 17	5.78	6 – 9	28.25	16 – 17	3.24
19 – 20	6.91	16 – 17	3.24	18 – 19	2.61
22 – 24	5.6	18 – 19	2.61	23 – 24	1.47
24 – 25	1.7	23 – 24	1.47		
$\sum P_{min}$	190.53	$\sum P_{min}$	182.93	$\sum P_{min}$	154.69

Figure 4.7 shows the one line diagram of the islanding solution. The graph model of the islanding solution is shown in appendix B (Figure B-1).

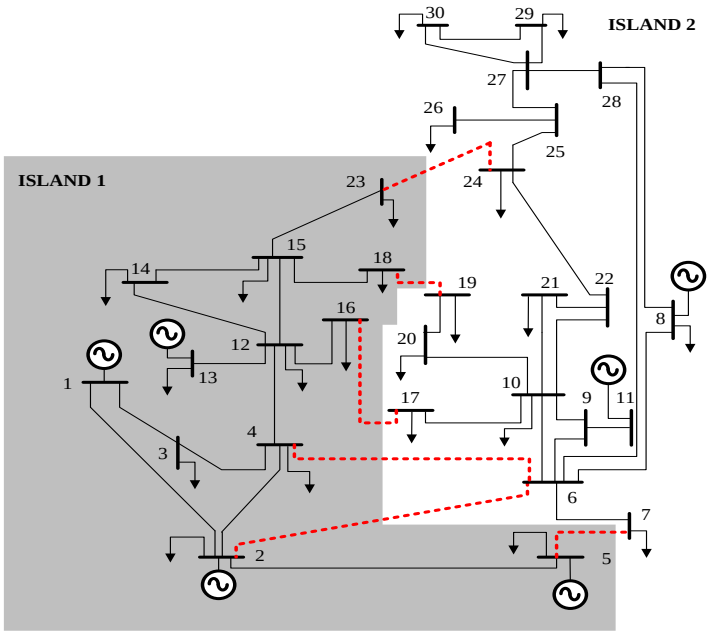

Figure 4.7: Islanding solution for case 1

Figure 4.8 shows the convergence curve for case 1 of both optimization techniques. The figure shows that the modified ABC based on discrete values is able to achieve the global minima compared to the modified PSO based on discrete values.

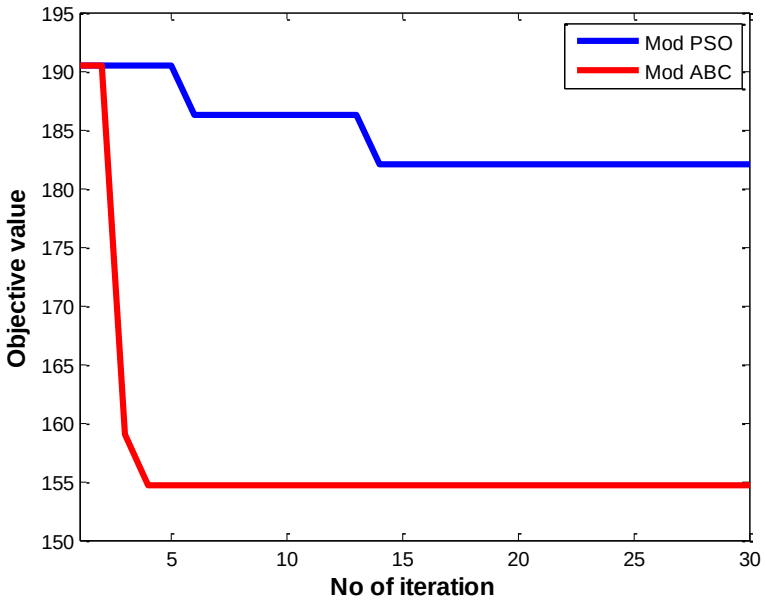

Figure 4.8: Convergence curve for Case 1

Table 4.5: First island information for Case 1

Buses 12 (1 – 5, 12 – 16, 18, 23)		
Generating Bus	**Pre-Splitting**	**Post-Splitting**
1*	261.13	128.01
2	40	40
5	0	0
13	0	0
$\sum P_{Generation}$ (MW)	301.13	168.01
$\sum P_{Load}$ (MW)	161.4	161.4
$\sum P_{Loss}$ (MW)	16.44	6.61
$\sum P_{imbalance}$ (MW)	123.29	0

**** slack bus***

Table 4.5 shows the islanding information for island 1. The pre-splitting column indicates the generation value (P_G) and load demand (P_{Load}) in each island before bus data reassignment is carried out. In island 1, a significant value in surplus power ($P_{imbalance}$) of 123.29 MW is available. This is due to the fact that the slack bus (Bus 1) is located in this island. The generator data detailing the maximum generation of each bus is given in Table A-1. Bus data reassignment is carried out based on the new line configuration in island 1 and load flow is carried out determine the new power flow in the transmission lines and the slack bus. The generation value in the slack bus is reduced to meet the power balance in the island as shown in the post-splitting column.

Table 4.6: Second island information for Case 1

Buses 18 (6 – 11, 17, 19 – 22, 24 - 30)		
Generating Bus	**Pre-Splitting**	**Post-Splitting**
8	0	61.71*
11	0	61.65
$\sum P_{Generation}$ (MW)	0	123.36
$\sum P_{Load}$ (MW)	122	122
$\sum P_{Loss}$ (MW)	1.3	1.36
$\sum P_{imbalance}$ (MW)	-123.3	0

**** slack bus***

Table 4.6 shows the islanding information for island 2. In island 2, a huge deficit in generation of 123.3 MW is experienced due to the fact that in this particular test case, the slack bus which is responsible for the total generation of power in the system is located in Island 1. As such, bus data reassignment is carried out and bus 8 is chosen as the slack bus. However, the deficit value is far larger than the maximum generation

capability of bus 8 which is 100 MW as seen in Table A-1. In order to address the deficit in generation value, the load demand is shared equally by generating bus 8 and 11 (PV bus). The post-splitting column shows that the load-generation balance in the island is met. In both islands, we can observe that the load-generation balance is maintained. The line losses are also taken into account to ensure that proper power balance criteria are met.

Table 4.7 shows the power flow in each of the lines after the large scale power system has been split into two islands. This analysis is carried out to ensure that there is no overloading once the islands are formed. P_{flow} denotes the power flowing in the lines and the P_{max} represents the maximum power rating of the lines. The P_{util} *(%)* shows the percentage of power utilized by the respective transmission lines. The results show that the power flow is well within the maximum allowable capacity of the transmission lines.

Table 4.7: Transmission Lines Power Flow Analysis for Case 1

Parameters of transmission lines in island 1					**Parameters of transmission lines in island 2**				
From Bus	**To Bus**	**P_{flow}**	**P_{max}**	**P_{util} (%)**	**From Bus**	**To Bus**	**P_{flow}**	**P_{max}**	**P_{util} (%)**
1	2	93.44	208	44.92	6	7	22.97	208	11.04
1	3	34.57	208	16.62	6	8	24.24	51.2	47.34
2	4	11.84	104	11.39	6	9	12.16	104	11.69
2	5	98.41	208	47.31	6	10	5.32	51.2	10.39
3	4	31.69	208	15.23	6	28	8.03	51.2	15.69
4	12	35.73	104	34.36	8	28	7.47	51.2	14.59
12	13	0.00	104	0.00	9	10	49.49	104	47.59
12	14	6.84	51.2	13.35	9	11	61.65	104	59.28
12	15	14.18	51.2	27.70	10	17	9.04	51.2	17.65
12	16	3.51	51.2	6.86	10	20	11.90	51.2	23.23
14	15	0.58	25.6	2.26	10	21	18.61	51.2	36.35
15	18	3.20	25.6	12.50	10	22	9.47	51.2	18.49
15	18	3.21	25.6	12.54	19	20	9.54	51.2	18.63
					21	22	0.94	51.2	1.84
					22	24	10.33	25.6	40.33
					24	25	1.47	25.6	5.75
					25	26	3.55	25.6	13.87
					25	27	2.13	25.6	8.34
					27	28	15.45	104	14.86
					27	29	6.21	25.6	24.24
					27	30	7.11	25.6	27.78
					29	30	3.71	25.6	14.49

The optimum network splitting algorithm is able to scour the search space and find the optimal network splitting solution which adheres to the system constraints. The network splitting solution is deemed optimum only after load-generation balance constraint and transmission line power flow constraint is met. In this case, load shedding algorithm is not initiated as the generating unity capacity is available to meet the load demand in each island.

4.5 Case 2: IEEE 30-Bus Test System (Coherency set 2)

4.5.1 First Phase: Edge reduction for Case 2

In this case, the IEEE 30-bus test system with a different group of coherent generators set is analyzed. The system parameters as reported by (W. Liu et al., 2007) are listed in Table 4.8.

Table 4.8: System Parameters for Case 2

Desired number of islands:	2
Coherent group of generators:	Group 1 = {1, 2, 5, 8, 13}
	Group 2 = {11}

In the first phase of investigation, the edge reduction algorithm is carried out to determine the initial number of transmission lines which needs to be disconnected to result in the desired number of islands with the coherent group of generators. The red lines indicate transmission lines which remain intact while the blue lines indicate transmission lines that are disconnected. The edge reduction algorithm is applied for the IEEE 30-bus test system as shown in Figure 4.9. The initial search space is reduced to 5 lines as an initial solution.

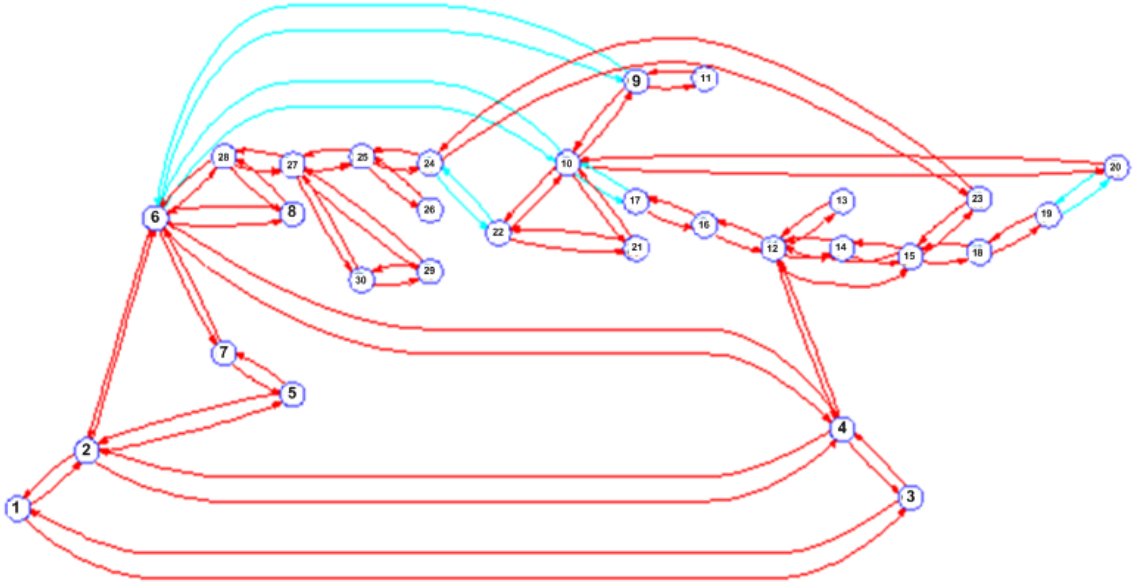

Figure 4.9: Edge reduction algorithm for Case 2

Table 4.9: Initial network splitting solution for Case 2

Initial splitting solution	Power flow (MW)
6 – 9	28.25
6 – 10	15.83
10 – 17	5.78
19 – 20	6.91
22 – 24	5.6
$\sum P_{min}$	62.37

Table 4.9 shows the initial network splitting solution obtained after the edge reduction algorithm has been implemented. The initial minimal power-flow disruption obtained ($\sum P_{min}$) is 62.37 MW. This initial solution is then passed on to the second phase to find the optimum network splitting solution.

4.5.2 Second Phase: Modified ABC optimization for Case 2

The proposed modified ABC optimization is applied to the test system and the optimum network splitting solution is obtained for the test case as shown in Table 4.10. The optimum number of lines to be disconnected is six and the minimal power-flow disruption obtained is 53.11 MW. This optimized minimal power-flow disruption value is lower than the reported value of 66.53 MW based on the reported investigation (W. Liu et al., 2007) and value of 57.23 MW based on the modified PSO.

Table 4.10: Optimum network splitting solution for Case 2

Reported investigation (W. Liu et al., 2007)	Power flow (MW)	Modified PSO	Power flow (MW)	Modified ABC	Power flow (MW)
6 – 9	28.25	6 – 9	28.25	6 – 9	28.25
6 – 10	15.83	6 – 10	15.83	6 – 10	15.83
10 – 20	9.2	16 – 17	3.24	16 – 17	3.24
15 – 23	4.72	18 – 19	2.61	18 – 19	2.61
16 – 17	3.2	22 – 24	5.6	23 – 24	1.47
25 – 27	5.29	24 – 25	1.70	24 – 25	1.70
$\sum P_{min}$	66.53	$\sum P_{min}$	57.23	$\sum P_{min}$	53.11

Figure 4.10 shows the one line diagram of the islanding solution. The graph model of the islanding solution is shown in appendix B (Figure B-2).

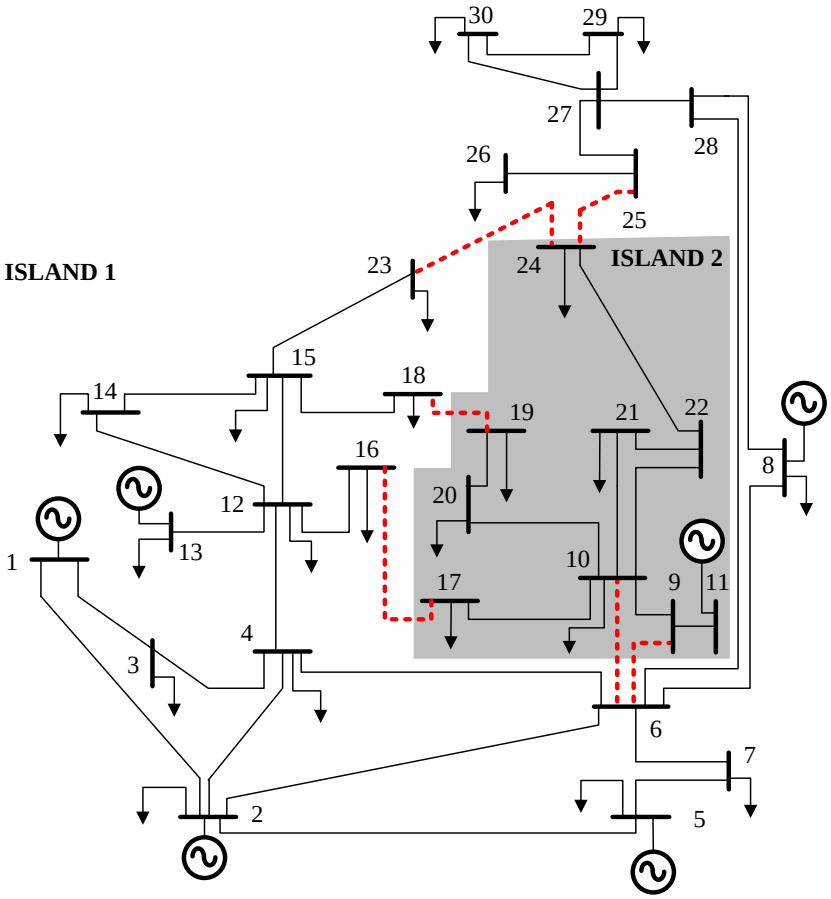

Figure 4.10: Islanding solution for case 2

Figure 4.11 shows the convergence curve for case 2 of both optimization techniques. The figure shows that the modified ABC based on discrete values is able to achieve the global minima compared to the modified PSO based on discrete values.

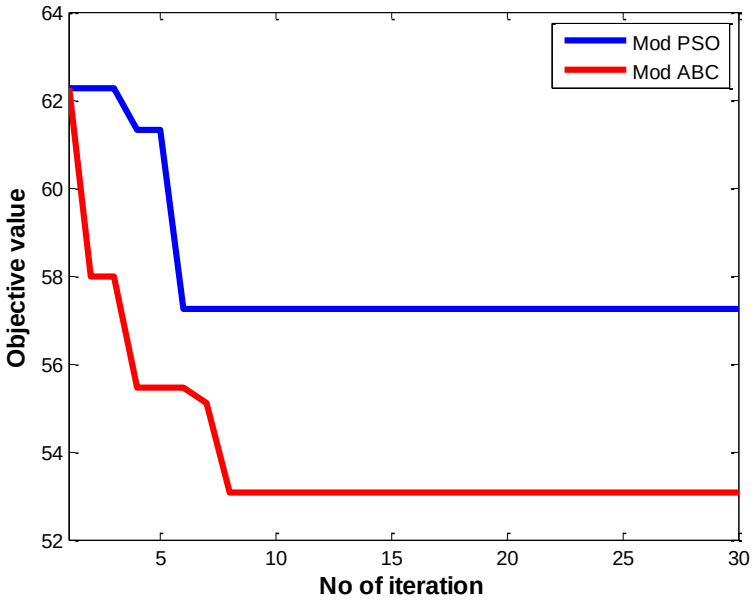

Figure 4.11: Convergence curve for Case 2

Table 4.11: First island information for Case 2

Buses 21 (1 – 8, 12 – 16, 18, 23, 25 – 30)		
Generating Bus	**Pre-Splitting**	**Post-Splitting**
1*	261.13	202.03
2	40	40
5	0	0
8	0	0
13	0	0
$\sum P_{Generation}$ (MW)	301.13	242.03
$\sum P_{Load}$ (MW)	230.7	230.7
$\sum P_{Loss}$ (MW)	17.36	11.33
$\sum P_{imbalance}$ (MW)	53.07	0

**** slack bus***

Table 4.11 shows the islanding information for island 1. In island 1, a surplus power ($P_{imbalance}$) of 53.07 MW is available. This is similar to Case 1, as the slack bus (Bus 1) is located in this island. Bus data reassignment is carried out based on the new line configuration in island 1 and load flow is carried out determine the new power flow in the transmission lines and the slack bus. The generation value in the slack bus is then reduced to 202.03 MW to meet the power balance in the island as shown in the post-splitting column.

Table 4.12: Second island information for Case 2

Buses 9 (9 – 11, 17, 19 – 22, 24)		
Generating Bus	**Pre-Splitting**	**Post-Splitting**
11	0	53.37*
$\sum P_{Generation}$ **(MW)**	0	53.37
$\sum P_{Load}$ **(MW)**	52.7	52.7
$\sum P_{Loss}$ **(MW)**	0.37	0.67
$\sum P_{imbalance}$ **(MW)**	-53.07	0

**** slack bus***

Table 4.12 shows the islanding information for island 2. In island 2, a deficit in generation of 53.07 MW is experienced. This is due to the fact that the slack bus is located in Island 1. As such, bus data reassignment is carried out and bus 11, which is the only generation bus in island 2 is chosen as the slack bus. Since the load imbalance value is less than the maximum generation capacity of bus 11, no load shedding is required. The bus 11 takes the role as slack bus and provides the generation capacity for the loads attached in the particular island. The post-splitting column shows that the load-generation balance in the island is met.

The transmission line power flow analysis is carried out and results show that that the power flow is well within the maximum allowable capacity of the transmission lines. The complete result of the transmission line power flow analysis is included in the Appendix section (Table B-1).

4.6 Case 3: IEEE 30-Bus Test System (Coherency set 3)

4.6.1 First Phase: Edge reduction for Case 3

In this case, the IEEE 30-bus test system based on a different group of coherent generators set is analyzed. The system parameters as reported by (Zhao et al., 2003) are listed in Table 4.13.

Table 4.13: System Parameters for Case 3

Desired number of islands:	3
Coherent group of generators:	Group 1 = {1, 2, 5, 13}
	Group 2 = {8}
	Group 3 = {11}

In the first phase of investigation, the edge reduction algorithm is carried out to determine the initial number of transmission lines which needs to be disconnected to result in the desired number of islands with the coherent group of generators. The edge reduction algorithm is applied for the IEEE 30-bus test system as shown in Figure 4.12. The initial search space is reduced to 9 lines as an initial solution.

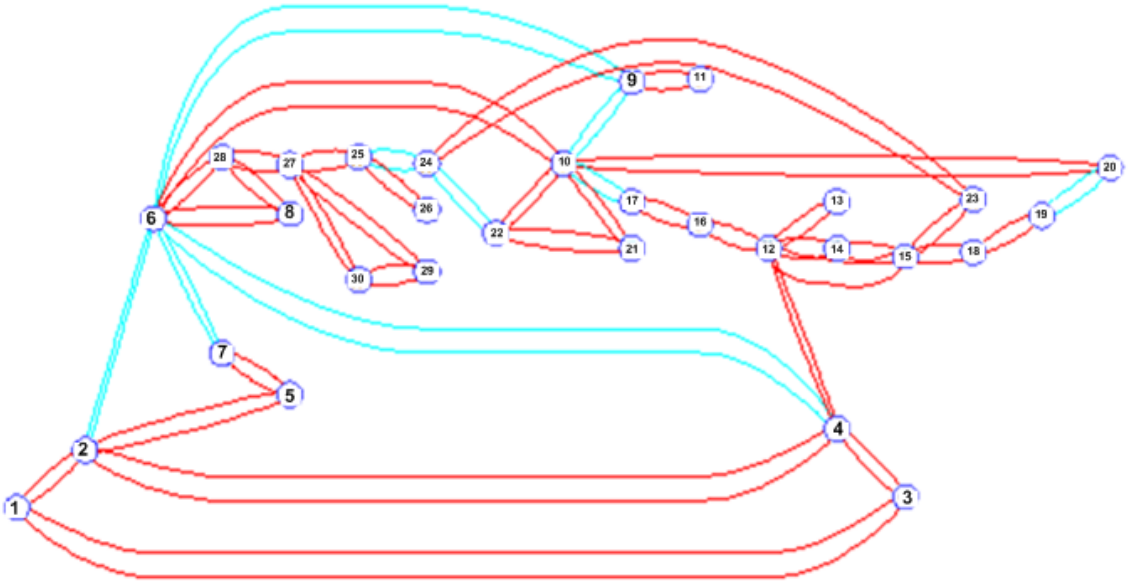

Figure 4.12: Edge reduction algorithm for Case 3

Table 4.14: Initial network splitting solution for Case 3

Initial splitting solution	**Power flow (MW)**
2 – 6	61.93
4 – 6	71.07
6 – 7	37.52
6 – 9	28.25
9 – 10	28.25
10 – 17	5.78
19 – 20	6.91
22 – 24	5.60
24 – 25	1.70
$\sum P_{min}$	247.02

Table 4.14 shows the initial network splitting solution obtained after the edge reduction algorithm has been implemented. The initial minimal power-flow disruption obtained ($\sum P_{min}$) is 247.02 MW. This initial solution is then passed on to the second phase to find the optimum network splitting solution.

4.6.2 Second Phase: Modified ABC optimization for Case 3

The proposed modified ABC optimization is applied to the test system and the optimum network splitting solution is obtained for the test case as shown in Table 4.15. The optimum number of lines to be disconnected is eight and the minimal power-flow disruption obtained is211.18 MW. This optimized minimal power-flow disruption value is lower than the reported value of 242.94 MW based on the reported investigation (W. Liu et al., 2007; Zhao et al., 2003) and value of 230.80 MW based on the modified PSO. Furthermore, the number of lines disconnected is also lower than the reported value and the modified PSO technique.

Table 4.15: Optimum network splitting solution for Case 3

Reported investigation (W. Liu et al., 2007; Zhao et al., 2003)	**Power flow (MW)**	**Modified PSO**	**Power flow (MW)**	**Modified ABC**	**Power flow (MW)**
2 – 6	61.93	2 – 6	61.93	2 – 6	61.93
4 – 6	71.07	4 – 6	71.07	4 – 6	71.07
6 – 7	37.52	5 – 7	14.36	5 – 7	14.36
6 – 9	29.62	6 – 9	28.25	6 – 9	28.25
6 – 28	19.14	6 – 28	19.14	9 – 10	28.25
10 – 17	5.78	8 – 28	0.48	16 – 17	3.24
10 – 22	7.57	9 – 10	28.25	18 – 19	2.61
19 – 20	6.91	16 – 17	3.24	23 – 24	1.47
21 – 22	1.91	18 -19	2.61		
23 – 24	1.47	23 – 24	1.47		
$\sum P_{min}$	242.94	$\sum P_{min}$	230.80	$\sum P_{min}$	211.18

Figure 4.13 shows the one line diagram of the islanding solution. The graph model of the islanding solution is shown in appendix B (Figure B-3).

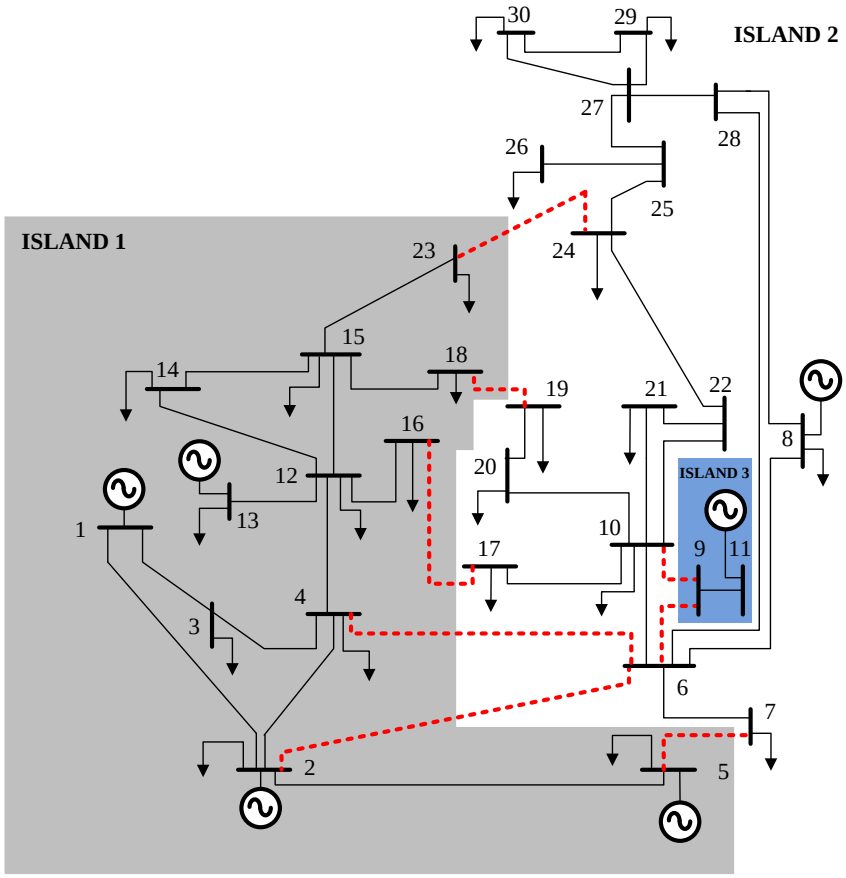

Figure 4.13: Islanding solution for case 3

Figure 4.14 shows the convergence curve for case 3 of both optimization techniques. The figure shows that the modified ABC based on discrete values is able to achieve the global minima compared to the modified PSO based on discrete values.

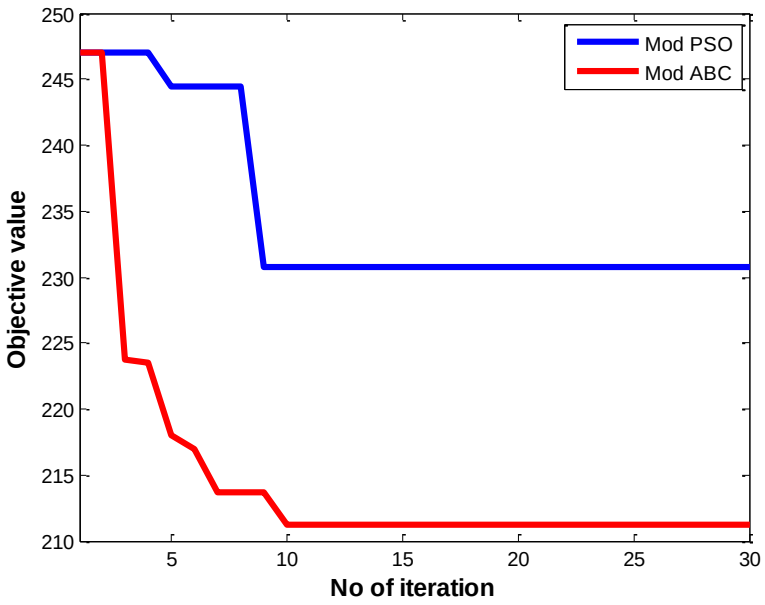

Figure 4.14: Convergence curve for Case 3

Table 4.16: First island information for Case 3

Buses 12 (1 – 5, 12 – 16, 18, 23)		
Generating Bus	**Pre-Splitting**	**Post-Splitting**
1*	261.13	128.01
2	40	40
5	0	0
13	0	0
$\sum P_{Generation}$ (MW)	301.13	168.01
$\sum P_{Load}$ (MW)	161.4	161.4
$\sum P_{Loss}$ (MW)	16.44	6.61
$\sum P_{imbalance}$ (MW)	123.29	0

**** slack bus***

Table 4.16 shows the islanding information for island 1. In island 1, a surplus power ($P_{imbalance}$) of 123.29 MW is available. The slack bus (Bus 1) is located in this island. Bus data reassignment is carried out based on the new line configuration in island 1 and load flow is carried out determine the new power flow in the transmission lines and the slack bus. The generation value in the slack bus is then reduced to 128.01 MW to meet the power balance in the island as shown in the post-splitting column.

Table 4.17: Second island information for Case 3

Buses 16 (6 – 8, 10, 17, 19 – 22, 24 – 30)		
Generating Bus	**Pre-Splitting**	**Post-Splitting**
8	0	96.24*
$\sum P_{Generation}$ (MW)	0	96.24
$\sum P_{Load}$ (MW)	122	93.57
$\sum P_{Loss}$ (MW)	1.3	2.67
$\sum P_{imbalance}$ (MW)	-123.3	0

**** slack bus***

Table 4.17 shows the islanding information for island 2. In island 2, a deficit in generation of 123.3MW is experienced. This is due to the fact that the slack bus is located in Island 1. As such, bus data reassignment is carried out and bus 8, which is the only generation bus in island 2 is chosen as the slack bus. However, the power imbalance value is greater than the maximum generation capability of generator (bus 8) which is at 100 MW as seen in Table A-1. Since there are no other generator buses to share the load, load shedding has to be initiated. The load shedding percentage was 23.30%. This means total amount of 28.43 MW of load has been shed. The post-

splitting column shows that the generator is now providing 96.24 MW and subsequently the load-generation balance in the island is met.

Table 4.18: Third island information for Case 3

Buses 2 (9, 11)		
Generating Bus	**Pre-Splitting**	**Post-Splitting**
11	0	0*
$\sum P_{Generation}$ **(MW)**	0	0
$\sum P_{Load}$ **(MW)**	0	0
$\sum P_{Loss}$ **(MW)**	0	0
$\sum P_{imbalance}$ **(MW)**	0	0

**** slack bus***

In the third island, there are only two buses which are bus 9 and bus 11. Since bus 9 is not connected to any load, then bus 11, which takes the role of generator bus is not providing any power. This can be seen in pre-splitting and post-splitting column in Table 4.18 as no power flow is recorded between the generator and load. This case is similar to case 1 with the only difference being that the island 2 only contains a single generator bus (bus 8). As such it can be observed the results are similar for island 1 and the algorithm reacts to changes accordingly for island 2. This shows the adaptability of the algorithm to deal with different scenarios which can arise in the network splitting scenario.

The transmission line power flow analysis is carried out and results show that that the power flow is well within the maximum allowable capacity of the transmission lines. The complete result of the transmission line power flow analysis is included in the Appendix section (Table B-2).

4.7 Case 4: IEEE 39-Bus Test System (Coherency set 1)

Figure 4.15 shows the graph model of the original IEEE 39-bus test system.

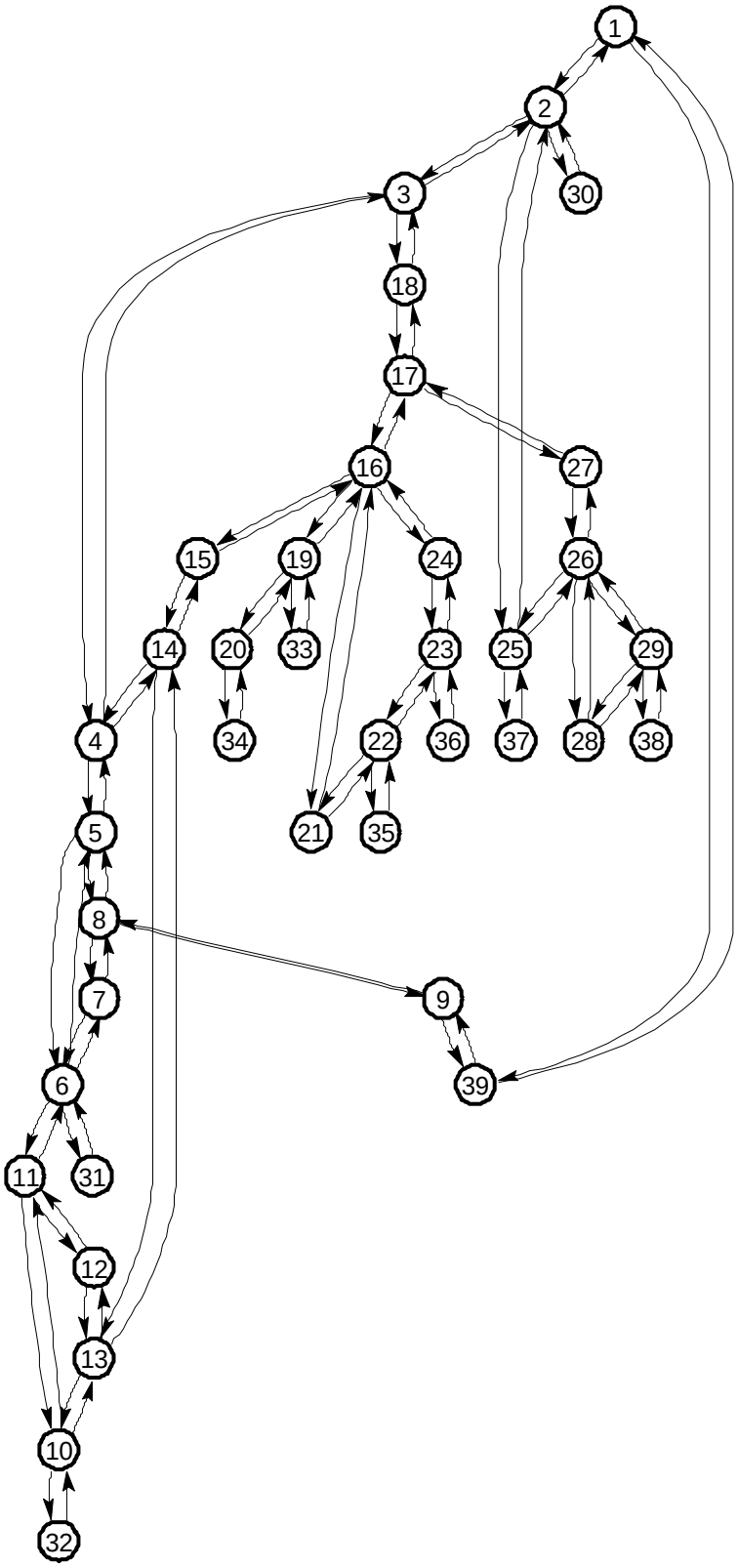

Figure 4.15: Graph model of IEEE 39-bus test system

4.7.1 First Phase: Edge reduction for Case 4

In this case, the original IEEE 39-bus test system is analyzed based on investigation presented by (L. Liu et al., 2009). The system parameters as reported by (L. Liu et al., 2009) are listed in Table 4.19.

Table 4.19: System Parameters for Case 4

Desired number of islands:	2
Coherent group of generators:	Group 1 = {30, 31, 32, 37, 38, 39}
	Group 2 = {33, 34, 35, 36}

In the first phase of investigation, the edge reduction algorithm is carried out to determine the initial number of transmission lines which needs to be disconnected to result in the desired number of islands with the coherent group of generators. The edge reduction algorithm is applied for the IEEE 39-bus test system as shown in Figure 4.16. The initial search space of 46 possible transmission line combinations ($\approx 7.0369 \times 10^{13}$) is reduced to 2 lines as an initial solution.

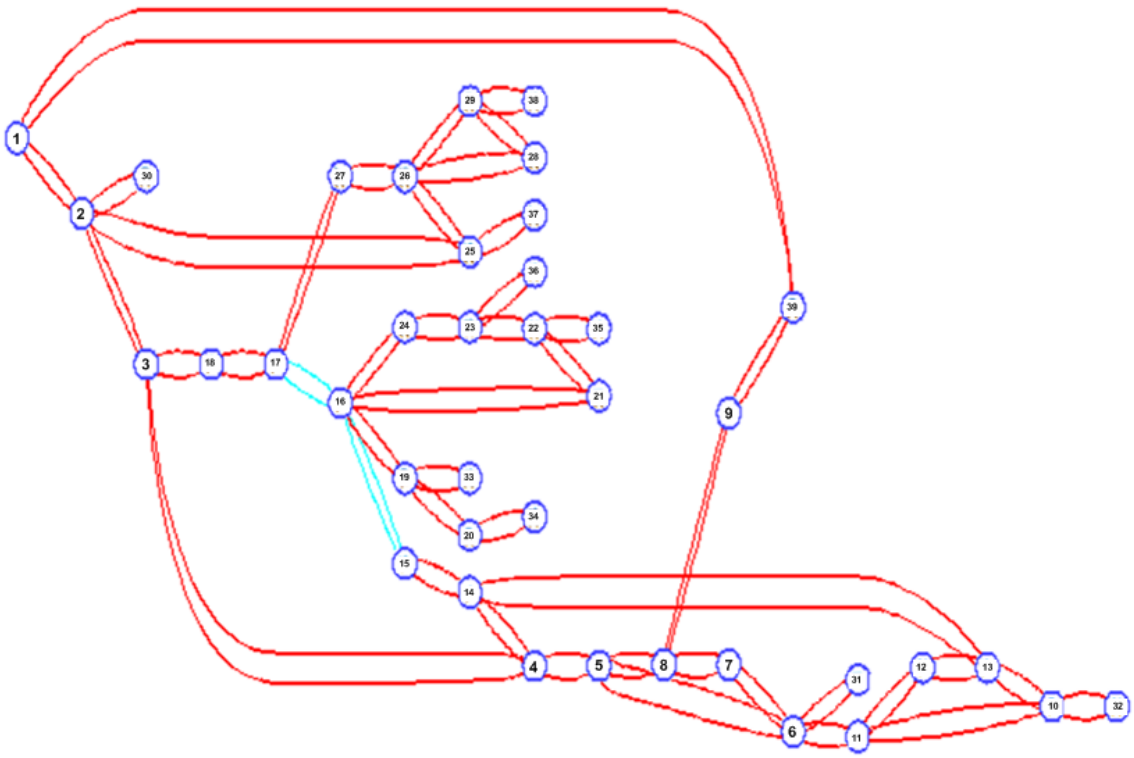

Figure 4.16: Edge reduction algorithm for Case 4

Table 4.20: Initial network splitting solution for Case 4

Initial splitting solution	Power flow (MW)
15 – 16	287.26
16 – 17	206.86
$\sum P_{min}$	494.12

Table 4.20 shows the initial network splitting solution obtained after the edge reduction algorithm has been implemented. The initial minimal power-flow disruption obtained ($\sum P_{min}$) is 494.12 MW. This initial solution is then passed on to the second phase to find the optimum network splitting solution.

4.7.2 Second Phase: Modified ABC optimization for Case 4

The proposed modified ABC optimization is applied to the test system and the optimum network splitting solution is obtained for the test case as shown in Table 4.21. The optimum number of lines to be disconnected is two and the minimal power-flow disruption obtained is 240.48 MW. This optimized minimal power-flow disruption value is lower than the reported value of 335.38 MW based on the reported investigation (W. Liu et al., 2007). The modified PSO is able to achieve the same value of 240.48 MW. Furthermore, the number of lines disconnected is also lower than the reported value.

Table 4.21: Optimum network splitting solution for Case 4

Reported investigation (W. Liu et al., 2007)	Power flow (MW)	Modified PSO	Power flow (MW)	Modified ABC	Power flow (MW)
3 – 18	40.15	14 – 15	33.61	14 – 15	33.61
15 – 16	287.26	16 – 17	206.86	16 – 17	206.86
17 – 27	7.97				
$\sum P_{min}$	335.38	$\sum P_{min}$	240.48	$\sum P_{min}$	240.48

Figure 4.17 shows the one line diagram of the islanding solution.

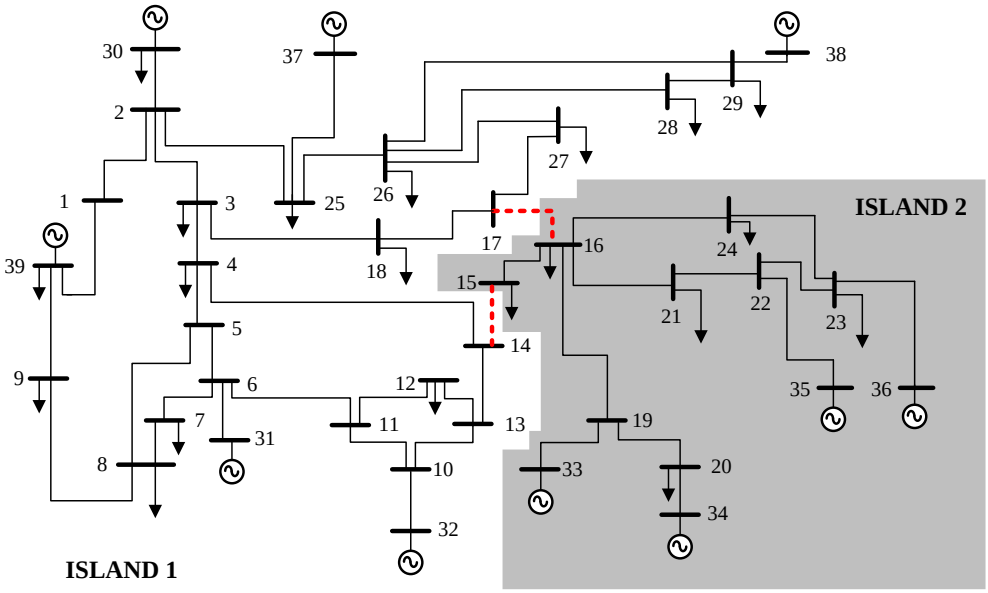

Figure 4.17: Islanding solution for case 4

Figure 4.18 shows the convergence curve for case 4 of both optimization techniques. The figure shows that both the modified ABC based on discrete values and the modified PSO based on discrete values are able to achieve the global minima. However, the modified ABC optimization technique is able to reach global minima in less number of iteration compared to the modified PSO. In this case, the number of lines disconnected in the initial solution and the optimum number of lines to be disconnected are the same. Not many changes in the transmission lines are required to obtain to optimum network splitting solution.

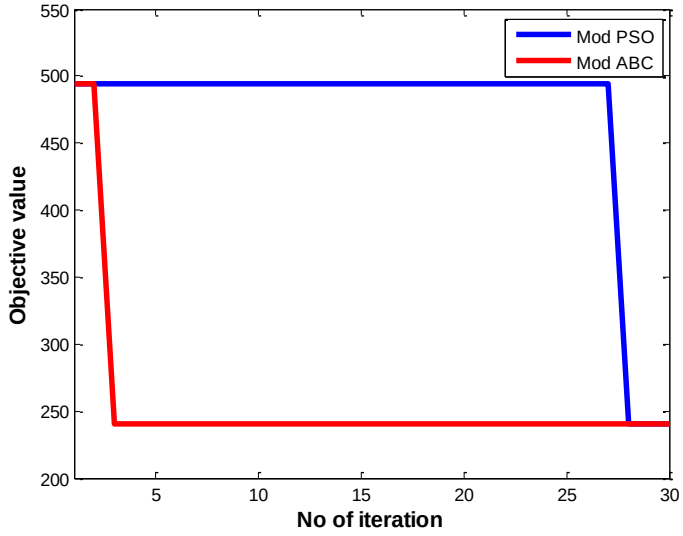

Figure 4.18: Convergence curve for Case 4

Table 4.22: First island information for Case 4

Buses 27 (1 – 14, 17 - 18, 25 - 32, 37 - 39)		
Generating Bus	**Pre-Splitting**	**Post-Splitting**
30	250	278.80
31*	582.25	618.02
32	650	678.8
37	540	564
38	830	858.8
39	1000	1028.8
$\sum P_{Generation}$ **(MW)**	3852.25	4027.22
$\sum P_{Load}$ **(MW)**	3997.53	3997.53
$\sum P_{Loss}$ **(MW)**	27.52	29.69
$\sum P_{imbalance}$ **(MW)**	-172.8	0

**** slack bus***

Table 4.22 shows the islanding information for island 1. In island 1, an imbalance of 172.8 MW of power is experienced. Since the slack bus (bus 31) is located in this island, bus data reassignment can be carried out and load flow analysis can be calculated. However, based on the generator data shown in Table A-2, the slack bus will not be able to absorb the total power imbalance as the maximum limit of the generator is 646 MW. Due to that, the load is shared equally between all the generators. The post-splitting columns shows that the all the generator bus value has been increased to meet the load demand and further ensure that the load-generation balance in the island is met.

Table 4.23: Second island information for Case 4

Buses 12 (15 – 16, 19 – 24, 33 – 36)		
Generating Bus	**Pre-Splitting**	**Post-Splitting**
33	632	632
34	508	508
35	650	474.78*
36	560	560
$\sum P_{Generation}$ **(MW)**	2350	2174.78
$\sum P_{Load}$ **(MW)**	2159.1	2159.1
$\sum P_{Loss}$ **(MW)**	18.11	15.68
$\sum P_{imbalance}$ **(MW)**	172.79	0

**** slack bus***

Table 4.23 shows the islanding information for island 2. In island 2, a surplus generation of 172.79 MW is available. The slack bus is located in island 1. The bus data reassignment is carried out and the generator bus with the largest generating capability, bus 35 is selected as the slack bus. Load flow analysis is then carried out and the slack

bus value is reduced to meet load-generation balance in the island. The transmission line power flow analysis is carried out and results show that that the power flow is well within the maximum allowable capacity of the transmission lines. The complete result of the transmission line power flow analysis is included in the Appendix section (Table B-3).

4.8 Case 5: IEEE 39-Bus Test System (Coherency set 2)

4.8.1 First Phase: Edge reduction for Case 5

In this case, the original IEEE 39-bus test system is analyzed based on investigation presented by (L. Liu et al., 2009). The system parameters as reported by (L. Liu et al., 2009) are listed in Table 4.24.

Table 4.24: System Parameters for Case 5

Desired number of islands:	3
Coherent group of generators:	Group 1 = {30, 37, 38}
	Group 2 = {31, 32, 39}
	Group 3 = {33, 34, 35, 36}

In the first phase of investigation, the edge reduction algorithm is carried out to determine the initial number of transmission lines which needs to be disconnected to result in the desired number of islands with the coherent group of generators. The edge reduction algorithm is applied for the IEEE 39-bus test system as shown in Figure 4.19. The initial search space is reduced to 4 lines as an initial solution.

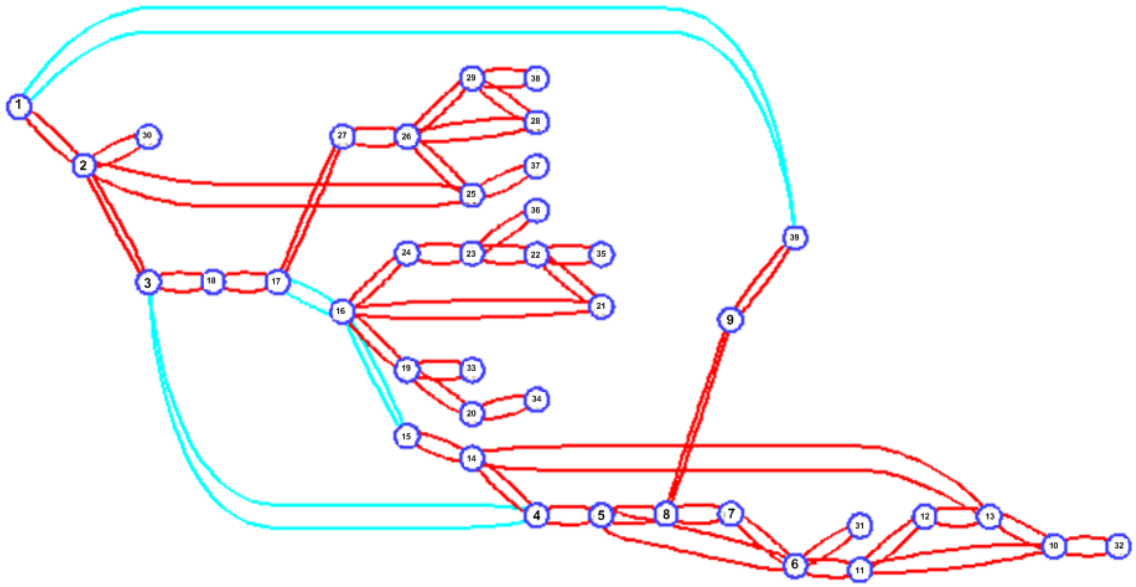

Figure 4.19: Edge reduction algorithm for Case 5

Table 4.25: Initial network splitting solution for Case 5

Initial splitting solution	Power flow (MW)
1 – 39	121.23
3 – 4	71.63
15 – 16	287.26
16 – 17	206.86
$\sum P_{min}$	686.98

Table 4.25 shows the initial network splitting solution obtained after the edge reduction algorithm has been implemented. The initial minimal power-flow disruption obtained ($\sum P_{min}$) is 686.98 MW. This initial solution is then passed on to the second phase to find the optimum network splitting solution.

4.8.2 Second Phase: Modified ABC optimization for Case 5

The proposed modified ABC optimization is applied to the test system and the optimum network splitting solution is obtained for the test case as shown in Table 4.26. The optimum number of lines to be disconnected is four and the minimal power-flow disruption obtained is 433.34 MW. This optimized minimal power-flow disruption value is lower than the reported value of 686.98 MW based on the reported

investigation (W. Liu et al., 2007). The modified PSO similarly is able to achieve the value of 433.34 MW.

Table 4.26: Optimum network splitting solution for Case 5

Reported investigation (W. Liu et al., 2007)	Power flow (MW)	Modified PSO	Power flow (MW)	Modified ABC	Power flow (MW)
1 – 39	121.23	1 – 39	121.23	1 – 39	121.23
3 – 4	71.63	3 – 4	71.63	3 – 4	71.63
15 – 16	287.26	14 – 15	33.61	14 – 15	33.61
16 – 17	206.86	16 – 17	206.86	16 – 17	206.86
$\sum P_{min}$	686.98	$\sum P_{min}$	433.34	$\sum P_{min}$	433.34

Figure 4.20 shows the one line diagram of the islanding solution.

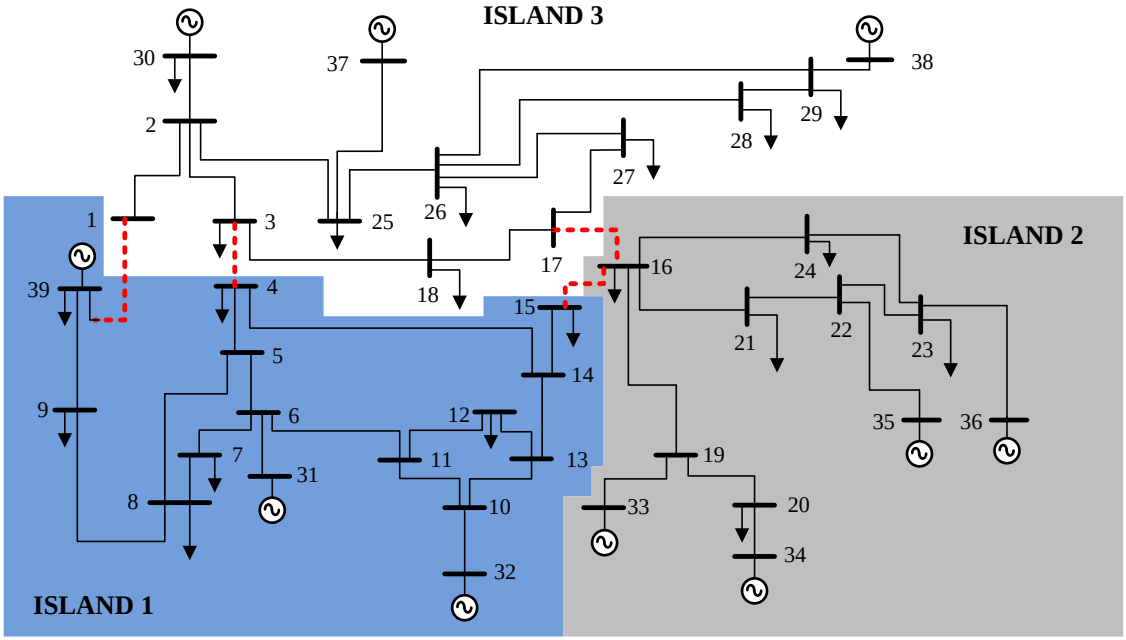

Figure 4.20: Islanding solution for case 5

Figure 4.21 shows the convergence curve for case 5 of both optimization techniques. The figure shows that both the modified ABC based on discrete values and the modified PSO based on discrete values are able to achieve the global minima similar to case 4. Similarly, the modified ABC optimization technique is able to reach global minima in less number of iterations compared to the modified PSO.

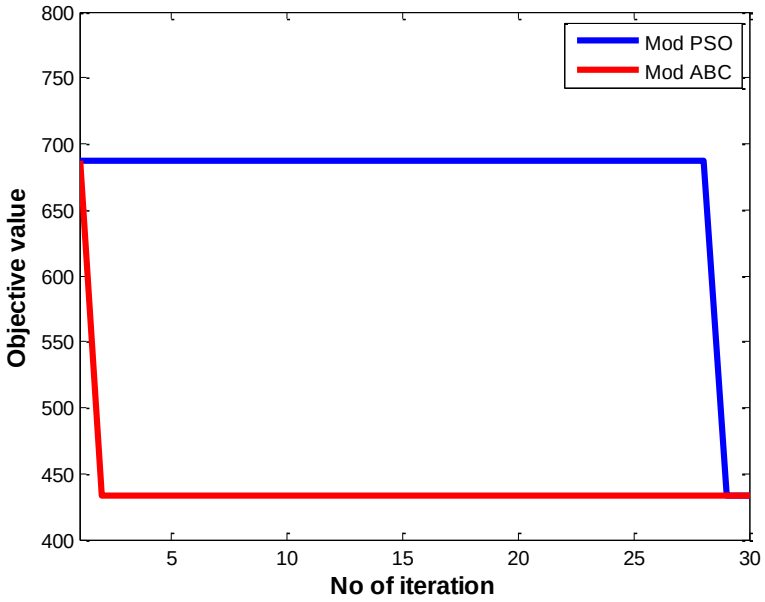

Figure 4.21: Convergence curve for Case 5

Table 4.27: First island information for Case 5

Buses 14 (4 – 14, 31 – 32, 39)		
Generating Bus	**Pre-Splitting**	**Post-Splitting**
31*	582.25	638.03
32	650	702.88
39	1000	1052.88
$\sum P_{Generation}$ (MW)	2232.25	2393.79
$\sum P_{Load}$ (MW)	2384.03	2384.03
$\sum P_{Loss}$ (MW)	6.83	9.76
$\sum P_{imbalance}$ (MW)	-158.63	0

**** slack bus***

Table 4.27 shows the islanding information for island 1. In island 1, an imbalance of 158.63 MW of power is experienced. Since the slack bus (bus 31) is located in this island, bus data reassignment can be carried out and load flow analysis can be calculated. However, based on the generator data shown in Table A-2, the slack bus will not be able to absorb the total power imbalance as the maximum limit of the generator is 646 MW. Due to that, the load is shared equally between all three generators. The post-splitting columns shows that the all the generator bus value has been increased to meet the load demand and further ensure that the load-generation balance in the island is met.

Table 4.28: Second island information for Case 5

Buses 12 (15 – 16, 19 – 24, 33 – 36)		
Generating Bus	**Pre-Splitting**	**Post-Splitting**
33	632	632
34	508	508
35	650	474.78*
36	560	560
$\sum P_{Generation}$ (MW)	2350	2174.78
$\sum P_{Load}$ (MW)	2159.1	2159.1
$\sum P_{Loss}$ (MW)	18.11	15.68
$\sum P_{imbalance}$ (MW)	172.79	0

**** slack bus***

Table 4.28 shows the islanding information for island 2. This island contains the same number of buses as in island 2 of Case 4. As such, similar value can be seen in the power values for generator buses, load buses and line losses.

Table 4.29: Third island information for Case 5

Buses 13 (1 – 3, 17 – 18, 25 – 30, 37 - 38)		
Generating Bus	**Pre-Splitting**	**Post-Splitting**
30	250	262.4*
37	540	540
38	830	830
$\sum P_{Generation}$ (MW)	1620	1632.4
$\sum P_{Load}$ (MW)	1613.5	1613.5
$\sum P_{Loss}$ (MW)	20.68	18.90
$\sum P_{imbalance}$ (MW)	-14.18	0

**** slack bus***

Table 4.29 shows the islanding information for island 3. In the pre-splitting column, it can be seen that a small value of power imbalance exists. As such, the bus data reassignment and load flow analysis for the island is evaluated. The largest generator bus in the island which is bus 30 is chosen as the slack bus. The slack bus absorbs the additional load demand and the load-generation balance in the island is met.

The transmission line power flow analysis is carried out and results show that that the power flow is well within the maximum allowable capacity of the transmission lines. The complete result of the transmission line power flow analysis is included in the Appendix section (Table B-4).

4.9 Case 6: IEEE 39-Bus Test System (Coherency set 3)

Figure 4.22 shows the graph model of the modified IEEE 39-bus test system.

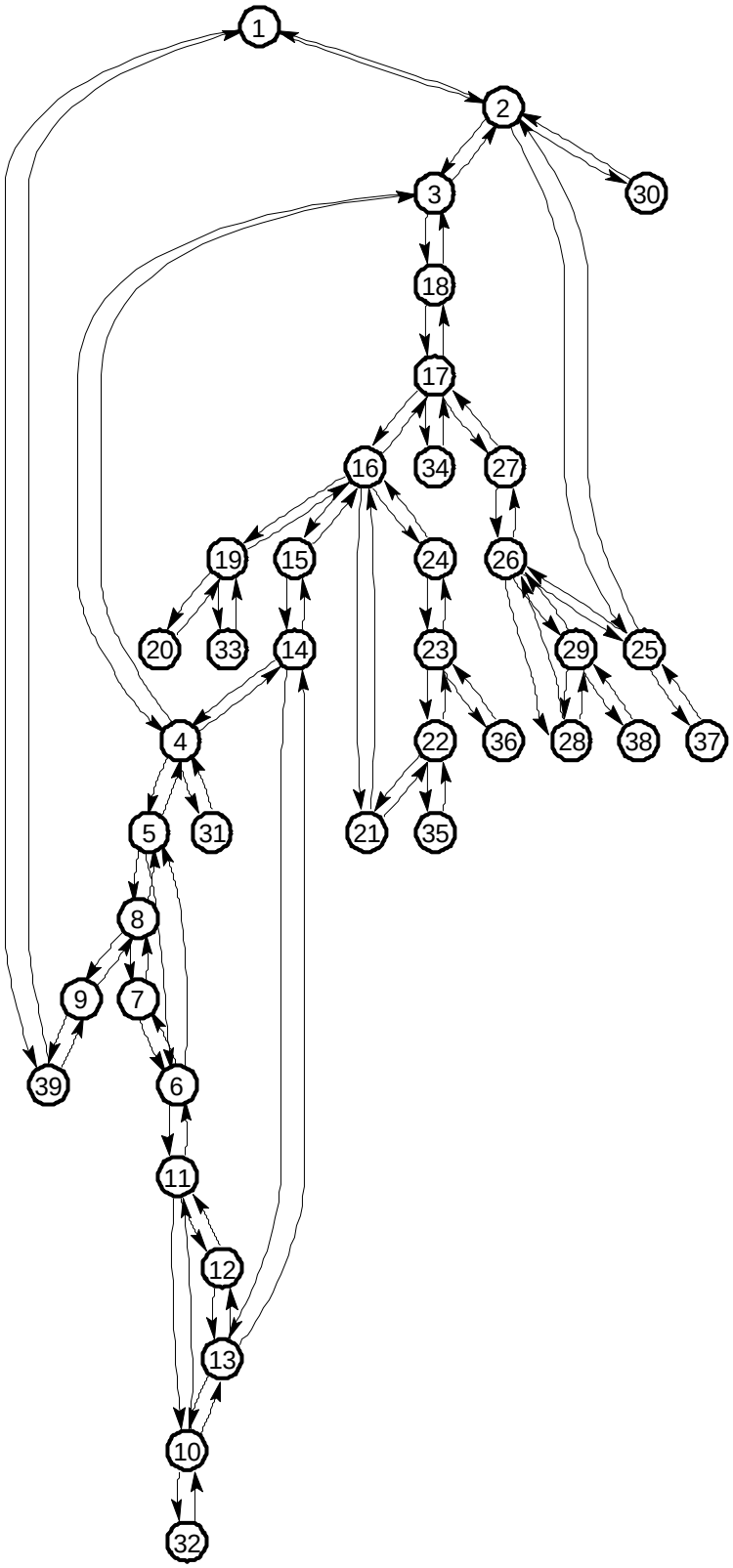

Figure 4.22: Graph model of modified IEEE 39-bus test system

4.9.1 First Phase: Edge reduction for Case 6

In this case, the modified IEEE 39-bus test system is analyzed based on the investigation and results presented by (Aghamohammadi & Shahmohammadi, 2012). The system parameters are listed in Table 4.30.

Table 4.30: System Parameters for Case 6

Desired number of islands:	4
Coherent group of generators:	Group 1 = {30, 31, 37}
	Group 2 = {33, 35, 36}
	Group 3 = {34, 38}
	Group 4 = {32, 39}

Initially, the edge reduction algorithm is carried out to determine the initial number of transmission lines which needs to be disconnected to result in the desired number of islands with the coherent group of generators. The edge reduction algorithm is applied for the modified IEEE 39-bus test system as shown in Figure 4.23. The initial search space of 46 possible transmission line combinations is reduced to 9 lines as an initial solution.

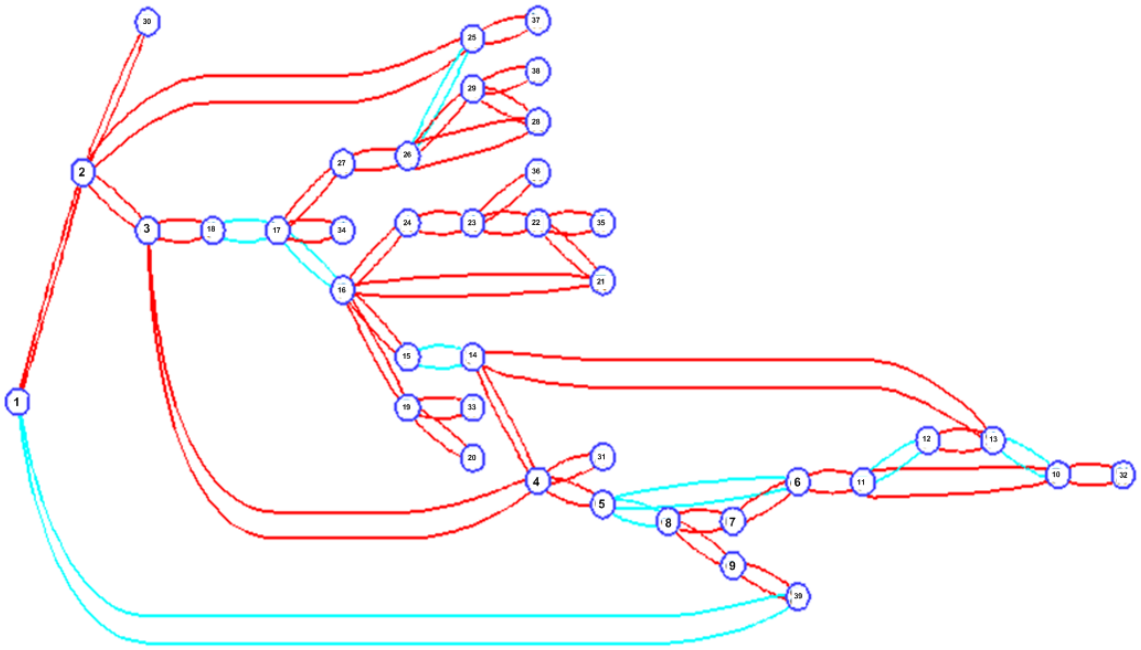

Figure 4.23: Edge reduction algorithm for Case 6

Table 4.31: Initial network splitting solution for Case 6

Initial splitting solution	Power flow (MW)
1 – 39	163.14
5 – 6	111.83
5 – 8	335.59
10 – 13	175.25
11 – 12	10.22
14 – 15	72.64
16 – 17	260.25
17 – 18	222.54
25 – 26	67.39
$\sum P_{min}$	1418.84

Table 4.31 shows the initial network splitting solution obtained after the edge reduction algorithm has been implemented. The initial minimal power-flow disruption obtained ($\sum P_{min}$) is 1418.84 MW. This initial solution is then passed on to the second phase to find the optimum network splitting solution.

4.9.2 Second Phase: Modified ABC optimization for Case 6

The proposed modified ABC optimization is applied to the test system and the optimum network splitting solution is obtained for the test case as shown in Table 4.32. The optimum number of lines to be disconnected is seven and the minimal power-flow disruption obtained is 935.31 MW. This optimized minimal power-flow disruption value is lower than the reported value of 1380.64 MW (Aghamohammadi & Shahmohammadi, 2012) and the modified PSO value of 1218.72 MW. Furthermore, the number of lines disconnected is also lower than the reported value.

Table 4.32: Optimum network splitting solution for Case 6

Reported investigation (Aghamohammadi & Shahmohammadi, 2012)	Power flow (MW)	Modified PSO	Power flow (MW)	Modified ABC	Power flow (MW)
1 – 2	164.13	1 – 39	163.14	1 – 39	163.14
4 – 5	224.19	4 – 5	224.19	3 – 18	64.21
10 – 13	175.25	11 – 12	10.22	4 – 5	224.19
12 – 13	18.79	13 – 14	156.34	4 – 14	83.49
15 – 16	248.10	14 – 15	72.64	14 – 15	72.64
16 – 17	260.25	16 – 17	260.25	16 – 17	260.25
17 – 18	222.54	17 – 18	222.54	25 – 26	67.39
25 – 26	67.39	22 – 23	42.01		
		25 – 26	67.39		
$\sum P_{min}$	1380.64	$\sum P_{min}$	1218.72	$\sum P_{min}$	935.31

Figure 4.24 shows the one line diagram of the islanding solution.

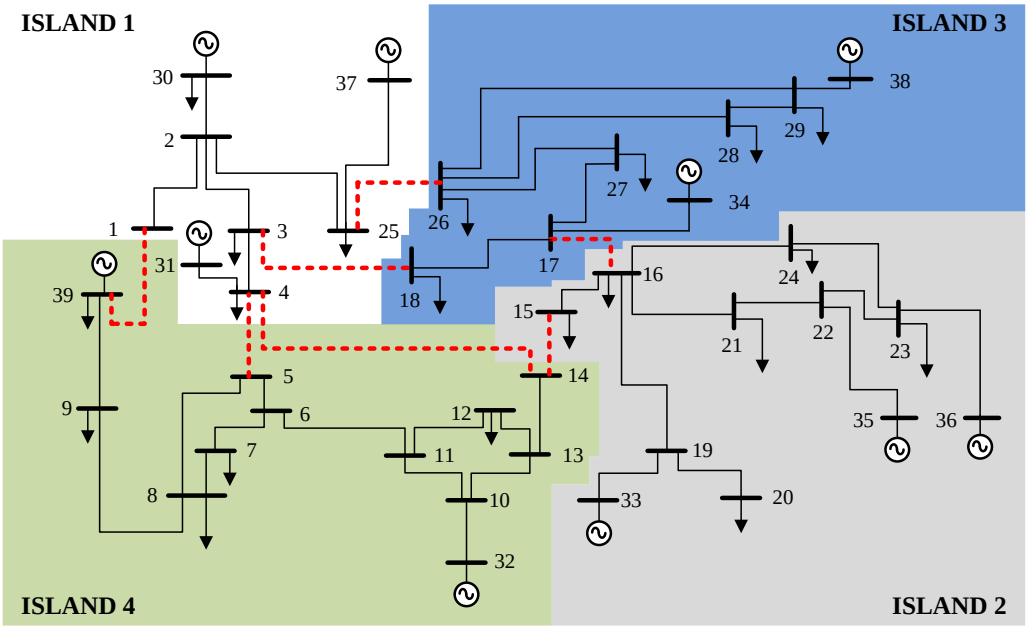

Figure 4.24: Islanding solution for case 6

Figure 4.25 shows the convergence curve for case 6 of both optimization techniques. The figure shows that the modified ABC based on discrete values is able to achieve the global minima compared to the modified PSO based on discrete values.

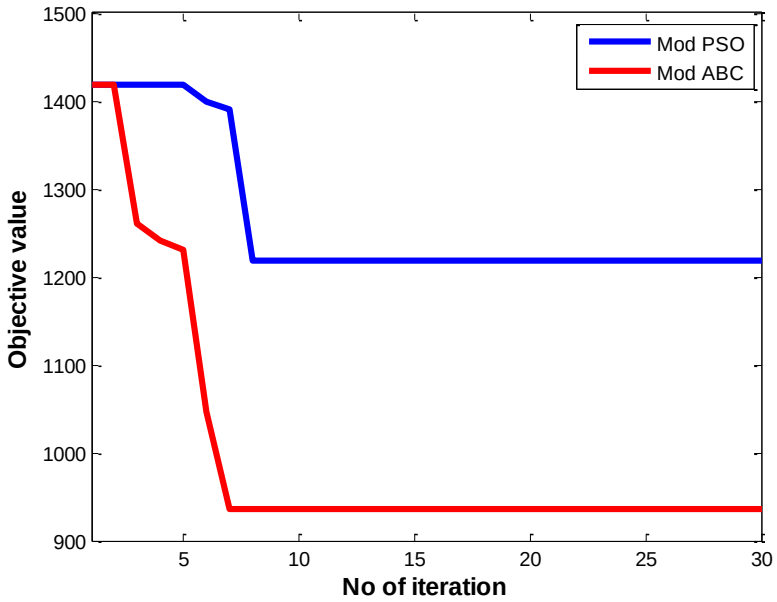

Figure 4.25: Convergence curve for Case 6

Table 4.33: First island information for Case 6

Buses 8 (1 – 4, 25, 30 – 31, 37)		
Generating Bus	**Pre-Splitting**	**Post-Splitting**
30	250	250
31*	582.25	281.69
37	540	540
$\sum P_{Generation}$ **(MW)**	1372.25	1071.69
$\sum P_{Load}$ **(MW)**	1055.2	1055.2
$\sum P_{Loss}$ **(MW)**	15.70	16.49
$\sum P_{imbalance}$ **(MW)**	301.35	0

**** slack bus***

Table 4.33 shows the islanding information for island 1. In island 1, a surplus power of 310.25 301.35 MW is experienced. The slack bus (bus 31) is located in this island. Bus data reassignment and the load flow analysis is carried out and the generation level for bus 31 is reduced to meet the load-generation balance.

Table 4.34: Second island information for Case 6

Buses 11 (15 – 16, 19 – 24, 33, 35 - 36)		
Generating Bus	**Pre-Splitting**	**Post-Splitting**
33	632	652
35	650	655.59*
36	560	580
$\sum P_{Generation}$ **(MW)**	1842	1887.59
$\sum P_{Load}$ **(MW)**	2159.1	1871.29
$\sum P_{Loss}$ **(MW)**	13.18	16.30
$\sum P_{imbalance}$ **(MW)**	-330.28	0

**** slack bus***

In island 2, a deficit of 330.28 MW of power is experienced as shown in Table 4.34. In order to maintain load-generation balance in island 2, initially bus data reassignment is carried out by selecting bus 35 as the slack bus. However the power imbalance value is greater than the maximum generation capacity of bus 35 which is at 652 MW as shown in Table A-2. To address the shortfall in generation, all the generators (bus 33 and 36) are operated at their maximum values. Despite this effort, the generators are still not able to cope with the load demand. In order to ensure successful post islanding operation, load shedding is carried out. A total amount of 13.33% (287.81 MW) of load is shed and load-generation balance in island 2 is met.

Table 4.35: Third island information for Case 6

Buses 8 (17 – 18, 26 - 29, 34, 38)		
Generating Bus	**Pre-Splitting**	**Post-Splitting**
34	508	508
38	830	567.83*
$\sum P_{Generation}$ (MW)	1338	1075.82
$\sum P_{Load}$ (MW)	1067.5	1067.5
$\sum P_{Loss}$ (MW)	11.43	8.32
$\sum P_{imbalance}$ (MW)	259.07	0

**** slack bus***

Table 4.35 shows the islanding information for island 3. In island 3, there is a surplus of 259.07 MW. This is similar to scenario in island 1. In this island, through bus data reassignment, bus 38 is chosen as the slack bus for this island. The slack bus generation level is reduced proportionally and load-generation balance is maintained.

Table 4.36: Fourth island information for Case 6

Buses 12 (5 - 14, 32, 39)		
Generating Bus	**Pre-Splitting**	**Post-Splitting**
32	650	725
39	1000	1100*
$\sum P_{Generation}$ (MW)	1650	1825
$\sum P_{Load}$ (MW)	1874.83	1816.72
$\sum P_{Loss}$ (MW)	5.77	8.28
$\sum P_{imbalance}$ (MW)	-230.6	0

**** slack bus***

In island 4, a deficit of 230.6 MW of power is experienced as shown in Table 4.36. Bus 39 is chosen as the slack bus in this island based on bus data reassignment. Despite increasing the generators to their maximum limit, the load demand could not be met. This condition is similar to the scenario in island 2. With regards to this, load shedding is applied and total of 3.05% (58.11 MW) of load is shed. The post splitting column shows that the load-generation balance is maintained after load shedding is carried out. The transmission line power flow analysis is carried out and results show that that the power flow is well within the maximum allowable capacity of the transmission lines. The complete result of the transmission line power flow analysis is included in the Appendix section (Table B-5).

4.10 Case 7: IEEE 118-Bus Test System (Coherency set 1)

Figure 4.26 shows the graph model of the IEEE 118-bus test system.

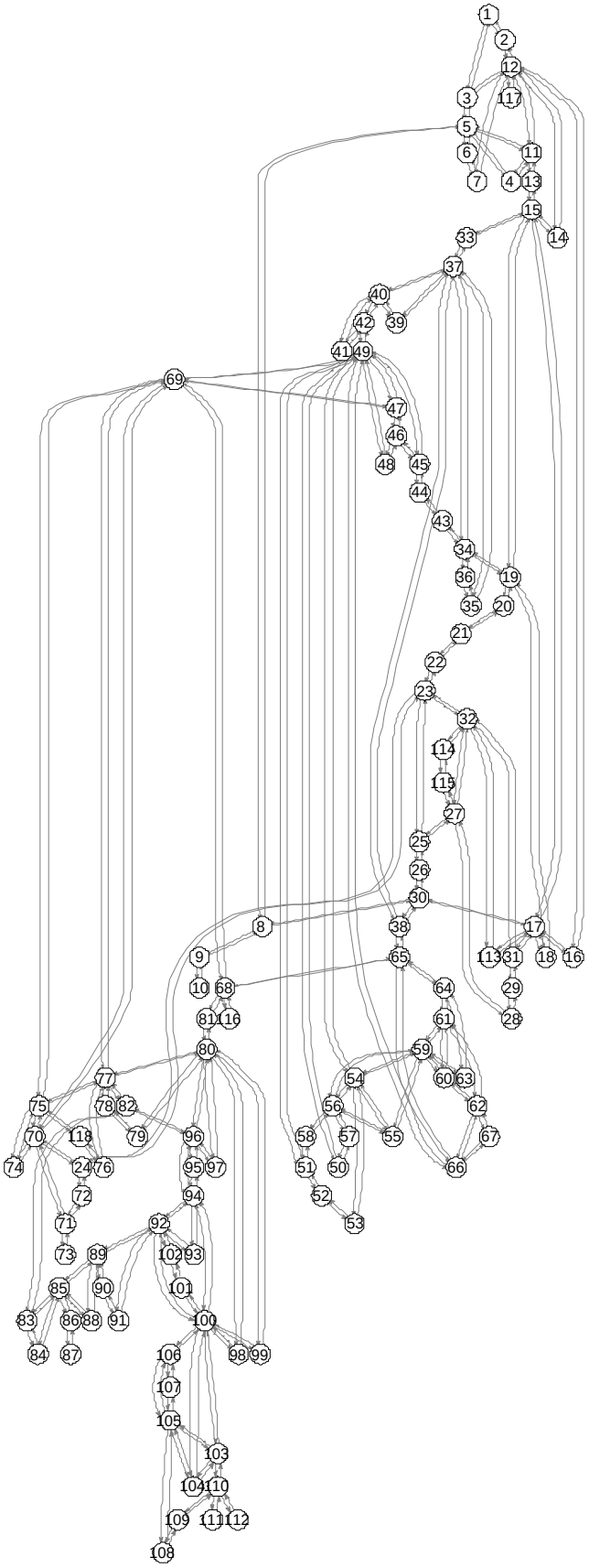

Figure 4.26: Graph model of IEEE 118-bus test system

4.10.1 First Phase: Edge reduction for Case 7

This large scale power system is a complex interconnection of 118 nodes and 186 edges. Based on the investigation carried out by in (Ding et al., 2013), the system parameters are listed in Table 4.37.

Table 4.37: System Parameters for Case 7

Desired number of islands:	3
Coherent group of generators:	Group 1 = {10, 12, 25, 26, 31}
	Group 2 = {46, 49, 54, 59, 61, 65, 66, 69, 80}
	Group 3 = {87, 89, 100, 103, 111}

Initially, the edge reduction algorithm is carried out to determine the initial number of transmission lines which needs to be disconnected to result in the desired number of islands with the coherent group of generators. The edge reduction algorithm is applied for the IEEE 118-bus test system as shown in Figure 4.27. The initial search space of 46 possible transmission line combinations ($\approx 9.808 \times 10^{55}$) is reduced to 13 lines as an initial solution.

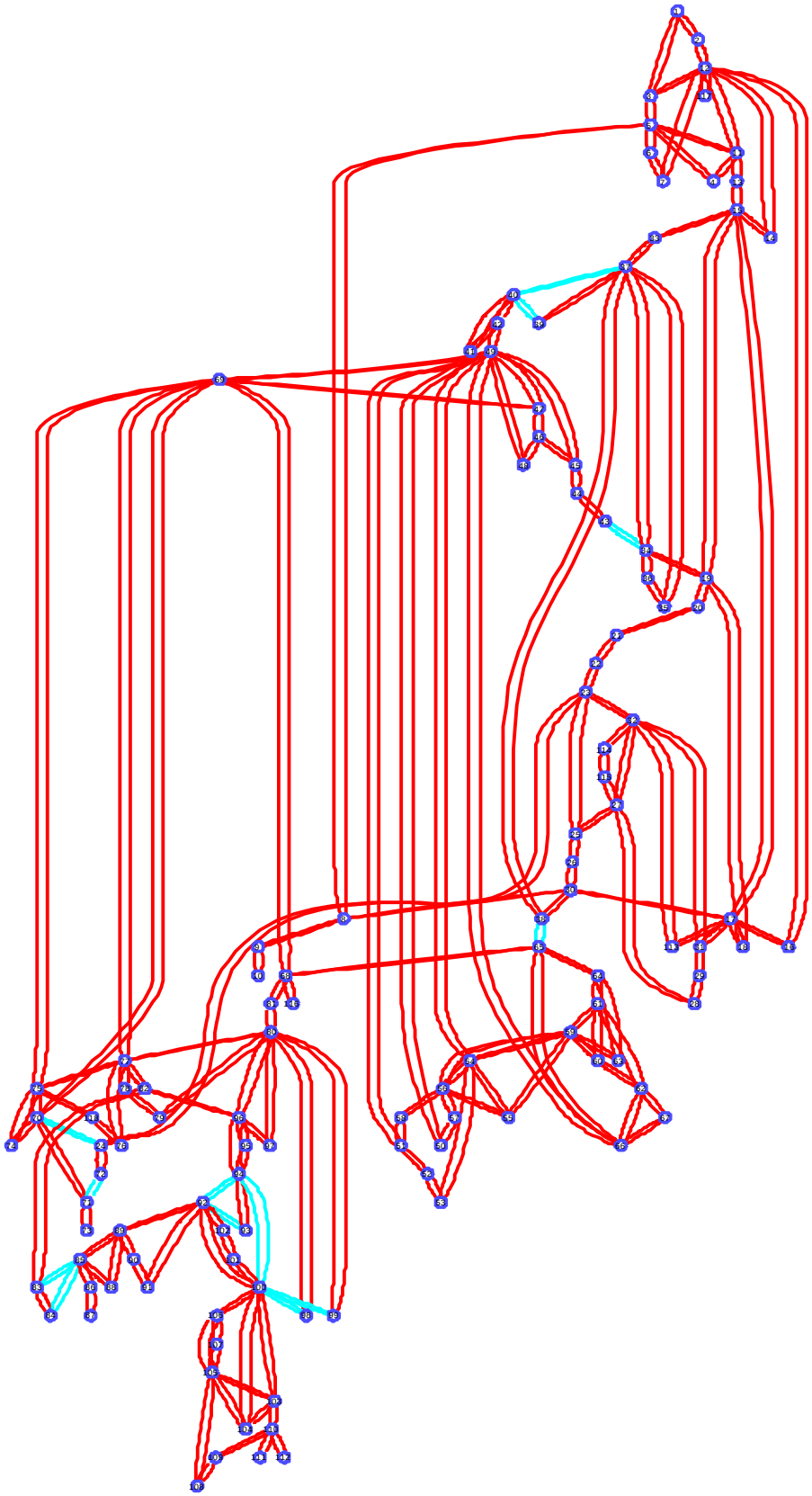

Figure 4.27: Edge reduction algorithm for Case 7

Table 4.38: Initial network splitting solution for Case 7

Initial splitting solution	Power flow (MW)
24 – 70	5.36
34 – 43	3.01
37 – 40	45.86
38 – 65	189.76
39 – 40	28.52
71 – 72	10.35
83 – 85	43.35
84 – 85	37.15
92 – 93	57.88
92 – 94	52.36
94 – 100	4.63
98 – 100	5.45
99 – 100	22.93
$\sum P_{min}$	506.61

Table 4.38 shows the initial network splitting solution obtained after the edge reduction algorithm has been implemented. The initial minimal power-flow disruption obtained ($\sum P_{min}$) is 506.61 MW. This initial solution is then passed on to the second phase to find the optimum network splitting solution.

4.10.2 Second Phase: Modified ABC optimization for Case 7

The proposed modified ABC optimization is applied to the test system and the optimum network splitting solution is obtained for the test case as shown in Table 4.39. The optimum number of lines to be disconnected is nine and the minimal power-flow disruption obtained is 142.17 MW. This optimized minimal power-flow disruption value is similar to the reported value of 142.17 MW (Ding et al., 2013). However, it is better than the modified PSO value of 506.61 MW.

Table 4.39: Optimum network splitting solution for Case 7

Reported investigation (Ding et al., 2013)	Power flow (MW)	Modified PSO	Power flow (MW)	Modified ABC	Power flow (MW)
15 – 33	6.47	24 – 70	5.36	15 – 33	6.47
19 – 34	4.42	34 – 43	3.01	19 – 34	4.42
23 – 24	9.44	37 – 40	45.86	23 – 24	9.44
30 – 38	63.54	38 – 65	189.76	30 – 38	63.54
77 – 82	3.50	39 – 40	28.52	77 – 82	3.50
80 – 96	18.87	71 – 72	10.35	80 – 96	18.87
80 – 99	19.37	83 – 85	43.35	80 – 99	19.37
96 – 97	11.12	84 – 85	37.15	96 – 97	11.12
98 – 100	5.45	92 – 93	57.88	98 – 100	5.45
		92 – 94	52.36		
		94 – 100	4.63		
		98 – 100	5.45		
		99 – 100	22.93		
$\sum P_{min}$	142.17	$\sum P_{min}$	506.61	$\sum P_{min}$	142.17

Figure 4.28 shows the one line diagram of the islanding solution.

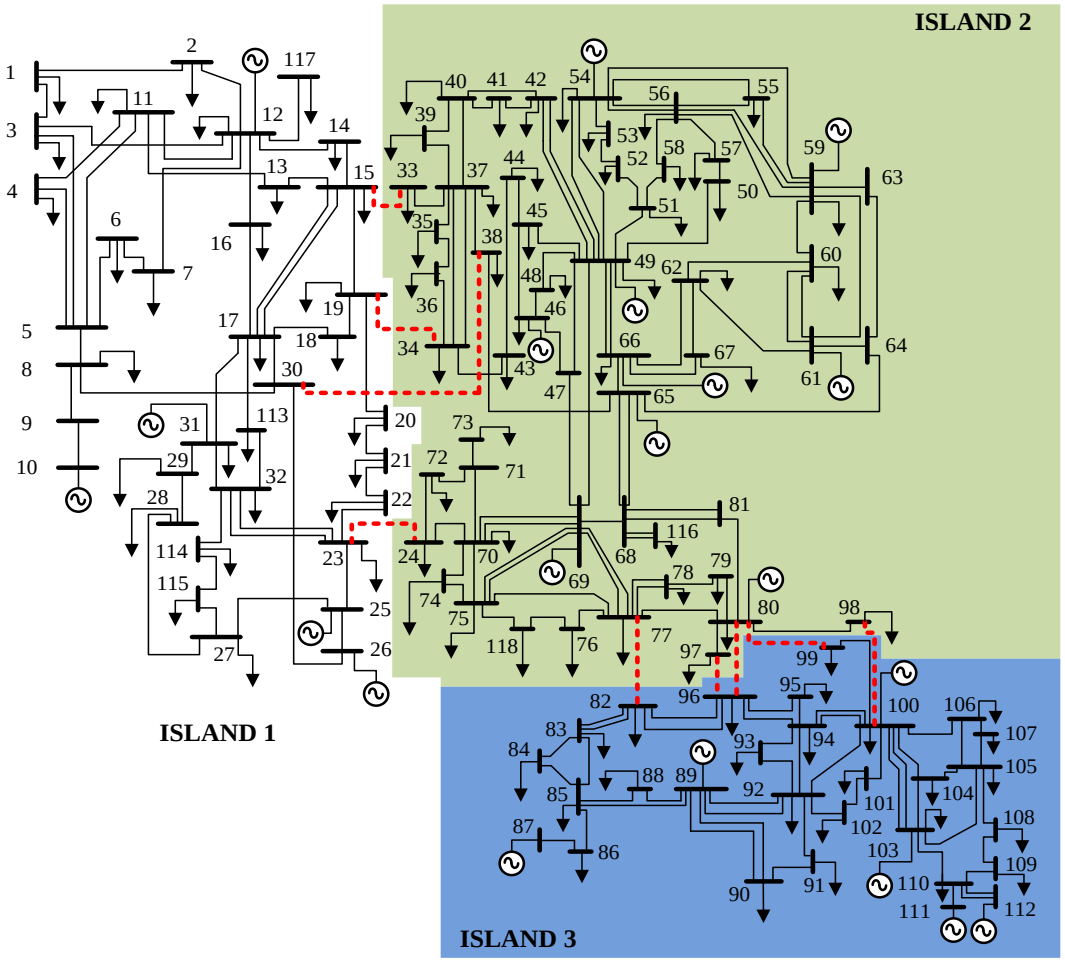

Figure 4.28: Islanding solution for case 7

Figure 4.29 shows the convergence curve for case 7 of both optimization techniques. The figure shows that the modified ABC based on discrete values is able to achieve the

global minima whereas the modified PSO based on discrete values is not able to converge to find the optimum solution.

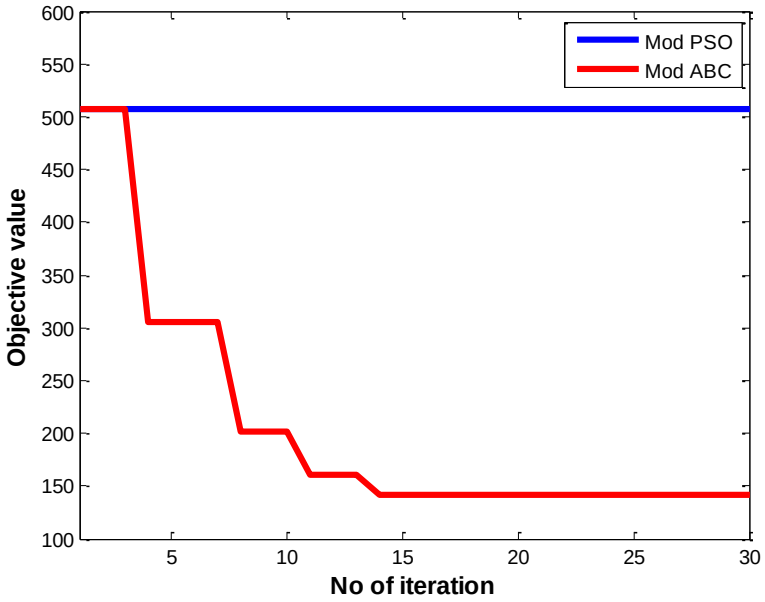

Figure 4.29: Convergence curve for Case 7

Table 4.40: First island information for Case 7

Buses 35 (1 – 23, 25 – 32, 113 – 115, 117)		
Generating Bus	**Pre-Splitting**	**Post-Splitting**
10	450	371.83*
12	85	85
25	220	220
26	314	314
31	7	7
$\sum P_{Generation}$ (MW)	1076	997.83
$\sum P_{Load}$ (MW)	963	963
$\sum P_{Loss}$ (MW)	38.26	34.83
$\sum P_{imbalance}$ (MW)	74.74	0

**** slack bus***

Table 4.40 shows the islanding information for island 1. In island 1, a surplus power of 74.74 MW is experienced. Bus data reassignment and load flow analysis is carried out and bus 10 is chosen as the slack bus since the slack bus is not originally located in this island. The slack bus generation is then reduced to meet the load-generation balance.

Table 4.41: Second island information for Case 7

Buses 54 (24, 33 – 81, 97 – 98, 116, 118)		
Generating Bus	**Pre-Splitting**	**Post-Splitting**
46	19	19
49	204	204
54	48	48
59	155	155
61	160	160
65	391	391
66	392	392
69*	511.92	551.92
80	477	477
$\sum P_{Generation}$ (MW)	2357.92	2397.92
$\sum P_{Load}$ (MW)	2333	2333
$\sum P_{Loss}$ (MW)	59.70	64.92
$\sum P_{imbalance}$ (MW)	-34.78	0

**** slack bus***

In island 2, a deficit power imbalance of 52.95 MW is observed as shown in Table 4.41. The slack bus (bus 69) is located in this island. When bus data reassignment and load flow analysis is carried out, the slack bus caters for the power imbalance. The power imbalance is lower than the maximum generation capability of bus 69 (805.2 MW) as shown in Table A-3. Once the generation value is increased, the load-generation balance criteria is met as seen in the post-splitting column.

Table 4.42: Third island information for Case 7

Buses 29 (82 – 96, 99 – 112)		
Generating Bus	**Pre-Splitting**	**Post-Splitting**
87	4	4
89	607	653.07*
100	252	252
103	40	40
111	36	36
$\sum P_{Generation}$ (MW)	939	985.07
$\sum P_{Load}$ (MW)	946	946
$\sum P_{Loss}$ (MW)	32.95	39.07
$\sum P_{imbalance}$ (MW)	-39.95	0

**** slack bus***

Table 4.42 shows the islanding information for island 3. In the pre-splitting column, it can be seen that a small value of power imbalance of 49.34 MW exists. As such, the bus data reassignment and load flow analysis for the island is evaluated. The largest

generator bus in the island which is bus 89 is chosen as the slack bus. The slack bus absorbs the additional load demand and the load-generation balance in the island is met.

In this case, the load shedding was not carried out as the load-generation balance was met as the generators were still able to provide the required power. The transmission line power flow analysis is carried out and results show that that the power flow is well within the maximum allowable capacity of the transmission lines. The complete result of the transmission line power flow analysis is included in the Appendix section (Table B-6).

4.11 Case 8: IEEE 118-Bus Test System (Coherency set 2)

4.11.1 First Phase: Edge reduction for Case 8

In this case, the IEEE 118-bus test system is analyzed based on investigation presented by (Tortós & Terzija, 2012). The system parameters as reported by (Tortós & Terzija, 2012) are listed in Table 4.43.

Table 4.43: System Parameters for Case 8

Desired number of islands:	2
Coherent group:	Group 1 = {10,12,25,26,31}
of generators	Group 2 = {46,49,54,59,61,65,66,69,80,87,89, 100,103,111}

In the first phase of investigation, the edge reduction algorithm is carried out to determine the initial number of transmission lines which needs to be disconnected to result in the desired number of islands with the coherent group of generators. The edge reduction algorithm is applied for the IEEE 118-bus test system as shown in Figure 4.30. The initial search space is reduced to 6 lines as an initial solution.

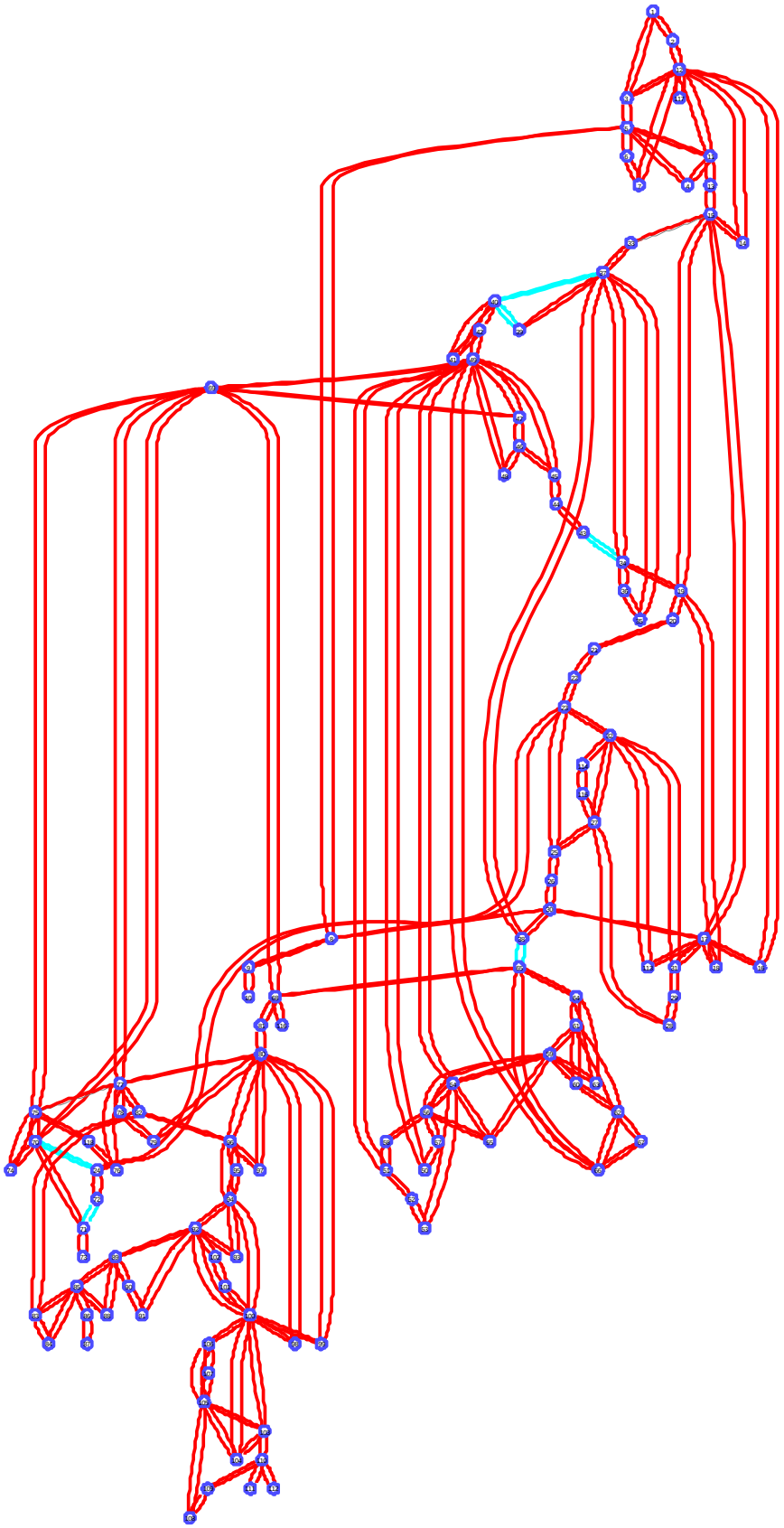

Figure 4.30: Edge reduction algorithm for Case 8

Table 4.44: Initial network splitting solution for Case 8

Initial splitting solution	Power flow (MW)
24 – 70	5.36
34 – 43	3.01
37 – 40	45.86
38 – 65	189.76
39 – 40	28.52
71 – 72	10.35
$\sum P_{min}$	282.86

Table 4.44 shows the initial network splitting solution obtained after the edge reduction algorithm has been implemented. The initial minimal power-flow disruption obtained ($\sum P_{min}$) is 282.86 MW. This initial solution is then passed on to the second phase to find the optimum network splitting solution.

4.11.2 Second Phase: Modified ABC optimization for Case 8

The proposed modified ABC optimization is applied to the test system and the optimum network splitting solution is obtained for the test case as shown in Table 4.45. The optimum number of lines to be disconnected is two and the minimal power-flow disruption obtained is 227.20 MW. This optimized minimal power-flow disruption value is lower than the reported value of 235.82 MW based on the reported investigation (Tortós & Terzija, 2012) and 277.74 based on the modified PSO.

Table 4.45: Optimum network splitting solution for Case 8

Reported investigation (Tortós & Terzija, 2012)	Power flow (MW)	Modified PSO	Power flow (MW)	Modified ABC	Power flow (MW)
24 – 70	5.36	24 – 70	5.36	24 – 70	5.36
34 – 43	3.01	24 – 72	1.73	24 – 72	1.73
38 – 65	189.76	34 – 43	3.01	34 – 43	3.01
40 – 41	17.12	38 – 65	189.76	38 – 65	189.76
40 – 42	10.22	40 – 41	17.12	40 – 41	17.12
71 - 72	10.35	40 – 42	10.22	40 – 42	10.22
		45 – 49	50.54		
$\sum P_{min}$	235.82	$\sum P_{min}$	277.74	$\sum P_{min}$	227.20

Figure 4.31 shows the one line diagram of the islanding solution.

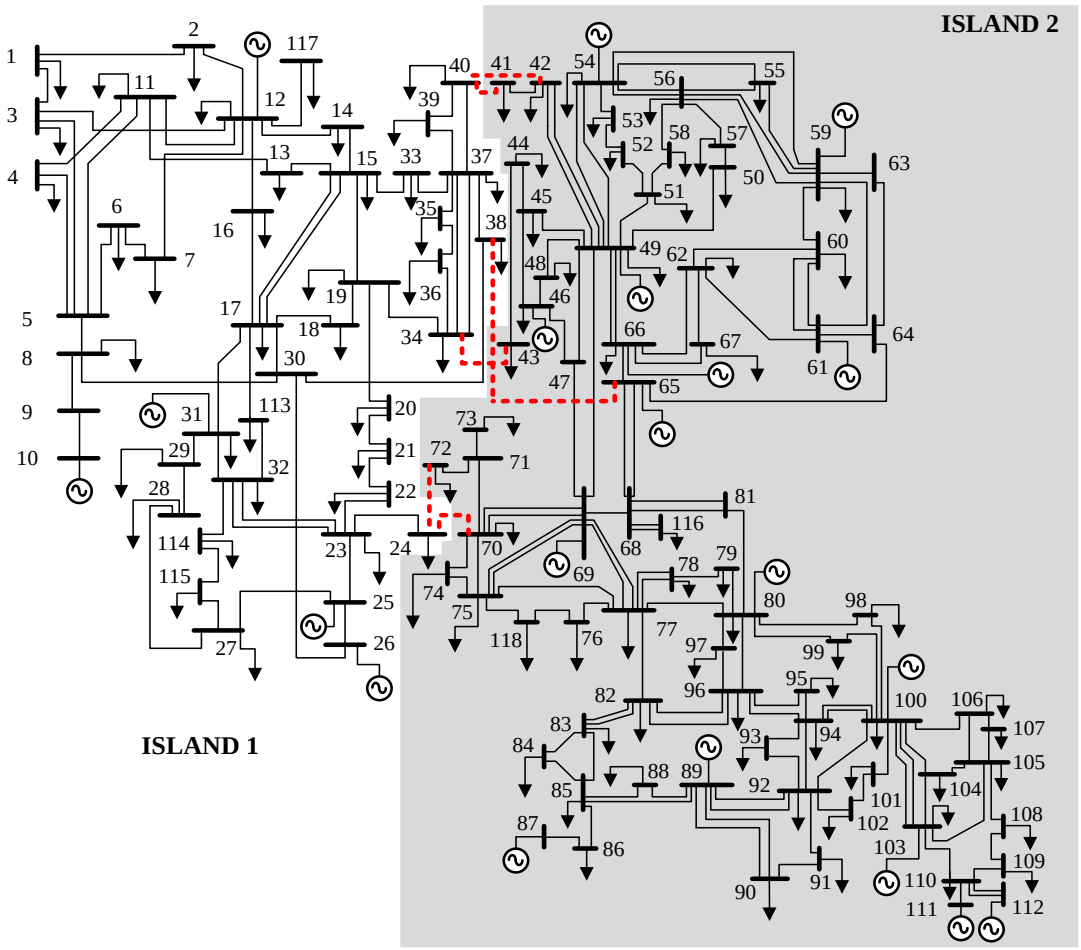

Figure 4.31: Islanding solution for case 8

Figure 4.32 shows the convergence curve for case 8 of both optimization techniques. The figure shows that both the modified ABC based on discrete values is able to converge to the global minima compared to the modified PSO based on discrete values.

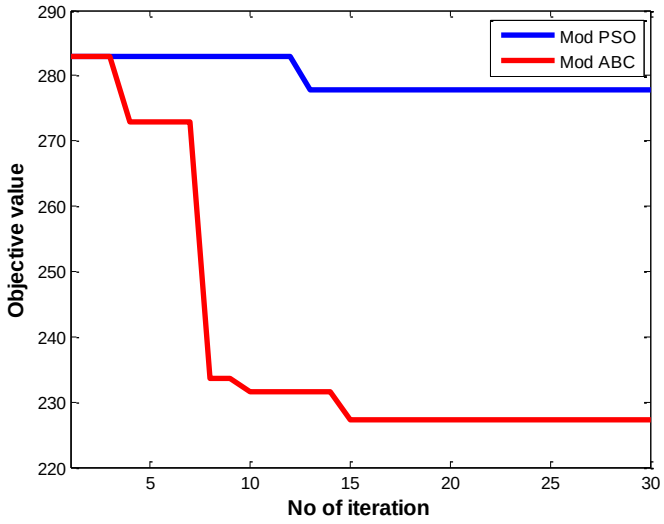

Figure 4.32: Convergence curve for Case 8

Table 4.46: First island information for Case 8

Buses 44 (1 – 40, 113 – 115, 117)		
Generating Bus	**Pre-Splitting**	**Post-Splitting**
10	450	491.33*
12	85	121.85
25	220	256.85
26	314	350.85
31	7	43.85
$\sum P_{Generation}$ (MW)	1076	1264.74
$\sum P_{Load}$ (MW)	1215	1215
$\sum P_{Loss}$ (MW)	44.57	49.74
$\sum P_{imbalance}$ (MW)	-183.57	0

**** slack bus***

This island contains 44 buses. In order to meet the power imbalance, the generating units are increased. Bus 10 is chosen as the slack bus. Bus data reassignment and load flow analysis is carried out. However, based on the generator data shown in Table A-3, the slack bus will not be able to absorb the total power imbalance as the maximum limit of the generator is 550 MW. Due to that, the load is shared equally between all five generating units. The post-splitting columns shows that the all the generator bus value has been increased to meet the load demand and further ensure that the load-generation balance in the island is met

Table 4.47: Second island information for Case 8

Buses 74 (41 – 112, 116, 118)		
Generating Bus	**Pre-Splitting**	**Post-Splitting**
46	19	19
49	204	204
54	48	48
59	155	155
61	160	160
65	391	391
66	392	392
69*	511.92	328.91
80	477	477
87	4	4
89	607	607
100	252	252
103	40	40
111	36	36
$\sum P_{Generation}$ (MW)	3296.92	3113.91
$\sum P_{Load}$ (MW)	3027	3027
$\sum P_{Loss}$ (MW)	86.34	86.91
$\sum P_{imbalance}$ (MW)	183.58	0

**** slack bus***

Table 4.47 shows the islanding information for island 2 in which the slack bus is located. In island 2, a surplus power of 156.91 MW is experienced. Bus data reassignment and load flow analysis is carried out and the slack bus generation is subsequently reduced to meet the load-generation balance. In this case, the load shedding was not carried out as the load-generation balance was met as the generators were still able to provide the required power. The transmission line power flow analysis is carried out and results show that that the power flow is well within the maximum allowable capacity of the transmission lines. The complete result of the transmission line power flow analysis is included in the Appendix section (Table B-7).

4.12 Case 9: IEEE 118-Bus Test System (Coherency set 3)

4.12.1 First Phase: Edge reduction for Case 9

In this case, the IEEE 118-bus test system is analyzed based on investigation presented by (L. Liu et al., 2009) The system parameters as reported by (L. Liu et al., 2009) are listed in Table 4.48.

Table 4.48: System Parameters for Case 9

Desired number of islands:	2
Coherent group:	Group 1 = {10,12,25,26,31,46,49,54,59,61,65,66,69,80}
of generators	Group 2 = {87,89,100,103,111}

In the first phase of investigation, the edge reduction algorithm is carried out to determine the initial number of transmission lines which needs to be disconnected to result in the desired number of islands with the coherent group of generators. The edge reduction algorithm is applied for the IEEE 118-bus test system as shown in Figure 4.33. The initial search space is reduced to 5 lines as an initial solution.

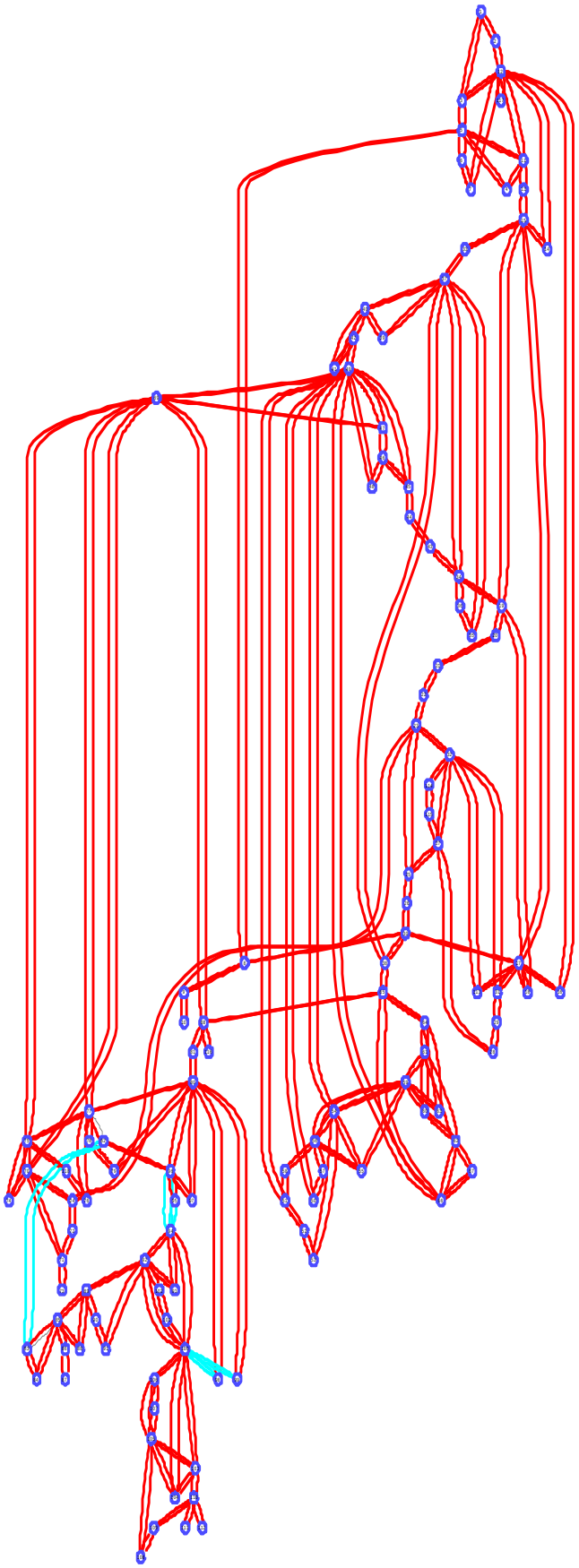

Figure 4.33: Edge reduction algorithm for Case 9

Table 4.49: Initial network splitting solution for Case 9

Initial splitting solution	Power flow (MW)
82 – 83	47.74
94 – 95	40.98
94 – 96	19.89
98 – 100	5.45
99 – 100	22.93
$\sum P_{min}$	136.98

Table 4.49 shows the initial network splitting solution obtained after the edge reduction algorithm has been implemented. The initial minimal power-flow disruption obtained ($\sum P_{min}$) is 136.98 MW. This initial solution is then passed on to the second phase to find the optimum network splitting solution.

4.12.2 Second Phase: Modified ABC optimization for Case 9

The proposed modified ABC optimization is applied to the test system and the optimum network splitting solution is obtained for the test case as shown in Table 4.50. The optimum number of lines to be disconnected is two and the minimal power-flow disruption obtained is 93.77 MW. This optimized minimal power-flow disruption value is lower than the reported value of 176.08 MW based on the reported investigation (L. Liu et al., 2009) and 119.49 based on the modified PSO. Furthermore, the number of lines disconnected is also lower than the reported value and the modified PSO technique.

Table 4.50: Optimum network splitting solution for Case 9

Reported investigation (L. Liu et al., 2009)	Power flow (MW)	Modified PSO	Power flow (MW)	Modified ABC	Power flow (MW)
80 – 96	18.87	80 – 99	19.37	80 – 99	19.37
80 – 97	26.32	82 – 83	47.74	82 – 83	47.74
80 – 98	28.77	83 – 84	25.72	94 – 96	19.89
82 – 96	10.11	94 – 96	19.89	95 – 96	1.32
83 – 84	25.72	95 – 96	1.32	98 – 100	5.45
83 – 85	43.35	98 – 100	5.45		
99 – 100	22.93				
$\sum P_{min}$	176.08	$\sum P_{min}$	119.49	$\sum P_{min}$	93.77

Figure 4.34 shows the one line diagram of the islanding solution.

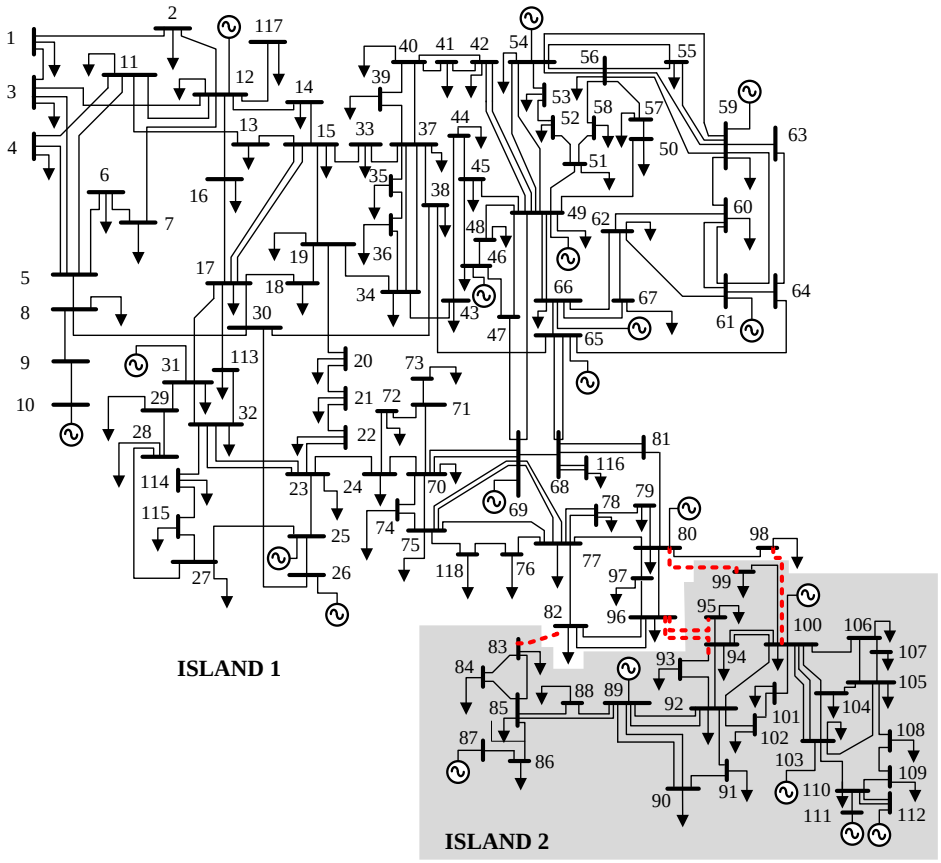

Figure 4.34: Islanding solution for case 9

Figure 4.35 shows the convergence curve for case 9 of both optimization techniques. The figure shows that both the modified ABC based on discrete values is able to converge to the global minima compared to the modified PSO based on discrete values.

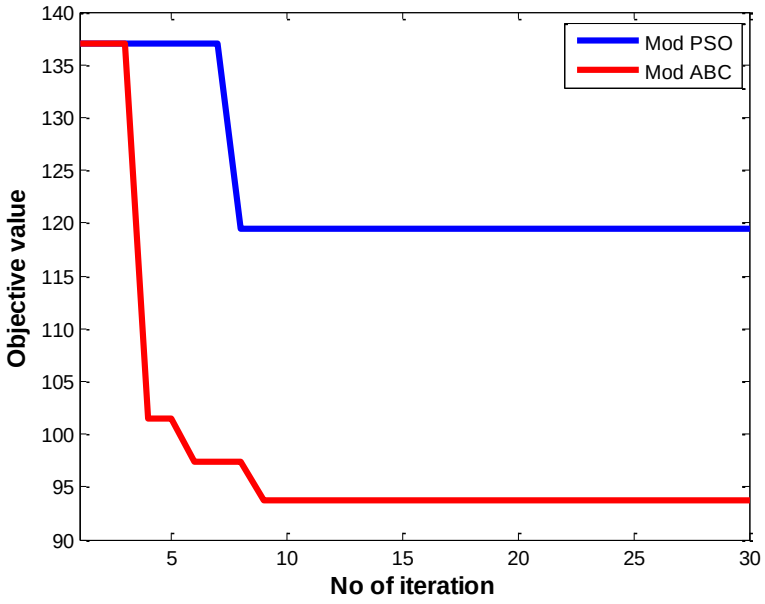

Figure 4.35: Convergence curve for Case 9

Table 4.51: First island information for Case 9

Buses 91 (1 – 82, 96 – 98, 113 – 118)		
Generating Bus	**Pre-Splitting**	**Post-Splitting**
10	450	450
12	85	85
25	220	220
26	314	314
31	7	7
46	19	19
49	204	204
54	48	48
59	155	155
61	160	160
65	391	391
66	392	392
69*	511.92	566.12
80	477	477
$\sum P_{Generation}$ **(MW)**	3433.92	3488.12
$\sum P_{Load}$ **(MW)**	3388	3388
$\sum P_{Loss}$ **(MW)**	96.45	100.12
$\sum P_{imbalance}$ **(MW)**	-50.53	0

**** slack bus***

In island 1, a deficit power imbalance of 50.53 MW is observed as shown in Table 4.51. The slack bus (bus 69) is located in this island. The bus data reassignment and load flow analysis is carried out and it is evaluated that the slack bus is able to cater for the power imbalance. Once the generation value of the slack bus is increased, the load-generation balance criteria is met as seen in the post-splitting column.

Table 4.52: Second island information for Case 9

Buses 27 (83 – 95, 99 – 112)		
Bus	**Generation**	
	Pre-Splitting	**Post-Splitting**
87	4	4
89	607	551.26*
100	252	252
103	40	40
111	36	36
$\sum P_{Generation}$ **(MW)**	939	883.27
$\sum P_{Load}$ **(MW)**	854	854
$\sum P_{Loss}$ **(MW)**	32.53	29.27
$\sum P_{imbalance}$ **(MW)**	52.47	0

**** slack bus***

Table 4.52 shows the islanding information for island 2. In island 2, a surplus power of 52.47 MW is experienced. Bus data reassignment and load flow analysis is carried out

and bus 89 is chosen as the slack bus since the slack bus is not originally located in this island. The slack bus generation is then reduced to meet the load-generation balance.

The transmission line power flow analysis is carried out and results show that that the power flow is well within the maximum allowable capacity of the transmission lines. The complete result of the transmission line power flow analysis is included in the Appendix section (Table B-8).

4.13 Summary

In this chapter, the proposed optimal network splitting algorithm for large scale power system is presented. The algorithm consists of two main phases. In the first phase, the edge reduction algorithm is implemented. The edge reduction algorithm presents the initial set of transmission lines to be disconnected in shortest time possible. Once the initial line configuration is obtained, the modified ABC optimization is implemented to obtain the optimum splitting solution.

In order to further highlight the advantage of the proposed modified ABC optimization, the algorithm is compared to modified PSO technique. The convergence test was carried out and it was clearly seen that the proposed modified ABC optimization is able to perform better in all the nine test cases. The proposed modified ABC optimization forages the search space to obtain the solution with minimal power flow disruption with the least possible number of lines to be disconnected. This is validated by implementing the proposed algorithm on the IEEE 30-bus, 39-bus and 118-bus test system. The obtained solution is also compared with published results. In eight of the test cases, better results were achieved and for case seven, similar results were achieved.

The algorithm also incorporates bus load shedding scheme and transmission line power flow analysis in order to determine the post islanding stability of the system. This is because, in this research, the network splitting solution is deemed optimum when these criteria are also met. The main contribution highlighted here however is the flexibility and adaptability of the proposed algorithm. The objective function can be easily changed to include different objective functions such as line stability index or power imbalance in each islands. Reactive power and multi objective consideration can also be easily incorporated in the algorithm.

CHAPTER 5: VALIDATION OF PROPOSED LOAD FREQUENCY CONTROL OPTIMIZATION

5.1 Introduction

In this chapter, the multi objective ABC optimization and online wavelet filter developed in Chapter 3 is implemented. Three different LFC test cases based on the islanded areas obtained in Chapter 4 are used in this chapter for further investigation. In this research, the frequency stability in the islanded areas is one of the important concerns of this investigation. In order to realize this, the multi objective ABC optimization based on weighted sum approach is used to find the optimal tuning parameters for the PID. In order to verify the tuning performance of the multi objective ABC optimization technique, comparative investigation is carried out with the multi objective PSO technique. The optimum PID parameter and weightage set is then selected based on the Least Average Error (LAE) performance index.

The online wavelet filter is subsequently implemented to filter out the noisy ACE signal. A comparative investigation with the conventional low pass filter is carried out to highlight the performance of the wavelet filter. The signal integrity index is used to evaluate the performance of each filtering technique and further investigation is carried out to show the importance of wavelet selection in determining the performance of the wavelet filter. The complete details pertaining to the optimal PID parameters and the online wavelet filter are presented. The system parameters of the LFC model are included in the appendix section (Appendix C).

5.2 LFC Test System

In order to validate the effectiveness of the proposed multi objective ABC optimization technique in tuning the PID parameters of the LFC, three different test systems are used. In each test system a different test case based on the investigation carried out in Chapter 4 is used to evaluate the performance of the tuning algorithm. Comparative investigation between the multi objective ABC optimization tuning technique and multi objective PSO tuning technique is carried out to further highlight the effectiveness of the proposed tuning algorithm. The test cases used are:

a) Case 1 (Chapter 4 – Section 4.4)

   In this test case, the LFC model of the IEEE 30-bus test system shown in Section 4.4 is designed and the LFC for each island is optimally tuned.

b) Case 6 (Chapter 4 – Section 4.9)

   In this test case, the LFC model of the modified IEEE 39-bus test system shown in Section 4.9 is designed and the LFC for each island is optimally tuned.

c) Case 7 (Chapter 4 – Section 4.10)

   In this test case, the LFC model of the IEEE 118-bus test system shown in Section 4.10 is designed and the LFC for each island is optimally tuned.

The load variation test is carried out in order to observe the tuning capability of the proposed controller optimization technique. In the load variation test, the load demand for each island is varied in the range of ±50% of the total load demand based on a step size of 25% to observe the frequency response of the system under different loading

conditions. This test is carried out to observe the performance of the generators in each area as a standalone network when the load is increased or decreased.

Once the optimum values of the PID parameters for the LFC has been obtained, the performance of the online wavelet filter is evaluated. This is done by comparing the noisy Area Control Error (ACE) signal of the online wavelet filter against the ACE signal from the conventional low pass filter and ACE signal without a filter. The signal integrity index is evaluated and the results of the investigation are shown. The choice of wavelet selection is then further highlighted by varying the performance of the online wavelet filter with the following wavelets:

a) Daubechies 1 (db1)
b) Daubechies 5 (db5)
c) Daubechies 9 (db9)
d) Symlets 1 (sym1)
e) Symlets 5 (sym5)
f) Symlets 9 (sym9)
g) Coiflets 1 (coif1)
h) Coiflets 3 (coif3)
i) Coiflets 5 (coif5)

5.3 LFC Test Case 1

In this investigation, the LFC model of IEEE 30-bus test systems shown in Chapter 4 (Section 4.4) is realized. In this case, the power system network is split into two islands. In island 1, there are four generating units represented by generators in bus 1, 2, 5 and 13. In island 2, there are two generating units represented by generators in bus 8 and 11. Details of the load modeling are given in Appendix C. The parameters for the two area power system are given in Table C-1.

5.3.1 Load variation investigation in Island 1

The nominal load demand for island 1 is fixed as per the load demand shown for the optimum network splitting solution shown in Section 4.4. In order to further analyze the performance of the load frequency control in a standalone network, the load demand in the respective island is increased and decreased in a step size of 25% to 50% based on the aggregated maximum generation capability of the generators. The information of IEEE 30-bus generator data is given in Table A-1. Table 5.1 shows the load demand (P_{Load}) and the maximum generation capability (P_{Gmax}) of the generators in island 1.

Table 5.1: First island information for LFC Test Case 1

Generation	
Bus	**P_{Gmax}**
1	360.2
2	140
5	100
13	100
$\sum P_{Gmax}$ (MW)	700.2
Load	
$\sum P_{Load}$ (MW)	161.4

This means that the generators are able to cater for an additional load demand of 538.8 MW before the load-generation equilibrium is violated. In the load increment phase, the nominal load demand for island 1 is initially increased by 25% to 0.135 pu MW and subsequently by 50% to 0.269 pu MW. In the load decrement phase, the nominal load

demand for island 1 is initially decreased by 25% to -0.135 pu MW and subsequently by 50% to -0.269 pu MW.

Table 5.2 shows the weightage set and the corresponding performance index based on LAE for load variation investigation of island 1 for both multi objective ABC and multi objective PSO based optimization technique.

Table 5.2: Weightage set and corresponding performance index based on LAE of Island 1 for LFC Test Case 1

w_1	w_2	η_{LAE}							
		ΔP_L = +50%		ΔP_L = +25%		ΔP_L = -50%		ΔP_L = -25%	
		PSO	**ABC**	**PSO**	**ABC**	**PSO**	**ABC**	**PSO**	**ABC**
1	0	1.87	5.86	2.23	6.03	2.38	6.51	0.40	6.12
0.9	0.1	0.71	5.87	6.27	6.43	4.68	6.61	5.96	6.16
0.8	0.2	1.84	6.00	1.18	7.24	0.00046	8.18	3.43	6.33
0.7	0.3	8.63	6.37	2.28	8.02	2.40	9.44	5.55	6.44
0.6	0.4	1.97	6.38	7.80	12.76	2.32	10.96	3.54	6.53
0.5	0.5	1.70	11.24	3.73	13.22	1.98	14.23	2.31	7.25
0.4	0.6	2.00	19.05	2.69	13.79	2.81	21.42	6.69	12.89
0.3	0.7	10.03	13.53	3.00	13.59	11.59	18.11	2.54	12.48
0.2	0.8	2.30	6.69	3.89	7.27	3.75	7.93	0.68	6.92
0.1	0.9	7.57	6.87	5.81	6.68	5.21	7.92	2.86	6.39
0	1	2.30	6.77	2.16	6.54	2.38	7.84	6.65	6.30

Referring to the information presented in Table 5.2, it can be seen that the overall performance of the ABC based optimization technique is better than PSO based optimization technique. The best overall performance of both the optimization techniques are shown in Table 5.3.

Table 5.3: Optimum weightage set and LAE of Island 1 for LFC Test Case 1

Optimization technique	**Load demand (pu MW)**	**Weightage set**		η_{LAE}
		w_1	w_2	
ABC	0.269	0.4	0.6	19.05
PSO		0.3	0.7	10.03
ABC	0.135	0.4	0.6	13.79
PSO		0.6	0.4	7.80
ABC	-0.269	0.4	0.6	21.42
PSO		0.3	0.7	11.59
ABC	-0.135	0.4	0.6	12.89
PSO		0.4	0.6	6.69

From the Table 5.3, it can be seen that the ABC technique is able to achieve a higher LAE compared to PSO based on a consistent weightage set of w_1 = 0.4 and w_2 = 0.6. Table 5.4 shows the optimal PID parameters and the system performance when the load is varied for both optimization technique based on the optimum weightage set.

Table 5.4: Optimal PID controller gains and system performance of Island 1 for LFC Test Case 1

		Controller paramters			**System performance**	
	ΔP_L	**K_{p1}**	**T_{i1}**	**T_{d1}**	**Settling time (s)**	**Max. overshoot (Hz)**
ABC	+50%	0.314	0.954	0.443	9.394	-0.00570
PSO		0.302	1.218	0.450	11.68	-0.00570
ABC	+25%	0.311	1.023	0.444	11.663	-0.00286
PSO		0.279	1.163	0.412	12.368	-0.00287
ABC	-50%	0.3	1.053	0.493	11.380	0.00569
PSO		0.221	0.754	1.000	12.853	0.00568
ABC	-25%	0.308	0.848	0.445	9.661	0.00286
PSO		0.267	0.834	0.517	11.122	0.00286

Figures 5.1 – 5.4 shows the system's frequency deviation step response and generator power response for both optimization technique based on their optimum values.

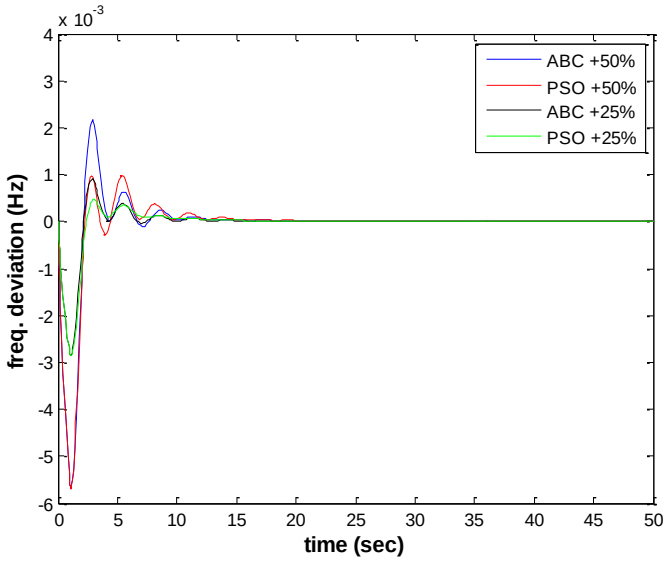

Figure 5.1: Frequency deviation step response for load increment in island 1 for LFC Test Case 1

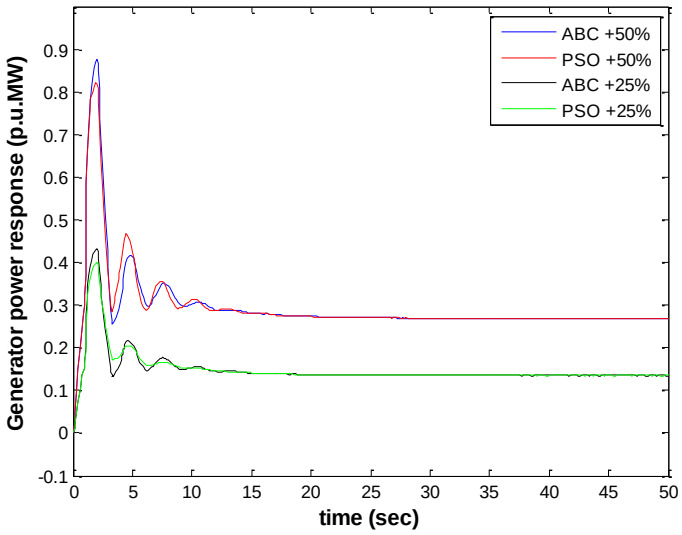

Figure 5.2: Generator power response for load increment in island 1 for LFC Test Case 1

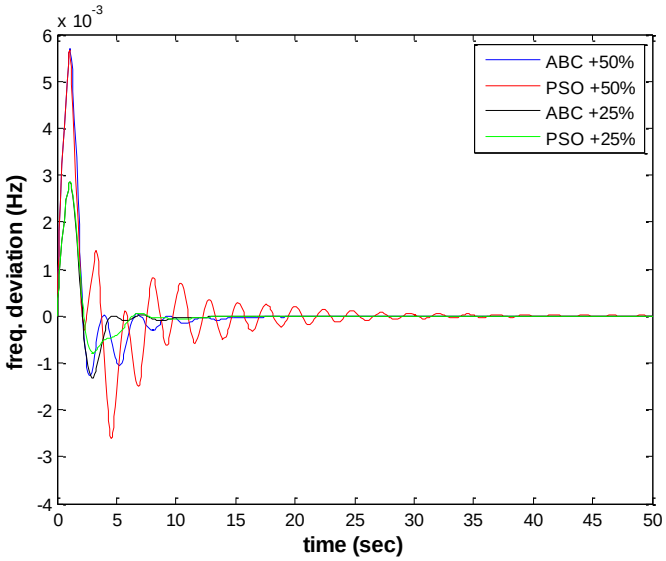

Figure 5.3: Frequency deviation step response for load decrement in island 1 for LFC Test Case 1

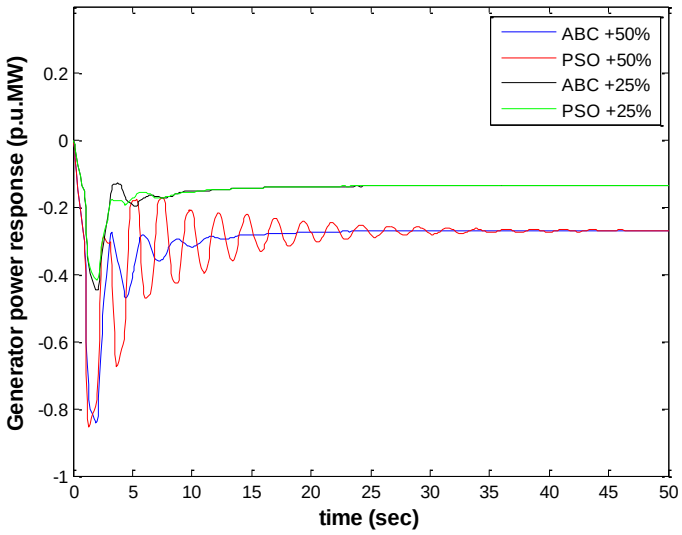

Figure 5.4: Generator power response for load decrement in island 1 for LFC Test Case 1

In Island 1 which operates as a standalone network, it can be seen that the ABC tuned LFC is able to settle the system in allowable settling time with reasonable maximum overshoot and undershoot value. No major issues such as oscillation in the islands or prolonged under frequency or over frequency value is observed.

5.3.2 Online wavelet filter implementation in island 1

In order to highlight the performance of the online wavelet filter, the ACE signal of the ABC optimized LFC is analyzed. High frequency noise is added to the system and the performance of the system is evaluated. The Gaussian white noise function in Matlab Simulink is used to add the high frequency noise component in the LFC model. Four different output signals are obtained each for the load increment and load decrement investigation to highlight the performance of the online wavelet filter. Figures 5.5 – 5.8 shows the ACE signal analysis for the load increment investigation and Figure is 5.9 – 5.12 shows the ACE signal analysis for the load decrement investigation. The ***db1*** wavelet is selected as the default wavelet to be used.

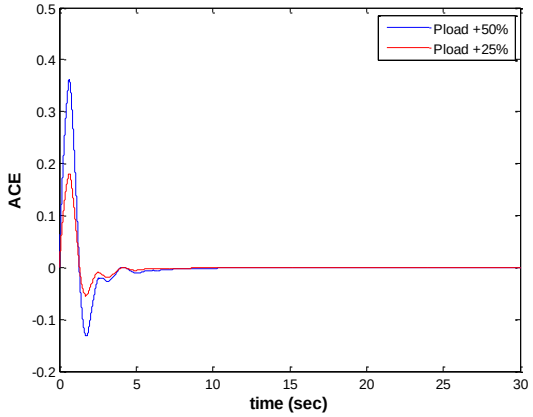

Figure 5.5: Clean ACE signal for load increment in island 1 for LFC Test Case 1

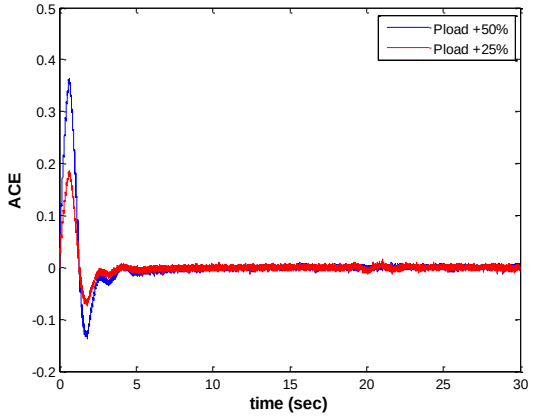

Figure 5.6: Noisy ACE signal for load increment in island 1 for LFC Test Case 1

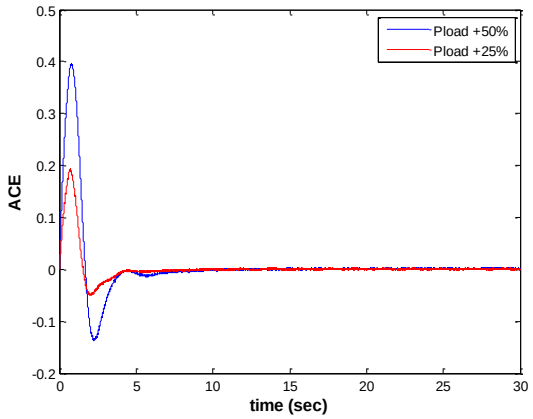

Figure 5.7: Noisy ACE signal with conventional low pass filter for load increment in island 1 for LFC Test Case 1

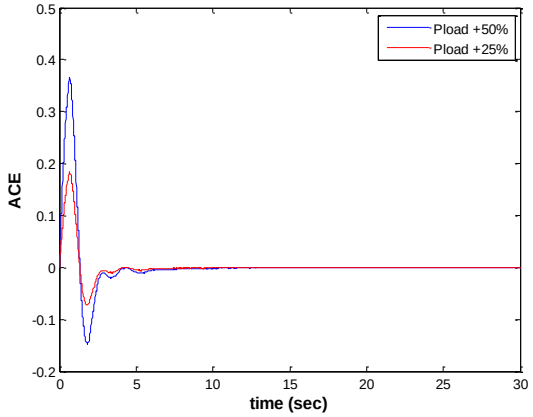

Figure 5.8: Noisy ACE signal with wavelet filter for load increment in island 1 for LFC Test Case 1

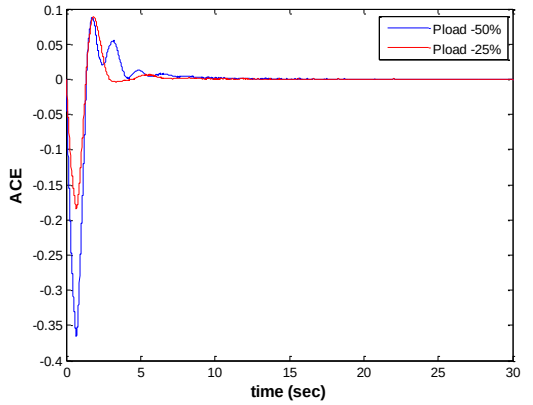

Figure 5.9: Clean ACE signal for load decrement in island 1 for LFC Test Case 1

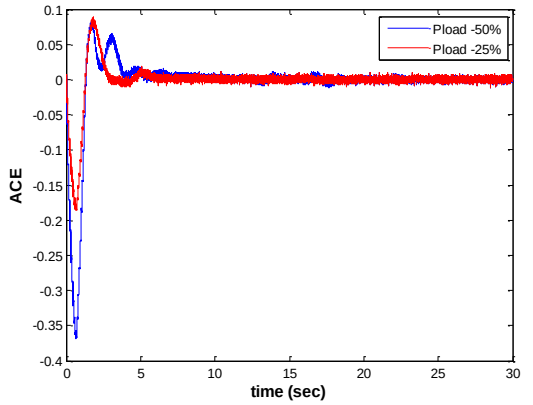

Figure 5.10: Noisy ACE signal for load decrement in island 1 for LFC Test Case 1

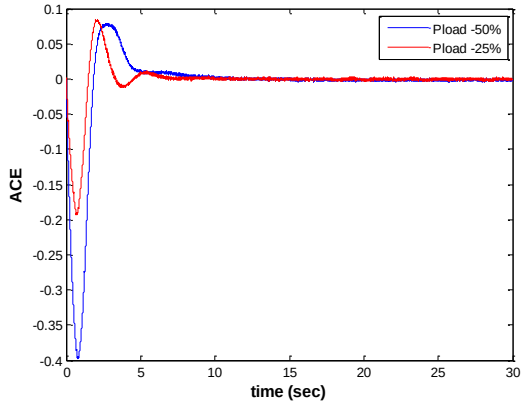

Figure 5.11: Noisy ACE signal with conventional low pass filter for load decrement in island 1 for LFC Test Case 1

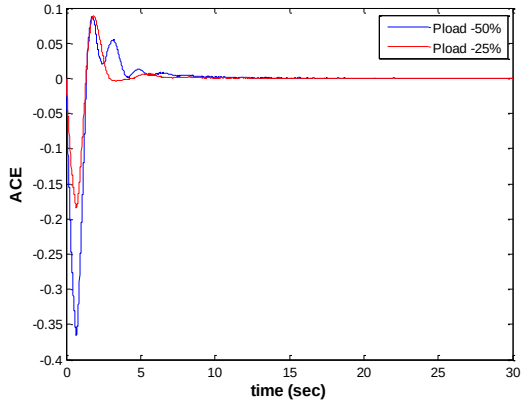

Figure 5.12: Noisy ACE signal with wavelet filter for load decrement in island 1 for LFC Test Case 1

Figure 5.5 and 5.9 shows the clean ACE signal with no noise component present. Figure 5.6 and 5.10 shows the ACE signal with presence of noise. Figure 5.7 and 5.11 shows the noisy ACE signal which is filtered conventional low pass filter. Figure 5.8 and 5.12 shows the noisy ACE signal filtered by online wavelet filter. Based on the figures, it can be clearly seen that the online wavelet filtered ACE signal shows a closer resemblance to the clean ACE signal. The signal integrity index is then subsequently calculated to view the index of the signal similarity. Table 5.5 shows the signal integrity index for the load increment investigation in island 1. An index value of 1 shows the closest resemblance to the ideal noise free ACE signal. The wavelet filter signal is used as the benchmark to be compared against by the unfiltered ACE signal and the ACE signal filtered by the conventional low pass filter.

Table 5.5: Signal integrity index for load variation investigation in island 1 for LFC Test Case 1

ΔP_L	ACE signal	Signal integrity index
50%	Unfiltered	0.8195
	Low pass filter	0.8394
	Wavelet filter	1.000
25%	Unfiltered	0.7224
	Low pass filter	0.8796
	Wavelet filter	1.000
-50%	Unfiltered	0.8022
	Low pass filter	0.8203
	Wavelet filter	1.000
-25%	Unfiltered	0.7265
	Low pass filter	0.8792
	Wavelet filter	1.000

From Table 5.5 it can be seen that the ACE signal filtered by the wavelet filter shows closer resemblance to the ideal ACE signal with the least amount of noise. This is followed by the conventional low pass filter and finally the unfiltered signal with the most amount of noise. In order to further scrutinize the selection of wavelet type, nine different wavelets are investigated and the signal integrity index for each wavelet type is evaluated as are shown in the bar plot in Figure 5.13.

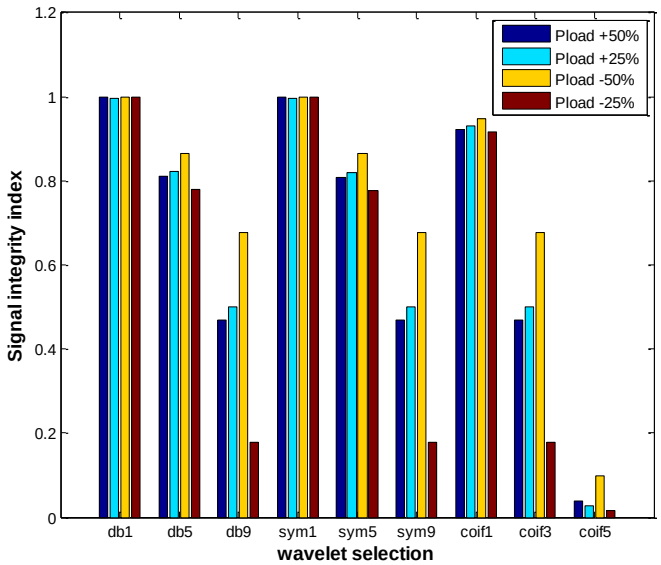

Figure 5.13: Signal integrity index for various wavelet choices in island 1 for LFC Test Case 1

Results in Figure 5.13 shows that the selection of wavelet type plays a very important role towards the performance of the online wavelet filter for the LFC problem. All four load demand levels of +25%, +50%,-25%, and -50% are investigated and the highest

signal integrity index are recorded. In the +50% and +25% load demand level, the highest signal integrity index of 1 and 0.9960 is recorded respectively. In the -50% and -25% load demand level, the highest signal integrity index of 0.9982 and 1 is recorded respectively. The indexes are attributed to the *daubechies1* wavelet and *symlet1* wavelet.

5.3.3 Load variation investigation in Island 2

The nominal load demand for island 2 is fixed as per the load demand shown for the optimum network splitting solution shown in Chapter 4 (Section 4.4). In order to further analyze the performance of the load frequency control in a standalone network, the load demand in the respective island is increased and decreased in a step size of 25% to 50% based on the aggregated maximum generation capability of the generators. The information of IEEE 30-bus generator data is given in Table A-1. Table 5.6 shows the load demand (P_{Load}) and the maximum generation capability (P_{Gmax}) of the generators in island 2.

Table 5.6: Second island information for LFC Test Case 1

Generation	
Bus	**P_{Gmax}**
8	100
11	100
$\sum P_{Gmax}$ (MW)	200
Load	
$\sum P_{Load}$ (MW)	122

This means that the generators are able to cater for an additional load demand of 78 MW before the load-generation equilibrium is violated. In the load increment phase, the nominal load demand for island 1 is initially increased by 25% to 0.0195 pu MW and subsequently by 50% to 0.039 pu MW. In the load decrement phase, the nominal load demand for island 2 is initially decreased by 25% to -0.0195 pu MW and subsequently by 50% to -0.039 pu MW.

Table 5.7 shows the weightage set and the corresponding performance index based on LAE for load variation investigation of island 2 for both multi objective ABC and multi objective PSO based optimization technique.

Table 5.7: Weightage set and corresponding performance index based on LAE of Island 2 for LFC Test Case 1

w_1	w_2	η_{LAE}							
		ΔP_L = +50%		ΔP_L = +25%		ΔP_L = -50%		ΔP_L = -25%	
		PSO	**ABC**	**PSO**	**ABC**	**PSO**	**ABC**	**PSO**	**ABC**
1	0	4.59	6.62	5.47	6.09	5.75	6.34	5.31	5.97
0.9	0.1	0.80	6.53	4.50	6.13	8.10	6.38	1.73	5.99
0.8	0.2	0.24	10.64	1.20	6.31	2.57	8.14	8.90	6.11
0.7	0.3	12.51	13.37	3.77	7.65	3.07	8.17	7.18	6.55
0.6	0.4	3.89	14.73	3.73	7.73	1.34	10.00	0.56	9.13
0.5	0.5	2.24	17.40	7.19	9.27	7.27	14.01	0.87	9.57
0.4	0.6	13.53	11.07	1.12	9.21	0.22	6.74	1.81	7.03
0.3	0.7	0.62	10.39	5.12	7.65	1.08	6.57	0.26	6.14
0.2	0.8	11.35	9.82	1.05	6.18	10.39	6.54	0.86	6.13
0.1	0.9	8.51	7.76	3.17	5.99	1.49	6.30	2.89	6.00
0	1	4.95	6.34	6.07	5.85	2.23	6.09	1.67	5.73

Referring to the information presented in Table 5.7, it can be seen that the overall performance of the ABC based optimization technique is better than PSO based optimization technique. The best overall performance of both the optimization techniques is shown in Table 5.8.

Table 5.8: Optimum weightage set and LAE of Island 2 for LFC Test Case 1

Optimization technique	**Load demand (pu MW)**	**Weightage set**		η_{LAE}
		w_1	w_2	
ABC	0.039	0.5	0.5	17.40
PSO		0.4	0.6	13.53
ABC	0.0195	0.5	0.5	9.27
PSO		0.5	0.5	7.19
ABC	-0.039	0.5	0.5	14.01
PSO		0.2	0.8	10.39
ABC	-0.0195	0.5	0.5	9.57
PSO		0.8	0.2	8.90

From the Table 5.8, it can be seen that the ABC technique is able to achieve a higher LAE compared to PSO based on a consistent weightage set of w_1 = 0.5 and w_2 = 0.5.

Table 5.9 shows the optimal PID parameters and the system performance when the load is varied for both optimization techniques based on the optimum weightage set.

Table 5.9: Optimal PID controller gains and system performance of Island 2 for LFC Test Case 1

		Controller paramters			System performance	
	ΔP_L	K_{p1}	T_{i1}	T_{d1}	Settling time (s)	Max. overshoot (Hz)
ABC	+50%	0.552	0.853	0.438	11.189	-0.00145
PSO		0.482	0.913	0.500	11.928	-0.00145
ABC	+25%	0.543	0.824	0.451	9.046	-0.000728
PSO		0.426	0.849	0.613	10.204	-0.000729
ABC	-50%	0.503	1.004	0.485	11.026	0.00145
PSO		0.481	0.780	0.532	11.890	0.00145
ABC	-25%	0.548	0.881	0.422	9.184	0.000726
PSO		0.541	0.848	0.497	11.134	0.000728

Figures 5.14 – 5.17 shows the system's frequency deviation step response and generator power response for both optimization technique based on their optimum values.

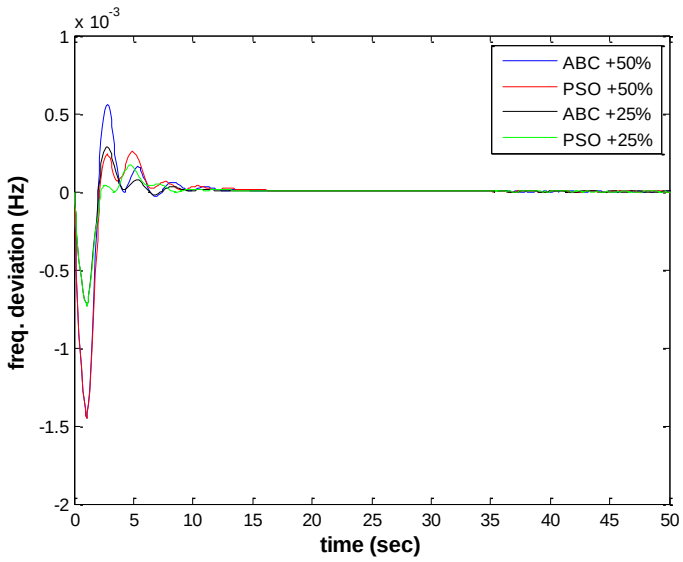

Figure 5.14: Frequency deviation step response for load increment in island 2 for LFC Test Case 1

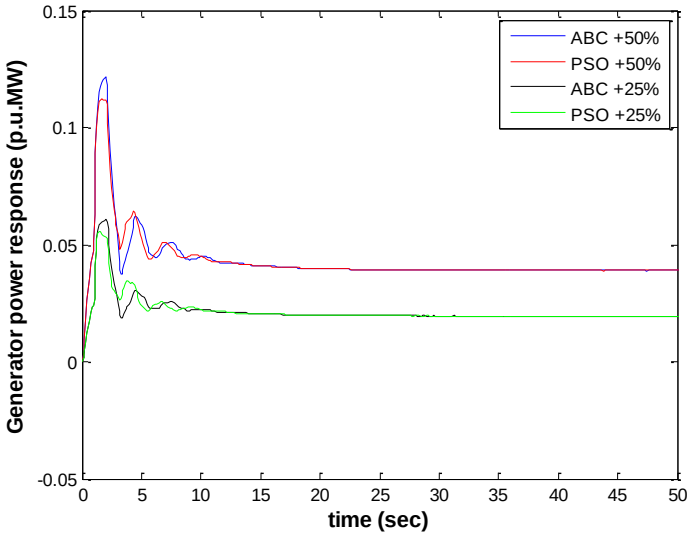

Figure 5.15: Generator power response for load increment in island 2 for LFC Test Case 1

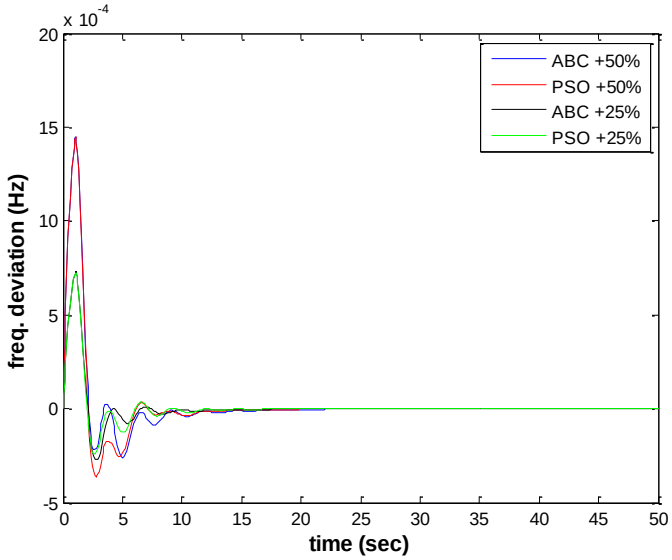

Figure 5.16: Frequency deviation step response for load decrement in island 2 for LFC Test Case 1

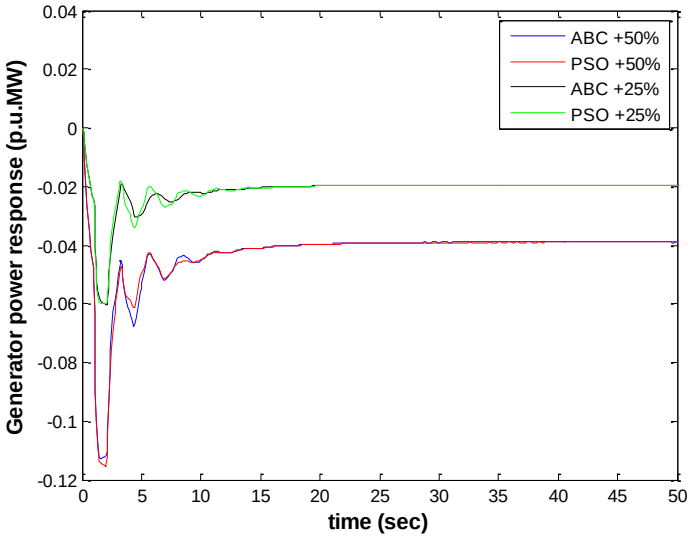

Figure 5.17: Generator power response for load decrement in island 2 for LFC Test Case 1

In island 2 which operates as a standalone network, it can be seen that the ABC tuned LFC is able to settle the system in allowable settling time with reasonable maximum overshoot and undershoot value. No major issues such as oscillation in the islands or prolonged under frequency or over frequency value is observed.

5.3.4 Online wavelet filter implementation in island 2

In order to highlight the performance of the online wavelet filter, the ACE signal of the ABC optimized LFC is analyzed. High frequency noise is added to the system and the performance of the system is evaluated. Four different output signals are obtained each for the load increment and load decrement investigation to highlight the performance of the online wavelet filter. Figures 5.18 – 5.21 shows the ACE signal analysis for the load increment investigation and Figures 5.22 – 5.25 shows the ACE signal analysis for the load decrement investigation. The ***db1*** wavelet is selected as the default wavelet to be used.

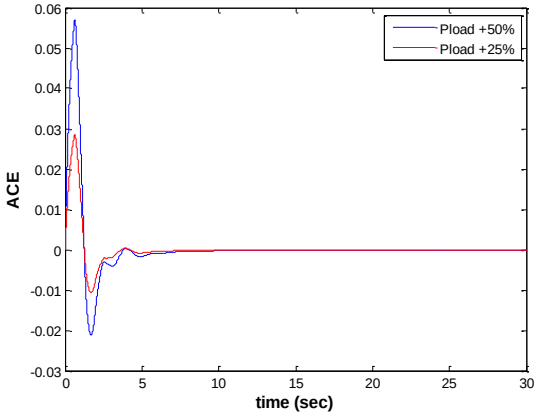

Figure 5.18: Clean ACE signal for load increment in island 2 for LFC Test Case 1

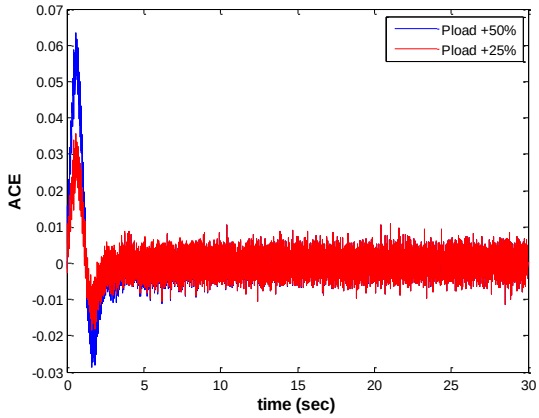

Figure 5.19: Noisy ACE signal for load increment in island 2 for LFC Test Case 1

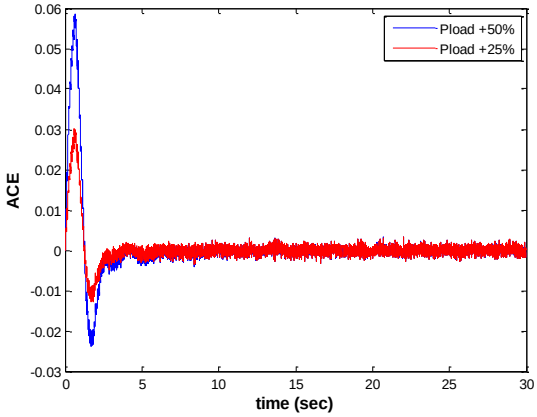

Figure 5.20: Noisy ACE signal with conventional low pass filter for load increment in island 2 for LFC Test Case 1

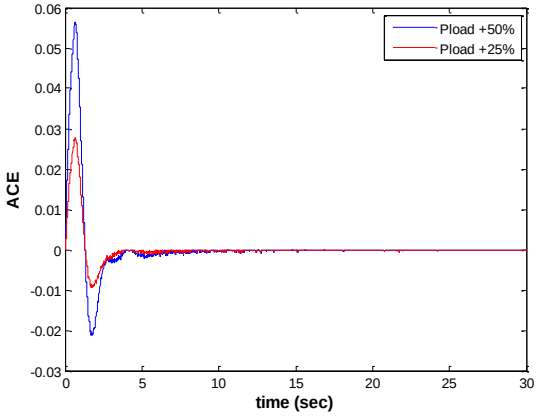

Figure 5.21: Noisy ACE signal with wavelet filter for load increment in island 2 for LFC Test Case 1

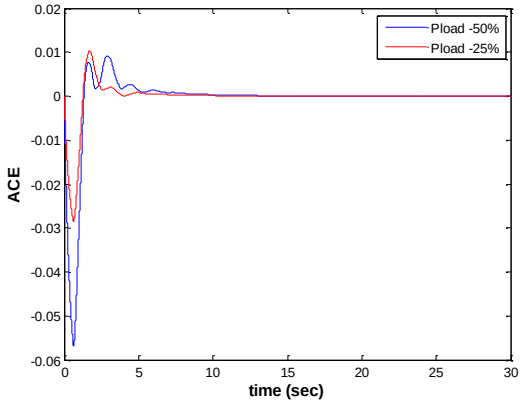

Figure 5.22: Clean ACE signal for load decrement in island 2 for LFC Test Case 1

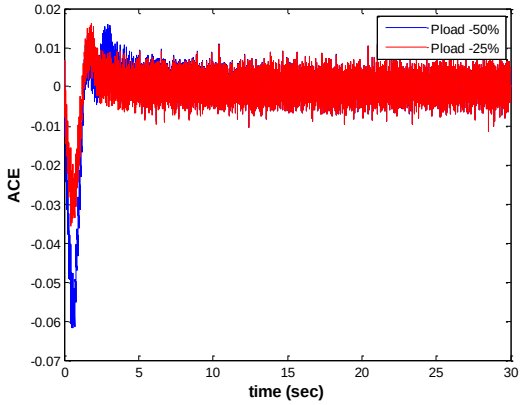

Figure 5.23: Noisy ACE signal for load decrement in island 2 for LFC Test Case 1

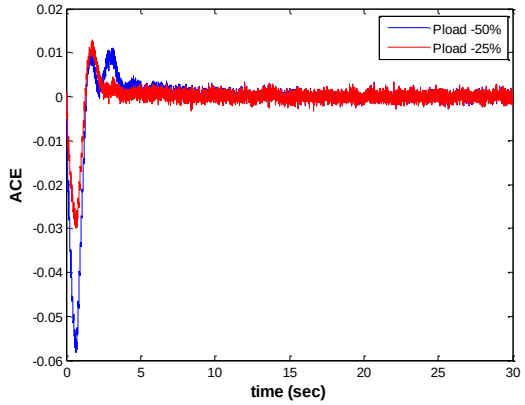

Figure 5.24: Noisy ACE signal with conventional low pass filter for load decrement in island 2 for LFC Test Case 1

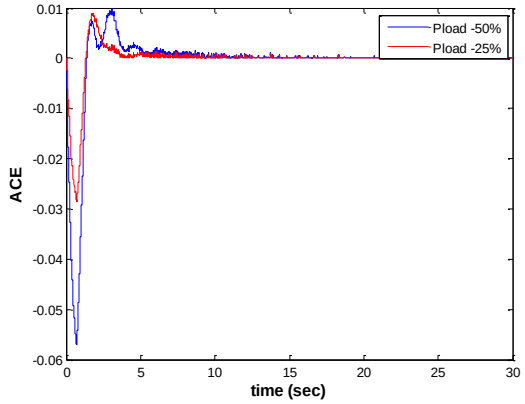

Figure 5.25: Noisy ACE signal with wavelet filter for load decrement in island 2 for LFC Test Case 1

Figure 5.18 and 5.22 shows the clean ACE signal with no noise component present. Figure 5.19 and 5.23 shows the ACE signal with presence of noise. Figure 5.20 and 5.24 shows the noisy ACE signal which is filtered conventional low pass filter. Figure 5.21 and 5.25 shows the noisy ACE signal filtered by online wavelet filter. Based on the figures, it can be clearly seen that the online wavelet filtered ACE signal shows a closer resemblance to the clean ACE signal. The signal integrity index is then subsequently calculated to view the index of the signal similarity. Table 5.10 shows the signal integrity index for the load increment investigation in island 1. An index value of 1 shows the closest resemblance to the ideal noise free ACE signal. The wavelet filter signal is used as the benchmark to be compared against by the unfiltered ACE signal and the ACE signal filtered by the conventional low pass filter.

Table 5.10: Signal integrity index for load variation investigation in island 2 for LFC Test Case 2

ΔP_L	ACE signal	Signal integrity index
50%	Unfiltered	0.5868
	Low pass filter	0.8284
	Wavelet filter	1.000
25%	Unfiltered	0.5033
	Low pass filter	0.7249
	Wavelet filter	1.000
-50%	Unfiltered	0.5895
	Low pass filter	0.8354
	Wavelet filter	1.000
-25%	Unfiltered	0.5107
	Low pass filter	0.7328
	Wavelet filter	1.000

From the table it can be seen that the ACE signal filtered by the wavelet filter shows closer resemblance to the ideal ACE signal with the least amount of noise. This is followed by the conventional low pass filter and finally the unfiltered signal with the most amount of noise. In order to further scrutinize the selection of wavelet type, nine different wavelets are investigated and the signal integrity index for each wavelet type is evaluated as are shown in the bar plot in Figure 5.26.

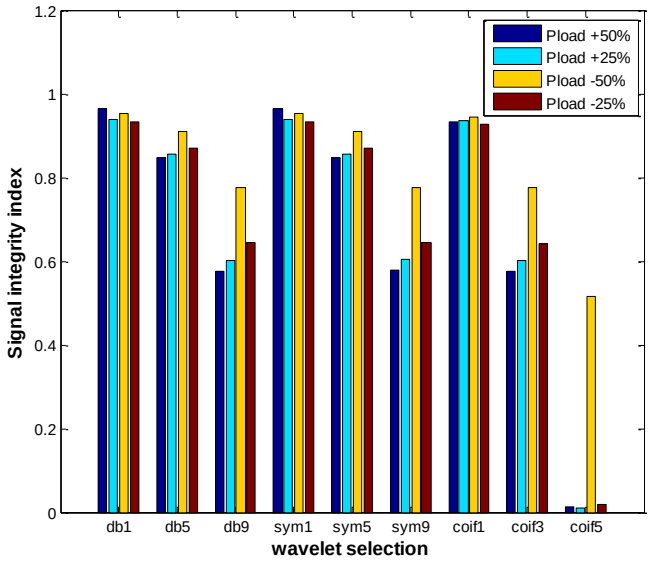

Figure 5.26: Signal integrity index for various wavelet choices in island 2 for LFC Test Case 1

Results in Figure 5.26 shows that the selection of wavelet type plays a very important role towards the performance of the online wavelet filter for the LFC problem. All four

load demand levels of +25%, +50%,-25%, and -50% are investigated and the highest signal integrity index are recorded. In the +50% and +25% load demand level, the highest signal integrity index of 0.9675 and 0.9399 is recorded respectively. In the -50% and -25% load demand level, the highest signal integrity index of 0.9555 and 0.9350 is recorded respectively. The indexes are attributed to the *daubechies1* wavelet and *symlet1* wavelet.

In this investigation for LFC test case 1, it can be seen that the optimum weightage set for island 1 is $w_1 = 0.4$ and $w_2 = 0.6$ and in island 2, the optimum weightage set $w_1 = 0.5$ and $w_2 = 0.5$. The best wavelet types to be used for the online wavelet filter for both islands are *daubechies1* and *symlet1*.

5.4 LFC Test Case 2

In this investigation, the LFC model of modified IEEE 39-bus test systems shown in Chapter 4 (Section 4.9) is realized. In this case, the power system network is split into four islands. In island 1, there are three generating units represented by generators in bus 30, 31 and 37. In island 2, there are three generating units represented by generators in bus 33, 35 and 36. In island 3, there are two generating units represented by generators in bus 34 and 38. In island 4, there are two generating units as well represented by generators in bus 32 and 39. Details of the load modeling are given in Appendix C. The parameters for the four area power system are given in Table C-2. In this test case, the investigation is carried out for one island only (island 3) since for the other islands the same process is implemented. However in island 2 and island 4 are not considered for the load increment investigation as according to the investigation carried out in Section 4.9, the generators in both these areas are operating at their maximum capability.

5.4.1 Load variation investigation in Island 3

The nominal load demand for island 3 is fixed as per the load demand shown for the optimum network splitting solution shown in Section 4.9. In order to further analyze the performance of the load frequency control in a standalone network, the load demand in the respective island is increased and decreased in a step size of 25% to 50% based on the aggregated maximum generation capability of the generators. The information of IEEE 39-bus generator data is given in Table A-2. Table 5.11 shows the load demand (P_{Load}) and the maximum generation capability (P_{Gmax}) of the generators in island 3.

Table 5.11: Third island information for LFC Test Case 2

Generation	
Bus	**P_{Gmax}**
34	508
38	865
$\sum P_{Gmax}$ (MW)	1373
Load	
$\sum P_{Load}$ (MW)	1067.5

This means that the generators are able to cater for an additional load demand of 305.5 MW before the load-generation equilibrium is violated. In the load increment phase, the nominal load demand for island 1 is initially increased by 25% to 0.0764 pu MW and subsequently by 50% to 0.153 pu MW. In the load decrement phase, the nominal load demand for island 1 is initially decreased by 25% to -0.0764 pu MW and subsequently by 50% to -0.153 pu MW.

Table 5.12 shows the weightage set and the corresponding performance index based on LAE for load variation investigation of island 2 for both multi objective ABC and multi objective PSO based optimization technique.

Table 5.12: Weightage set and corresponding performance index based on LAE of Island 3 for LFC Test Case 2

w_1	w_2	η_{LAE}							
		ΔP_L = +50%		ΔP_L = +25%		ΔP_L = -50%		ΔP_L = -25%	
		PSO	ABC	PSO	ABC	PSO	ABC	PSO	ABC
1	0	4.15	5.94	0.71	5.69	2.24	5.77	3.28	5.93
0.9	0.1	18.57	6.65	10.53	5.82	1.88	5.80	0.62	6.14
0.8	0.2	2.21	8.91	1.27	5.86	7.53	6.26	19.71	16.08
0.7	0.3	9.14	27.53	13.35	6.01	7.74	6.65	1.01	25.67
0.6	0.4	1.80	28.87	2.01	6.19	9.90	9.55	0.97	25.73
0.5	0.5	3.12	29.80	3.37	6.36	2.49	18.06	2.08	26.64
0.4	0.6	1.99	30.59	5.21	25.02	7.23	26.67	0.32	26.77
0.3	0.7	2.46	33.16	6.28	25.21	1.64	28.27	5.25	27.56
0.2	0.8	6.67	30.42	0.24	24.41	1.44	27.02	3.42	5.83
0.1	0.9	18.44	30.06	0.59	23.89	7.72	5.80	1.74	5.66
0	1	2.85	18.27	2.36	15.37	0.66	6.08	1.43	5.79

Referring to the information presented in Table 5.12, it can be seen that the overall performance of the ABC based optimization technique is better than PSO based optimization technique. The best overall performance of both the optimization techniques is shown in Table 5.13.

Table 5.13: Optimum weightage set and LAE of Island 3 for LFC Test Case 2

Optimization technique	Load demand (pu MW)	Weightage set		η_{LAE}
		w_1	w_2	
ABC	0.153	0.3	0.7	33.16
PSO		0.9	0.1	18.57
ABC	0.0764	0.3	0.7	25.21
PSO		0.7	0.3	13.35
ABC	-0.153	0.3	0.7	28.27
PSO		0.6	0.4	9.90
ABC	-0.0764	0.3	0.7	27.56
PSO		0.8	0.2	19.71

From the Table 5.13, it can be seen that the ABC technique is able to achieve a higher LAE compared to PSO based on a consistent weightage set of w_1 = 0.3 and w_2 = 0.7. Table 5.14 shows the optimal PID parameters and the system performance when the load is varied for both optimization techniques based on the optimum weightage set.

Table 5.14: Optimal PID controller gains and system performance of Island 3 for LFC Test Case 2

		Controller paramters			System performance	
	ΔP_L	K_{p1}	T_{i1}	T_{d1}	Settling time (s)	Max. overshoot (Hz)
ABC	+50%	0.672	1.270	0.622	12.518	-0.00310
PSO		0.635	1.487	0.616	12.630	-0.00310
ABC	+25%	0.685	1.278	0.597	12.673	-0.00154
PSO		0.528	1.872	0.468	15.421	-0.00158
ABC	-50%	0.705	1.028	0.542	10.780	0.00311
PSO		0.599	1.042	0.771	12.019	0.00309
ABC	-25%	0.68	1.290	0.601	12.633	0.00154
PSO		0.341	1.522	1.513	16.067	0.00154

Figures 5.27 – 5.30 shows the system's frequency deviation step response and generator power response for both optimization technique based on their optimum values.

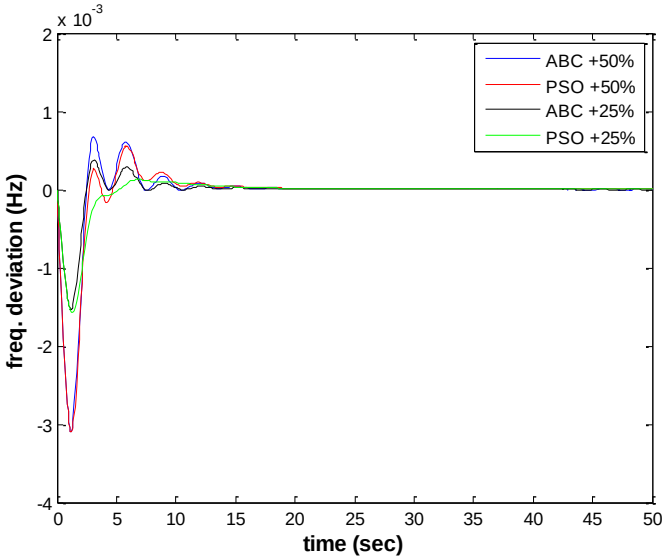

Figure 5.27: Frequency deviation step response for load increment in island 3 for LFC Test Case 2

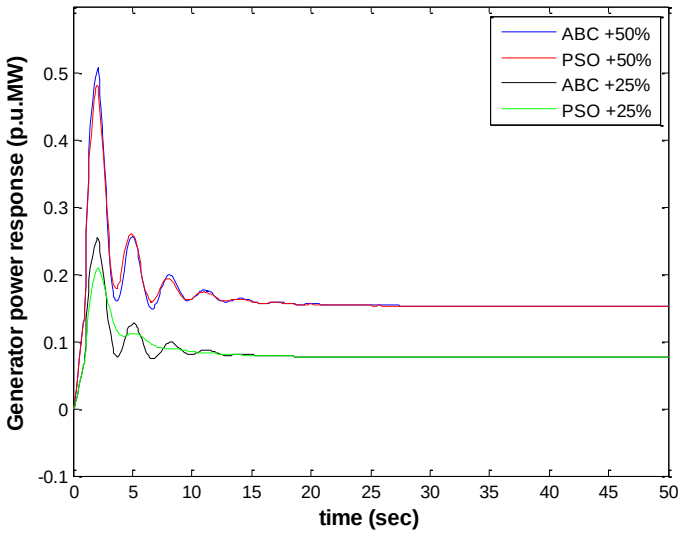

Figure 5.28: Generator power response for load increment in island 3 for LFC Test Case 2

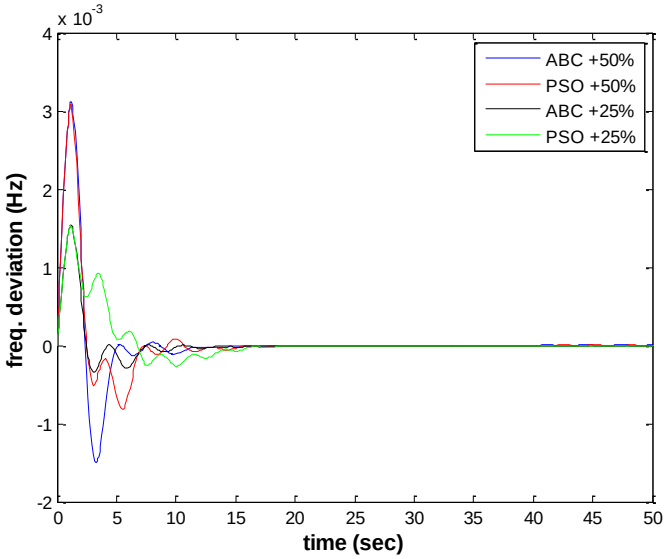

Figure 5.29: Frequency deviation step response for load decrement in island 3 for LFC Test Case 2

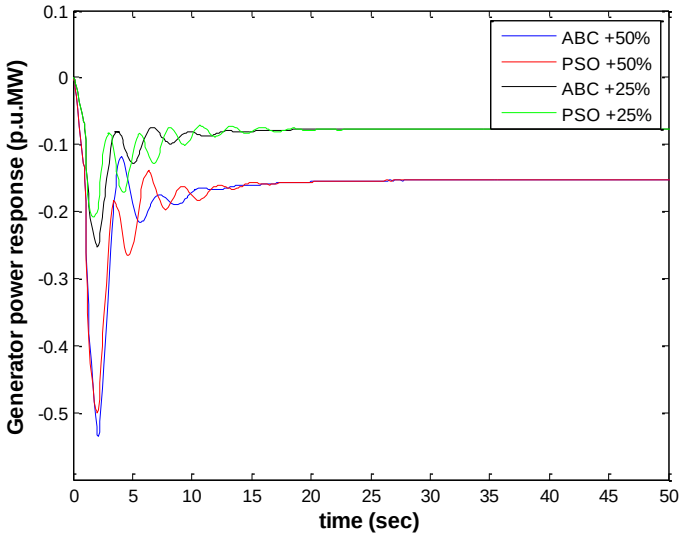

Figure 5.30: Generator power response for load decrement in island 3 for LFC Test Case 2

In island 3 which operates as a standalone network, it can be seen that the ABC tuned LFC is able to settle the system in allowable settling time with reasonable maximum overshoot and undershoot value. No major issues such as oscillation in the islands or prolonged under frequency or over frequency value is observed.

5.4.2 Online wavelet filter implementation in island 3 for LFC Test Case 2

In order to highlight the performance of the online wavelet filter, the ACE signal of the ABC optimized LFC is analyzed. High frequency noise is added to the system and the performance of the system is evaluated. Four different output signals are obtained each for the load increment and load decrement investigation to highlight the performance of the online wavelet filter. Figures 5.31 – 5.34 shows the ACE signal analysis for the load increment investigation and Figures 5.35 – 5.38 shows the ACE signal analysis for the load decrement investigation. The ***db1*** wavelet is selected as the default wavelet to be used.

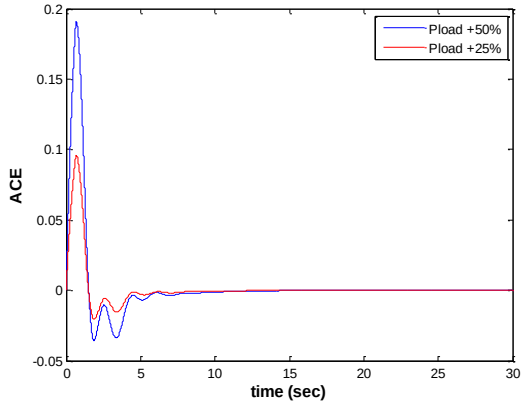

Figure 5.31: Clean ACE signal for load increment in island 3 for LFC Test Case 2

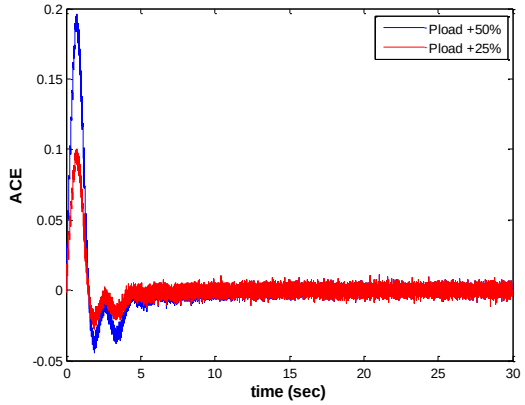

Figure 5.32: Noisy ACE signal for load increment in island 3 for LFC Test Case 2

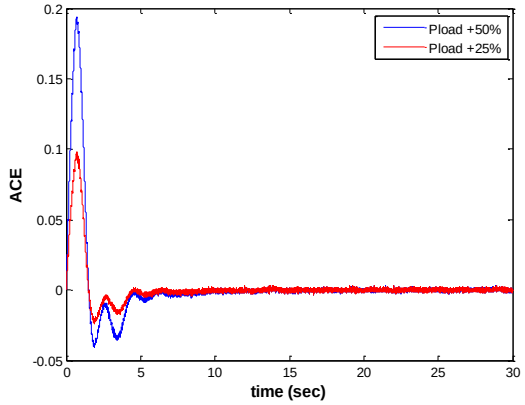

Figure 5.33: Noisy ACE signal with conventional low pass filter for load increment in island 3 for LFC Test Case 2

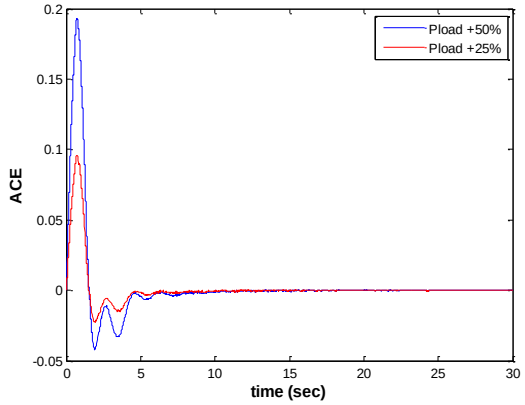

Figure 5.34: Noisy ACE signal with wavelet filter for load increment in island 3 for LFC Test Case 2

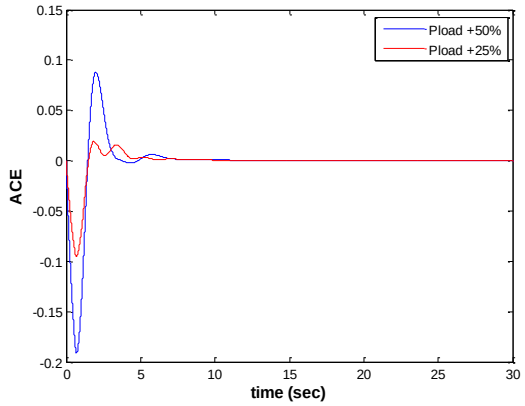

Figure 5.35: Clean ACE signal for load increment in island 3 for LFC Test Case 2

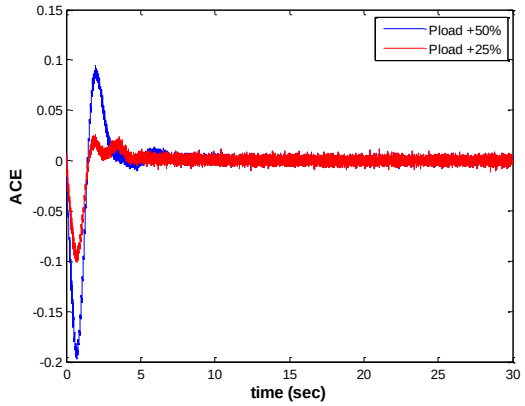

Figure 5.36: Noisy ACE signal for load increment in island 3 for LFC Test Case 2

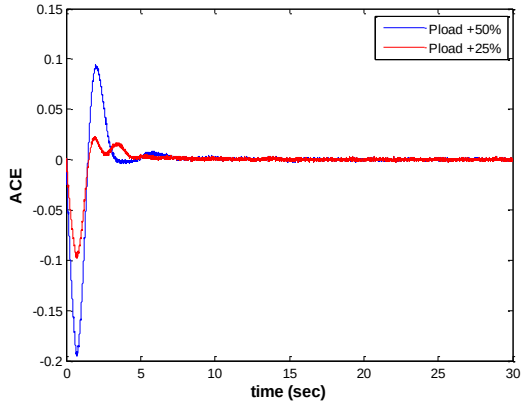

Figure 5.37: Noisy ACE signal with conventional low pass filter for load increment in island 3 for LFC Test Case 2

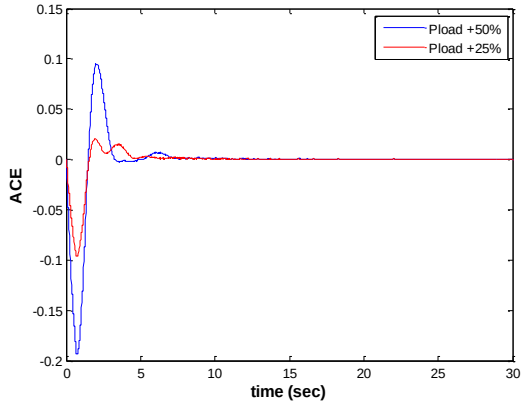

Figure 5.38: Noisy ACE signal with wavelet filter for load increment in island 3 for LFC Test Case 2

Figure 5.31 and 5.35 shows the clean ACE signal with no noise component present. Figure 5.32 and 5.36 shows the ACE signal with presence of noise. Figure 5.33 and 5.37 shows the noisy ACE signal which is filtered conventional low pass filter. Figure 5.34 and 5.38 shows the noisy ACE signal filtered by online wavelet filter. Based on the figures, it can be clearly seen that the online wavelet filtered ACE signal shows a closer resemblance to the clean ACE signal. The signal integrity index is then subsequently calculated to view the index of the signal similarity. Table 5.15 shows the signal integrity index for the load increment investigation in island 1. An index value of 1 shows the closest resemblance to the ideal noise free ACE signal. The wavelet filter signal is used as the benchmark to be compared against by the unfiltered ACE signal and the ACE signal filtered by the conventional low pass filter.

Table 5.15: Signal integrity index for load variation investigation in Island 3 for LFC Test Case 2

ΔP_L	ACE signal	Signal integrity index
50%	Unfiltered	0.7235
	Low pass filter	0.9556
	Wavelet filter	1.000
25%	Unfiltered	0.6423
	Low pass filter	0.8939
	Wavelet filter	1.000
-50%	Unfiltered	0.7372
	Low pass filter	0.9608
	Wavelet filter	1.000
-25%	Unfiltered	0.6454
	Low pass filter	0.8949
	Wavelet filter	1.000

From the table it can be seen that the ACE signal filtered by the wavelet filter shows closer resemblance to the ideal ACE signal with the least amount of noise. This is followed by the conventional low pass filter and finally the unfiltered signal with the most amount of noise. In order to further scrutinize the selection of wavelet type, nine different wavelets are investigated and the signal integrity index for each wavelet type is evaluated as are shown in the bar plot in Figure 5.39.

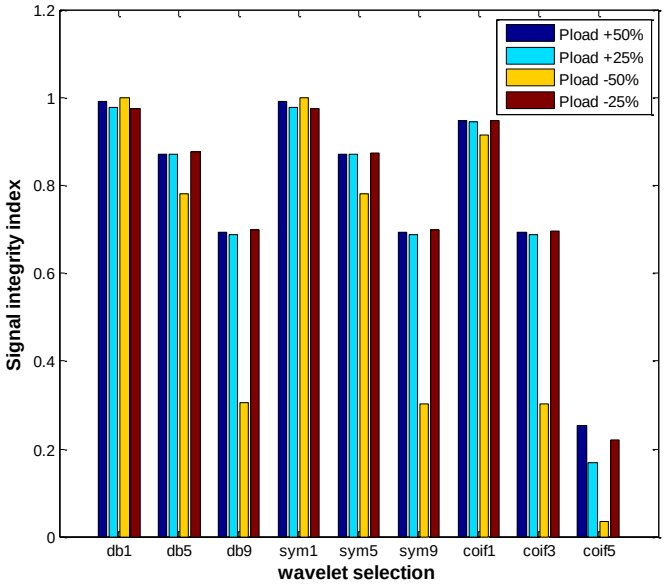

Figure 5.39: Signal integrity index for various wavelet choices in island 3 for LFC Test Case 2

Results in Figure 5.39 shows that the selection of wavelet type plays a very important role towards the performance of the online wavelet filter for the LFC problem. All four load demand levels of +25%, +50%,-25%, and -50% are investigated and the highest signal integrity index are recorded. In the +50% and +25% load demand level, the highest signal integrity index of 0.9920 and 0.9794 is recorded respectively. In the -50% and -25% load demand level, the highest signal integrity index of 1.000 and 0.9767 is recorded respectively. The indexes are attributed to the *daubechies1* wavelet and *symlet1* wavelet.

In this investigation for LFC test case 2, it can be seen that the optimum weightage set for island 1 is $w_1 = 0.3$ and $w_2 = 0.7$ and the best wavelet types to be used for the online wavelet filter for island 3 are *daubechies1* and *symlet1*.

5.5 LFC Test Case 3

In this investigation, the LFC model of IEEE 118-bus test systems shown in Chapter 4 (Section 4.10) is realized. In this case, the power system network is split into three islands. In island 1, there are five generating units represented by generators in bus 10, 12, 25, 26 and 31. In island 2, there are nine generating units represented by generators in bus 46, 49, 54, 59, 61, 65, 66, 69 and 80. In island 3, there are five generating units represented by generators in bus 87, 89, 100, 103 and 111. Details of the load modeling are given in Appendix C. The parameters for the three area power system are given in Table C-3. In this test case, the investigation is carried out for one island only (island 2) since for the other islands the same process is implemented.

5.5.1 Load variation investigation in Island 2

The nominal load demand for island 2 is fixed as per the load demand shown for the optimum network splitting solution in Section 4.10. In order to further analyze the performance of the load frequency control in a standalone network, the load demand in the respective island is increased and decreased in a step size of 25% to 50% based on the aggregated maximum generation capability of the generators. The information of IEEE 118-bus generator data is given in Table A-3. Table 5.16 shows the load demand (P_{Load}) and the maximum generation capability (P_{Gmax}) of the generators in island 2.

Table 5.16: Second island information for LFC Test Case 3

Generation	
Bus	**P_{Gmax}**
46	119
49	304
54	148
59	255
61	260
65	491
66	492
69	805.2
80	577
$\sum P_{Gmax}$ (MW)	3451.2
Load	
$\sum P_{Load}$ (MW)	2333

This means that the generators are able to cater for an additional load demand of 1118.2 MW before the load-generation equilibrium is violated. In the load increment phase, the nominal load demand for island 1 is initially increased by 25% to 0.28 pu MW and subsequently by 50% to 0.559 pu MW. In the load decrement phase, the nominal load demand for island 1 is initially decreased by 25% to -0.28 pu MW and subsequently by 50% to -0.559 pu MW. Table 5.17 shows the weightage set and the corresponding performance index based on LAE for load variation investigation of island 2 for both multi objective ABC and multi objective PSO based optimization technique.

Table 5.17: Weightage set and corresponding performance index based on LAE for Island 2 for LFC Test Case 3

w_1	w_2	η_{LAE}							
		ΔP_L = +50%		ΔP_L = +25%		ΔP_L = -50%		ΔP_L = -25%	
		PSO	ABC	PSO	ABC	PSO	ABC	PSO	ABC
1	0	1.41	52.75	5.46	12.89	2.01	6.13	4e-47	6.78
0.9	0.1	8e-04	58.42	5e-13	12.93	3.55	6.21	8e-34	6.85
0.8	0.2	2.44	59.45	2e-51	13.37	0.21	6.28	1.19	6.89
0.7	0.3	4e-07	62.27	1e-54	13.44	2.39	6.32	2e-03	6.95
0.6	0.4	4e-12	64.37	3e-07	13.51	4.52	6.35	0.45	6.95
0.5	0.5	2.55	66.32	2.13	13.57	0.85	6.36	5e-13	7.04
0.4	0.6	3e-03	76.51	1e-37	13.95	9e-28	6.40	7e-55	7.05
0.3	0.7	6e-22	60.67	2e-10	13.73	4.66	6.37	5.07	6.94
0.2	0.8	1e-32	59.32	7e-34	13.53	1e-32	6.38	9e-07	6.93
0.1	0.9	1e-24	57.32	4e-08	13.49	2.46	6.35	3e-27	6.86
0	1	2e-11	54.23	5e-21	13.22	0.55	6.16	4e-39	6.85

Referring to the information presented in Table 5.17, it can be seen that the overall performance of the ABC based optimization technique is better than PSO based optimization technique. The best overall performance of both the optimization techniques is shown in Table 5.18.

Table 5.18: Optimum weightage set and LAE for Island 2 for LFC Test Case 3

Optimization technique	Load demand (pu MW)	Weightage set		η_{LAE}
		w_1	w_2	
ABC	0.559	0.4	0.6	76.51
PSO		0.5	0.5	2.55
ABC	0.28	0.4	0.6	13.95
PSO		1	0	5.46
ABC	-0.559	0.4	0.6	6.40
PSO		0.3	0.7	4.66
ABC	-0.28	0.4	0.6	7.05
PSO		0.3	0.7	5.07

From the table 5.118, it can be seen that the ABC technique is able to achieve a higher LAE compared to PSO based on a consistent weightage set of w_1 = 0.4 and w_2 = 0.6. Table 5.19 shows the optimal PID parameters and the system performance when the load is varied for both optimization technique based on the optimum weightage set.

Table 5.19: Optimal PID controller gains and system performance for Island 2 for LFC Test Case 3

		Controller paramters			System performance	
	ΔP_L	K_{p1}	T_{i1}	T_{d1}	Settling time (s)	Max. overshoot (Hz)
ABC	+50%	0.213	0.705	0.469	9.384	-0.00174
PSO		0.2	1.942	0.200	15.883	-0.00175
ABC	+25%	0.212	0.702	0.467	9.395	-0.00087
PSO		0.217	0.923	0.553	13.380	-0.00087
ABC	-50%	0.212	0.695	0.472	9.388	0.00174
PSO		0.202	0.944	0.550	10.926	0.00174
ABC	-25%	0.212	0.700	0.467	9.392	0.00087
PSO		0.2	1.227	0.465	13.349	0.000871

Figures 5.40 – 5.43 shows the system's frequency deviation step response and generator power response for both optimization technique based on their optimum values.

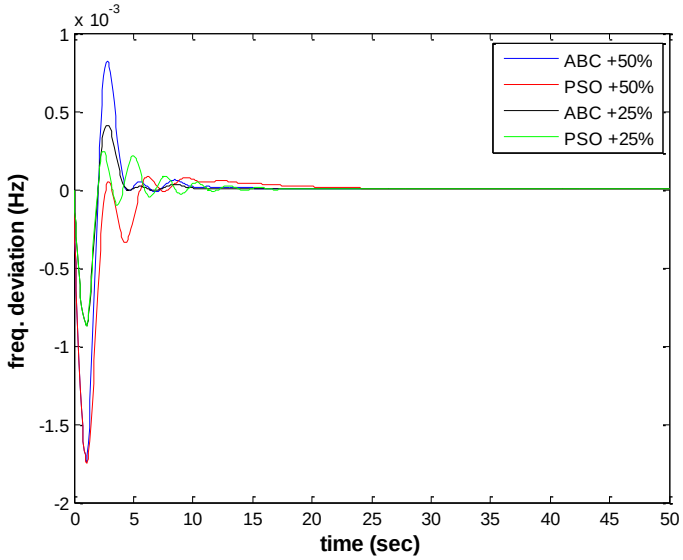

Figure 5.40: Frequency deviation step response for load increment in island 2 for LFC Test Case 3

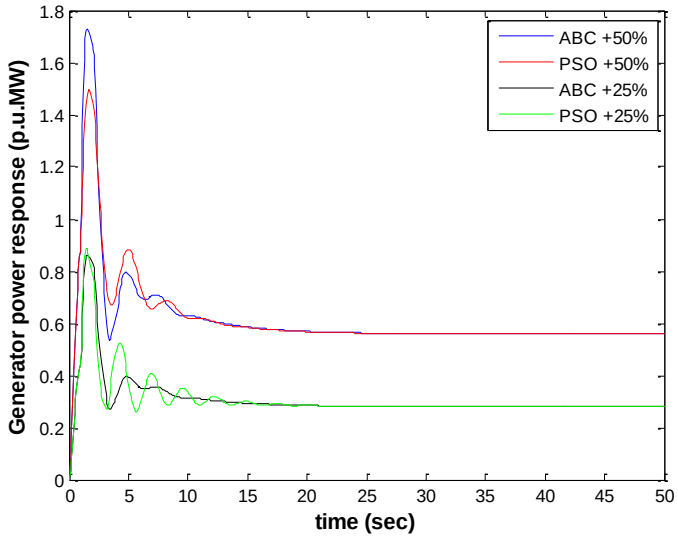

Figure 5.41: Generator power response for load increment in island 2 for LFC Test Case 3

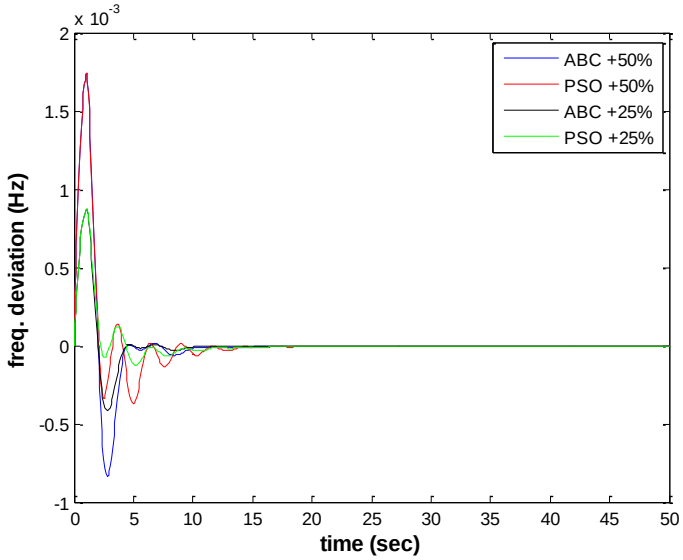

Figure 5.42: Frequency deviation step response for load decrement in island 2 for LFC Test Case 3

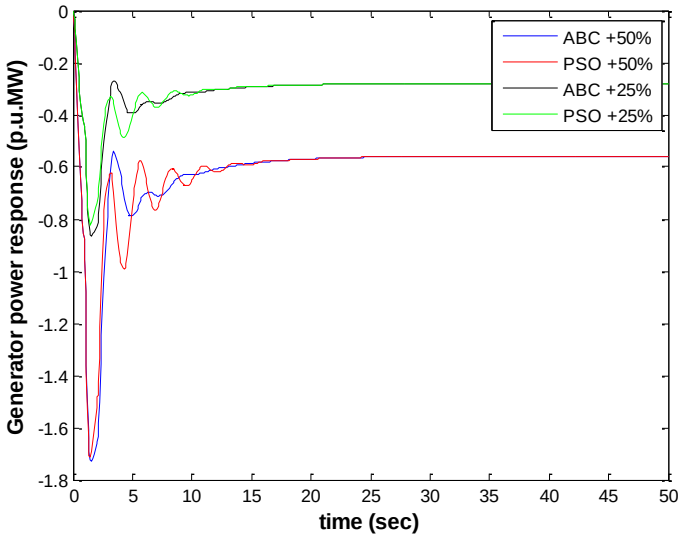

Figure 5.43: Generator power response for load decrement in island 2 for LFC Test Case 3

In island 2 which operates as a standalone network, it can be seen that the ABC tuned LFC is able to settle the system in allowable settling time with reasonable maximum overshoot and undershoot value. No major issues such as oscillation in the islands or prolonged under frequency or over frequency value is observed.

5.5.2 Online wavelet filter implementation in island 2 for LFC Test Case 3

In order to highlight the performance of the online wavelet filter, the ACE signal of the ABC optimized LFC is analyzed. High frequency noise is added to the system and the performance of the system is evaluated. Four different output signals are obtained each for the load increment and load decrement investigation to highlight the performance of the online wavelet filter. Figures 5.44 – 5.47 shows the ACE signal analysis for the load increment investigation and Figures 5.48 – 5.51 shows the ACE signal analysis for the load decrement investigation. The ***db1*** wavelet is selected as the default wavelet to be used.

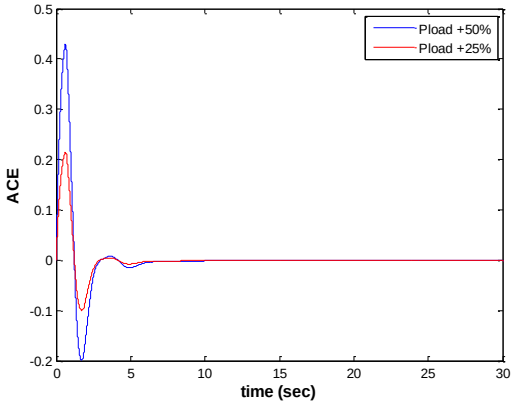

Figure 5.44: Clean ACE signal for load increment in island 2 for LFC Test Case 3

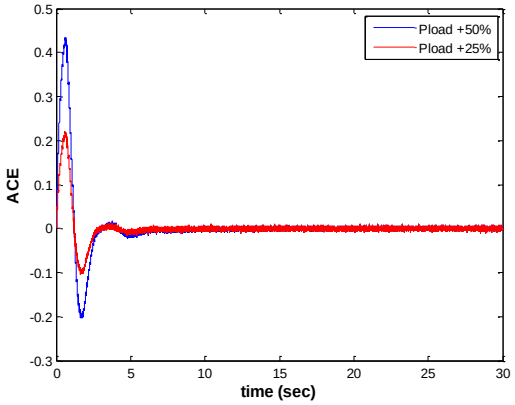

Figure 5.45: Noisy ACE signal for load increment in island 2 for LFC Test Case 3

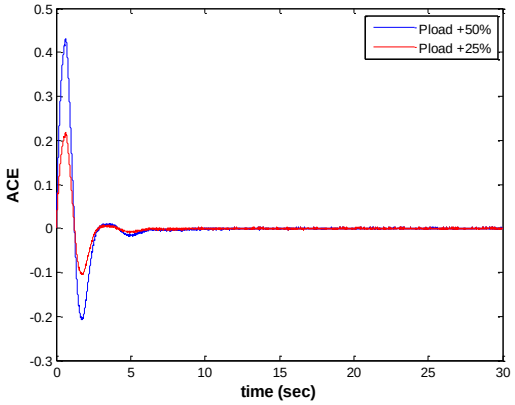

Figure 5.46: Noisy ACE signal with conventional low pass filter for load increment in island 2 for LFC Test Case 3

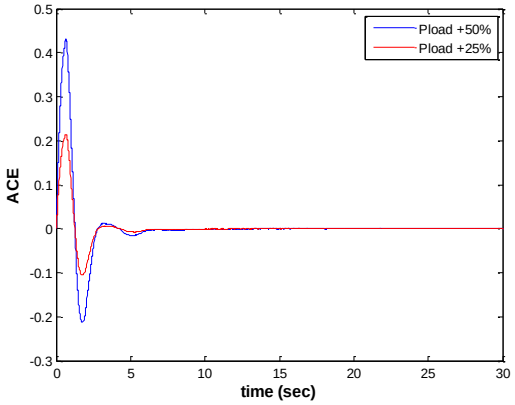

Figure 5.47: Noisy ACE signal with wavelet filter for load increment in island 2 for LFC Test Case 3

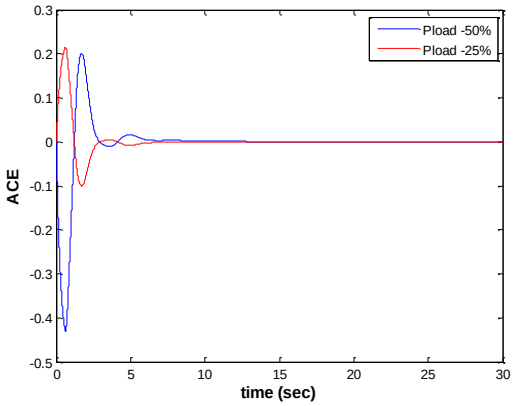

Figure 5.48: Clean ACE signal for load decrement in island 2 for LFC Test Case 3

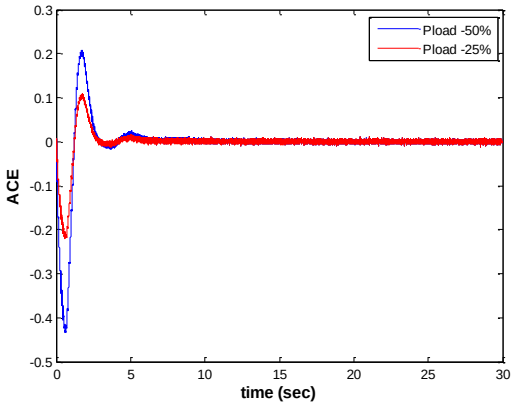

Figure 5.49: Noisy ACE signal for load decrement in island 2 for LFC Test Case 3

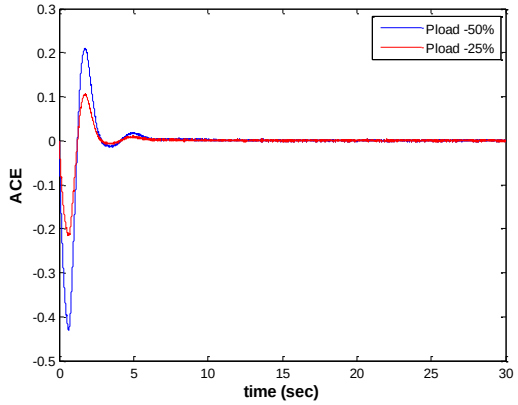

Figure 5.50: Noisy ACE signal with conventional low pass filter for load decrement in island 2 for LFC Test Case 3

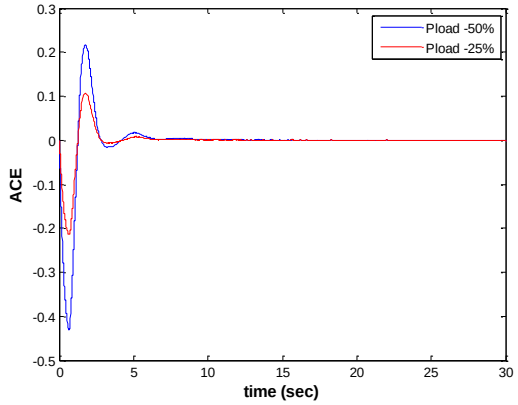

Figure 5.51: Noisy ACE signal with wavelet filter for load decrement in island 2 for LFC Test Case 3

Figure 5.44 and 5.48 shows the clean ACE signal with no noise component present. Figure 5.45 and 5.49 shows the ACE signal with presence of noise. Figure 5.46 and 5.50 shows the noisy ACE signal which is filtered conventional low pass filter. Figure 5.47 and 5.51 shows the noisy ACE signal filtered by online wavelet filter. Based on the figures, it can be clearly seen that the online wavelet filtered ACE signal shows a closer resemblance to the clean ACE signal. The signal integrity index is then subsequently calculated to view the index of the signal similarity. Table 5.20 shows the signal integrity index for the load increment investigation in island 1. An index value of 1 shows the closest resemblance to the ideal noise free ACE signal. The wavelet filter signal is used as the benchmark to be compared against by the unfiltered ACE signal and the ACE signal filtered by the conventional low pass filter.

Table 5.20: Signal integrity index for load variation investigation in island 2 for LFC Test Case 3

ΔP_L	ACE signal	Signal integrity index
50%	Unfiltered	0.8417
	Low pass filter	0.9899
	Wavelet filter	1.000
25%	Unfiltered	0.7560
	Low pass filter	0.9693
	Wavelet filter	1.000
-50%	Unfiltered	0.8408
	Low pass filter	0.9987
	Wavelet filter	1.000
-25%	Unfiltered	0.7447
	Low pass filter	0.9692
	Wavelet filter	1.000

From the table it can be seen that the ACE signal filtered by the wavelet filter shows closer resemblance to the ideal ACE signal with the least amount of noise. This is followed by the conventional low pass filter and finally the unfiltered signal with the most amount of noise. In order to further scrutinize the selection of wavelet type, nine different wavelets are investigated and the signal integrity index for each wavelet type is evaluated as are shown in the bar plot in Figure 5.52.

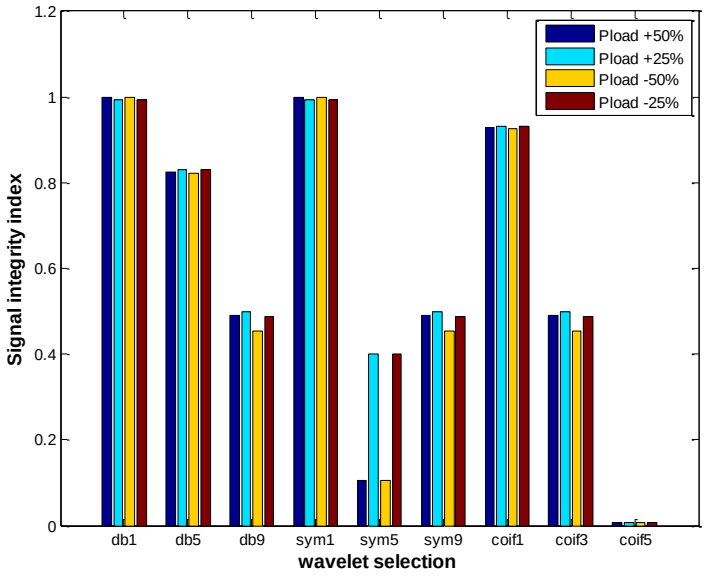

Figure 5.52: Signal integrity index for various wavelet choices in island 2 for LFC Test Case 3

Results in Figure 5.52 shows that the selection of wavelet type plays a very important role towards the performance of the online wavelet filter for the LFC problem. All four

load demand levels of +25%, +50%,-25%, and -50% are investigated and the highest signal integrity index are recorded. In the +50% and +25% load demand level, the highest signal integrity index of 1.000 and 0.9927 is recorded respectively. In the -50% and -25% load demand level, the highest signal integrity index of 1.000 and 0.9934 is recorded respectively. The indexes are attributed to the *daubechies1* wavelet and *symlet1* wavelet. In this investigation for LFC test case 3, it can be seen that the optimum weightage set for island 2 is w_1 = 0.4 and w_2 = 0.6 and the best wavelet types to be used for the online wavelet filter are *daubechies1* and *symlet1*.

5.6 Summary

In this chapter, the load frequency stability of each islands are investigated and analyzed. The frequency stability which is one of the post islanding criteria is of utmost importance in order to ensure a successful network splitting operation. This is due to the fact that if the frequency stability is not maintained, the islands might not be able to perform as a standalone network. This will further defeat the purpose of the network splitting operation if network is unable to resume operation in delivering power to meet the load demand.

The LFC models for each case (IEEE 30-bus, 39-bus and 118-bus test system) are developed based on their system parameters. The multi objective ABC optimization based on weighted sums is then used to optimally tune the PID parameters of the controller to obtain the best system performance based on the frequency response's settling time and maximum overshoot value. The multi objective PSO technique based on weighted sum is also implemented to test and verify the performance of the multi objective ABC optimization technique.

In order to validate the robustness of the ABC tuned LFC, the LFC model is subjected to load variation Investigation. In this test, the load is initially increased proportionally to the load demand in the particular island to 25% and 50%. Subsequently, the load is decreased by the same percentage to observe the system performance. Based on the results obtained, it can be seen that the ABC optimization technique is able to optimally tune the PID parameters of the LFC. The weightage set for each island remains consistent for the ABC optimization technique compared to PSO technique. The ABC optimization technique is also able to provide better performance as shown by the LAE performance index. The frequency response in each area changes according to the load demand as the maximum overshoot in each case is experienced when the load demand is at +50% and the minimum overshoot value is observed when the load demand is at -50%. Despite the load variation, the system controller is still able to respond and damp the oscillation for optimum system performance.

Subsequently the online wavelet filter is implemented and investigation is carried out to observe the performance of the proposed online wavelet filter. High frequency noise component is added to the system and the online wavelet filter was successfully able to filter out the unwanted noise in the system. A comparative investigation is carried out with a conventional low pass filter and the signal integrity index shows that the online wavelet filter performs well in effectively filtering out the noise while at the same time maintaining the signal integrity. Further investigation was carried out and it was found that the *daubechies1* wavelet and *symlet1* wavelet proves to be the best wavelet to be used in the online wavelet filter.

CHAPTER 6: CONCLUSION AND FUTURE WORK

6.1 Conclusion

In network splitting, it is of crucial importance to limit the propagation of cascaded failure in the system which could lead to total blackout in the power system. If a major generating unit is suddenly unavailable, the power balance in the network is jeopardized. The resulting event will have a dire consequence on the security of the whole network. As such, it is of crucial importance to isolate and limit the faulted section of the network. However, network splitting is a challenging task since the formation of each island is based upon the coherent group of generators. Furthermore, the transmission line to be disconnected has to be chosen carefully in order to ensure transient stability in the islanded areas. Once the formation of islands has been realized, the post-islanding frequency stability has to be taken into account to ensure that the islands are able operate as standalone network. This will be extremely useful for network operators or planning engineers to view the optimum islanding solution before it is implemented.

In this research, a proposed modified ABC optimization program based on discrete values was developed for the network splitting problem. The proposed scheme utilizes graph theory to identify the busses and lines connected in the system. Conventional approaches in network splitting problem is usually tasked to find the best solution. The difference of this proposed approach is to find the optimum solution to island the network while considering the associated system constraints. This is extremely important for network planning engineers and future research as the information available from this investigation can be used as a benchmark to identify the most practical and feasible network splitting solution to island the network. The

proposed optimum network splitting algorithm is tested on nine different test cases based on three different IEEE tests system (IEEE 30-bus, IEEE 39-bus and IEEE-118 bus). Initially the edge reduction algorithm is applied to obtain the initial solution. It is verified that by using the edge reduction algorithm, the search space can be reduced to find the initial solution for the optimization process. Subsequently the proposed modified ABC optimization technique is implemented to obtain the optimum network splitting solution. The results clearly show that the modified ABC optimization technique is able to obtain the optimum network splitting solution. In order to verify this, comparative investigation was carried out against published results and modified PSO technique. The result of the investigation further highlights the performance of the modified ABC optimization technique as it is able to find the optimal solution faster and more accurately.

In order to successfully implement the network splitting solution, the post-islanding frequency stability has to be maintained. This is achieved by analyzing the feasibility and stability of each island. The power balance in each island is observed to maintain stability. The generators in the islands are driven to their maximum capability to ensure power imbalance does not occur. In the event the generators are not able to serve the load demand, the load shedding scheme is applied. Furthermore, the splitting solution chosen is ensured that it does not violate the transmission line's maximum power carrying capability. The test results in Chapter 4 prove the proposed algorithm's ability in different scenarios based on power imbalance in each island. Despite different islanding solutions based on the coherency of the generators, the load-generation balance in each island is maintained by increasing the generation level to meet the load demand in the islanded areas. In the event that the load generation balance is not met due to insufficient generation capability as seen in island 3 for case 3 and in island 2 &

4 in case 6, the load shedding algorithm is initiated. The load-generation balance is then maintained and transmission line power flow analysis is further carried out. Results show that the line's maximum power carrying capability is not violated.

To further ensure the successful operation of the islanded areas, the frequency response in each island is evaluated. This is carried out by modeling the AGC of the islanded area based on the IEEE 30-bus test case, IEEE 39-bus test case and IEEE 118-bus test case. Load variation investigation is carried out and the frequency response based on the settling time and maximum overshoot value is analyzed. The proposed controller optimization technique is implemented based on three different network splitting scenarios. The multi objective ABC optimization technique is implemented to find the optimum PID parameters Based on the LAE performance index, it can be concluded that the multi objective ABC optimization technique is able to perform better in finding the optimum PID parameters compared to the multi objective PSO technique. According to the simulation result, the proposed controller optimization technique is able to settle the frequency response of the system in shortest time possible with least amount of overshoot value. This is extremely important when the islands are operating as standalone network, as the islands have to be able to cater to load demand in the area and operate in similar fashion as to how the grid reacts to changes in load demand. A consistent weightage set is also observed for the multi objective ABC optimization technique in the islanded area.

In this investigation, different physical constraints were incorporated in the LFC model to further represent the practical system. High frequency noise component often impede the controllers performance by subjecting the controller to react to unwanted signal changes. The online wavelet filter is implemented to reduce the impact of high

frequency noise in the LFC model. Comparative investigation is carried out against the conventional low pass filter and it was verified that the wavelet filter can effectively filter out the high frequency noise in the input signal to the controller. The signal integrity index shows that the output signal filtered by wavelet filter contains the least amount of noise. This is important so that the LFC is able to reject rapid control signal variation presented due to the noise. Further investigation has proven that the *daubechies1* and *symlet1* wavelet are the best wavelet type to be used.

6.2 Future Work

In order to further improve the investigation, the following tasks are to be carried out:

1. Currently, the optimum network splitting algorithm only considers the power balance criteria and transmission line power flow analysis. In order to further ascertain the stability of the islanded solution, the voltage profile of the buses should also be considered. This criteria can be integrated in the modified ABC optimization program as a constraint to be adhered to when the network splitting is carried out.

1. The proposed algorithm only considers active power balance while neglecting the reactive power in the system. This is because the reactive power can be compensated locally. However, in future, the reactive power status of the system should also be incorporated in the algorithm so that the network splitting solution provides the reactive power information in each islanded area.

3. Load shedding scheme implemented in the proposed network splitting algorithm is a simple algorithm based on the ratio of generation and load. Further improvement has to be made in order to ensure that the load shedding scheme is more advanced. This

can be achieved by incorporating different aspects such as priority of load and optimum load level to be shed.

4. The research currently considers the post islanding frequency stability by incorporating the optimized LFC. In future, the voltage stability of the islands can be also be evaluated by incorporating the automatic voltage regulator (AVR) in the control system model.

5. The multi objective optimization used in this investigation is based on the weighted sum approach. An optimal pareto front can be obtained using the multi objective optimization based on pareto. The pareto approach will further fine tune the optimal weightage set of the PID parameters.

6. The PID controller used in for the LFC in this research is the conventional PID controller. Further improvement can be made in the controller selection to enhance the control system performance. The fractional order PID ($PI^{\lambda}D^{\mu}$) which is gaining wide attention from researchers will further improve the dynamic performance and robustness of the LFC.

REFERENCES

Abedinia, O., Shayanfar, H., Wyns, B., & Ghasemi, A. (2011). *Design of robust PSS to improve stability of composed LFC and AVR using ABC in deregulated environment.* Paper presented at the 13th International conference on Artificial Intelligence (ICAI 2011).

Abu-Mouti, F., & El-Hawary, M. (2009). *Modified artificial bee colony algorithm for optimal distributed generation sizing and allocation in distribution systems.* Paper presented at the 2009 IEEE Electrical Power & Energy Conference (EPEC).

Aditya. (2003). Design of load frequency controllers using genetic algorithm for two area interconnected hydro power system. *Electric Power Components and Systems, 31*(1), 81-94.

Aghamohammadi, M. R., & Shahmohammadi, A. (2012). Intentional islanding using a new algorithm based on ant search mechanism. *International Journal of Electrical Power & Energy Systems, 35*(1), 138-147.

Aldeen, M., & Trinh, H. (1992). Combined modal and singular perturbation approach to decentralized control. *International journal of systems science, 23*(5), 741-764.

Andersson, G., Donalek, P., Farmer, R., Hatziargyriou, N., Kamwa, I., Kundur, P., . . . Sanchez-Gasca, J. (2005). Causes of the 2003 major grid blackouts in North America and Europe, and recommended means to improve system dynamic performance. *IEEE Transactions on Power Systems, 20*(4), 1922-1928.

Astrom KJ, & Hagglund T. (1995). PID Controllers: Theory, Design and Tuning (2nd ed.). USA: Instrument Society of America.

Azzam, M. (1999). Robust automatic generation control. *Energy Conversion and Management, 40*(13), 1413-1421.

Balasundaram, P., & Akilandam, C. I. (2012). ABC Algorithm based Load-Frequency Controller for an interconnected Power System Considering nonlinearities and Coordinated with UPFC and RFB. *International Journal of Engineering and Innovative Technology, 1*.

Basturk, B., & Karaboga, D. (2006). *An artificial bee colony (ABC) algorithm for numeric function optimization.* Paper presented at the IEEE swarm intelligence symposium.

Beaufays, F., Abdel-Magid, Y., & Widrow, B. (1994). Application of neural networks to load-frequency control in power systems. *Neural Networks, 7*(1), 183-194.

Bevrani, H. (2009). *Robust power system frequency control* (Vol. 85): Springer.

Bevrani, H., Mitani, Y., & Tsuji, K. (2004a). Robust decentralised load-frequency control using an iterative linear matrix inequalities algorithm. *IEE Proceedings-Generation, Transmission and Distribution, 151*(3), 347-354.

Bevrani, H., Mitani, Y., & Tsuji, K. (2004b). Sequential design of decentralized load frequency controllers using μ synthesis and analysis. *Energy Conversion and Management, 45*(6), 865-881.

Birch, A., Sapeluk, A., & Ozveren, C. (1994). *An enhanced neural network load frequency control technique.* Paper presented at the International Conference on Control, 1994.

Bohn, E., & Miniesy, S. M. (1972). Optimum load-frequency sampled-data control with randomly varying system disturbances. *IEEE Transactions on Power Apparatus and Systems*(5), 1916-1923.

Bondy, J. A., & Murty, U. S. R. (1976). *Graph theory with applications* (Vol. 6): Macmillan London.

Brace, K. S., Rudell, R. L., & Bryant, R. E. (1991). *Efficient implementation of a BDD package.* Paper presented at the Proceedings of the 27th ACM/IEEE design automation conference.

Bryant, R. E. (1992). Symbolic Boolean manipulation with ordered binary-decision diagrams. *ACM Computing Surveys (CSUR), 24*(3), 293-318.

Chang, C., & Fu, W. (1997). Area load frequency control using fuzzy gain scheduling of PI controllers. *Electric Power Systems Research, 42*(2), 145-152.

Chang, C., Fu, W., & Wen, F. (1998). Load frequency control using genetic-algorithm based fuzzy gain scheduling of PI controllers. *Electric machines and power systems, 26*(1), 39-52.

Chang, J.-L. (2003). Robust Sliding-Mode Control with Disturbance Attenuation Using Only Output Feedback. *JSME International Journal Series C, 46*(1), 239-244.

Chaturvedi, D., Satsangi, P., & Kalra, P. (1999). Load frequency control: a generalised neural network approach. *International Journal of Electrical Power & Energy Systems, 21*(6), 405-415.

Chen, J., & Li, J. (2012). An application of rough sets to graph theory. *Information Sciences, 201*, 114-127.

Chidambaram, I., & Francis, R. (2011). *Automatic generation control of a two area reheat interconnected power system based on CPS using fuzzy neural network.* Paper presented at the 2011 International Conference on Emerging Trends in Electrical and Computer Technology (ICETECT).

Chow, J. H., Galarza, R., Accari, P., & Price, W. (1995). Inertial and slow coherency aggregation algorithms for power system dynamic model reduction. *IEEE Transactions on Power Systems, 10*(2), 680-685.

Committee on Enhancing the Robustness and Resilience of Future Electrical Transmission and Distribution in the United States to Terrorist Attack. (2012). *Terrorism and the Electric Power Delivery System* (pp. 146). Retrieved from

http://www.nap.edu/catalog/12050/terrorism-and-the-electric-power-delivery-system

Daneshfar, F., & Bevrani, H. (2010). Load–frequency control: a GA-based multi-agent reinforcement learning. *IET generation, transmission & distribution, 4*(1), 13-26.

DeMello, F., Mills, R., & B'rells, W. (1973). Automatic generation control part ii-digital control techniques. *Power Apparatus and Systems, IEEE Transactions on*(2), 716-724.

Demiroren, N. S. S., H. Lale Zeynelgil, Aysen. (2001). Automatic generation control by using ANN technique. *Electric Power Components and Systems, 29*(10), 883-896.

Dhanalakshmi, R., & Palaniswami, S. (2012). ANFIS based Neuro-Fuzzy Controller in LFC of Wind-Micro Hydro-Diesel Hybrid Power System. *International Journal of computer applications, 42*(6), 28-35.

Ding, L., Gonzalez-Longatt, F. M., Wall, P., & Terzija, V. (2013). Two-step spectral clustering controlled islanding algorithm. *IEEE Transactions on Power Systems, 28*(1), 75-84.

Dola, H. M., & Chowdhury, B. H. (2006). *Intentional islanding and adaptive load shedding to avoid cascading outages.* Paper presented at the IEEE Power Engineering Society General Meeting.

Dy Liacco, T. E. (1967). The adaptive reliability control system. *IEEE Transactions on Power Apparatus and Systems*(5), 517-531.

Elgerd, O. I., & Fosha, C. E. (1970). Optimum megawatt-frequency control of multiarea electric energy systems. *IEEE Transactions on Power Apparatus and Systems*, 556-563.

Ford, J. J., Bevrani, H., & Ledwich, G. (2009). Adaptive load shedding and regional protection. *International Journal of Electrical Power & Energy Systems, 31*(10), 611-618.

Fu, X., & Wang, X. (2011). Determination of load shedding to provide voltage stability. *International Journal of Electrical Power & Energy Systems, 33*(3), 515-521.

Ghasemi, & A, H. S. (2011). Market based LFC design using artificial bee colony. *International Journal on Technical and Physical Problems of Engineering, 3*(6), 1-10.

Golpira, H., & Bevrani, H. (2011). Application of GA optimization for automatic generation control design in an interconnected power system. *Energy Conversion and Management, 52*(5), 2247-2255.

Gozde, H., Cengiz Taplamacioglu, M., & Kocaarslan, İ. (2012). Comparative performance analysis of Artificial Bee Colony algorithm in automatic generation

control for interconnected reheat thermal power system. *International Journal of Electrical Power & Energy Systems, 42*(1), 167-178.

Gozde, H., Taplamacioglu, M. C., & Kocaarslan, I. (2012). Comparative performance analysis of Artificial Bee Colony algorithm in automatic generation control for interconnected reheat thermal power system. *International Journal of Electrical Power & Energy Systems, 42*(1), 167-178.

Graps, A. (1995). An introduction to wavelets. *IEEE Computational Science & Engineering, 2*(2), 50-61.

Ha, Q., & Trinh, H. (2000). A variable structure-based controller with fuzzy tuning for load-frequency control. *International Journal of power and energy systems, 20*(3), 146-154.

Hain, Y., & Schweitzer, I. (1997). Analysis of the power blackout of June 8, 1995 in the Israel Electric Corporation. *IEEE Transactions on Power Systems, 12*(4), 1752-1758.

Hardiman, R. C., Kumbale, M., & Makarov, Y. V. (2004). *An advanced tool for analyzing multiple cascading failures.* Paper presented at the International Conference on Probabilistic Methods Applied to Power Systems.

Hari, L., Kothari, M., & Nanda, J. (1991). *Optimum selection of speed regulation parameters for automatic generation control in discrete mode considering generation rate constraints.* Paper presented at the IEE Proceedings C (Generation, Transmission and Distribution).

Hassani, A., & Treijs, J. (1975). *An overview of standard and parallel genetic algorithms.* Paper presented at the IDT Workshop on Interesting Results in Computer Science and Engineering, Mälardalen University.

Hemamalini, S., & Simon, S. P. (2010). Economic/emission load dispatch using artificial bee colony algorithm. *ACEEE International Journal on Electrical and Power Engineering, 1*(2).

Hemeida, A. M. (2005). Wavelet neural network load frequency controller. *Energy Conversion and Management, 46*(9), 1613-1630.

Hemmati, R., Shirvani Boroujeni, S. M., Delafkar, H., & Boroujeni, A. S. (2011). PID Controller Adjustment using PSO for Multi Area Load Frequency Control. *Australian Journal of Basic & Applied Sciences, 5*(3).

Huang, S.-J., & Liu, X.-Z. (2013). Application of artificial bee colony-based optimization for fault section estimation in power systems. *International Journal of Electrical Power & Energy Systems, 44*(1), 210-218.

Hussein, T. A Genetic Algorithm for Optimum Design of PID Controller in Load Frequency Control. *World Academy of Science, Engineering and Technology, 6*(10), 1205-1208.

Imai, H., & Iri, M. (1987). An optimal algorithm for approximating a piecewise linear function. *Journal of information processing, 9*(3), 159-162.

Jain, Y. K., & Bhandare, S. K. (2011). Min Max Normalization Based Data Perturbation Method for Privacy Protection. *International Journal of Computer & Communication Technology (IJCCT), 2*(8).

Javidan, J., & Ghasemi, A. (2013). A novel fuzzy RPID controller for multiarea AGC with IABC optimization. *Journal of Engineering, 2013*.

Jayanthi, R., & Chidambaram, I. (2012). Power System Restoration Index for Load Frequency Control Assessment Using Artificial Bee Colony Algorithm in a Two-Area Reheat Interconnected Power System Co-ordinated with SMES Units. *International Journal of Soft Computing and Engineering (IJSCE) ISSN*, 2231-2307.

Jin, M., Sidhu, T. S., & Sun, K. (2007). A new system splitting scheme based on the unified stability control framework. *IEEE Transactions on Power Systems, 22*(1), 433-441.

Jovanovic, S. (1999). Self-tuning steam turbine controller in a multi-machine power system. *IEEE Transactions on Energy Conversion, 14*(4), 1578-1581.

Karaboga, D. (2005). An idea based on honey bee swarm for numerical optimization: Technical report-tr06, Erciyes University, Engineering Faculty, Computer Engineering Department.

Karaboga, D., & Akay, B. (2009). A survey: algorithms simulating bee swarm intelligence. *Artificial Intelligence Review, 31*(1-4), 61-85.

Karaboga, D., Akay, B., & Ozturk, C. (2007). Artificial bee colony (ABC) optimization algorithm for training feed-forward neural networks *Modeling decisions for artificial intelligence* (pp. 318-329): Springer.

Karaboga, D., & Basturk, B. (2007a). Artificial bee colony (ABC) optimization algorithm for solving constrained optimization problems *Foundations of Fuzzy Logic and Soft Computing* (pp. 789-798): Springer.

Karaboga, D., & Basturk, B. (2007b). A powerful and efficient algorithm for numerical function optimization: artificial bee colony (ABC) algorithm. *Journal of global optimization, 39*(3), 459-471.

Karaboga, D., & Basturk, B. (2008). On the performance of artificial bee colony (ABC) algorithm. *Applied Soft Computing, 8*(1), 687-697.

Karaboga, D., Gorkemli, B., Ozturk, C., & Karaboga, N. (2014). A comprehensive survey: artificial bee colony (ABC) algorithm and applications. *Artificial Intelligence Review, 42*(1), 21-57.

Kazemi, A., & Andami, H. (2004). A decentralized fuzzy logic enhanced variable structure controller applied to load frequency control system. *IRANIAN JOURNAL OF SCIENCE AND TECHNOLOGY, 28*(B3), 295-303.

Kenndy, J., & Eberhart, R. (1995). *Particle swarm optimization.* Paper presented at the Proceedings of IEEE International Conference on Neural Networks.

Killingsworth, N. J., & Krstic, M. (2006). PID tuning using extremum seeking: Online, model-free performance optimization. *Control Systems, IEEE, 26*(1), 70-79.

Kirschen, D. S. (2002). Power system security. *Power Engineering Journal, 16*(5), 241-248.

Klinger, C., & Owen Landeg, V. M. (2014). Power Outages, Extreme Events and Health: A Systematic Review of the Literature from 2011-2012. *PLoS currents, 6*.

Koren, Y. (2005). Drawing graphs by eigenvectors: Theory and practice. *Computers & Mathematics with Applications, 49*(11), 1867-1888.

Kothari, M., Nanda, J., Kothari, D., & Das, D. (1989). Discrete-mode automatic generation control of a two-area reheat thermal system with new area control error. *IEEE Transactions on Power Systems, 4*(2), 730-738.

Kundur, P., Balu, N. J., & Lauby, M. G. (1994). *Power system stability and control* (Vol. 7): McGraw-hill New York.

Kundur, P., Taylor, C., & Pourbeik, P. (2007). Blackout experiences and lessons, best practices for system dynamic performance, and the role of new technologies. *IEEE Task Force Report*.

Kwatny, H., Kalnitsky, K., & Bhatt, A. (1975). An optimal tracking approach to load-frequency control. *IEEE Transactions on Power Apparatus and Systems, 94*(5), 1635-1643.

Lee, H. J., Park, J. B., & Joo, Y. H. (2006). Robust load-frequency control for uncertain nonlinear power systems: A fuzzy logic approach. *Information Sciences, 176*(23), 3520-3537.

Lim, K., Wang, Y., & Zhou, R. (1996). *Robust decentralised load-frequency control of multi-area power systems.* Paper presented at the IEE Proceedings-Generation, Transmission and Distribution.

Liu, L., Liu, W., Cartes, D. A., & Chung, I.-Y. (2009). Slow coherency and Angle Modulated Particle Swarm Optimization based islanding of large-scale power systems. *Advanced Engineering Informatics, 23*(1), 45-56.

Liu, W., Liu, L., Cartes, D. A., & Venayagamoorthy, G. K. (2007). Binary particle swarm optimization based defensive islanding of large scale power systems. *Technomathematics Research Foundation, international Journal of Computer Science & Applications, 4*(3), 69-83.

Lu, C.-F., Liu, C.-C., & Wu, C.-J. (1995). Effect of battery energy storage system on load frequency control considering governor deadband and generation rate constraint. *IEEE Transactions on Energy Conversion, 10*(3), 555-561.

Maharana, M. K., & Swarup, K. (2010). Graph theoretic approach for preventive control of power systems. *International Journal of Electrical Power & Energy Systems, 32*(4), 254-261.

Makarov, Y. V., Reshetov, V. I., Stroev, A., & Voropai, N. I. (2005). Blackout prevention in the united states, Europe, and Russia. *Proceedings of the IEEE, 93*(11), 1942-1955.

Masiala, M., Ghribi, M., & Kaddouri, A. (2004). *An adaptive fuzzy controller gain scheduling for power system load-frequency control.* Paper presented at the IEEE International Conference onIndustrial Technology, 2004, IEEE ICIT'04.

Mills, R., & B'Rells, W. (1973). Automatic Generation Control Part I-Process Modeling. *IEEE Transactions on Power Apparatus and Systems*(2), 710-715.

Morison, K., Wang, L., & Kundur, P. (2004). Power system security assessment. *IEEE Power and Energy Magazine, 2*(5), 30-39.

Najafi, S., Hosseinian, S., & Abedi, M. (2010). Evaluation of Interconnected Power Systems Splitting. *Electric Power Components and Systems, 38*(11), 1248-1268.

Nanda, J., Kothari, M., & Satsang, P. (1983). *Automatic generation control of an interconnected hydrothermal system in continuous and discrete modes considering generation rate constraints.* Paper presented at the Control theory and applications, IEE proceedings D.

New Straits Times. (2015). TNB taking steps to rectify Puchong power outage, *http://www2.nst.com.my/streets/central/tnb-taking-steps-to-rectify-puchong-power-outage-1.330347*.

Ng, C.-K., Li, D., & Zhang, L.-S. (2007). Discrete global descent method for discrete global optimization and nonlinear integer programming. *Journal of global optimization, 37*(3), 357-379.

Oysal, Y., Yilmaz, A. S., & Koklukaya, E. (2005). A dynamic wavelet network based adaptive load frequency control in power systems. *International Journal of Electrical Power & Energy Systems, 27*(1), 21-29.

P. A. Trodden, W. A. Bukhsh, A. Grothey, & K. I. M. McKinnon. *Optimization-based Islanding of Power Networks using Piecewise Linear AC Power Flow*. Retrieved from http://www.maths.ed.ac.uk/~agr/pwl_ac_paper.pdf

Pan, C., & Liaw, C. (1989). An adaptive controller for power system load-frequency control. *IEEE Transactions on Power Systems, 4*(1), 122-128.

Pan, Q.-K., Tasgetiren, M. F., Suganthan, P. N., & Chua, T. J. (2011). A discrete artificial bee colony algorithm for the lot-streaming flow shop scheduling problem. *Information Sciences, 181*(12), 2455-2468.

Panda, G., Panda, S., & Ardil, C. (2009). Automatic generation control of interconnected power system with generation rate constraints by hybrid neuro

fuzzy approach. *World Academy of Science, Engineering and Technology, 52*, 543-548.

Pandey, S. K., Mohanty, S. R., & Kishor, N. (2013). A literature survey on load–frequency control for conventional and distribution generation power systems. *Renewable and Sustainable Energy Reviews, 25*, 318-334.

Paramasivam, B., & Chidambaram, I. (2011). Design of Load-frequency Controller using Artificial Bee Colony Algorithm for an Interconnected Power System Coordinated with UPFC and RFB. *International Journal of computer applications, 36*.

Peiravi, A., & Ildarabadi, R. (2009). A fast algorithm for intentional islanding of power systems using the multilevel kernel k-means approach. *Journal of Applied Sciences, 9*(12), 2247-2255.

Phadke, A., & Thorp, J. S. (1996). Expose hidden failures to prevent cascading outages [in power systems]. *IEEE Computer Applications in Power, 9*(3), 20-23.

Pourbeik, P., Kundur, P. S., & Taylor, C. W. (2006). The anatomy of a power grid blackout. *IEEE Power and Energy Magazine, 4*(5), 22-29.

Prakash, S., & Sinha, S. (2014). Simulation based neuro-fuzzy hybrid intelligent PI control approach in four-area load frequency control of interconnected power system. *Applied Soft Computing, 23*, 152-164.

Ramesh, S., & Krishnan, A. (2009). Modified genetic algorithm based load frequency controller for interconnected power system. *International Journal of Electrical Power Engineering, 3*(1), 26-30.

Rao, R. S., Narasimham, S., & Ramalingaraju, M. (2008). Optimization of distribution network configuration for loss reduction using artificial bee colony algorithm. *International Journal of Electrical Power and Energy Systems Engineering, 1*(2), 116-122.

Rathor, S., Acharya, D., Gude, S., & Mishra, P. (2011). *Application of artificial bee colony optimization for load frequency control*. Paper presented at the 2011 World Congress on Information and Communication Technologies (WICT).

Ray, G., Prasad, A., & Prasad, G. (1999). A new approach to the design of robust load-frequency controller for large scale power systems. *Electric Power Systems Research, 51*(1), 13-22.

Rerkpreedapong, D., Hasanovic, A., & Feliachi, A. (2003). Robust load frequency control using genetic algorithms and linear matrix inequalities. *IEEE Transactions on Power Systems, 18*(2), 855-861.

Rosas-Casals, M., & Solé, R. (2011). Analysis of major failures in Europe's power grid. *International Journal of Electrical Power & Energy Systems, 33*(3), 805-808.

Ross, C. (1966). Error adaptive control computer for interconnected power systems. *IEEE Transactions on Power Apparatus and Systems*(7), 742-749.

Ross, C. W., & Green, T. A. (1972). Dynamic performance evaluation of a computer controlled electric power system. *IEEE Transactions on Power Apparatus and Systems*(3), 1158-1165.

Rubaai, A., & Udo, V. (1992). An adaptive control scheme for load-frequency control of multiarea power systems Part I. Identification and functional design. *Electric Power Systems Research, 24*(3), 183-188.

Ruohonen, K. (2008). Graph Theory. 114. Retrieved from http://math.tut.fi/~ruohonen/english.html website: math.tut.fi/~ruohonen/GT_English.pdf

Sakaguchi, T., & Matsumoto, K. (1983). Development of a knowledge based system for power system restoration. *IEEE Transactions on Power Apparatus and Systems*(2), 320-329.

Senroy, N., Heydt, G. T., & Vittal, V. (2006). Decision tree assisted controlled islanding. *IEEE Transactions on Power Systems, 21*(4), 1790-1797.

Sepulveda, R., Melin, P., Rodriguez, A., Mancilla, A., & Montiel, O. (2006). Analyzing the effects of the footprint of uncertainty in type-2 fuzzy logic controllers. *Engineering Letters, 13*(2), 1-12.

Shabani, H., Vahidi, B., & Ebrahimpour, M. (2013). A robust PID controller based on imperialist competitive algorithm for load-frequency control of power systems. *ISA transactions, 52*(1), 88-95.

Sharifi, A., Sabahi, K., Shoorehdeli, M. A., Nekoui, M., & Teshnehlab, M. (2008). *Load frequency control in interconnected power system using multi-objective PID controller*. Paper presented at the SMCia'08, IEEE Conference on Soft Computing in Industrial Applications.

Sharma, A., Parmar, K. S., & Gupta, S. (2012). Automatic Generation Control of Multi Area Power System using ANN Controller. *International Journal of Computer Science and Telecommunications, 3*(3), 55 - 59.

Shayeghi, H. (2008). A robust decentralized power system load frequency control. *Journal of Electrical Engineering, 59*(6), 281-293.

Shayeghi, H., Jalili, A., & Shayanfar, H. (2007). Robust modified GA based multi-stage fuzzy LFC. *Energy Conversion and Management, 48*(5), 1656-1670.

Shayeghi, H., Jalili, A., & Shayanfar, H. (2008). Multi-stage fuzzy load frequency control using PSO. *Energy Conversion and Management, 49*(10), 2570-2580.

Shayeghi, H., Shayanfar, H., & Jalili, A. (2009). Load frequency control strategies: A state-of-the-art survey for the researcher. *Energy Conversion and Management, 50*(2), 344-353.

Skiena, S. (1990). Dijkstra's Algorithm. *Implementing Discrete Mathematics: Combinatorics and Graph Theory with Mathematica, Reading, MA: Addison-Wesley*, 225-227.

Smith, T. B. (2003). Privatising electric power in Malaysia and Thailand: politics and infrastructure development policy. *Public Administration and Development, 23*(3), 273-283.

Soundarrajan, A., Sumathi, S., & Sundar, C. (2010). Particle swarm optimization based LFC and AVR of autonomous power generating system. *IAENG International Journal of Computer Science, 37*(1), 37-31.

Stankovic, A., Tadmor, G., & Sakharuk, T. (1998). On robust control analysis and design for load frequency regulation. *IEEE Transactions on Power Systems, 13*(2), 449-455.

Sun, K., Zheng, D. Z., & Lu, Q. (2003). Splitting strategies for islanding operation of large-scale power systems using OBDD-based methods. *IEEE Transactions on Power Systems, 18*(2), 912-923.

Tacker, E., Lee, C., Reddoch, T., Tan, T., & Julich, P. (1972). Optimal control of interconnected, electric energy systems—A new formulation. *Proceedings of the IEEE, 60*(10), 1239-1241.

Talaq, J., & Al-Basri, F. (1999). Adaptive fuzzy gain scheduling for load frequency control. *IEEE Transactions on Power Systems, 14*(1), 145-150.

Taylor, C., & Cresap, R. L. (1976). Real-time power system simulation for automatic generation control. *IEEE Transactions on Power Apparatus and Systems, 95*(1), 375-384.

Tiranuchit, A., & Thomas, R. (1988). A posturing strategy against voltage instabilities in electric power systems. *IEEE Transactions on Power Systems, 3*(1), 87-93.

Tortós, J. Q., & Terzija, V. (2012). *Controlled islanding strategy considering power system restoration constraints.* Paper presented at the 2012 IEEE Power and Energy Society General Meeting.

Toulabi, M., Shiroei, M., & Ranjbar, A. (2014). Robust analysis and design of power system load frequency control using the Kharitonov's theorem. *International Journal of Electrical Power & Energy Systems, 55*, 51-58.

Trodden, P. A., Bukhsh, W. A., Grothey, A., & McKinnon, K. I. (2014). Optimization-based islanding of power networks using piecewise linear AC power flow. *IEEE Transactions on Power Systems, 29*(3), 1212-1220.

Union for the Coordination of Transmission of Electricity. (2003). Interim Report of the Investigation Committee on the 28 September 2003 blackout in Italy (pp. 62).

University of Washington. (1999). Power Systems Test Case Archive. *http://www.ee.washington.edu/research/pstca/*.

Velusami, S., & Romar, K. (1997). Design of observer-based decentralized load-frequency controllers for interconnected power systems. *International journal of power & energy systems, 17*(2), 152-160.

Vournas, C. D., Nikolaidis, V. C., & Tassoulis, A. A. (2006). Postmortem analysis and data validation in the wake of the 2004 Athens blackout. *IEEE Transactions on Power Systems, 21*(3), 1331-1339.

Wang, C., Vittal, V., & Sun, K. (2011). OBDD-based sectionalizing strategies for parallel power system restoration. *IEEE Transactions on Power Systems, 26*(3), 1426-1433.

Wang, X., Shao, W., & Vittal, V. (2005). *Adaptive corrective control strategies for preventing power system blackouts.* Paper presented at the 15th Power Systems Computation Conference, Liège, Belgium.

Wang, X., & Vittal, V. (2004). *System islanding using minimal cutsets with minimum net flow.* Paper presented at the IEEE PES Power Systems Conference and Exposition, 2004.

Wang, Y., Zhou, R., & Wen, C. (1993). *Robust load-frequency controller design for power systems.* Paper presented at the IEE proceedings C (generation, transmission and distribution).

Wang, Y., Zhou, R., & Wen, C. (1994). *New robust adaptive load-frequency control with system parametric uncertainties.* Paper presented at the IEE Proceedings Generation, Transmission and Distribution, .

Wong, J. J., Su, C. T., Liu, C. S., & Chang, C. L. (2007). Study on the 729 blackout in the Taiwan power system. *International Journal of Electrical Power & Energy Systems, 29*(8), 589-599.

Yang, B., Vittal, V., & Heydt, G. T. (2006). Slow-Coherency-Based Controlled Islanding - A Demonstration of the Approach on the August 14, 2003 Blackout Scenario. *IEEE Transactions on Power Systems, 21*(4), 1840-1847.

Yeşil, E., Güzelkaya, M., & Eksin, I. (2004). Self tuning fuzzy PID type load and frequency controller. *Energy Conversion and Management, 45*(3), 377-390.

Yongjian, Y., & Yumei, L. (2007). A new discrete filled function algorithm for discrete global optimization. *Journal of Computational and Applied Mathematics, 202*(2), 280-291.

You, H., Vittal, V., & Wang, X. (2004). Slow coherency-based islanding. *IEEE Transactions on Power Systems, 19*(1), 483-491.

You, H., Vittal, V., & Yang, Z. (2003). Self-healing in power systems: an approach using islanding and rate of frequency decline-based load shedding. *IEEE Transactions on Power Systems, 18*(1), 174-181.

Zhang, C.-K., Jiang, L., Wu, Q., He, Y., & Wu, M. (2013). Delay-Dependent Robust Load Frequency Control for Time Delay Power Systems. *2013 IEEE Power and Energy Society General Meeting (PES).*

Zhao, Q., Sun, K., Zheng, D.-Z., Ma, J., & Lu, Q. (2003). A study of system splitting strategies for island operation of power system: A two-phase method based on OBDDs. *IEEE Transactions on Power Systems, 18*(4), 1556-1565.

Zimmerman, R., Murillo-Sanchez, C., & Gan, D. (2009). MATPOWER: A MATLAB power system simulation package 2006.

Zin, A. A. M., Hafiz, H. M., & Wong, W. (2004). *Static and dynamic under-frequency load shedding: a comparison.* Paper presented at the PowerCon 2004. 2004 International Conference on Power System Technology, 2004. .

Zribi, M., Al-Rashed, M., & Alrifai, M. (2005). Adaptive decentralized load frequency control of multi-area power systems. *International Journal of Electrical Power & Energy Systems, 27*(8), 575-583.

LIST OF PUBLICATIONS AND PAPERS PRESENTED

Journal

Naidu, K., Mokhlis, H., & Bakar, A. (2014). Multiobjective optimization using weighted sum artificial bee colony algorithm for load frequency control. *International Journal of Electrical Power & Energy Systems, 55*, 657-667.

Naidu, K., Mokhlis, H., Bakar, A., Terzija, V., & Illias, H. (2014). Application of firefly algorithm with online wavelet filter in automatic generation control of an interconnected reheat thermal power system. *International Journal of Electrical Power & Energy Systems, 63*, 401-413.

Conference

Naidu, K., Mokhlis, H., & Bakar, A. (2013). *Application of firefly algorithm (FA) based optimization in load frequency control for interconnected reheat thermal power system.* Paper presented at the 2013 IEEE Jordan Conference on Applied Electrical Engineering and Computing Technologies (AEECT).

Mokhlis, H., Naidu, K., Bakar, A., & Terzija, V. *Performance Investigation Of Abc Algorithm For Automatic Generation Control Of A Three Area Interconnected Power System*. Paper presented at the ACE.

APPENDIX A

Table A-1

IEEE 30-bus generator data (Zimmerman et al., 2009)

Bus	Type	Qmax	Qmin	Pmax	Pmin
1	Slack	10	0	360.2	0
2	PV	50	-40	140	0
5	PV	40	-40	100	0
8	PV	40	-10	100	0
11	PV	24	-6	100	0
13	PV	24	-6	100	0

Table A-2

IEEE 39-bus generator data (Zimmerman et al., 2009)

Bus	Type	Qmax	Qmin	Pmax	Pmin
30	PV	400	140	1040	0
31	Slack	300	-100	646	0
32	PV	300	150	725	0
33	PV	250	0	652	0
34	PV	167	0	508	0
35	PV	300	-100	687	0
36	PV	240	0	580	0
37	PV	250	0	564	0
38	PV	300	-150	865	0
39	PV	300	-100	1100	0

Table A-3

IEEE 118-bus generator data (Zimmerman et al., 2009)

Bus	Type	Qmax	Qmin	Pmax	Pmin
10	PV	200	-147	550	0
12	PV	120	-35	185	0
25	PV	140	-47	320	0
26	PV	1000	-1000	414	0
31	PV	300	-300	107	0
46	PV	100	-100	119	0
49	PV	210	-85	304	0
54	PV	300	-300	148	0
59	PV	180	-60	255	0
61	PV	300	-100	260	0
65	PV	200	-67	491	0
66	PV	200	-67	492	0
69	Slack	300	-300	805.2	0
80	PV	280	-165	577	0
87	PV	1000	-100	104	0
89	PV	300	-210	707	0
100	PV	155	-50	352	0
103	PV	40	-15	140	0
111	PV	1000	-100	136	0

Table A-4

Load Flow Analysis Data for IEEE 30-bus Test System

From bus	To bus	P (MW)	Q (MVar)	S (MVA)
1	2	177.72	22.13	179.09
1	3	83.42	3.40	83.49
2	4	45.64	0.55	45.64
2	5	82.99	1.70	83.00
2	6	61.93	1.10	61.94
3	4	78.20	4.89	78.36
4	6	71.07	9.34	71.68
4	12	43.31	2.03	43.36
5	7	14.36	12.07	18.76
6	7	37.52	1.77	37.57
6	8	29.62	3.22	29.79
6	9	28.25	4.11	28.54
6	10	15.83	1.96	15.95
6	28	19.14	8.11	20.79
8	28	0.48	2.33	2.38
9	10	28.25	23.54	36.77
9	11	0.00	29.30	29.30
10	17	5.78	3.25	6.64
10	20	9.20	3.04	9.69
10	21	15.71	10.72	19.02
10	22	7.57	5.06	9.11
12	13	0.00	18.75	18.75
12	14	7.84	2.88	8.35
12	15	17.47	8.59	19.46
12	16	6.81	4.55	8.19
14	15	1.55	1.11	1.91
15	18	5.85	2.29	6.29
15	23	4.72	4.41	6.46
16	17	3.24	2.62	4.17
18	19	2.61	1.31	2.92
19	20	6.91	2.14	7.24
21	22	1.91	0.75	2.06
22	24	5.60	4.18	6.99
23	24	1.47	2.73	3.10
24	25	1.70	0.08	1.70
25	26	3.55	2.37	4.27
25	27	5.29	2.36	5.79
27	28	18.60	5.74	19.46
27	29	6.20	1.69	6.43
27	30	7.11	1.69	7.30
29	30	3.71	0.61	3.76

Table A-5

Load Flow Analysis Data for IEEE 39-bus (original) Test System

From bus	To bus	P (MW)	Q (MVar)	S (MVA)
1	2	121.82	149.84	193.11
1	39	121.23	10.01	121.64
2	3	355.07	95.40	367.67
2	25	231.95	192.46	301.40
2	30	250.00	110.12	273.18
3	4	71.63	163.92	178.89
3	18	40.15	17.57	43.83
4	5	165.17	81.51	184.19
4	14	264.46	17.24	265.02
5	6	485.87	104.28	496.93
5	8	320.22	20.11	320.85
6	7	428.07	5.32	428.11
6	11	341.69	34.39	343.42
6	31	573.05	163.17	595.83
7	8	193.20	82.69	210.15
8	9	10.52	177.59	177.90
9	39	17.03	170.48	171.33
10	11	344.76	63.71	350.59
10	13	305.24	43.08	308.27
10	32	650.00	101.57	657.89
11	12	2.59	39.39	39.48
12	13	6.01	50.33	50.69
13	14	298.88	82.06	309.94
14	15	33.61	72.14	79.59
15	16	287.26	119.62	311.17
16	17	206.86	200.38	288.00
16	19	454.55	239.13	513.62
16	21	331.32	0.10	331.32
16	24	42.00	116.90	124.22
17	18	198.39	14.45	198.92
17	27	7.97	162.31	162.50
19	20	174.57	81.55	192.68
19	33	632.00	99.14	639.73
20	34	508.00	72.72	513.18
21	22	608.02	104.36	616.91
22	23	41.98	73.60	84.73
22	35	650.00	177.96	673.92
23	24	353.04	17.57	353.47
23	36	560.00	27.81	560.69
25	26	82.11	150.67	171.59
25	37	540.00	221.11	583.51
26	27	274.33	120.61	299.67
26	28	142.33	102.41	175.34
26	29	191.76	145.81	240.90
28	29	349.84	118.97	369.52
29	38	830.00	142.41	842.13

Table A-6

Load Flow Analysis Data for IEEE 39-bus (modified) Test System

From bus	To bus	P (MW)	Q (MVar)	S (MVA)
1	2	164.13	157.70	227.62
1	39	163.14	4.10	163.19
2	3	327.12	141.40	356.37
2	25	246.72	189.23	310.94
2	30	250.00	145.88	289.45
3	4	67.73	158.57	172.43
3	18	64.21	66.48	92.42
4	5	224.19	56.55	231.22
4	14	83.49	55.10	100.03
4	31	573.51	152.65	593.48
5	6	111.83	2.09	111.85
5	8	335.59	29.11	336.85
6	7	370.65	3.37	370.67
6	11	484.07	8.77	484.15
7	8	136.05	69.78	152.90
8	9	52.31	174.07	181.76
9	39	58.85	173.38	183.09
10	11	474.75	28.46	475.61
10	13	175.25	3.02	175.27
10	32	650.00	31.48	650.76
11	12	10.22	42.16	43.38
12	13	18.79	46.91	50.53
13	14	156.34	30.01	159.20
14	15	72.64	51.72	89.17
15	16	248.10	100.33	267.61
16	17	260.25	47.82	264.61
16	19	54.95	164.28	173.23
16	21	331.19	33.82	332.91
16	24	41.96	138.08	144.31
17	18	222.54	61.17	230.79
17	27	22.71	196.04	197.35
17	34	508.00	159.58	532.48
19	20	683.51	172.20	704.87
19	33	632.00	10.00	632.08
21	22	607.99	140.73	624.07
22	23	42.01	76.00	86.84
22	35	650.00	216.73	685.18
23	24	353.05	5.95	353.10
23	36	560.00	49.82	562.21
25	26	67.39	129.81	146.26
25	37	540.00	199.06	575.52
26	27	259.81	161.07	305.69
26	28	142.48	89.50	168.25
26	29	191.67	132.78	233.17
28	29	349.98	105.71	365.59
29	38	830.00	117.01	838.21

Table A-7

Load Flow Analysis Data for IEEE 118-bus Test System

From bus	To bus	P (MW)	Q (MVar)	S (MVA)
1	2	12.25	4.65	13.10
1	3	39.04	9.56	40.19
2	12	32.48	11.38	34.42
3	5	69.59	9.13	70.19
3	12	9.71	2.63	10.06
4	5	103.14	23.04	105.68
4	11	63.95	2.51	64.00
5	6	88.13	2.80	88.18
5	8	337.73	65.82	344.08
5	11	76.86	0.16	76.86
6	7	35.21	5.40	35.62
7	12	16.15	6.59	17.44
8	9	445.52	81.96	453.00
8	30	74.64	96.02	121.62
9	10	450.00	148.86	473.98
11	12	33.92	30.06	45.32
11	13	34.84	4.73	35.16
12	14	18.06	4.36	18.58
12	16	7.52	0.79	7.56
12	117	20.15	1.70	20.22
13	15	0.55	8.61	8.63
14	15	3.98	2.05	4.48
15	17	104.91	11.15	105.50
15	19	11.47	12.96	17.31
15	33	6.47	8.75	10.88
16	17	17.64	1.97	17.75
17	18	80.11	33.35	86.77
17	30	233.29	78.03	245.99
17	31	16.26	12.09	20.27
17	113	3.37	20.42	20.69
18	19	19.17	5.33	19.89
19	20	10.12	6.11	11.82
19	34	4.42	1.67	4.72
20	21	28.28	6.45	29.01
21	22	42.68	1.32	42.70
22	23	53.66	0.29	53.66
23	24	9.44	15.99	18.56
23	25	166.41	15.61	167.14
23	32	92.23	6.56	92.46
24	70	5.36	9.56	10.96
24	72	1.73	0.84	1.92
25	26	87.49	69.45	111.70
25	27	141.08	14.18	141.79
26	30	226.51	115.36	254.20
27	28	32.00	2.94	32.13
27	32	11.33	12.85	17.13
27	115	20.57	4.05	20.96
28	29	14.79	6.85	16.30
29	31	9.28	5.17	10.63
30	38	63.54	61.25	88.25
31	32	29.54	3.93	29.80
32	113	2.74	14.83	15.08
32	114	9.53	7.23	11.97
33	37	16.71	4.94	17.42
34	36	30.29	11.99	32.57
34	37	97.03	54.74	111.40
34	43	3.01	0.25	3.02
35	36	0.81	9.75	9.78
35	37	33.97	16.86	37.92
37	38	250.14	86.18	264.57
37	39	56.58	8.29	57.18

37	40	45.86	1.36	45.88
38	65	189.76	109.95	219.32
39	40	28.52	0.92	28.54
40	41	17.12	1.51	17.18
40	42	10.22	0.52	10.24
41	42	20.12	3.43	20.41
42	49	63.17	0.29	63.17
42	49	66.17	4.14	66.30
43	44	15.17	12.10	19.41
44	45	31.41	7.48	32.29
45	46	36.09	3.27	36.24
45	49	50.54	2.15	50.59
46	47	31.00	0.52	31.00
46	48	14.57	3.55	15.00
47	49	9.51	4.77	10.64
47	69	58.22	14.61	60.03
48	49	34.79	5.43	35.21
49	50	53.53	9.58	54.38
49	51	66.46	15.10	68.16
49	54	37.54	9.23	38.66
49	54	36.36	19.04	41.05
49	66	129.57	2.18	129.59
49	66	132.45	7.18	132.65
49	69	48.28	16.42	51.00
50	57	35.76	7.29	36.50
51	52	28.43	3.69	28.67
51	58	18.82	4.02	19.25
52	53	10.26	0.78	10.29
53	54	12.85	2.40	13.07
54	55	7.74	13.11	15.22
54	56	17.39	4.34	17.93
54	59	30.97	1.35	31.00
55	56	20.25	57.30	60.78
55	59	35.87	1.46	35.90
56	57	23.11	8.92	24.77
56	58	6.72	4.07	7.85
56	59	29.33	6.34	30.01
56	59	30.09	1.48	30.13
59	60	44.28	0.26	44.28
59	61	52.97	0.04	52.97
59	63	151.93	58.88	162.94
60	61	113.29	6.61	113.48
60	62	9.34	5.76	10.98
61	62	26.66	14.69	30.43
61	64	32.91	64.47	72.39
62	66	36.99	6.87	37.62
62	67	23.61	7.57	24.79
63	64	152.35	29.82	155.24
64	65	186.23	25.30	187.94
65	66	1.10	14.19	14.23
65	68	13.91	75.91	77.18
66	67	52.21	11.49	53.46
68	69	123.68	31.80	127.71
68	81	47.54	0.75	47.54
68	116	184.71	410.28	449.94
69	70	108.44	1.56	108.45
69	75	110.02	7.25	110.26
69	77	63.27	0.96	63.28
70	71	16.38	0.66	16.39
70	74	16.78	11.22	20.19
70	75	0.56	9.42	9.43
71	72	10.35	0.02	10.35
71	73	6.00	0.96	6.08
74	75	51.76	1.59	51.79
75	77	34.80	1.03	34.81
75	118	41.06	29.96	50.83

76	77	62.42	22.69	66.42
76	118	7.66	15.85	17.60
77	78	46.34	17.52	49.54
77	80	95.33	40.29	103.50
77	80	97.07	35.37	103.32
77	82	3.50	27.88	28.10
78	79	24.79	5.09	25.31
79	80	64.61	36.88	74.40
80	81	47.54	0.03	47.54
80	96	18.87	15.16	24.21
80	97	26.32	19.85	32.97
80	98	28.77	4.26	29.09
80	99	19.37	5.25	20.07
82	83	47.74	24.68	53.74
82	96	10.11	6.79	12.18
83	84	25.72	13.30	28.95
83	85	43.35	9.34	44.35
84	85	37.15	7.81	37.96
85	86	17.14	8.11	18.96
85	88	50.76	13.60	52.55
85	89	72.68	4.40	72.81
86	87	4.00	4.23	5.82
88	89	100.15	0.39	100.15
89	90	110.29	10.73	110.81
89	90	107.42	1.74	107.43
89	92	202.47	30.45	204.75
89	92	198.39	40.21	202.43
90	91	0.63	3.62	3.68
91	92	9.50	11.97	15.28
92	93	57.88	10.50	58.82
92	94	52.36	14.06	54.21
92	100	31.09	14.73	34.40
92	102	44.44	8.09	45.17
93	94	45.00	16.02	47.77
94	95	40.98	9.58	42.08
94	96	19.89	8.89	21.79
94	100	4.63	41.02	41.28
95	96	1.32	17.30	17.35
96	97	11.12	15.18	18.82
98	100	5.45	11.30	12.54
99	100	22.93	1.64	22.99
100	101	16.81	20.14	26.24
100	103	121.07	7.62	121.31
100	104	56.39	7.83	56.93
100	106	60.62	5.32	60.85
101	102	39.19	9.27	40.28
103	104	32.29	6.08	32.86
103	105	42.94	5.29	43.26
103	110	60.57	1.08	60.58
104	105	48.68	2.14	48.73
105	106	8.68	0.49	8.69
105	107	26.68	4.56	27.07
105	108	23.98	13.28	27.41
106	107	24.06	4.83	24.54
108	109	21.78	11.37	24.57
109	110	13.72	13.13	18.99
110	111	36.00	2.80	36.11
110	112	69.46	33.55	77.14
114	115	1.51	7.19	7.35

APPENDIX B

Article B-1

In Section 4, nine different test cases were evaluated and the optimum network splitting solutions were obtained. The one line diagram of the islanding solution was shown in each of those sections (Section 4.4 – Section 4.12). In this section, the graph models of the optimum network splitting are shown.

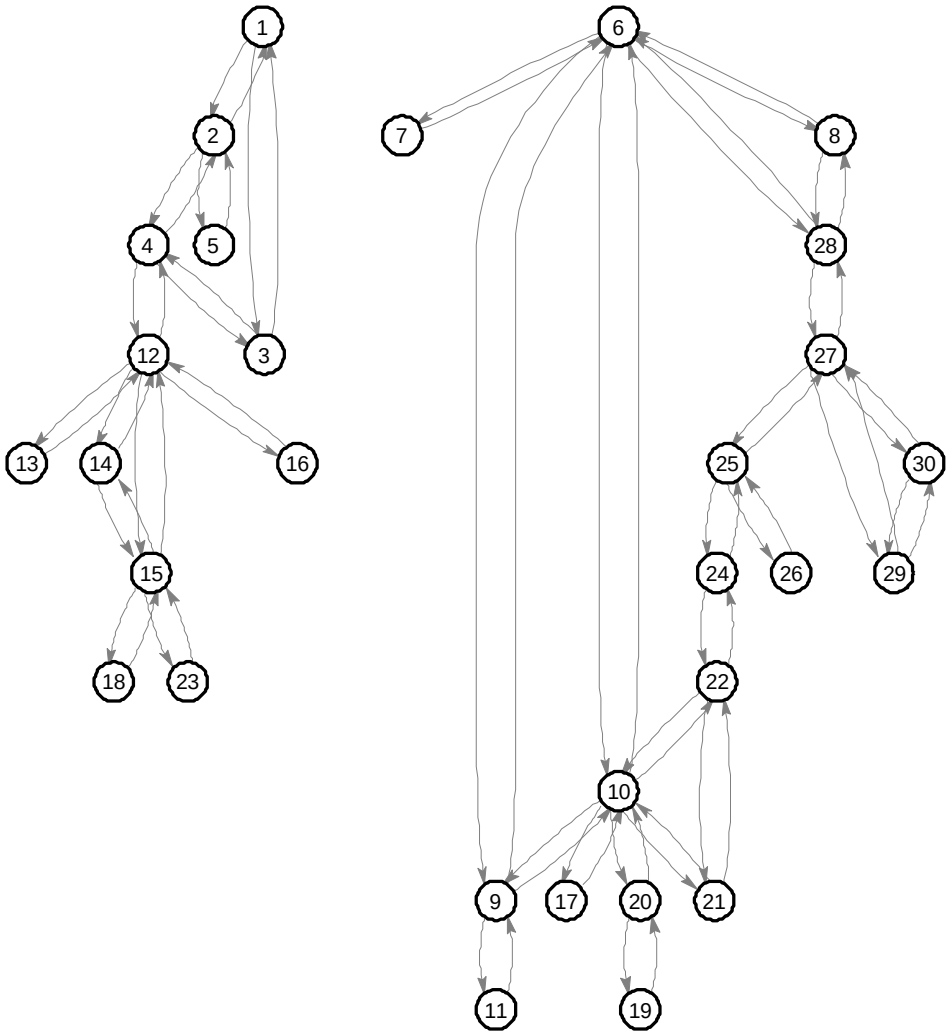

Figure B-1: Graph model for islanding solution for case 1

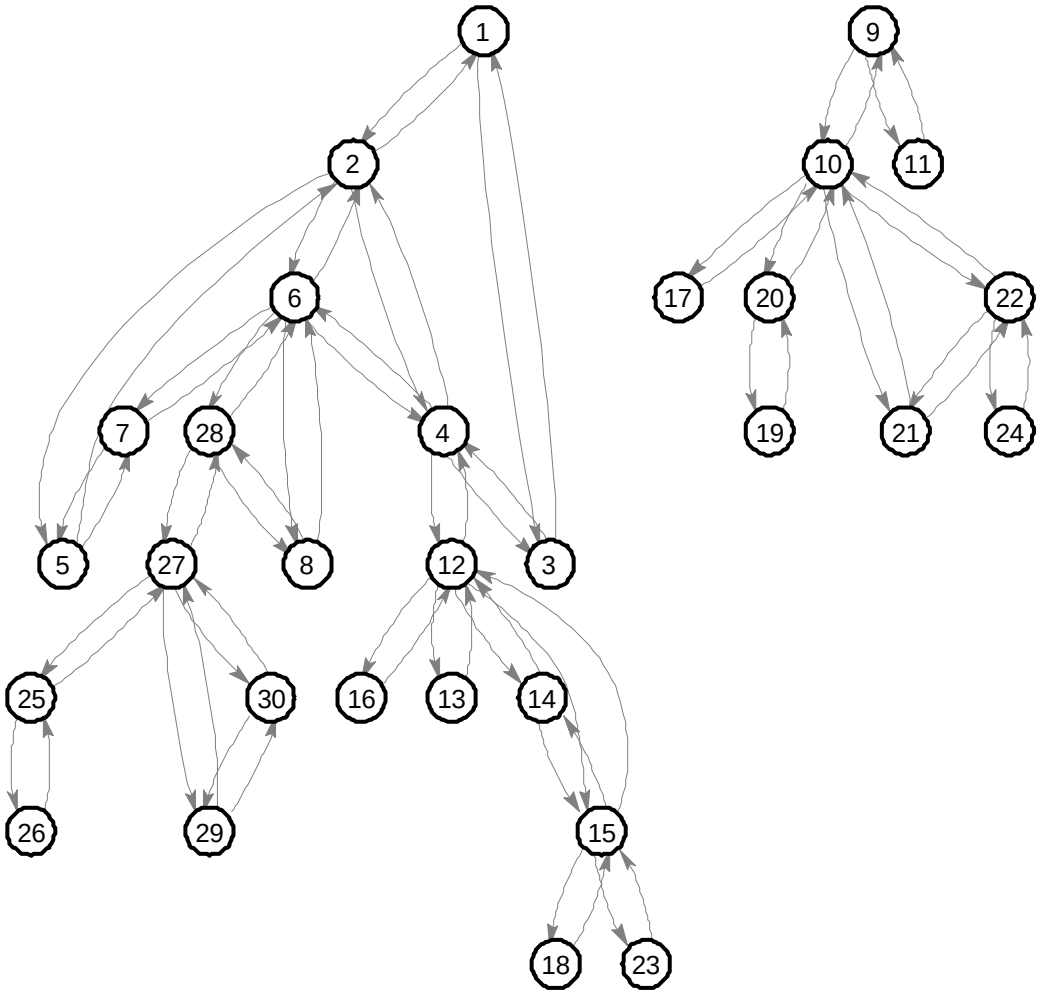

Figure B-2: Graph model for islanding solution for case 2

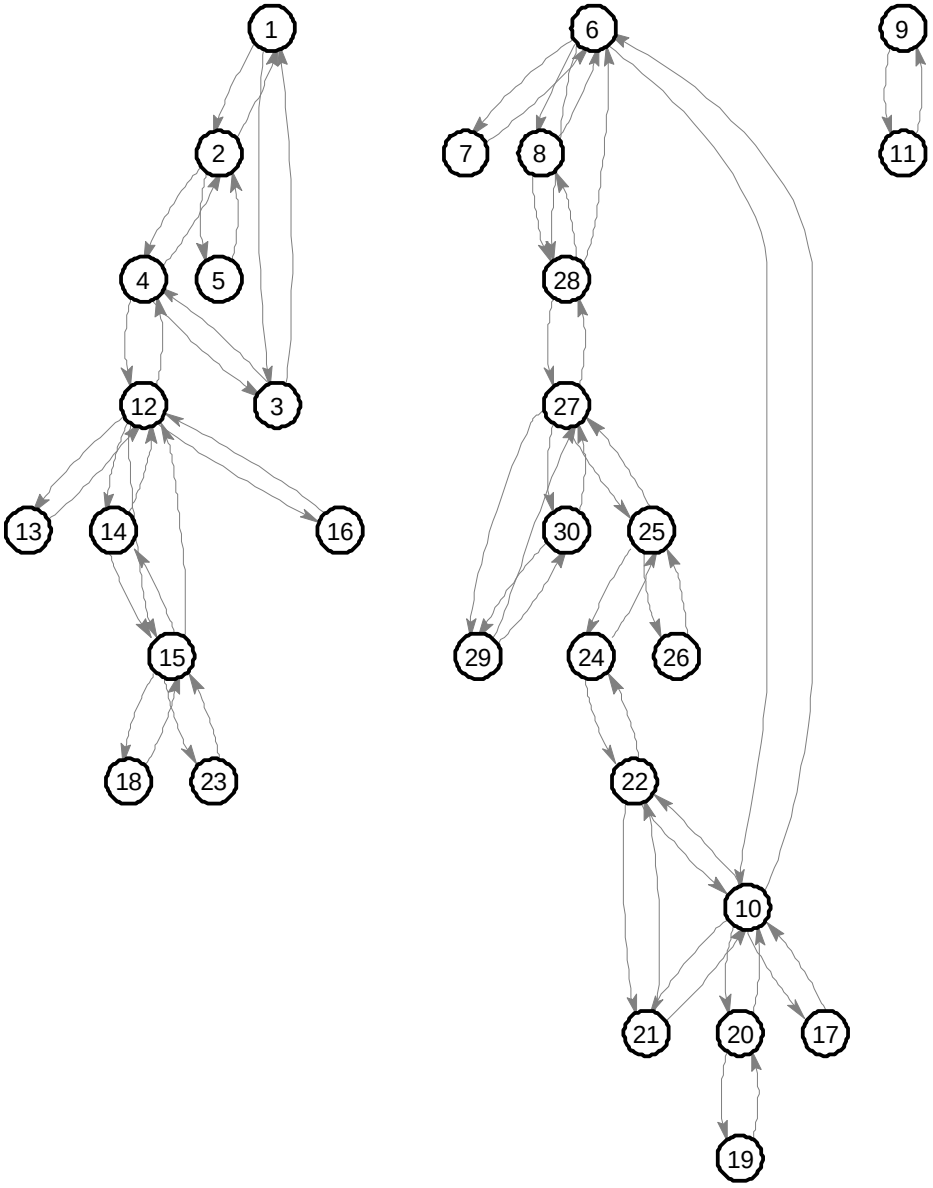

Figure B-3: Graph model for islanding solution for case 3

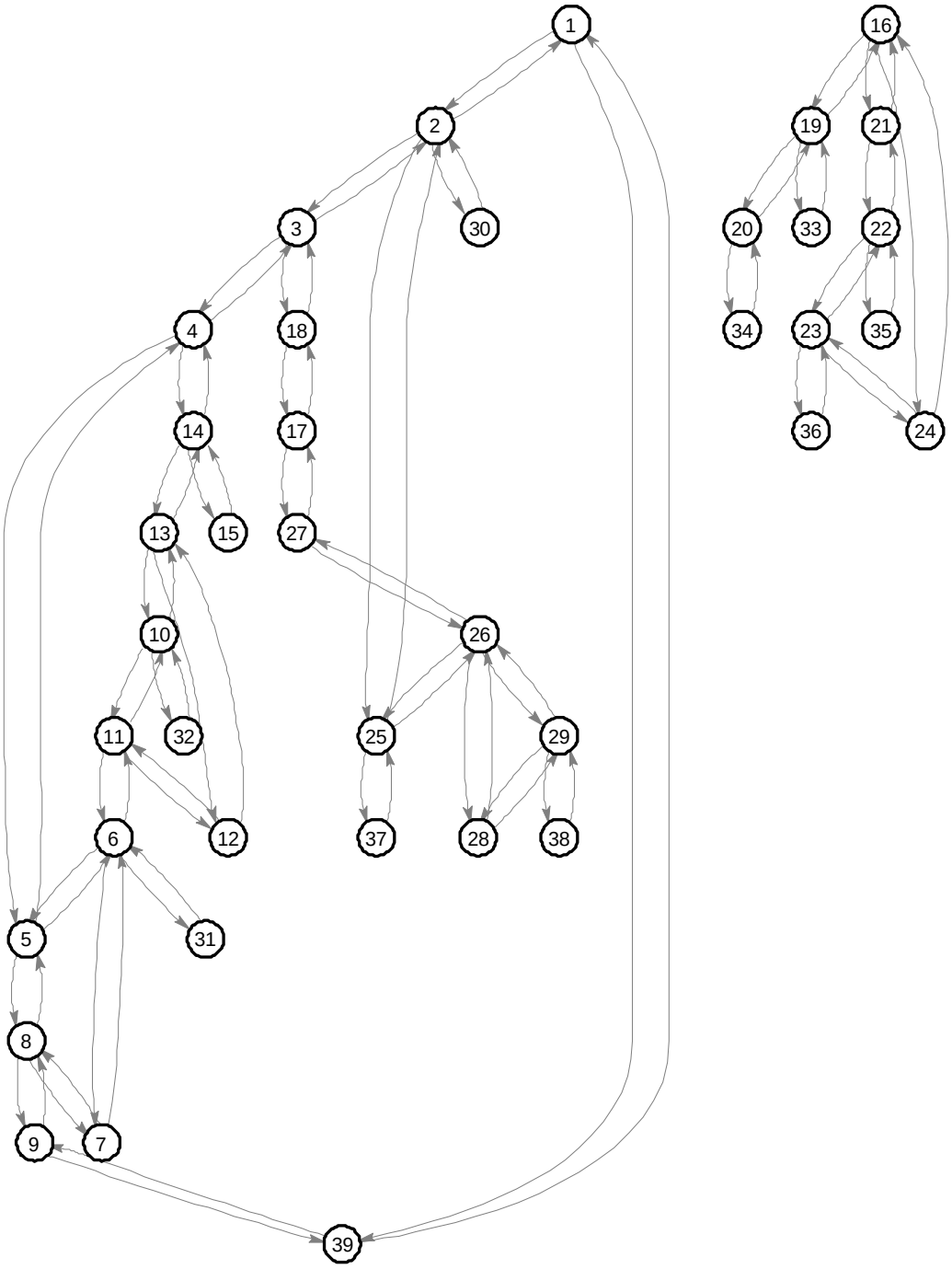

Figure B-4: Graph model for islanding solution for case 4

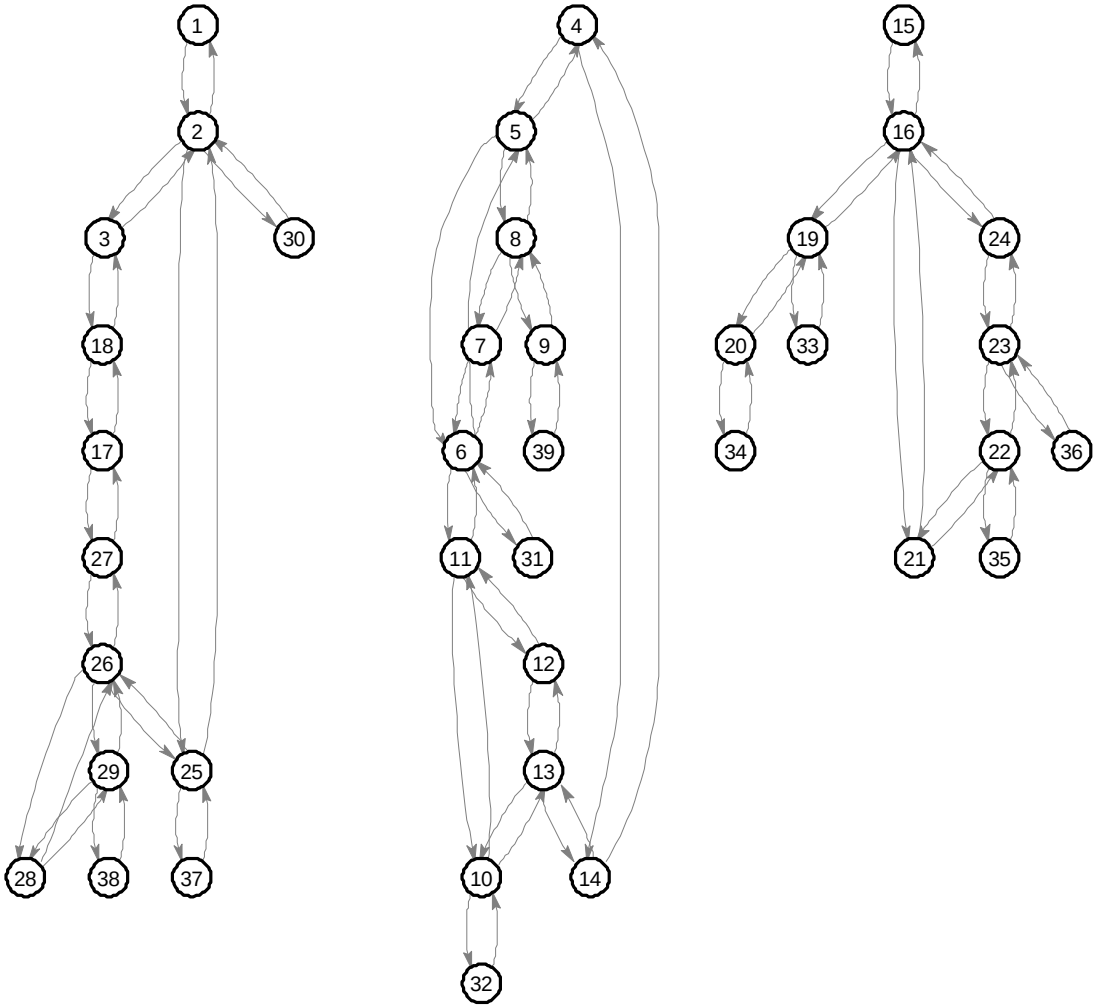

Figure B-5: Graph model for islanding solution for case 5

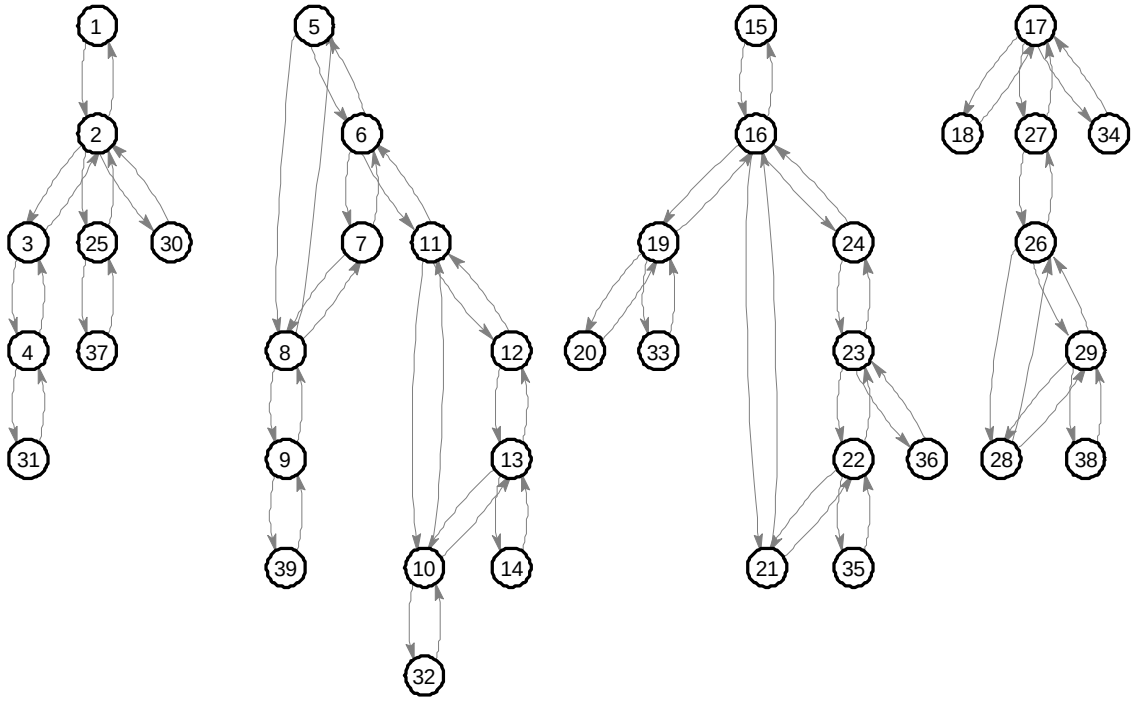

Figure B-6: Graph model for islanding solution for case 6

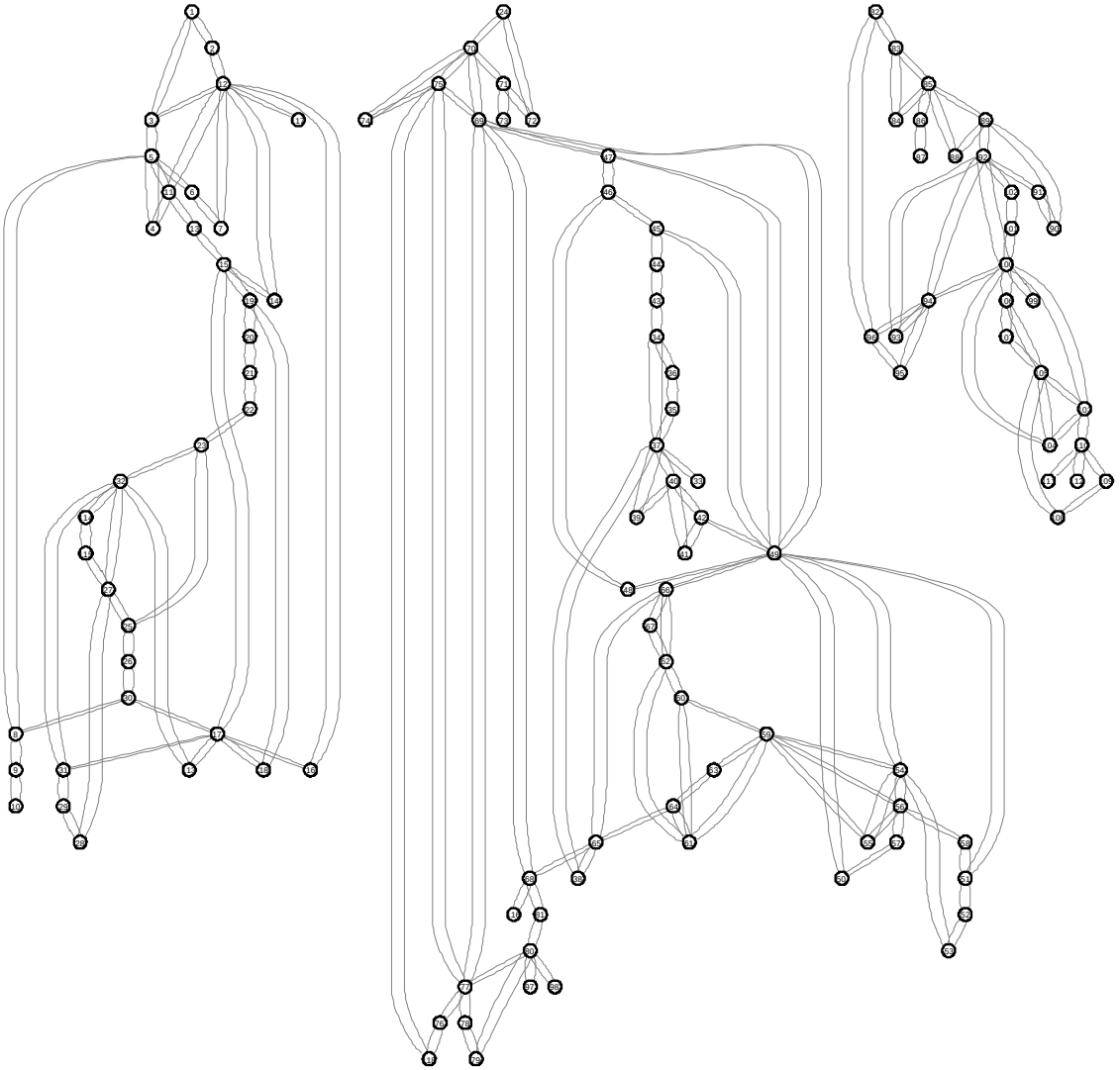

Figure B-7: Graph model for islanding solution for case 7

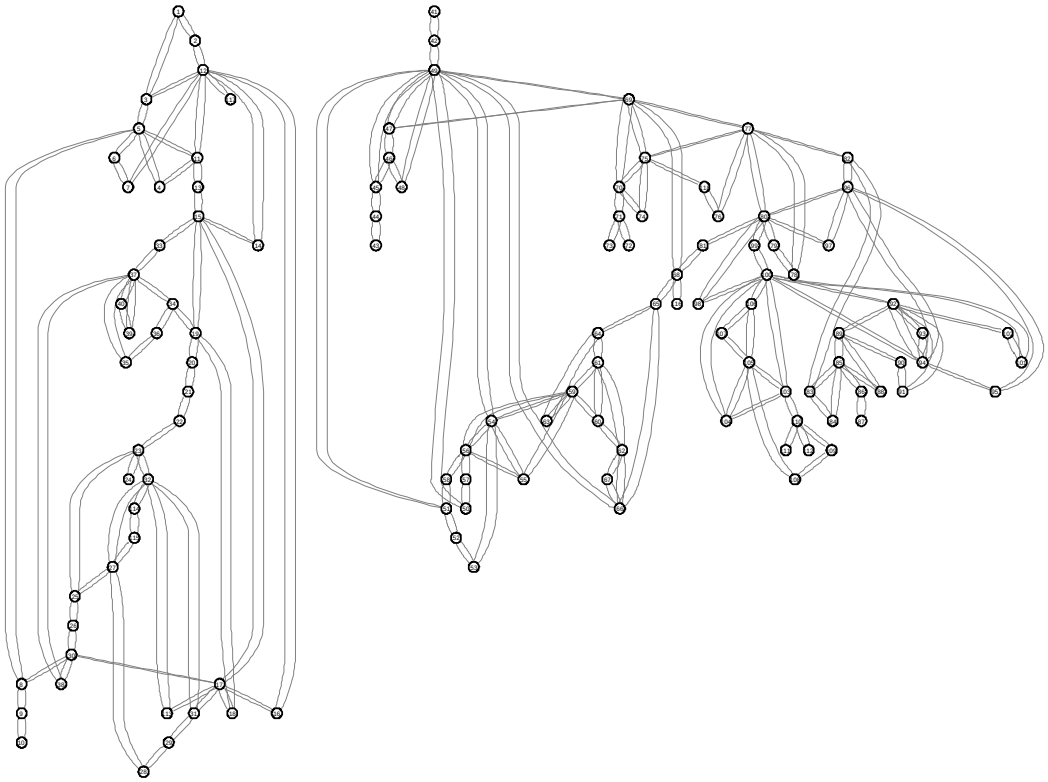

Figure B-8: Graph model for islanding solution for case 8

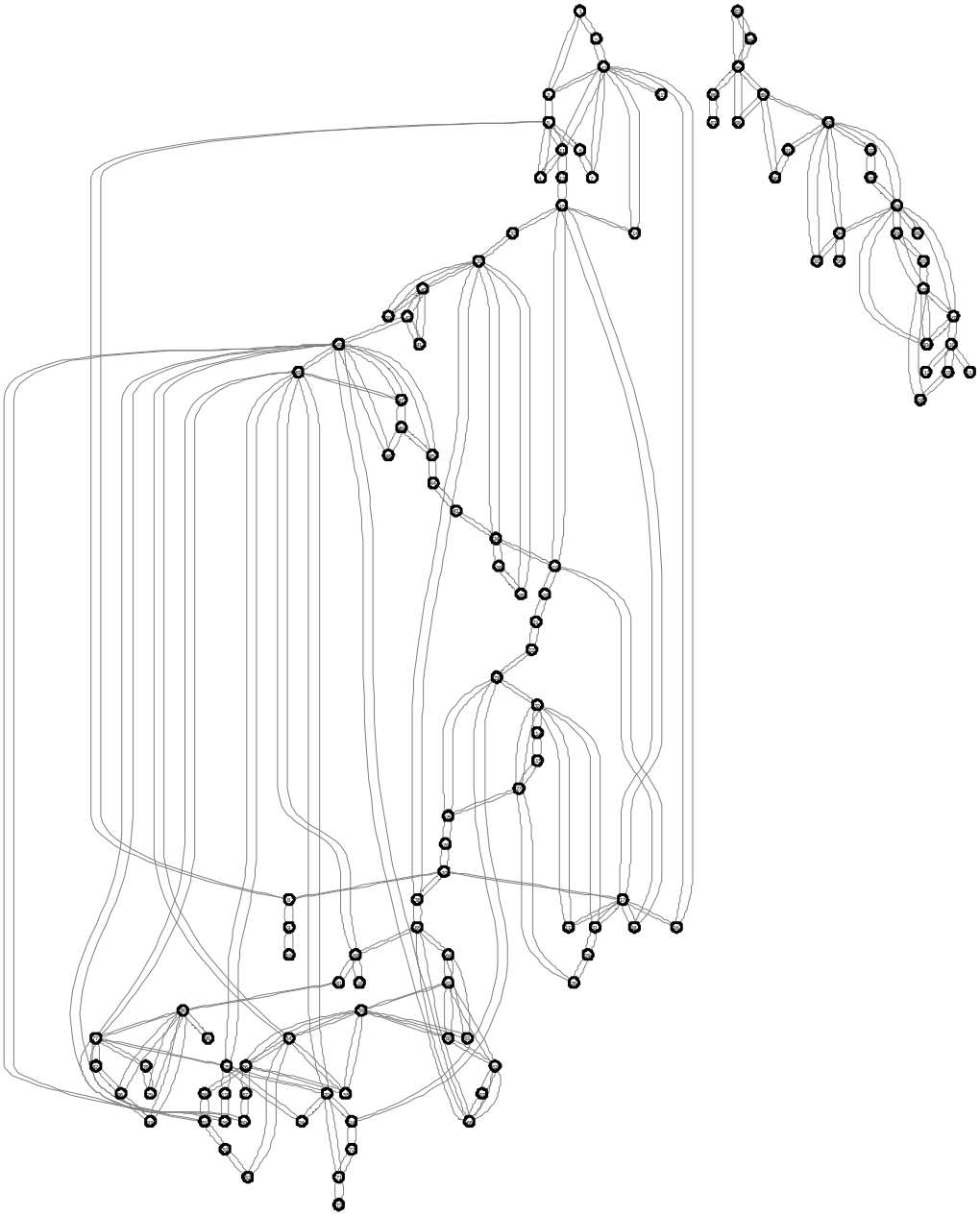

Figure B-9: Graph model for islanding solution for case 9

Table B-1

Transmission Lines Power Flow Analysis for Case 2

Parameters of transmission lines in island 1					Parameters of transmission lines in island 2				
From Bus	**To Bus**	**P_{flow}**	**P_{max}**	**P_{util} (%)**	**From Bus**	**To Bus**	**P_{flow}**	**P_{max}**	**P_{util} (%)**
1	2	138.40	208	66.54	9	10	53.37	104	51.32
1	3	63.63	208	30.59	9	11	53.37	104	51.32
2	4	33.66	104	32.37	10	17	9.04	51.2	17.66
2	5	75.04	208	36.08	10	20	11.90	51.2	23.25
2	6	44.71	104	42.99	10	21	17.73	51.2	34.63
3	4	59.59	208	28.65	10	22	8.90	51.2	17.38
4	6	48.88	144	33.94	19	20	9.54	51.2	18.63
4	12	35.74	104	34.36	21	22	0.06	51.2	0.11
5	7	21.88	112	19.54	22	24	8.86	25.6	34.62
6	7	45.21	208	21.74					
6	8	29.23	51.2	57.10					
6	28	17.80	51.2	34.77					
8	28	0.88	51.2	1.72					
12	13	0.00	104	0.00					
12	14	6.84	51.2	13.36					
12	15	14.19	51.2	27.71					
12	16	3.51	51.2	6.86					
14	15	0.58	25.6	2.26					
15	18	3.21	25.6	12.55					
15	23	3.20	25.6	12.50					
25	26	3.55	25.6	13.86					
25	27	3.55	25.6	13.86					
27	28	16.87	104	16.22					
27	29	6.20	25.6	24.22					
27	30	7.10	25.6	27.75					
29	30	3.71	25.6	14.48					

Table B-2

Transmission Lines Power Flow Analysis for Case 3

Parameters of transmission lines in island 1					Parameters of transmission lines in island 2				
From Bus	**To Bus**	**P_{flow}**	**P_{max}**	**P_{util} (%)**	**From Bus**	**To Bus**	**P_{flow}**	**P_{max}**	**P_{util} (%)**
1	2	93.44	208	44.92	6	7	17.61	208	8.46
1	3	34.57	208	16.62	6	8	43.26	51.2	84.39
2	4	11.84	104	11.39	6	10	28.52	51.2	55.71
2	5	98.41	208	47.31	6	28	10.92	51.2	21.33
3	4	31.69	208	15.23	8	28	15.58	51.2	30.44
4	12	35.73	104	34.36	10	17	6.94	51.2	13.56
12	13	0.00	104	0.00	10	20	9.17	51.2	17.90
12	14	6.84	51.2	13.35	10	21	6.07	51.2	11.85
12	15	14.18	51.2	27.70	10	22	1.89	51.2	3.70
12	16	3.51	51.2	6.86	19	20	7.33	51.2	14.31
14	15	0.58	25.6	2.26	21	22	7.41	51.2	14.48
15	18	3.20	25.6	12.50	22	24	5.59	25.6	21.84
15	18	3.21	25.6	12.54	24	25	12.85	25.6	50.20
					25	26	2.72	25.6	10.64
					25	27	16.10	25.6	62.87
					27	28	26.28	104	25.27
					27	29	4.75	25.6	18.54
					27	30	5.44	25.6	21.25
					29	30	2.84	25.6	11.09

Parameters of transmission lines in island 3				
From Bus	**To Bus**	**P_{flow}**	**P_{max}**	**P_{util} (%)**
9	11	0.00	104	0.00

Table B-3

Transmission Lines Power Flow Analysis for Case 4

Parameters of transmission lines in island 1					Parameters of transmission lines in island 2				
From Bus	**To Bus**	**P_{flow}**	**P_{max}**	**P_{util} (%)**	**From Bus**	**To Bus**	**P_{flow}**	**P_{max}**	**P_{util} (%)**
1	2	89.77	960	9.35	15	16	321.12	960	33.45
1	39	88.45	1600	5.53	16	19	454.57	960	47.35
2	3	397.22	800	49.65	16	21	217.54	960	22.66
2	25	212.63	800	26.58	16	24	18.22	960	1.90
2	30	281.33	1440	19.54	19	20	174.62	1440	12.13
3	4	23.35	800	2.92	19	33	632.00	1440	43.89
3	18	95.98	800	12.00	20	34	508.00	1440	35.28
4	5	211.07	960	21.99	21	22	493.52	1440	34.27
4	14	313.43	800	39.18	22	23	18.74	960	1.95
5	6	529.06	1920	27.56	22	35	474.78	1440	32.97
5	8	317.42	1440	22.04	23	24	292.27	960	30.44
6	7	433.89	1440	30.13	23	36	560.00	1440	38.89
6	11	355.00	768	46.22					
6	31	608.82	2880	21.14					
7	8	198.98	1440	13.82					
8	9	7.55	1440	0.52					
9	39	15.93	1440	1.11					
10	11	358.13	960	37.30					
10	13	320.67	960	33.40					
10	32	685.36	1440	47.59					
11	12	2.62	800	0.33					
12	13	5.97	800	0.75					
13	14	314.31	960	32.74					
17	18	62.34	960	6.49					
17	27	62.34	960	6.49					
25	26	125.23	960	13.04					
25	37	564.00	1440	39.17					
26	27	344.83	960	35.92					
26	28	156.30	960	16.28					
26	29	206.05	960	21.46					
28	29	363.96	960	37.91					
29	38	870.34	1920	45.33					

Table B-4

Transmission Lines Power Flow Analysis for Case 5

Parameters of transmission lines in island 1

From Bus	To Bus	P_{flow}	P_{max}	P_{util} (%)
4	5	189.68	960	19.76
4	14	311.61	800	38.95
5	6	542.51	1920	28.26
5	8	352.20	1440	24.46
6	7	465.82	1440	32.35
6	11	380.63	768	49.56
6	31	628.77	2880	21.83
7	8	230.63	1440	16.02
8	9	59.49	1440	4.13
9	39	49.95	1440	3.47
10	11	382.50	960	39.84
10	13	320.38	960	33.37
10	32	709.81	1440	49.29
11	12	1.25	800	0.16
12	13	7.35	800	0.92
13	14	312.57	960	32.56

Parameters of transmission lines in island 2

From Bus	To Bus	P_{flow}	P_{max}	P_{util} (%)
15	16	321.12	960	33.45
16	19	454.57	960	47.35
16	21	217.54	960	22.66
16	24	18.22	960	1.90
19	20	174.62	1440	12.13
19	33	632.00	1440	43.89
20	34	508.00	1440	35.28
21	22	493.52	1440	34.27
22	23	18.74	960	1.95
22	35	474.78	1440	32.97
23	24	292.27	960	30.44
23	36	560.00	1440	38.89

Parameters of transmission lines in island 3

From Bus	To Bus	P_{flow}	P_{max}	P_{util} (%)
1	2	0.21	960	0.02
2	3	432.52	800	54.07
2	25	173.06	800	21.63
2	30	262.40	1440	18.22
3	18	108.29	800	13.54
17	18	49.94	960	5.20
17	27	49.94	960	5.20
25	26	140.98	960	14.69
25	37	540.00	1440	37.50
26	27	332.21	960	34.61
26	28	142.03	960	14.79
26	29	191.92	960	19.99
28	29	349.58	960	36.41
29	38	830.00	1920	43.23

Table B-5

Transmission Lines Power Flow Analysis for Case 6

Parameters of transmission lines in island 1					Parameters of transmission lines in island 2				
From Bus	To Bus	P_{flow}	P_{max}	P_{util} (%)	From Bus	To Bus	P_{flow}	P_{max}	P_{util} (%)
1	2	0.20	960	0.02	15	16	278.24	960	28.98
2	3	554.66	800	69.33	16	19	56.82	960	5.92
2	25	314.25	800	39.28	16	21	393.66	960	41.01
2	30	250.00	1440	17.36	16	24	114.4	960	11.92
3	4	228.64	800	28.58	19	20	592.09	1440	41.12
4	31	272.49	2880	9.46	19	33	652	1440	45.28
25	37	540	1440	37.50	21	22	634.41	1440	44.06
					22	23	21.19	960	2.21
					22	35	655.59	1440	45.53
					23	24	385.05	960	40.11
					23	36	580	1440	40.28

Parameters of transmission lines in island 3					Parameters of transmission lines in island 4				
From Bus	To Bus	P_{flow}	P_{max}	P_{util} (%)	From Bus	To Bus	P_{flow}	P_{max}	P_{util} (%)
17	18	158.17	960	16.48	5	6	318.2	1920	16.57
17	27	347.46	960	36.19	5	8	318	1440	22.08
17	34	508	1440	35.28	6	7	392.93	1440	27.29
26	27	64.79	960	6.75	6	11	714.72	768	93.06
26	28	12.33	960	1.28	7	8	165.31	1440	11.48
26	29	62.54	960	6.51	8	9	24.32	1440	1.69
28	29	219.05	960	22.82	9	39	30.68	1440	2.13
29	38	567.82	1920	29.57	10	11	689.29	960	71.80
					10	13	35.71	960	3.72
					10	32	732.01	1440	50.83
					11	12	27.37	800	3.42
					12	13	35.7	800	4.46
					13	14	0.1	960	0.01

Table B-6

Transmission Lines Power Flow Analysis for Case 7

Parameters of transmission lines in island 1

From Bus	To Bus	P_{flow}	P_{max}	P_{util} (%)	From Bus	To Bus	P_{flow}	P_{max}	P_{util} (%)
24	72	2.54	280	0.91	55	59	36.37	280	12.99
24	70	10.49	280	3.75	56	58	6.38	280	2.28
33	37	23.24	280	8.30	56	57	22.69	280	8.10
34	43	3.13	280	1.12	56	59	29.11	280	10.40
34	36	31.27	280	11.17	56	59	30.53	280	10.90
34	37	87.42	800	10.93	59	60	44.55	280	15.91
35	36	0.17	280	0.06	59	61	53.27	280	19.02
35	37	32.98	280	11.78	59	63	153.23	800	19.15
37	40	39.82	280	14.22	60	62	9.19	280	3.28
37	39	50.57	280	18.06	60	61	113.72	800	14.21
37	38	234.04	800	29.26	61	62	27.04	280	9.66
38	65	238.82	800	29.85	61	64	34.02	800	4.25
39	40	22.73	280	8.12	62	67	23.34	280	8.34
40	41	11.40	280	4.07	62	66	36.71	280	13.11
40	42	16.06	280	5.73	63	64	153.66	800	19.21
41	42	25.92	280	9.26	64	65	188.67	800	23.58
42	49	68.99	280	24.64	65	66	6.19	800	0.77
42	49	72.59	280	25.92	65	68	42.99	800	5.37
43	44	21.44	280	7.66	66	67	51.93	280	18.55
44	45	37.78	280	13.49	68	81	78.79	800	9.85
45	46	39.51	280	14.11	68	69	149.13	800	18.64
45	49	53.84	280	19.23	68	116	184.71	800	23.09
46	48	15.20	280	5.43	69	77	59.09	280	21.10
46	47	33.86	280	12.09	69	70	108.75	800	13.59
47	49	6.10	280	2.18	69	70	112.42	800	14.05
47	69	65.18	280	23.28	70	75	2.68	280	0.96
48	49	35.42	280	12.65	70	74	14.18	280	5.06
49	54	35.91	280	12.83	70	71	20.71	280	7.40
49	54	37.07	280	13.24	71	73	6.01	280	2.15
49	50	52.34	280	18.69	71	72	14.64	280	5.23
49	69	55.00	280	19.64	74	75	54.41	280	19.43
49	51	65.93	280	23.55	75	77	37.52	280	13.40
49	66	132.27	800	16.53	75	118	38.75	280	13.84
49	66	135.27	800	16.91	76	118	5.41	280	1.93
50	57	35.34	280	12.62	76	77	64.75	280	23.13
51	58	18.48	280	6.60	77	78	43.29	280	15.46
51	52	28.27	280	10.10	77	80	47.57	800	5.95
52	53	10.09	280	3.61	77	80	103.61	800	12.95
53	54	13.01	280	4.65	78	79	27.84	280	9.94
54	55	7.61	280	2.72	79	80	67.71	280	24.18
54	56	16.97	280	6.06	80	97	15.05	280	5.37
54	59	31.48	280	11.24	80	98	34.27	280	12.24
55	56	19.91	280	7.11	80	81	78.79	800	9.85

Parameters of transmission lines in island 2

From Bus	To Bus	P_{flow}	P_{max}	P_{util} (%)
1	2	13.20	280	4.71
1	3	38.08	280	13.60
2	12	33.44	280	11.94
3	12	10.94	280	3.91
3	5	67.35	280	24.05
4	11	59.48	280	21.24
4	5	98.66	800	12.33
5	11	71.80	280	25.64
5	6	83.94	280	29.98

Parameters of transmission lines in island 3

From Bus	To Bus	P_{flow}	P_{max}	P_{util} (%)
82	96	3.43	280	1.23
82	83	57.86	320	18.08
83	84	31.01	280	11.07
83	85	48.61	280	17.36
84	85	42.59	280	15.21
85	86	17.22	800	2.15
85	88	56.62	280	20.22
85	89	77.93	280	27.83
86	87	4.00	800	0.50

5	8	321.74	800	40.22	88	89	106.20	800	13.27
6	7	31.10	280	11.11	89	90	59.57	800	7.45
7	12	12.06	280	4.31	89	90	59.57	800	7.45
8	30	15.29	280	5.46	89	92	70.89	800	8.86
8	9	445.52	800	55.69	89	90	113.41	800	14.18
9	10	450.00	800	56.25	89	92	225.07	800	28.13
11	12	29.18	280	10.42	90	91	5.12	280	1.83
11	13	30.31	280	10.82	92	100	38.11	280	13.61
12	16	1.66	280	0.59	92	102	51.37	280	18.35
12	14	12.93	280	4.62	92	94	62.04	280	22.16
12	117	20.15	280	7.19	92	93	67.59	280	24.14
13	15	3.93	280	1.40	93	94	54.39	280	19.43
14	15	1.12	280	0.40	94	100	6.32	280	2.26
15	19	11.33	280	4.05	94	96	28.57	280	10.21
15	17	107.93	800	13.49	94	95	48.95	280	17.48
16	17	23.60	280	8.43	95	96	6.44	280	2.30
17	113	0.55	280	0.20	99	100	42.31	280	15.11
17	31	13.31	280	4.75	100	101	23.47	280	8.38
17	18	81.52	280	29.11	100	104	56.39	280	20.14
17	30	237.91	800	29.74	100	106	60.62	280	21.65
18	19	20.59	280	7.35	100	103	121.07	800	15.13
19	20	13.22	280	4.72	101	102	46.03	280	16.44
20	21	31.41	280	11.22	103	104	32.29	280	11.53
21	22	45.86	280	16.38	103	105	42.94	280	15.33
22	23	56.95	280	20.34	103	110	60.57	280	21.63
23	32	97.25	224	43.41	104	105	48.68	280	17.39
23	25	165.12	800	20.64	105	106	8.68	280	3.10
25	26	87.37	800	10.92	105	108	23.98	280	8.56
25	27	142.25	800	17.78	105	107	26.68	280	9.53
26	30	226.63	800	28.33	106	107	24.06	280	8.59
27	32	11.40	280	4.07	108	109	21.78	280	7.78
27	115	20.60	280	7.36	109	110	13.72	280	4.90
27	28	32.96	280	11.77	110	111	36.00	280	12.86
28	29	15.74	280	5.62	110	112	69.46	280	24.81
29	31	8.34	280	2.98					
31	32	31.54	280	11.26					
32	113	5.56	800	0.70					
32	114	9.50	280	3.39					
114	115	1.48	280	0.53					

Table B-7

Transmission Lines Power Flow Analysis for Case 8

Parameters of transmission lines in island 1

From Bus	To Bus	P_{flow}	P_{max}	P_{util} (%)	From Bus	To Bus	P_{flow}	P_{max}	P_{util} (%)
1	2	13.21	280	4.72	19	34	16.98	280	6.07
1	3	38.07	280	13.60	19	20	18.64	280	6.66
2	12	33.45	280	11.95	20	21	36.92	280	13.19
3	12	10.96	280	3.91	21	22	51.50	280	18.39
3	5	67.32	280	24.04	22	23	62.85	280	22.45
4	11	61.44	280	21.94	23	24	13.07	280	4.67
4	5	100.63	800	12.58	23	32	91.88	224	41.02
5	11	74.02	280	26.44	23	25	179.54	800	22.44
5	6	83.89	280	29.96	25	26	67.78	800	8.47
5	8	325.86	800	40.73	25	27	145.09	800	18.14
6	7	31.06	280	11.09	26	30	283.08	800	35.38
7	12	12.01	280	4.29	27	32	15.34	280	5.48
8	30	126.14	280	45.05	27	115	22.72	280	8.11
8	9	485.64	800	60.70	27	28	29.51	280	10.54
9	10	491.33	800	61.42	28	29	12.33	280	4.40
11	12	21.37	280	7.63	29	31	11.73	280	4.19
11	13	42.19	280	15.07	30	38	199.18	280	71.14
12	16	15.74	280	5.62	31	32	21.18	280	7.56
12	117	20.15	280	7.19	32	114	7.39	280	2.64
12	14	27.86	280	9.95	32	113	16.89	800	2.11
13	15	7.77	280	2.78	33	37	4.78	280	1.71
14	15	13.68	280	4.89	34	36	33.66	280	12.02
15	19	17.14	280	6.12	34	37	76.13	800	9.52
15	33	28.10	280	10.04	35	36	2.35	280	0.84
15	17	115.75	800	14.47	35	37	30.85	280	11.02
16	17	9.36	280	3.34	37	40	42.12	280	15.04
17	31	10.16	280	3.63	37	39	53.02	280	18.94
17	113	10.58	280	3.78	37	38	197.39	800	24.67
17	18	87.48	280	31.24	39	40	25.09	280	8.96
17	30	203.14	800	25.39	114	115	0.63	280	0.22
18	19	26.45	280	9.45	19	34	16.98	280	6.07
					19	20	18.64	280	6.66

Parameters of transmission lines in island 2

From Bus	To Bus	P_{flow}	P_{max}	P_{util} (%)	From Bus	To Bus	P_{flow}	P_{max}	P_{util} (%)
41	42	37.63	280	13.44	75	118	36.91	280	13.18
42	49	66.82	280	23.86	75	77	40.03	280	14.29
42	49	70.18	280	25.07	76	118	3.59	280	1.28
43	44	18.22	280	6.51	76	77	66.68	280	23.82
44	45	34.51	280	12.32	77	82	6.77	320	2.12
45	46	36.56	280	13.06	77	78	40.17	280	14.35
45	49	53.48	280	19.10	77	80	50.78	800	6.35
46	48	16.56	280	5.91	77	80	110.31	800	13.79
46	47	29.49	280	10.53	78	79	30.96	280	11.06
47	49	20.49	280	7.32	79	80	70.89	280	25.32
47	69	44.67	280	15.95	80	81	18.35	800	2.29
48	49	36.80	280	13.14	80	96	19.76	280	7.06
49	54	34.08	280	12.17	80	96	20.02	280	7.15
49	69	34.37	280	12.28	80	97	27.47	280	9.81
49	54	35.31	280	12.61	80	98	29.29	280	10.46
49	50	51.40	280	18.36	82	96	12.82	280	4.58
49	51	63.89	280	22.82	82	83	48.33	320	15.10
49	66	143.37	800	17.92	83	84	25.96	280	9.27
49	66	146.90	800	18.36	83	85	43.72	280	15.61
50	57	33.69	280	12.03	84	85	37.40	280	13.36
51	58	17.19	280	6.14	85	86	17.14	800	2.14

51	52	27.64	280	9.87	85	88	51.07	280	18.24
52	53	9.47	280	3.38	85	89	73.00	280	26.07
53	54	13.63	280	4.87	86	87	4.00	800	0.50
54	55	7.09	280	2.53	88	89	100.46	800	12.56
54	56	15.36	280	5.49	89	90	57.91	800	7.24
54	59	33.41	280	11.93	89	92	63.35	800	7.92
55	56	18.59	280	6.64	89	90	110.24	800	13.78
55	59	38.26	280	13.66	89	92	202.04	800	25.26
56	58	5.10	280	1.82	90	91	0.56	280	0.20
56	57	21.10	280	7.54	91	92	9.57	280	3.42
56	59	30.73	280	10.98	92	100	30.89	280	11.03
56	59	32.23	280	11.51	92	102	44.24	280	15.80
59	60	45.76	280	16.34	92	94	52.25	280	18.66
59	61	54.59	280	19.50	92	93	57.77	280	20.63
59	63	157.92	800	19.74	93	94	44.89	280	16.03
60	62	8.75	280	3.12	94	100	3.99	280	1.43
60	61	115.38	800	14.42	94	96	20.12	280	7.19
61	62	28.30	280	10.11	94	95	41.18	280	14.71
61	64	38.27	800	4.78	95	96	1.12	280	0.40
62	67	22.49	280	8.03	96	97	12.26	280	4.38
62	66	35.84	280	12.80	98	100	4.94	280	1.76
63	64	158.37	800	19.80	99	100	22.42	280	8.01
64	65	197.67	800	24.71	100	101	16.62	280	5.93
65	66	27.70	800	3.46	100	104	56.39	280	20.14
65	68	165.62	800	20.70	100	106	60.62	280	21.65
66	67	51.06	280	18.24	100	103	121.07	800	15.13
68	69	1.18	800	0.15	101	102	39.00	280	13.93
68	81	18.35	800	2.29	103	104	32.29	280	11.53
68	116	184.57	800	23.07	103	105	42.94	280	15.33
69	77	43.73	280	15.62	103	110	60.57	280	21.63
69	70	98.89	800	12.36	104	105	48.68	280	17.39
69	75	103.00	800	12.88	105	106	8.68	280	3.10
70	75	0.89	280	0.32	105	108	23.98	280	8.56
70	74	15.61	280	5.58	105	107	26.68	280	9.53
70	71	18.13	280	6.47	106	107	24.06	280	8.59
71	73	6.01	280	2.15	108	109	21.78	280	7.78
71	72	12.07	280	4.31	109	110	13.72	280	4.90
74	75	52.97	280	18.92	110	111	36.00	280	12.86
					110	112	69.46	280	24.81

Table B-8

Transmission Lines Power Flow Analysis for Case 9

Parameters of transmission lines in island 1									
From Bus	**To Bus**	**P_{flow}**	**P_{max}**	**P_{util} (%)**	**From Bus**	**To Bus**	**P_{flow}**	**P_{max}**	**P_{util} (%)**
1	2	12.25	280	4.38	45	46	36.28	280	12.96
1	3	39.03	280	13.94	45	49	50.52	280	18.04
2	12	32.48	280	11.60	46	48	14.45	280	5.16
3	12	9.71	280	3.47	46	47	31.31	280	11.18
3	5	69.59	280	24.85	47	49	8.38	280	2.99
4	11	63.94	280	22.84	47	69	59.81	280	21.36
4	5	103.14	800	12.89	48	49	34.66	280	12.38
5	11	76.86	280	27.45	49	54	36.52	280	13.04
5	6	88.13	280	31.47	49	54	37.70	280	13.47
5	8	337.71	800	42.21	49	69	49.89	280	17.82
6	7	35.20	280	12.57	49	50	53.68	280	19.17
7	12	16.14	280	5.77	49	51	66.65	280	23.80
8	30	74.66	280	26.66	49	66	128.64	800	16.08
8	9	445.52	800	55.69	49	66	131.48	800	16.44
9	10	450.00	800	56.25	50	57	35.91	280	12.83
11	12	33.91	280	12.11	51	58	18.94	280	6.76
11	13	34.83	280	12.44	51	52	28.49	280	10.18
12	16	7.51	280	2.68	52	53	10.31	280	3.68
12	14	18.05	280	6.45	53	54	12.79	280	4.57
12	117	20.15	280	7.19	54	55	7.79	280	2.78
13	15	0.55	280	0.20	54	56	17.54	280	6.26
14	15	3.98	280	1.42	54	59	30.80	280	11.00
15	33	6.47	280	2.31	55	56	20.37	280	7.27
15	19	11.45	280	4.09	55	59	35.70	280	12.75
15	17	104.90	800	13.11	56	58	6.83	280	2.44
16	17	17.64	280	6.30	56	57	23.25	280	8.30
17	113	3.34	280	1.19	56	59	28.55	280	10.19
17	31	16.23	280	5.80	56	59	29.94	280	10.69
17	18	80.09	280	28.60	59	60	44.18	280	15.78
17	30	233.21	800	29.15	59	61	52.86	280	18.88
18	19	19.16	280	6.84	59	63	151.48	800	18.93
19	34	4.42	280	1.58	60	62	9.39	280	3.36
19	20	10.15	280	3.63	60	61	113.14	800	14.14
20	21	28.31	280	10.11	61	62	26.53	280	9.47
21	22	42.71	280	15.25	61	64	32.53	800	4.07
22	23	53.69	280	19.18	62	67	23.70	280	8.47
23	24	9.24	280	3.30	62	66	37.08	280	13.24
23	32	92.29	224	41.20	63	64	151.90	800	18.99
23	25	166.31	800	20.79	64	65	185.39	800	23.17
24	72	1.63	280	0.58	65	66	0.65	800	0.08
24	70	5.46	280	1.95	65	68	17.07	800	2.13
25	26	87.39	800	10.92	66	67	52.30	280	18.68
25	27	141.08	800	17.64	68	81	24.13	800	3.02
26	30	226.61	800	28.33	68	69	143.91	800	17.99
27	32	11.33	280	4.05	68	116	184.70	800	23.09
27	115	20.56	280	7.34	69	77	83.37	280	29.78
27	28	32.01	280	11.43	69	75	111.29	800	13.91
28	29	14.80	280	5.29	69	75	116.57	800	14.57
29	31	9.28	280	3.31	70	75	2.60	280	0.93
30	38	63.73	280	22.76	70	71	16.47	280	5.88
31	32	29.57	280	10.56	70	74	18.44	280	6.58
32	113	2.77	800	0.35	71	73	6.00	280	2.14
32	114	9.54	280	3.41	71	72	10.44	280	3.73
33	37	16.71	280	5.97	74	75	50.11	280	17.90
34	43	2.86	280	1.02	75	77	29.11	280	10.40
34	36	30.30	280	10.82	75	118	45.28	280	16.17

34	37	96.89	800	12.11	76	118	11.83	280	4.23
35	36	0.80	280	0.28	76	77	58.04	280	20.73
35	37	33.96	280	12.13	77	82	31.12	320	9.73
37	40	45.75	280	16.34	77	80	45.04	800	5.63
37	39	56.47	280	20.17	77	80	45.73	800	5.72
37	38	249.79	800	31.22	77	80	45.73	800	5.72
38	65	189.20	800	23.65	77	80	99.78	800	12.47
39	40	28.42	280	10.15	78	79	26.05	280	9.30
40	42	10.33	280	3.69	79	80	65.89	280	23.53
40	41	17.01	280	6.08	80	81	24.13	800	3.02
41	42	20.22	280	7.22	80	98	34.27	280	12.24
42	49	63.27	280	22.60	80	96	34.91	280	12.47
42	49	66.28	280	23.67	80	97	42.29	280	15.10
43	44	15.33	280	5.47	82	96	23.28	280	8.32
44	45	31.56	280	11.27	96	97	26.96	280	9.63
					114	115	1.51	280	0.54

Parameters of transmission lines in island 2

From Bus	To Bus	P_{flow}	P_{max}	P_{util} (%)	From Bus	To Bus	P_{flow}	P_{max}	P_{util} (%)
83	84	6.43	280	2.30	94	100	17.01	280	6.07
83	85	13.69	280	4.89	94	95	42.37	280	15.13
84	85	17.53	280	6.26	100	101	17.76	280	6.34
85	86	17.17	800	2.15	100	104	56.39	280	20.14
85	88	26.30	280	9.39	100	106	60.62	280	21.65
85	89	46.76	280	16.70	100	103	121.07	800	15.13
86	87	4.00	800	0.50	101	102	40.16	280	14.34
88	89	75.09	800	9.39	103	104	32.29	280	11.53
89	90	57.74	800	7.22	103	105	42.94	280	15.33
89	92	62.48	800	7.81	103	110	60.57	280	21.63
89	90	109.92	800	13.74	104	105	48.68	280	17.39
89	92	199.28	800	24.91	105	106	8.68	280	3.10
90	91	0.10	280	0.04	105	108	23.98	280	8.56
91	92	10.03	280	3.58	105	107	26.68	280	9.53
92	100	32.07	280	11.45	106	107	24.06	280	8.59
92	102	45.42	280	16.22	108	109	21.78	280	7.78
92	94	49.09	280	17.53	109	110	13.72	280	4.90
92	93	54.63	280	19.51	110	111	36.00	280	12.86
93	94	41.87	280	14.95	110	112	69.46	280	24.81

APPENDIX C

Article C-1

Load Frequency Control (LFC) Modeling

In order to design the Load Frequency Control (LFC) model of the respective system, the system parameters are obtained from published data (Bevrani, 2009). The system parameters for each generating units are considered by referring to the MW rating of the generator. In order to model the load demand, the P_{Load} value shown in each island in the post-splitting column is taken into consideration when load damping (*D*) is evaluated. The load damping is calculated based on the following equation:

$$D = (d\%) * (P_{Load} / MVA_{base}) \quad \text{(C-1-1)}$$

where *D* represents the load damping value, *d* represents the damping constant (in percentage), P_{Load} represents the load demand in the island and MVA_{base} represents the common MVA base for the system. In this investigation for all the LFC models, the *d* is taken as 1.5% (Prabha Kundur et al., 1994).

C-1.1. LFC test case 1

Table C-1 shows the generating parameters of the two area power system obtained from datasheet given in (Bevrani, 2009). The P_{Load} for area 1 is 161.4 MW and the corresponding D is 2.421 Hz/pu. In area 2, the P_{Load} is 122 MW and the corresponding D is 1.83 Hz/pu. The maximum P_G in area 1 is 700.2 MW. By taking the load demand into consideration, the system is still able to cater to a maximum load demand of 538.8 MW. In area 2, the maximum P_G is 200 MW and the system is still able to cater a load of 78 MW. The reheat thermal parameters K_{ri} and T_{ri} are 0.5s and 10s respectively. The GRC for each generator is taken as 3%.

Table C-1

Generating unit parameters for IEEE 30-bus test system with multiple interconnected generators

Parameters	G1	G2	G3	G4	G5	G6
T_{Hi} (sec)	0.08	0.06	0.07	0.06	0.06	0.08
T_{Ti} (sec)	0.4	0.36	0.42	0.44	0.32	0.4
R_i (Hz/pu)	3.0	3.0	3.3	2.7273	2.6667	2.5
B_i (pu/Hz)	0.3483	0.3473	0.318	0.3827	0.3890	0.4140
2H (sec)	7	8.05	8.05	8.05	8.05	8.05

C-1.2. LFC test case 2

Table C-2 shows the generating parameters of the four area power system obtained from datasheet given in (Bevrani, 2009). The P_{Load} for area 1 is 1055.2 MW and the corresponding D is 1.5828 Hz/pu. In area 3, the P_{Load} 1067.5 MW and the corresponding D is 1.6013 Hz/pu. Area 2 and area 4 are not considered due to the fact that the no further increase is generation is possible as the maximum generation has been reached and load shedding has to be carried out in order to maintain generation load balance. The maximum P_G in area 1 is 2250 MW. By taking the load demand into consideration, the system is still able to cater to a maximum load demand of 1194.8 MW. In area 3, the maximum P_G is 1373 MW and the system is still able to cater a load of 305.5 MW.

The P_{Load} for area 2 is 1871.3 MW and the corresponding D is 2.807 Hz/pu. In area 4, the P_{Load} 1817.2 MW and the corresponding D is 2.7266 Hz/pu. The maximum P_G in area 2 is 1919 MW. The maximum P_G in area 4 is 1825 MW. The reheat thermal parameters K_{ri} and T_{ri} are 0.5s and 10s respectively. The GRC for each generator is taken as 3%.

Table C-2

Generating unit parameters for IEEE 39-bus test system with multiple interconnected generators

Parameters	G1	G2	G3	G4	G5	G6
T_{Hi} (sec)	0.06	0.06	0.06	0.06	0.06	0.06
T_{Ti} (sec)	0.44	0.36	0.05	0.36	0.05	0.05
R_i (Hz/pu)	2.7273	3	3	3	3	3
B_i (pu/Hz)	0.3827	0.3473	0.3473	0.3473	0.3473	0.3473
2H (sec)	12.102	7.2	30	7.2	7.2	30

Table C-2(continued)

Generating unit parameters for IEEE 39-bus test system with multiple interconnected generators

Parameters	**G7**	**G8**	**G9**	**G10**
T_{Hi} (sec)	0.06	0.06	0.08	0.06
T_{Ti} (sec)	0.05	0.32	0.4	0.44
R_i (Hz/pu)	3	2.667	2.8235	2.7273
B_i (pu/Hz)	0.3483	0.389	0.3692	0.3827
2H (sec)	30	9	7.482	12.102

C-1.3. LFC test case 3

Table C-3 shows the generating parameters of the three area power system obtained from datasheet given in (Bevrani, 2009). The P_{Load} for area 1 is 963 MW and the corresponding D is 1.4445 Hz/pu. In area 2, the P_{Load} is 2333 MW and the corresponding D is 3.4995 Hz/pu. In area 3 the P_{Load} is 946 MW and the corresponding D is 1.419 Hz/pu. The maximum P_G in area 1 is 1288 MW. By taking the load demand into consideration, the system is still able to cater to a maximum load demand of 325 MW. In area 2, the maximum P_G is 3451.2 MW and the system is still able to cater a load of 1118.2 MW. In area 3, the maximum P_G is 1439 MW and the system is still able to cater a load of 493 MW. The reheat thermal parameters K_{ri} and T_{ri} are 0.5s and 10s respectively. The GRC for each generator is taken as 3%.

Table C-3

Generating unit parameters for IEEE 118-bus test system with multiple interconnected generators

Parameters	G1	G2	G3	G4	G5
T_{Hi} (sec)	0.06	0.06	0.06	0.06	0.08
T_{Ti} (sec)	0.36	0.05	0.05	0.05	0.05
R_i (Hz/pu)	3	3	3	3	3
B_i (pu/Hz)	0.3473	0.3473	0.3473	0.3473	0.3483
2H (sec)	7.2	30	30	30	30

Table C-3(continued)

Generating unit parameters for IEEE 118-bus test system with multiple interconnected generators

Parameters	G6	G7	G8	G9	G10	G11	G12	G13	G14
T_{Hi} (sec)	0.07	0.07	0.07	0.07	0.07	0.06	0.06	0.07	0.06
T_{Ti} (sec)	0.05	0.05	0.05	0.05	0.05	0.05	0.05	0.3	0.05
R_i (Hz/pu)	3.3	3.3	3.3	3.3	3.3	3	3	2.8235	3
B_i (pu/Hz)	0.318	0.3827	0.318	0.3827	0.3827	0.3473	0.3473	0.3692	0.3473
2H (sec)	30	6	30	6	6	30	30	7.482	30

Table C-3(continued)

Generating unit parameters for IEEE 118-bus test system with multiple interconnected generators

Parameters	G15	G16	G17	G18	G19
T_{Hi} (sec)	0.07	0.08	0.07	0.08	0.08
T_{Ti} (sec)	0.05	0.4	0.05	0.05	0.05
R_i (Hz/pu)	3.3	2.8235	3.3	3	3
B_i (pu/Hz)	0.318	0.3692	0.3827	0.3483	0.3483
2H (sec)	30	7.482	6	30	30